APPLICATIONS OF THE PERTURBATIVE GRADIENT FLOW AT HIGHER ORDERS IN QUANTUM CHROMODYNAMICS

Von der Fakultät für Mathematik, Informatik und Naturwissenschaften der RWTH Aachen University zur Erlangung des akademischen Grades eines Doktors der der Naturwissenschaften genehmigte Dissertation

vorgelegt von

FABIAN LANGE
M. Sc.

aus Würzburg

Berichter: Prof. Dr. rer. nat. Robert V. Harlander
Prof. Dr. rer. nat. Michał Czakon

Tag der mündlichen Prüfung: 24.03.2021

ABSTRACT

The gradient flow formalism introduced ten years ago proved to be a useful tool for lattice simulations of Quantum Chromodynamics. Its flagship applications are new strategies to set the scale of these simulations. Another important feature is the smoothing property of the gradient flow, which improves renormalizability. In particular, operators composed of flowed fields do not require renormalization. Moreover, by utilizing the small-flow-time expansion, one obtains a relation between flowed and regular operators. For example, this allows to construct a regularization independent formula for the energy-momentum tensor, which can be used on the lattice. Other possible applications of the gradient flow formalism include the extraction of the strong coupling constant or parton distribution functions from lattice simulations. Many of these applications rely on input both from perturbative calculations and lattice simulations.

In this thesis we develop an automatized framework for higher-order perturbative calculations in the gradient flow formalism based on standard techniques for precision calculations in the Standard Model. Due to the complexity of the calculations in the gradient flow formalism, we codeveloped two open-source programs based on emerging algebraic techniques over finite fields. These programs are general and can be applied to a wide range of standard precision calculations as well.

This framework is then applied to compute vacuum expectation values of flowed operators, which we then use to define a gradient flow coupling and a gradient flow mass. Afterwards, we increase the accuracy of the gradient flow formula for the energy-momentum tensor to the next perturbative order. The results of both calculations are then combined to derive a flowed operator product expansion for current-current correlators, which might pave the way for an alternative determination of the hadronic corrections to the anomalous magnetic moment. Finally, we turn to flavor physics which is usually described by the electroweak Hamiltonian. We apply the small-flow-time expansion to the current-current operators of the Hamiltonian, which can be used to combine lattice simulations of hadronic matrix elements with the perturbative Wilson coefficients to obtain an overall theoretical prediction for Kaon and B meson mixing, for example.

ZUSAMMENFASSUNG

Der vor zehn Jahren eingeführte Gradientenflussformalismus hat sich als nützliches Werkzeug für Gittersimulationen in der Quantenchromodynamik erwiesen. Er findet dort insbesondere in neuen Strategien zur Fixierung der Skalen Anwendung. Eine weitere wichtige Eigenschaft ist das Ausschmieren von Feldern, was die Renormierbarkeit verbessert. Insbesondere müssen Operatoren, die aus geflossenen Feldern bestehen, nicht renormiert werden. Indem man darüber hinaus die Entwicklung in kleiner Flusszeit ausnutzt, kann man eine Relation zwischen geflossenen und regulären Operatoren herleiten. Damit kann man zum Beispiel eine regularisierungsunabhängige Formel für den Energie-Impuls-Tensor herleiten, die auf dem Gitter benutzt werden kann. Des Weiteren kann man möglicherweise den Gradientenfluss benutzen, um die starke Kopplungskonstante oder Partondichtefunktionen aus Gittersimulationen zu extrahieren. Viele der genannten Anwendungen benötigen sowohl störungstheoretische Rechnungen als auch Gittersimulationen.

In dieser Doktorarbeit entwickeln wir daher ein Framework für automatisierte Rechnungen im Gradientenflussformalismus zu höheren Ordnungen in der Störungstheorie. Es basiert auf üblichen Methoden, die für Präzisionsrechnungen im Standardmodell angewendet werden. Aufgrund der Komplexität der Rechnungen im Gradientenflussformalismus haben wir zwei Open-Source-Programme mitentwickelt, die auf aufstrebenden algebraischen Methoden über endlichen Körpern basieren. Diese Programme können nicht nur im Gradientenflussformalismus sondern auch in vielen gewöhnlicheren Präzisionsrechnungen Anwendung finden.

Mit Hilfe dieses Frameworks berechnen wir dann Vakuumerwartungswerte von geflossenen Operatoren, mit denen wir eine Gradientenflusskopplung und eine Gradientenflussmasse definieren. Danach erhöhen wir die Genauigkeit der Gradientflussformel des Energie-Impuls-Tensors zur nächsten störungstheoretischen Ordnung. Die Ergebnisse dieser beiden Rechnungen werden dann zur geflossenen Operatorproduktentwicklung für Strom-Strom-Korrelatoren kombiniert. Mit deren Hilfe erhält man möglicherweise eine alternative Berechnungsmethode der hadronischen Korrekturen zum anomalen magnetischen Moment. Zum Schluss wenden wir uns der Flavorphysik zu, die üblicherweise vom elektroschwachen Hamilton-Operator beschrieben wird. Wir wenden die Entwicklung in kleiner Flusszeit auf dessen Strom-Strom-Operatoren an. Dies könnte zum Beispiel eine alternative Zusammensetzung der theoretischen Vorhersage der Kaon- und B-Meson-Mischungen aus Gittersimulationen der hadronischen Matrixelemente und den perturbativen Wilson-Koeffizienten ermöglichen.

EIDESSTATTLICHE ERKLÄRUNG

Ich, Fabian Lange, erkläre hiermit, dass diese Dissertation und die darin dargelegten Inhalte die eigenen sind und selbstständig, als Ergebnis der eigenen originären Forschung, generiert wurden.

Hiermit erkläre ich an Eides statt

1. Diese Arbeit wurde vollständig oder größtenteils in der Phase als Doktorand dieser Fakultät und Universität angefertigt;

2. Sofern irgendein Bestandteil dieser Dissertation zuvor für einen akademischen Abschluss oder eine andere Qualifikation an dieser oder einer anderen Institution verwendet wurde, wurde dies klar angezeigt;

3. Wenn immer andere eigene- oder Veröffentlichungen Dritter herangezogen wurden, wurden diese klar benannt;

4. Wenn aus anderen eigenen- oder Veröffentlichungen Dritter zitiert wurde, wurde stets die Quelle hierfür angegeben. Diese Dissertation ist vollständig meine eigene Arbeit, mit der Ausnahme solcher Zitate;

5. Alle wesentlichen Quellen von Unterstützung wurden benannt;

6. Wenn immer ein Teil dieser Dissertation auf der Zusammenarbeit mit anderen basiert, wurde von mir klar gekennzeichnet, was von anderen und was von mir selbst erarbeitet wurde;

7. Teile dieser Arbeit wurden zuvor veröffentlicht und zwar in:

   [FL1] R. V. Harlander, Y. Kluth und F. Lange, *The two-loop energy–momentum tensor within the gradient-flow formalism*, *Eur. Phys. J. C* **78** (2018) 944, DOI: 10.1140/epjc/s10052-018-6415-7, arXiv: 1808.09837 [hep-lat], Erratum: *Eur. Phys. J. C* **79** (2019) 858, DOI: 10.1140/epjc/s10052-019-7327-x.

   [FL2] J. Klappert und F. Lange, *Reconstructing rational functions with* `FireFly`, *Comput. Phys. Commun.* **247** (2020) 106951, DOI: 10.1016/j.cpc.2019.106951, arXiv: 1904.00009 [cs.SC].

   [FL3] J. Artz, R. V. Harlander, F. Lange, T. Neumann und M. Prausa, *Results and techniques for higher order calculations within the gradient-flow formalism*, *JHEP* **06** (2019) 121, DOI: 10.1007/JHEP06(2019)121, arXiv: 1905.00882 [hep-lat], Erratum: *JHEP* **10** (2019) 032, DOI: 10.1007/JHEP10(2019)032.

   [FL4] J. Klappert, S. Y. Klein und F. Lange, *Interpolation of dense and sparse rational functions and other improvements in FireFly*, *Comput. Phys. Commun.* **264** (2021) 107968, DOI: 10.1016/j.cpc.2021.107968, arXiv: 2004.01463 [cs.MS].

[FL5] R. V. Harlander, F. Lange und T. Neumann, *Hadronic vacuum polarization using gradient flow*, *JHEP* **08** (2020) 109, DOI: 10.1007/JHEP08(2020)109, arXiv: 2007.01057 [hep-lat].

[FL6] J. Klappert, F. Lange, P. Maierhöfer und J. Usovitsch, *Integral reduction with Kira 2.0 and finite field methods*, *Comput. Phys. Commun.* **266** (2021) 108024, DOI: 10.1016/j.cpc.2021.108024, arXiv: 2008.06494 [hep-ph].

Karlsruhe, den 3. August 2021

LIST OF PUBLICATIONS

The research presented in this thesis was conducted at the Institute for Theoretical Particle Physics and Cosmology at RWTH Aachen University from November 2017 to October 2020. The contents of this thesis are partly based on work with other authors and have been published previously or are prepared for publication. Chapters 2, 4, and 5 as well as Section 3.1 are based on Ref. [FL3]. The remainder of Chapter 3 is based on Refs. [FL2, FL4, FL6]. Chapter 6 is based on Ref. [FL1] and Chapter 7 is based on Ref. [FL5]. My contributions to these publications are specified in the corresponding chapters.

[FL1] R. V. Harlander, Y. Kluth, and F. Lange, *The two-loop energy–momentum tensor within the gradient-flow formalism*, *Eur. Phys. J. C* **78** (2018) 944, DOI: 10.1140/epjc/s10052-018-6415-7, arXiv: 1808.09837 [hep-lat], Erratum: *Eur. Phys. J. C* **79** (2019) 858, DOI: 10.1140/epjc/s10052-019-7327-x.

[FL2] J. Klappert and F. Lange, *Reconstructing rational functions with* `FireFly`, *Comput. Phys. Commun.* **247** (2020) 106951, DOI: 10.1016/j.cpc.2019.106951, arXiv: 1904.00009 [cs.SC].

[FL3] J. Artz, R. V. Harlander, F. Lange, T. Neumann, and M. Prausa, *Results and techniques for higher order calculations within the gradient-flow formalism*, *JHEP* **06** (2019) 121, DOI: 10.1007/JHEP06(2019)121, arXiv: 1905.00882 [hep-lat], Erratum: *JHEP* **10** (2019) 032, DOI: 10.1007/JHEP10(2019)032.

[FL4] J. Klappert, S. Y. Klein, and F. Lange, *Interpolation of dense and sparse rational functions and other improvements in FireFly*, *Comput. Phys. Commun.* **264** (2021) 107968, DOI: 10.1016/j.cpc.2021.107968, arXiv: 2004.01463 [cs.MS].

[FL5] R. V. Harlander, F. Lange, and T. Neumann, *Hadronic vacuum polarization using gradient flow*, *JHEP* **08** (2020) 109, DOI: 10.1007/JHEP08(2020)109, arXiv: 2007.01057 [hep-lat].

[FL6] J. Klappert, F. Lange, P. Maierhöfer, and J. Usovitsch, *Integral reduction with Kira 2.0 and finite field methods*, *Comput. Phys. Commun.* **266** (2021) 108024, DOI: 10.1016/j.cpc.2021.108024, arXiv: 2008.06494 [hep-ph].

CONTENTS

Part I

APPLICATIONS OF THE PERTURBATIVE GRADIENT FLOW AT HIGHER ORDERS IN QUANTUM CHROMODYNAMICS

1 INTRODUCTION

Even though the Yang-Mills flow equation was already introduced by Atiyah and Bott in 1983 in the context of studying the Yang-Mills functional over a Riemann surface [1], it only appeared in 2006 in the context of lattice gauge theories, when Narayanan and Neuberger studied the large-N behavior of smeared Wilson loops [2]. In 2009, Lüscher formulated its discrete version to construct "trivializing" maps which map lattice gauge theories to their strong-coupling limit, hoping to improve the efficiency of lattice simulations [3]. A year later, he studied the smoothing properties of the gradient flow and discovered that the gauge fields obeying this flow equation and defined at non-vanishing flow time are smoothed fields which do not require a field renormalization [4]. Moreover, the introduced flow-time scale can be used to set the scale of lattice simulations. New scale setting strategies based on the gradient flow formalism, eventually superseding previous methods, drove the prominence of the formalism, see e.g. Refs. [4–6].

While *flowed*[1] quark fields do require a field renormalization [7], the renormalization properties of the gradient flow extend to flowed composite operators, which are finite when expressed through renormalized parameters and fields [8]. Therefore, they do not mix under *renormalization group* (RG) running. Furthermore, by performing a so-called *small-flow-time expansion* of flowed operators, one obtains a relation between flowed and regular operators related by a flow-time dependent mixing matrix. By inverting the mixing matrix, one obtains a flowed *operator product expansion* (OPE) (also called *smeared* OPE in Ref. [9]), which expresses the regular operators through the better behaved flowed operators. The Wilson coefficients can be calculated perturbatively while matrix elements of the flowed operators can be computed on the lattice. This was utilized by Makino and Suzuki to construct a regularization independent formula for the *energy-momentum tensor* (EMT) of *Quantum Chromodynamics* (QCD) [10, 11], which, in contrast, requires a sophisticated renormalization strategy when expressed through regular operators. This already led to promising thermodynamical results [12–16].

Other, still theoretical, applications of the gradient flow formalism include the extraction of the strong coupling α_s from lattice simulations [17–23] as well as a proposal to relate Euclidean quasi parton distribution functions on the lattice to perturbative light-cone parton distribution functions [24, 25]. Moreover, it can be used to study dualities in field theories [26–31].

Many of these applications require input from perturbative calculations. In this thesis, we thus develop an automatized framework for higher-order perturbative calculations in the gradient flow formalism based on many standard tools used for precision calculations

1 We use the terms *flowed* and *regular* to distinguish quantities defined at flow time $t > 0$ from those defined at $t = 0$.

in the Standard Model. Hence, the perturbative calculations throughout this thesis are performed at infinite volume. The inclusion of finite-volume effects requires different techniques such as *Numerical Stochastic Perturbation Theory*, see e.g. Ref. [22].

In Chapter 2, we review the gradient flow formalism as well as its perturbative treatment and derive the Feynman rules. The ensuing Feynman integrals are then solved with *integration-by-parts* (IBP) identities [32, 33] generalized to the gradient flow integrals in Chapter 3. However, no public program available was powerful enough to finish the reduction at three-loop level. We thus take a detour into strategies based on finite field and interpolation techniques, which, in the context of IBP reductions, only gained traction over the last decade [34–37]. At this point, we also describe our implementation of these strategies into the public programs `FireFly` and `Kira`. Afterwards in Chapter 4, we discuss the different calculational methods employed to compute the master integrals.

In Chapter 5, the techniques from the previous chapters are then exploited to calculate the *vacuum expectation value*s (VEVs) of some flowed operators to *next-to-next-to-leading order* (NNLO) accuracy, improving on and extending the results of Ref. [21]. These results are then used to define a *gradient flow coupling* and a *gradient flow mass*.

The Wilson coefficients of the flowed EMT are known to *next-to-leading order* (NLO) [10, 11]. In Chapter 6, we calculate them through NNLO, significantly reducing the scale uncertainty. Furthermore, we present the mixing matrix between the regular and flowed operators of the EMT.

The *vacuum polarization function*s (VPFs) of particles play important roles in both perturbative and non-perturbative physics. A prime example of the latter is the determination of anomalous magnetic moments [38, 39], which are usually obtained with the help of experimental data and dispersion relations. Only very recently lattice calculations have become competitive, leading to incompatible results [40]. In Chapter 7, we thus derive a flowed OPE for current-current correlators, which might pave the way for an alternative determination of the hadronic corrections to the anomalous magnetic moment and other observables. Moreover, we derive a general flow-time evolution equation for flowed operators.

Another area of large non-perturbative corrections is the physics of quark flavors. The perturbative electroweak corrections are usually captured in the Wilson coefficients of the effective electroweak Hamiltonian, while the hadronic matrix elements of the processes require a non-perturbative treatment on the lattice. However, the necessary matching between the different schemes in perturbative and lattice calculations is a large source of uncertainties. Therefore, we compute the mixing matrix between the regular and flowed current-current operators of the electroweak Hamiltonian in Chapter 8 as ingredient to the corresponding flowed OPE required to circumvent the scheme matching. While our results are still preliminary, they might be used to combine the hadronic contributions of Kaon or B meson mixing from the lattice with the perturbative Wilson coefficients.

2 THE YANG-MILLS GRADIENT FLOW IN PERTURBATION THEORY

In this chapter we introduce the gradient flow formalism and discuss its perturbative treatment. Section 2.1 introduces the eponymous flow equations and shows how they can be incorporated into the Lagrangian of QCD. They are perturbatively solved in Section 2.2 which provides us with the building blocks for the Feynman rules which are derived in Section 2.3. In Section 2.4 we introduce simple observables in the form of composite operators and discuss the renormalizability of the gradient flow formalism. The ensuing Feynman integrals are introduced in Section 2.5.

This chapter is based on parts of Ref. [41]. The Feynman rules were derived by Johannes Artz in the course of his Master's thesis [42] and some minor mistakes were corrected as part of this thesis.

2.1 THE FLOW EQUATIONS AND THE FLOWED LAGRANGIAN

In the following, we work in D-dimensional Euclidean space-time with $D = 4 - 2\epsilon$. The gradient flow formalism continues the gluon and quark fields $A^a_\mu(x)$ and $\psi^i_{\hat{\alpha}}(x)$ of regular QCD to $(D+1)$-dimensional fields $B^a_\mu(t,x)$ and $\chi^i_{\hat{\alpha}}(t,x)$ through the boundary conditions

$$B^a_\mu(t=0,x) = A^a_\mu(x)\,, \qquad \chi^i_{\hat{\alpha}}(t=0,x) = \psi^i_{\hat{\alpha}}(x) \tag{2.1}$$

and the flow equations [4, 7]

$$\begin{aligned} \partial_t B^a_\mu &= \mathcal{D}^{ab}_\nu G^b_{\nu\mu} + \kappa \mathcal{D}^{ab}_\mu \partial_\nu B^b_\nu, \\ \partial_t \chi &= \Delta\chi - \kappa \partial_\mu B^a_\mu T^a \chi, \\ \partial_t \bar{\chi} &= \bar{\chi}\overleftarrow{\Delta} + \kappa \bar{\chi} \partial_\mu B^a_\mu T^a, \end{aligned} \tag{2.2}$$

where the *flow time* t is a parameter of mass dimension minus two and we use the short-hand notation $\partial_t \equiv \frac{\partial}{\partial t}$. The $(D+1)$-dimensional field-strength tensor is defined as

$$G^a_{\mu\nu} = \partial_\mu B^a_\nu - \partial_\nu B^a_\mu + f^{abc} B^b_\mu B^c_\nu, \tag{2.3}$$

the covariant derivative in the adjoint representation is given by

$$\mathcal{D}^{ab}_\mu = \delta^{ab}\partial_\mu - f^{abc} B^c_\mu, \tag{2.4}$$

and

$$\Delta = \mathcal{D}^{\mathrm{F}}_\mu \mathcal{D}^{\mathrm{F}}_\mu, \qquad \overleftarrow{\Delta} = \overleftarrow{\mathcal{D}}^{\mathrm{F}}_\mu \overleftarrow{\mathcal{D}}^{\mathrm{F}}_\mu, \tag{2.5}$$

with the covariant derivative in the fundamental representation,

$$\mathcal{D}^{\mathrm{F}}_\mu = \partial_\mu + B^a_\mu T^a, \qquad \overleftarrow{\mathcal{D}}^{\mathrm{F}}_\mu = \overleftarrow{\partial}_\mu - B^a_\mu T^a. \tag{2.6}$$

As usual, the color indices of the adjoint representation are denoted by $a, b, c, \ldots$, while $\mu, \nu, \rho, \ldots$ are D-dimensional Lorentz indices. Color indices of the fundamental representation are denoted by $i, j, k, \ldots$, but they are suppressed throughout this thesis, unless required by clarity; similarly for spinor indices $\hat{\alpha}, \hat{\beta}, \hat{\gamma}, \ldots$. The symmetry generators T^a are understood in the fundamental representation. We refer to Appendix A for our conventions for the gauge group and the list of invariants.

κ is an additional gauge parameter introduced by the gauge transformations

$$\chi \to \chi' = \Lambda\chi \qquad \text{and} \qquad B_\mu^a T^a \to B_\mu^{a\prime} T^a = \Lambda B_\mu^a T^a \Lambda^{-1} + \Lambda\partial_\mu\Lambda^{-1} \tag{2.7}$$

with

$$\Lambda(t,x) = e^{-\int_0^t \mathrm{d}s\, \kappa\partial_\mu B_\mu^a(s,x)T^a}. \tag{2.8}$$

Of course, all observables are independent of the gauge parameter κ [4]. In perturbative calculations, it is usually most convenient to set $\kappa = 1$.

Note that the flow equations (2.2) have the form of a diffusion equation

$$\partial_t\phi(t,\vec{x}) = \nabla_x \cdot (\mathcal{D}(\phi,\vec{x})\nabla_x\phi(t,\vec{x})) \tag{2.9}$$

for the density of the diffusing material ϕ and the diffusion coefficient $\mathcal{D}$, where ∇_x is the nabla operator with respect to $\vec{x}$. For constant $\mathcal{D}$ the equation reduces to the heat equation. As the name already suggests, the equation smears out the density or, in our case, the fields, which makes the gradient flow formalism appealing for lattice QCD. The explicit smearing radius for the linear approximation of the flow equations (2.2) is derived in the next Section 2.2.

The flow equations (2.2) can be incorporated in a Lagrangian formalism by defining

$$\mathcal{L} = \mathcal{L}_{\text{QCD}} + \mathcal{L}_{\text{gauge-fixing}} + \mathcal{L}_{\text{ghost}} + \mathcal{L}_B + \mathcal{L}_\chi. \tag{2.10}$$

The first three terms constitute the regular Yang-Mills Lagrangian, with fermions added in the fundamental representation (quarks). Introducing an index f in order to distinguish different quark flavors of bare mass $m_{f,\mathrm{B}}$, the classical, gauge-fixing, and Faddeev-Popov ghost part are given by

$$\begin{aligned}
\mathcal{L}_{\text{QCD}} &= \frac{1}{4g_{\mathrm{B}}^2} F_{\mu\nu}^a F_{\mu\nu}^a + \sum_{f=1}^{n_{\mathrm{f}}} \bar{\psi}_f (\not{D}^{\mathrm{F}} + m_{f,\mathrm{B}})\psi_f, \\
\mathcal{L}_{\text{gauge-fixing}} &= \frac{1}{2g_{\mathrm{B}}^2\xi}(\partial_\mu A_\mu^a)^2, \\
\mathcal{L}_{\text{ghost}} &= \frac{1}{g_{\mathrm{B}}^2}\partial_\mu\bar{c}^a D_\mu^{ab} c^b,
\end{aligned} \tag{2.11}$$

respectively, where

$$F_{\mu\nu}^a = \partial_\mu A_\nu^a - \partial_\nu A_\mu^a + f^{abc} A_\mu^b A_\nu^c \tag{2.12}$$

is the regular field strength tensor and

$$D_\mu^{\mathrm{F}} = \partial_\mu + A_\mu^a T^a, \qquad D_\mu^{ab} = \delta^{ab}\partial_\mu - f^{abc} A_\mu^c \tag{2.13}$$

are the regular covariant derivatives in the fundamental and adjoint representation, respectively, g_B is the gauge coupling, ξ the QCD gauge parameter, and n_f the number of different quark flavors. The flow equations are incorporated by introducing Lagrange multiplier fields

$$L^a_\mu(t,x) \qquad \text{and} \qquad \lambda_f(t,x),\ \bar{\lambda}_f(t,x) \tag{2.14}$$

of mass dimensions 3 and 5/2 that otherwise carry the same quantum numbers as the flowed gluon and quark/antiquark fields B^a_μ and $\chi, \bar{\chi}$, respectively. Their Euler-Lagrange equations derived from

$$\begin{aligned}
\mathcal{L}_B &= -2\int_0^\infty \mathrm{d}t\, \mathrm{Tr}\left[L^a_\mu T^a\left(\partial_t B^b_\mu T^b - \mathcal{D}^{bc}_\nu G^c_{\nu\mu} T^b - \kappa \mathcal{D}^{bc}_\mu \partial_\nu B^c_\nu T^b\right)\right], \\
\mathcal{L}_\chi &= \sum_{f=1}^{n_\mathrm{f}} \int_0^\infty \mathrm{d}t \Big[\bar{\lambda}_f\left(\partial_t - \Delta + \kappa\left(\partial_\mu B^a_\mu\right) T^a\right)\chi_f + \bar{\chi}_f\left(\overleftarrow{\partial_t} - \overleftarrow{\Delta} - \kappa\left(\partial_\mu B^a_\mu\right) T^a\right)\lambda_f\Big],
\end{aligned} \tag{2.15}$$

indeed lead to Eq. (2.2) [7, 8].

Note that the Lagrangian (2.10) does not include flowed ghost fields $d^a(t,x)$ and $\bar{d}^a(t,x)$. They arise in the same way as the usual Faddeev-Popov ghosts $c^a(x)$ and $\bar{c}^a(x)$ due to gauge-fixing, and obey the initial condition

$$d^a(t,x)|_{t=0} = c^a(x). \tag{2.16}$$

Similar to the ghosts of the regular gauge fields, they always form closed loops as long as there are no external d^a or $\bar{d}^a$ fields which can be avoided by considering only physical degrees of freedom in amplitudes with external gluons. As becomes clear later, closed loops of only flowed fields vanish, so that one can omit d^a and $\bar{d}^a$ already at the level of the Lagrangian [8].

2.2 PERTURBATIVE SOLUTION OF THE FLOW EQUATIONS

Let us introduce the short-hand notation

$$\int_p \equiv \int \frac{\mathrm{d}^D p}{(2\pi)^D}, \qquad \int_x \equiv \int \mathrm{d}^D x, \tag{2.17}$$

where it should be clear from the context whether an integration variable is in position $(x, y, z, \ldots)$ or momentum space $(p, k, q, \ldots)$.

It is helpful to separate the flow equation (2.2) of the flowed gauge field $B^a_\mu(t,x)$ into a linear and a non-linear part [4]:

$$\begin{aligned}
&\partial_t B^a_\mu = \partial_\nu\partial_\nu B^a_\mu + (\kappa-1)\partial_\mu\partial_\nu B^a_\nu + R^a_\mu, \\
&R^a_\mu = 2f^{abc} B^b_\nu \partial_\nu B^c_\mu - f^{abc} B^b_\nu \partial_\mu B^c_\nu + (\kappa-1) f^{abc} B^b_\mu \partial_\nu B^c_\nu + f^{abe} f^{cde} B^b_\nu B^c_\nu B^d_\mu.
\end{aligned} \tag{2.18}$$

The linear equation can be solved by introducing the integration kernel

$$K_{\mu\nu}(t,x) = \int_p \frac{e^{\mathrm{i}px}}{p^2}\left(\left(\delta_{\mu\nu}p^2 - p_\mu p_\nu\right)e^{-tp^2} + p_\mu p_\nu\, e^{-\kappa t p^2}\right) \equiv \int_p e^{\mathrm{i}px}\widetilde{K}_{\mu\nu}(t,p), \tag{2.19}$$

which fulfills

$$\lim_{t\to 0} K_{\mu\nu}(t,x) = \delta_{\mu\nu}\delta^{(D)}(x). \tag{2.20}$$

Taking into account the initial condition (2.1), the full solution of the flow equation is then given by [8]

$$B^a_\mu(t,x) = \int_y K_{\mu\nu}(t,x-y)A^a_\nu(y) + \int_y\int_0^t \mathrm{d}s\, K_{\mu\nu}(t-s,x-y)R^a_\nu(s,y), \tag{2.21}$$

or, in momentum space,

$$\widetilde{B}^a_\mu(t,p) = \int_x e^{-\mathrm{i}px}B^a_\mu(t,x) = \widetilde{K}_{\mu\nu}(t,p)\widetilde{A}^a_\nu(p) + \int_0^t \mathrm{d}s\, \widetilde{K}_{\mu\nu}(t-s,p)\widetilde{R}^a_\nu(s,p). \tag{2.22}$$

By inserting the solution iteratively into itself, one can express the Fourier transform of the non-linear part of Eq. (2.18) as

$$\begin{aligned}\widetilde{R}^a_\mu(t,p) = \int_{q,l,k}(2\pi)^D\,\delta^{(D)}(p-q-l-k)\Big[&\delta^{(D)}(k)\cdot X^{abc}_{2,\mu\nu\rho}(q,l)\,\widetilde{B}^b_\nu(t,q)\widetilde{B}^c_\rho(t,l)\\ &+ X^{abcd}_{3,\mu\nu\rho\sigma}\,\widetilde{B}^b_\nu(t,q)\widetilde{B}^c_\rho(t,l)\widetilde{B}^d_\sigma(t,k)\Big],\end{aligned} \tag{2.23}$$

where

$$\begin{aligned}X^{abc}_{2,\mu\nu\rho}(q,l) &= -\mathrm{i}f^{abc}\big[(l-q)_\mu\delta_{\nu\rho} + 2q_\rho\delta_{\mu\nu} - 2l_\nu\delta_{\mu\rho} + (\kappa-1)(q_\nu\delta_{\mu\rho} - l_\rho\delta_{\mu\nu})\big],\\ X^{abcd}_{3,\mu\nu\rho\sigma} &= f^{abe}f^{cde}(\delta_{\mu\sigma}\delta_{\nu\rho} - \delta_{\mu\rho}\delta_{\nu\sigma}) + f^{ade}f^{bce}(\delta_{\mu\rho}\delta_{\nu\sigma} - \delta_{\mu\nu}\delta_{\rho\sigma})\\ &\quad + f^{ace}f^{dbe}(\delta_{\mu\nu}\delta_{\rho\sigma} - \delta_{\mu\sigma}\delta_{\nu\rho})\end{aligned} \tag{2.24}$$

The structure of X_3 is identical to the four-gluon vertex of regular QCD. When formulating the Feynman rules later, X_2 and X_3 describe the three- and four-point vertices of the flowed gluon fields.

The flow equation (2.2) for the flowed quark fields can be solved by again splitting it into a linear and a non-linear part,

$$\partial_t\chi = \partial_\mu\partial_\mu\chi + \Delta'\chi \quad \text{with} \quad \Delta' = (1-\kappa)\partial_\mu B^a_\mu T^a + 2B^a_\mu T^a\partial_\mu + B^a_\mu B^b_\mu T^a T^b. \tag{2.25}$$

The linear equation is solved by the integration kernel

$$K(t,x) = \int_p e^{\mathrm{i}px}e^{-tp^2} \equiv \int_p e^{\mathrm{i}px}\widetilde{K}(t,p), \tag{2.26}$$

with the help of which we can write the full solution as [7]

$$\chi(t,x) = \int_y K(t,x-y)\psi(y) + \int_y\int_0^t \mathrm{d}s\, K(t-s,x-y)\Delta'\chi(s,y). \tag{2.27}$$

Here and in what follows, we suppress the flavor index f unless required for clarity. The non-linear part of the Fourier-transformed field

$$\widetilde{\chi}(t,p) = \widetilde{K}(t,p)\widetilde{\psi}(p) + \int_0^t \mathrm{d}s\, \widetilde{K}(t-s,p)\widetilde{\Delta'\chi}(s,p) \tag{2.28}$$

can be expressed as

$$\begin{aligned}\widetilde{\Delta'\chi}(t,p) = \int_{q,l,r} (2\pi)^D \delta^{(D)}(p-q-l-r) \Big[\delta^{(D)}(l) \cdot Y^b_{1,\nu}(q,r) \widetilde{B}^b_\nu(t,q) \\ + \frac{1}{2} Y^{bc}_{2,\nu\rho} \widetilde{B}^b_\nu(t,q) \widetilde{B}^c_\rho(t,l) \Big] \widetilde{\chi}(t,r),\end{aligned} \tag{2.29}$$

where

$$Y^b_{1,\nu}(q,r) = \mathrm{i}\big(2r_\nu + (1-\kappa)q_\nu\big) T^b, \qquad Y^{bc}_{2,\nu\rho} = \delta_{\nu\rho}\big\{T^b, T^c\big\}. \tag{2.30}$$

These expressions lead to the three- and four-point vertices of the flowed quark fields. For $\bar{\chi}$ one proceeds analogously.

In the gauge $\kappa = 1$, the kernel $K_{\mu\nu}(t,x)$ for the gluons defined in Eq. (2.19) coincides with the kernel $K(t,x)$ for the quarks defined in Eq. (2.26) except for the trivial Lorentz structure. Both kernels can directly be solved and yield

$$K_{\mu\nu}(t,x) = \delta_{\mu\nu} K(t,x) = \delta_{\mu\nu} \int_p e^{\mathrm{i}px} e^{-tp^2} = \delta_{\mu\nu} \frac{\mathrm{e}^{\frac{-x^2}{4t}}}{(4\pi t)^{D/2}}. \tag{2.31}$$

Hence, both kernels smear out the fields over a spherical range with mean-squared radius $\sqrt{2Dt} \overset{D=4}{=} \sqrt{8t}$ [4, 7]. This radius characterizes a scale of the involved physics and is traditionally chosen as renormalization scale, see e.g. Refs. [4, 12–16, 21].

2.3 FEYNMAN RULES

We can now derive the Feynman rules for the Lagrangian (2.10). Since the Feynman rules for regular QCD are well known, we only derive the additional Feynman rules originating from the flowed constituents of the Lagrangian given in Eq. (2.15). Nonetheless, a complete list of the Feynman rules relevant for this thesis, including the QCD Feynman rules as well as the Feynman rules for the operators considered in the following chapters, can be found in Appendix B.

2.3.1 *(Flowed) Propagators*

The propagators for the flowed fields can easily be found by using the perturbative solutions of the flow equations derived in Section 2.2. Plugging in the solution of the flowed gluon field in momentum space in Eq. (2.22) into the two-point function, one finds [8]

$$\begin{aligned}\Big\langle \widetilde{B}^a_\mu(t,p) \widetilde{B}^b_\nu(s,q) \Big\rangle \Big|_{\mathrm{LO}} &= \widetilde{K}_{\mu\rho}(t,p) \widetilde{K}_{\nu\sigma}(s,q) \Big\langle \widetilde{A}^a_\rho(p) \widetilde{A}^b_\sigma(q) \Big\rangle \\ &= (2\pi)^D \delta^{(D)}(p+q)\, g_{\mathrm{B}}^2\, D^{ab}_{\mu\nu}(p, t+s, \xi, \kappa),\end{aligned} \tag{2.32}$$

where

$$D^{ab}_{\mu\nu}(p,t,\xi,\kappa) = \delta^{ab} \frac{1}{p^2} \left(\left(\delta_{\mu\nu} - \frac{p_\mu p_\nu}{p^2}\right) e^{-tp^2} + \xi \frac{p_\mu p_\nu}{p^2} e^{-\kappa t p^2} \right), \tag{2.33}$$

and we have used the result for the fundamental gluon propagator,

$$\left\langle \widetilde{A}^a_\mu(p)\widetilde{A}^b_\nu(q)\right\rangle\Big|_{\mathrm{LO}} = (2\pi)^D\delta^{(D)}(p+q)\, g_{\mathrm{B}}^2 D^{ab}_{\mu\nu}(p,0,\xi,0). \tag{2.34}$$

In order to render the propagator formally independent of the coupling g_{B}, it is useful to rescale the gluon field by the coupling, i.e. $B^a_\mu \to g_{\mathrm{B}} B^a_\mu$, which also applies to the fundamental gluon field $A^a_\mu = B^a_\mu\big|_{t=0}$. The factor g_{B}^2 is taken into account in the corresponding vertices further below.

Since the flowed gluon propagator coincides with the fundamental gluon propagator at $t+s=0$, we can express both of them by the same Feynman rule

$$s,\nu,b \overset{p}{\sim\!\sim\!\sim} t,\mu,a \qquad = \qquad D^{ab}_{\mu\nu}(p,t+s,\xi,\kappa). \tag{2.35}$$

We refer to this as the (flowed) gluon propagator. Eq. (2.35) also applies to the mixed propagator $\langle \widetilde{A}\widetilde{B}\rangle$, which is obtained by setting one of the two flow-time variables to zero.

The same can be done for flowed quark fields. Inserting their momentum space solution in Eq. (2.28) into the two-point function results in [42]

$$\begin{aligned}\left\langle \widetilde{\chi}^i_{\hat\alpha}(t,p)\widetilde{\bar\chi}^j_{\hat\beta}(s,q)\right\rangle\Big|_{\mathrm{LO}} &= \widetilde{K}(t,p)\widetilde{K}(s,q)\left\langle \widetilde{\psi}^i_{\hat\alpha}(p)\widetilde{\bar\psi}^j_{\hat\beta}(q)\right\rangle \\ &= (2\pi)^D\delta^{(D)}(p+q)\, S^{ij}_{\mathrm{F},\hat\alpha\hat\beta}(p,m_{\mathrm{B}},t+s),\end{aligned} \tag{2.36}$$

where

$$S^{ij}_{\mathrm{F},\hat\alpha\hat\beta}(p,m_{\mathrm{B}},t) = \delta^{ij}\frac{(-i\not{p}+m_{\mathrm{B}})_{\hat\alpha\hat\beta}}{p^2+m_{\mathrm{B}}^2}\, e^{-tp^2}, \tag{2.37}$$

and we have used the result for the fundamental quark propagator

$$\left\langle \widetilde{\psi}^i_{\hat\alpha}(p)\widetilde{\bar\psi}^j_{\hat\beta}(q)\right\rangle = (2\pi)^D\delta^{(D)}(p+q)\, S^{ij}_{\mathrm{F},\hat\alpha\hat\beta}(p,m_{\mathrm{B}},0). \tag{2.38}$$

Since one can express the fundamental propagator through the flowed propagator at vanishing flow times, both can be represented by the same Feynman rule

$$s,\hat\beta,j \overset{p}{\longrightarrow} t,\hat\alpha,i \qquad = \qquad S^{ij}_{\mathrm{F},\hat\alpha\hat\beta}(p,m_{\mathrm{B}},t+s). \tag{2.39}$$

We refer to this as the (flowed) quark propagator, which again includes the mixed propagators $\langle\psi\bar\chi\rangle$ and $\langle\chi\bar\psi\rangle$.

2.3.2 *Flow Lines*

Since there are no quadratic terms of the Lagrange multiplier fields L^a_μ, λ, and $\bar\lambda$ in Eq. (2.15), there are no propagators for these fields. However, the Lagrangian contains bilinear terms of a flowed field and a Lagrange multiplier field. For the gluon they read

$$\mathcal{L}^{(2)}_B = 2T_{\mathrm{R}}\int_0^\infty \mathrm{d}t L^a_\mu\left(\partial_t B^a_\mu - \partial_\nu\partial_\nu B^a_\mu + (1-\kappa)\partial_\mu\partial_\nu B^a_\nu\right). \tag{2.40}$$

Employing the path integral formalism, we can write the generating functional with the two source fields $J^a_{B,\mu}$ and $J^a_{L,\mu}$ as

$$Z\left[J^a_{B,\mu}, J^b_{L,\nu}\right] = \frac{1}{Z_0}\int \mathcal{D}L\mathcal{D}B\, \exp\left[-\int_x \left(\mathcal{L}^{(2)}_{\mathrm{B}} - \int_0^\infty \mathrm{d}t\, \left(J^a_{B,\mu}B^a_\mu + J^b_{L,\nu}L^b_\nu\right)\right)\right], \tag{2.41}$$

where $Z_0 = Z[0,0]$. The path integral can be solved by introducing the shifts

$$\begin{aligned} B^a_\mu(t,x) \to B'^a_\mu(t,x) &= B^a_\mu(t,x) + \int_y \int_0^\infty \mathrm{d}s\, H_{\mu\nu}(t-s, x-y) J^a_{L,\nu}(s,y), \\ L^a_\mu(t,x) \to L'^a_\mu(t,x) &= L^a_\mu(t,x) + \int_y \int_0^\infty \mathrm{d}s\, J^a_{B,\nu}(s,y) H_{\nu\mu}(s-t, y-x), \end{aligned} \tag{2.42}$$

which complete the square by demanding that $H_{\mu\nu}(t,x)$ obeys the equation

$$\left[(\partial_t - \partial_\sigma\partial_\sigma)\delta_{\mu\nu} + (1-\kappa)\partial_\mu\partial_\nu\right] H_{\nu\rho}(t,x) = \frac{1}{2T_{\mathrm{R}}}\delta_{\mu\rho}\delta(t)\delta^{(D)}(x). \tag{2.43}$$

Then, the generating functional can be written as

$$Z\left[J^a_{B,\mu}, J^b_{L,\nu}\right] = \exp\left[\int_{x,y}\int \mathrm{d}t\mathrm{d}s\, J^a_{B,\mu}(t,x)\delta^{ab}H_{\mu\nu}(t-s,x-y)J^b_{L,\nu}(s,y)\right]. \tag{2.44}$$

By taking functional derivatives, we find

$$\left\langle B^a_\mu(t,x)L^b_\nu(s,y)\right\rangle = \delta^{ab}H_{\mu\nu}(t-s,x-y) \tag{2.45}$$

for the two-point function at *leading order* (LO). Since the fundamental gluon field $A^a_\mu(x) = B^a_\mu(0,x)$ does not couple to the Lagrange multiplier field L^a_μ, and all flow-time variables are positive, one can impose the initial condition

$$\left\langle B^a_\mu(t,x)L^b_\nu(s,y)\right\rangle\Big|_{t=0} = 0 \quad \Rightarrow \quad H_{\mu\nu}(-s,x) = 0 \tag{2.46}$$

so that the unique solution becomes [8]

$$H_{\mu\nu}(t,x) = \frac{1}{2T_{\mathrm{R}}}\theta(t)K_{\mu\nu}(t,x). \tag{2.47}$$

We refer to the $\langle BL\rangle$ bilinear as *gluon flow line*. The inverse of the factor $\frac{1}{2T_{\mathrm{R}}}$ appears in the corresponding *flow vertices* further below. We can therefore discard it altogether and write

$$s,\nu,b \xrightarrow{\quad p \quad} t,\mu,a \qquad = \qquad \delta^{ab}\,\theta(t-s)\,\widetilde{K}_{\mu\nu}(t-s,p), \tag{2.48}$$

where $\widetilde{K}_{\mu\nu}(t,p)$ has been defined in Eq. (2.19), and the adjacent arrow indicates the direction towards increasing flow time as implied by the θ-distribution. As opposed to an actual propagator, the gluon flow line is a regular function for all p. Note that the

rescaling of the gauge fields $B_\mu^a \to g_\text{B} B_\mu^a$ leads to an additional factor $1/g_\text{B}$, which can also be absorbed by the flow vertices.

Similarly, one determines the mixed fermionic two-point function at LO as

$$\left\langle \chi^i_{\hat{\alpha}}(t,x)\bar{\lambda}^j_{\hat{\beta}}(s,y)\right\rangle = \delta_{\hat{\alpha}\hat{\beta}}\delta^{ij}G(t-s,x-y), \tag{2.49}$$

where $G(t,x)$ has to obey

$$(\partial_t - \partial_\mu\partial_\mu)G(t,x) = \delta(t)\delta^{(D)}(x) \tag{2.50}$$

to complete the square. With the condition

$$\left\langle \chi^i_{\hat{\alpha}}(t,x)\bar{\lambda}^j_{\hat{\beta}}(s,y)\right\rangle\Big|_{t=0} = 0 \quad \Rightarrow \quad G(-s,x) = 0, \tag{2.51}$$

the unique solution then reads [7]

$$G(t,x) = \theta(t)K(t,x). \tag{2.52}$$

The Fourier transformed expression defines the *fermion flow line* Feynman rule, where the θ-distribution again imposes a direction as indicated by the adjacent arrow pointing towards increasing flow time:

$$s,\hat{\beta},j \xrightarrow{\;p\;} t,\hat{\alpha},i \qquad = \qquad \delta_{\hat{\alpha}\hat{\beta}}\delta_{ij}\,\theta(t-s)\,\widetilde{K}(t-s,p), \tag{2.53}$$

where $\widetilde{K}(t,p)$ has been defined in Eq. (2.26). As usual, the arrow *on* the fermion line denotes the *charge flow* of the fermion. In this way, we have a unified Feynman rule for both the $\langle\chi\bar{\lambda}\rangle$ and the $\langle\lambda\bar{\chi}\rangle$ bilinear, where the latter can be obtained analogously as above and simply corresponds to reversing the direction of the charge flow:

$$s,\hat{\beta},j \xleftarrow{\;p\;} t,\hat{\alpha},i \qquad = \qquad \delta_{\hat{\alpha}\hat{\beta}}\delta_{ij}\,\theta(t-s)\,\widetilde{K}(t-s,p). \tag{2.54}$$

Since $\widetilde{K}(t,p)$ depends only quadratically on p, the momentum direction is irrelevant for the fermion flow lines.

2.3.3 *Flow Vertices*

Since $\mathcal{L}_B$ and $\mathcal{L}_\chi$ of Eq. (2.15) are proportional to a Lagrange multiplier field, the resulting vertices always involve at least one flow line. Such vertices are always associated with a flow-time parameter which is integrated over. We denote them by *flow vertices* and represent them by empty circles in Feynman diagrams. The corresponding Feynman rules can be derived straightforwardly. In this thesis, we define Feynman rules by assuming all momenta to be outgoing.

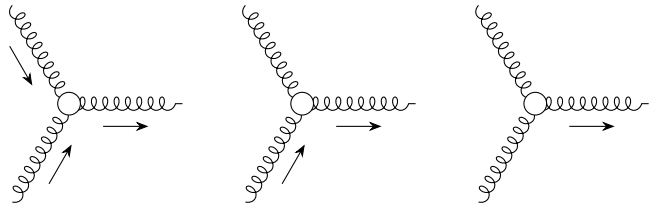

Figure 2.1: The three versions of the vertex X_2. Lines with an adjacent arrow denote flow lines, the others are flowed gluons.

The three-point gluon flow vertex is governed by X_2 [8]:

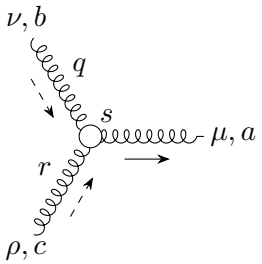

$$= -\mathrm{i}g_{\mathrm{B}} f^{abc} \int_0^\infty \mathrm{d}s \, \big(\delta_{\nu\rho}(r-q)_\mu + 2\delta_{\mu\nu}q_\rho - 2\delta_{\mu\rho}r_\nu + (\kappa-1)(\delta_{\mu\rho}q_\nu - \delta_{\mu\nu}r_\rho)\big). \tag{2.55}$$

The interaction terms of $\mathcal{L}_B$ involve exactly one Lagrange multiplier field $L(s)$, cf. Eq. (2.15). According to Eqs. (2.46) and (2.48), it must be contracted with a flowed gluon field $B(t)$ at larger flow time $t > s$. Thus, the vertex in Eq. (2.55) contains exactly one outgoing flow line. On the other hand, each of the two flowed gluon fields $B(s)$ in the interaction terms of $\mathcal{L}_B$ can be contracted either with a Lagrange multiplier field $L(t')$ at *smaller* flow time $t' < s$, resulting in an ingoing flow line, or with another flowed gluon field $B(s')$. In this sense, the Feynman rule (2.55) actually represents three vertices, displayed in Fig. 2.1: They all contain one outgoing flow line, while each of the other two lines can either be an ingoing flow line or a flowed gluon propagator.[1] The dashed arrows in Eq. (2.55) indicate lines which can be both a flow line or a propagator, while the solid arrows always denote flow lines.

Similarly, the four-point gluon flow vertex is governed by X_3 [8]:

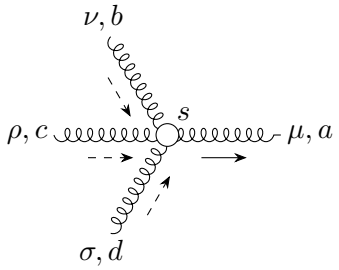

$$= -g_{\mathrm{B}}^2 \int_0^\infty \mathrm{d}s \, \big(f^{abe}f^{cde}(\delta_{\mu\rho}\delta_{\nu\sigma} - \delta_{\mu\sigma}\delta_{\nu\rho}) + f^{ace}f^{bde}(\delta_{\mu\nu}\delta_{\rho\sigma} - \delta_{\mu\sigma}\delta_{\nu\rho}) + f^{ade}f^{bce}(\delta_{\mu\nu}\delta_{\rho\sigma} - \delta_{\mu\rho}\delta_{\nu\sigma})\big). \tag{2.56}$$

Again, there is exactly one outgoing flow line, while the other three lines are either flowed gluons or incoming flow lines. This means that the Feynman rule (2.56) actually represents four different vertices.

1 The lines can also represent external "particles", of course.

Note that the factor $2T_R$, arising from the trace in Eq. (2.15), has been discarded in both vertices in accordance with the normalization of Eq. (2.48). Similarly, the factor of $1/g_B$ obtained from rescaling $B^a_\mu \to g_B B^a_\mu$ in Eq. (2.48) has been absorbed into the flow vertices.

Similar considerations applied to $\mathcal{L}_\chi$ lead to vertices involving flowed quark fields. For example, the quark flow vertex with one gluon is described by the Feynman rule [42]

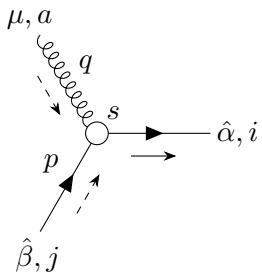

$$= \quad i g_B \, \delta_{\hat{\alpha}\hat{\beta}} T^a_{ij} \int_0^\infty ds \, (2p_\mu + (1-\kappa) q_\mu). \tag{2.57}$$

In this case, the fermion line with outgoing charge flow is also outgoing in the gradient flow, while the other two lines can be either flowed propagators, or ingoing flow lines. Thus, this Feynman rule actually represents four different vertices.

The complete list of Feynman rules can be found in Appendix B.

2.3.4 *Summary and further Remarks*

Let us summarize the main features of the Feynman rules for the gradient flow formalism and point out a few more details [8]:

1. Propagators and flow lines always carry an exponential factor $e^{\pm t p^2}$ for each vertex, where t is the flow time of the vertex.

2. Flow lines always start at a flow vertex. They end either at another flow vertex or an external operator. The θ-distribution $\theta(t-s)$ implies a flow-time direction, which we denote by an adjacent arrow in Feynman diagrams.

3. A flow vertex always has an outgoing flow line connected to it. The other lines are either incoming flow lines or flowed propagators. Each flow vertex is defined at a flow time s and implies an integration $\int_0^\infty ds$. The θ-distribution of the outgoing flow line restricts the integration to a finite upper limit t, i.e. $\int_0^t ds$.

4. Diagrams with closed flow-line loops vanish, because the integration interval shrinks to a point. Some of these diagrams are shown in Fig. 2.2. Hence, only diagrams whose flow lines form trees contribute to any observable.

2.4 OBSERVABLES AND RENORMALIZATION

With the Feynman rules derived, let us turn to actual calculations. Among the simplest quantities one can consider within the gradient flow formalism are *vacuum expectation*

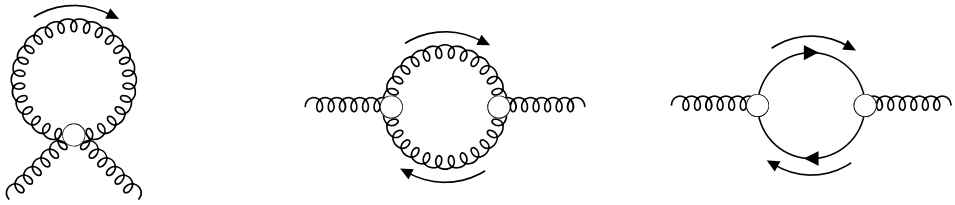

Figure 2.2: Diagrams with flow-line loops; they all vanish.

*value*s (VEVs) of gauge-invariant operators at finite flow time. It is one of the remarkable properties of the gradient flow formalism that these operators do not require any *ultra-violet* (UV) renormalization beyond that of regular QCD and that of the involved flowed fields [8]. This means that the operators do not mix under *renormalization group* (RG) running, which makes it particularly simple to combine results from different regularization schemes. Especially, one can easily match the results of lattice with perturbative calculations without having to compute the transformation between the lattice and the perturbative schemes. Hence, this feature opens promising prospects for a cross-fertilization of lattice and perturbative calculations, such as a possible lattice determination of $\alpha_s(M_Z)$, for example [21].

The renormalization of the coupling and the mass follows the usual prescription with the known QCD renormalization constants. Throughout this thesis, we employ the $\overline{\text{MS}}$ scheme. We refer to Appendix A.2 for the details.

The flowed gauge field $B^a_\mu(t,x)$ does not require renormalization [4, 8] so that for example matrix elements of the gluon action density,

$$E(t,x) \equiv \frac{1}{4} G^a_{\mu\nu}(t,x) G^a_{\mu\nu}(t,x), \tag{2.58}$$

are finite after just the renormalization of g and m_f. This allows for a direct comparison of results obtained in different regularization schemes.

On the contrary, flowed quark fields require a renormalization factor $Z_\chi^{1/2}(\alpha_s)$ in order to render Green's functions finite. In the $\overline{\text{MS}}$ scheme, it reads

$$Z_\chi^{-1}(\alpha_s) = 1 - \frac{\alpha_s}{4\pi}\frac{\gamma_{\chi,0}}{\epsilon} + \left(\frac{\alpha_s}{4\pi}\right)^2 \left[\frac{\gamma_{\chi,0}}{2\epsilon^2}\left(\gamma_{\chi,0} + \beta_0\right) - \frac{\gamma_{\chi,1}}{2\epsilon}\right] + \mathcal{O}(\alpha_s^3), \tag{2.59}$$

with

$$\begin{aligned} \gamma_{\chi,0} &= 3\,C_F, \\ \gamma_{\chi,1} &= \left(\frac{223}{6} - 8\ln 2\right) C_A C_F - \left(\frac{3}{2} + 8\ln 2\right) C_F^2 - \frac{22}{3} C_F T_R n_f. \end{aligned} \tag{2.60}$$

$\gamma_{\chi,0}$ has been computed in Ref. [7], whereas $\gamma_{\chi,1}$ has been obtained as part of this thesis by requiring that the NNLO calculations in Chapters 5 to 8 become finite. It has been first published in Ref. [43].

The scalar quark density

$$S(t,x) \equiv Z_\chi \sum_{f=1}^{n_\mathrm{f}} \bar{\chi}_f(t,x)\chi_f(t,x) \tag{2.61}$$

thus acquires an anomalous dimension, which prevents a direct comparison of results from different regularization schemes. Alternatively, one may work with *ringed quark fields* [11], which amounts to using

$$\mathring{Z}_\chi(t,\mu) = -\frac{2N_\mathrm{C}n_\mathrm{f}}{(4\pi t)^2} \cdot \frac{1}{\langle R(t)\rangle|_{m=0}} \tag{2.62}$$

instead of Z_χ in order to renormalize the quark fields, where

$$R(t,x) = \sum_{f=1}^{n_\mathrm{f}} \bar{\chi}_f(t,x) \overleftrightarrow{\mathcal{D}}^\mathrm{F} \chi_f(t,x) \tag{2.63}$$

is the quark kinetic operator with

$$\overleftrightarrow{\mathcal{D}}^\mathrm{F}_\mu = \mathcal{D}^\mathrm{F}_\mu - \overleftarrow{\mathcal{D}}^\mathrm{F}_\mu. \tag{2.64}$$

This corresponds to a "physical" renormalization scheme, which means that the anomalous dimension of the operator

$$\mathring{S}(t,x) = \zeta_\chi(t,\mu)\, S(t,x) \qquad \text{with} \qquad \zeta_\chi(t,\mu) \equiv Z_\chi^{-1}\mathring{Z}_\chi(t,\mu) \tag{2.65}$$

vanishes. In Eq. (2.62), we used the notation

$$\langle \mathcal{O}(t)\rangle \equiv \int \mathrm{d}^4x\, \langle \mathcal{O}(t,x)\rangle \tag{2.66}$$

for the zero-momentum Fourier transform of the VEV of an operator $\mathcal{O}(t,x)$, which we adopt in the following. As indicated, all quark masses are set to zero in Eq. (2.62). Of course, it immediately follows that

$$\langle \mathring{R}(t)\rangle\big|_{m=0} = -\frac{2N_\mathrm{C}n_\mathrm{f}}{(4\pi t)^2} \tag{2.67}$$

to all orders in perturbation theory.

The Feynman rules for the operators $E(t,x)$, $S(t,x)$, and $R(t,x)$ introduced above are obtained in the same manner as those described in Section 2.3. Expressing them in terms of the flowed fields $B(t,x)$ and $\chi_f(t,x)$, the operator $E(t,x)$ results in the bilinear gluon vertex

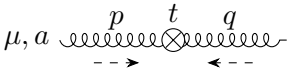

$$= \quad -g_\mathrm{B}^2\delta^{ab}\big(\delta_{\mu\nu}\, p\cdot q - p_\mu q_\nu\big), \tag{2.68}$$

the trilinear gluon vertex

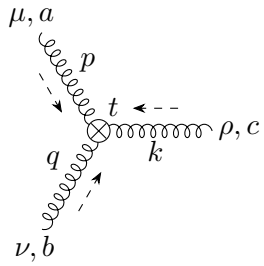

$$= \mathrm{i} g_{\mathrm{B}}^3 f^{abc} \big(\delta_{\mu\nu}(q-p)_\rho + \delta_{\nu\rho}(k-q)_\mu + \delta_{\mu\rho}(p-k)_\nu\big), \tag{2.69}$$

and the quartic gluon vertex

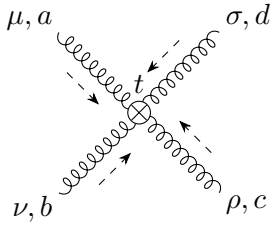

$$\begin{aligned} = \; & g_{\mathrm{B}}^4 \big(f^{abe} f^{cde} (\delta_{\mu\rho}\delta_{\nu\sigma} - \delta_{\mu\sigma}\delta_{\nu\rho}) \\ & + f^{ace} f^{bde} (\delta_{\mu\nu}\delta_{\rho\sigma} - \delta_{\mu\sigma}\delta_{\nu\rho}) \\ & + f^{ade} f^{bce} (\delta_{\mu\nu}\delta_{\rho\sigma} - \delta_{\mu\rho}\delta_{\nu\sigma}) \big), \end{aligned} \tag{2.70}$$

$S(t,x)$ corresponds to the single bilinear quark vertex

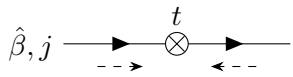

$$= \delta_{ij}\delta_{\hat{\alpha}\hat{\beta}}\,, \tag{2.71}$$

and $R(t,x)$ to the bilinear quark vertex

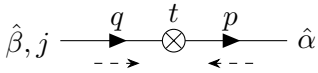

$$= \mathrm{i}\delta_{ij}(\not{p} - \not{q})_{\hat{\alpha}\hat{\beta}} \tag{2.72}$$

as well as the quark-gluon vertex

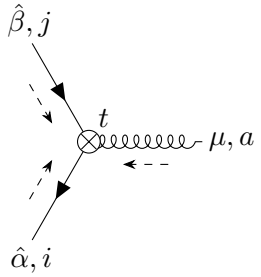

$$= -2 g_{\mathrm{B}} T^a_{ij} (\gamma_\mu)_{\hat{\alpha}\hat{\beta}}\,. \tag{2.73}$$

Similar to the flow vertices, the lines attached to these vertices are depicted with dashed arrows, indicating that they can be both flow lines and propagators. In contrast to the flow vertices, the flow time of all lines in these vertices is directed towards the corresponding operator. Therefore, these vertices set the largest flow time in the Feynman diagrams, which corresponds to the flow time the operator is defined at.[2]

2 If there are multiple operator insertions or external flow lines, this statement no longer holds, of course. Instead, these flow times are only larger than the flow times of all lines flowing towards them.

2.5 GRADIENT FLOW INTEGRALS

Similar to more common calculations in Quantum Field Theories, we end up with scalar Feynman integrals when the Feynman diagrams are translated to their mathematical expressions with the help of the Feynman rules.[3] A regular scalar L-loop Feynman integral in Euclidean space can be parametrized by

$$I(a_1, \ldots, a_N) = \int_{k_1,\ldots,k_L} \frac{1}{P_1^{a_1} \cdots P_N^{a_N}} \tag{2.74}$$

with the inverse propagators $P_j = q_j^2 + m_j^2$. The momenta q_j are linear combinations of the loop momenta k_i and external momenta p_n, where $n = 1, \ldots, E$ for $E+1$ external legs. Of course, there are no external momenta for vacuum integrals. The m_j are the propagator masses and the a_j are the integer propagator powers. To uniquely express every scalar product of momenta as a linear combination of the inverse propagators P_j, squared masses m_j^2, and external kinematical invariants, the set of P_j has to be complete and independent. Hence, the number of propagators is given by $N = \frac{L}{2}(L + 2E + 1)$ which includes auxiliary propagators that only appear in the numerator, i.e. with $a_j \leq 0$.

However, due to the exponential functions in the propagators and flow lines as well as the integrations introduced by the flow vertices, cf. Sections 2.3.1 to 2.3.3, this form is no longer sufficient for the gradient flow formalism. Instead, Eq. (2.74) generalizes to

$$\begin{aligned} &I(t_1^{\text{up}}, \ldots, t_F^{\text{up}}; T_1, \ldots, T_N; a_1, \ldots, a_N) \\ &\qquad = \left(\prod_{f=1}^{F} \int_0^{t_f^{\text{up}}} \mathrm{d}t_f \right) \int_{k_1,\ldots,k_L} \frac{\exp[-(T_1 q_1^2 + \cdots + T_N q_N^2)]}{P_1^{a_1} \cdots P_N^{a_N}}, \end{aligned} \tag{2.75}$$

where F is the number of flow-time integrations and the T_i are nonnegative linear combinations of the flow-time variables, e.g. $T_1 = t + t_1 - 2t_3$. Note that the integration variables t_f may appear as upper limit of a another integration, i.e. $t_{f'}^{\text{up}} = t_f$. Thus, the flow-time integrations are nested in general.

For all calculations in this thesis, we only compute matrix elements with a single operator insertion at flow time t. For the purpose of the integral reduction in Chapter 3, it is helpful to introduce dimensionless integration variables

$$u_f = \frac{t_f}{t_f^{\text{up}}} \tag{2.76}$$

such that the gradient flow integrals can be expressed as

$$\begin{aligned} &I(c_1, \ldots, c_F; T_1', \ldots, T_N'; a_1, \ldots, a_N) \\ &\qquad = t^F \left(\prod_{f=1}^{F} \int_0^1 \mathrm{d}u_f \, u_f^{c_f} \right) \int_{k_1,\ldots,k_L} \frac{\exp[-t(T_1' q_1^2 + \cdots + T_N' q_N^2)]}{P_1^{a_1} \cdots P_N^{a_N}}, \end{aligned} \tag{2.77}$$

3 For the calculation of the mixing matrix of the EMT operators in Chapter 6 we have to perform a tensor reduction first.

where the c_f are nonnegative integers and the T'_n are polynomials in u_f, e.g. $T'_1 = 1 + u_1 - 2u_1u_3$.

Throughout this thesis, all external momenta and masses are either directly set to zero or we perform an expansion. Thus, we only have to solve massless vacuum integrals. Since t is the only mass scale in the integral in this case, it can safely be set to one and its power can be restored by a dimensional analysis when needed.

Furthermore, all massless vacuum Feynman diagrams of a fixed loop order up to three loops belong to a single topology or one of its subtopologies. Hence, for each loop order all integrals can be expressed by the same choice of loop momenta and propagators, i.e. there is only one distinct set of P_j per order.

Note that Eq. (2.77) is more general than Eq. (2.75). For general c_f, the transformation from Eq. (2.77) back to Eq. (2.75) introduces factors of $t_f^{\tilde{c}_f}$ with nonzero powers $\tilde{c}_f$. However, all Feynman diagrams throughout this thesis only produce the "physical" integrals of Eq. (2.75). Thus, Eq. (2.77) defines additional auxiliary integrals which are required to perform the reduction to master integrals described in Chapter 3. These master integrals, potentially "non-physical", are then solved with the methods discussed in Chapter 4.

Each reduction strategy requires a systematic ordering of the integrals. Usually, integrals are assigned to so-called topologies based on their respective sets of propagators, i.e. their momenta and masses. Each topology then corresponds to a different number. As a measure of complexity it is useful to define the sum r of all positive powers and the negative sum of all non-positive powers s,

$$r \equiv \sum_{j=1}^{N} a_j \theta(a_j - \tfrac{1}{2}), \qquad s \equiv -\sum_{j=1}^{N} a_j \theta(\tfrac{1}{2} - a_j), \tag{2.78}$$

where $\theta(x)$ is the Heaviside step function. Usually, an integral with smaller numbers is considered simpler.

For the gradient flow integrals in Eq. (2.77), we have to introduce additional criteria. The most important one is the number of flow-time integrations and the corresponding exponential. Similar to the topology for regular Feynman integrals we assign an identification number to each combination, with smaller numbers for integrals with less flow-time integrations. Following Eq. (2.78), we also introduce the sum of all c_f

$$c \equiv \sum_{f=1}^{F} c_f. \tag{2.79}$$

For each integral we then compute an unique 64-bit identification number based on the numbers introduced above. Since there is only one topology, the most important aspects are the flow-time identification numbers followed by r and s. Thereafter, we assign numbers to the distributions of indices.

3

INTEGRAL REDUCTION

In this chapter, we describe how the integrals in Eq. (2.77) can be reduced to a smaller set of *master integrals* with the help of *integration-by-parts* (IBP) relations [32, 33] as well as similar relations for the flow-time integrations. Both types of relations are introduced in Section 3.1. In Section 3.2, we discuss strategies to actually perform the integral reduction. This mounts into a description of the Laporta algorithm [44] over finite fields in Section 3.3 and a discussion of algorithms to reconstruct rational functions from their images over finite fields. Finally, we briefly describe the reduction process for the gradient flow integrals encountered in this thesis in Section 3.4.

Section 3.1 is based on Ref. [41] and was worked out in my Master's thesis [45]. Sections 3.2 and 3.3 are based on Refs. [46–48]. My contributions to these publications are summarized in Section 3.3.

3.1 INTEGRATION-BY-PARTS RELATIONS FOR GRADIENT FLOW INTEGRALS

Since they were introduced in 1981 by Chetyrkin and Tkachov [32, 33], *integration-by-parts* (IBP) relations became a key ingredient of many precision calculations in high-energy physics. They are based on the fact that Feynman integrals vanish in dimensional regularization if a derivative w.r.t. one of the loop momenta is inserted, i.e.

$$\int_{k_1,\dots,k_L} \frac{\partial}{\partial k_i^\mu} \left(q_j^\mu \frac{1}{P_1^{a_1} \dots P_N^{a_N}} \right) = 0, \tag{3.1}$$

where q_j is an arbitrary momentum. On the other hand, the derivative can be calculated explicitly, which leads to a linear relation between Feynman integrals with different powers a_i of the propagators. Different combinations of $\frac{\partial}{\partial k_i^\mu} q_j^\mu$ lead to different linear relations in general.

Equivalent relations can be found with the help of *Lorentz-invariance* identities, which are obtained by taking antisymmetric derivatives w.r.t. external momenta [49]. Although they are not linearly independent of the IBP relations [50], they usually speed up the reduction process. Since there are no external momenta in our gradient flow integrals in Eq. (2.77), we cannot exploit the Lorentz-invariance identities.

On the other hand, the IBP relations can be trivially generalized to the gradient flow integrals, which leads to additional terms by taking the derivative of the exponentials.

Without external momenta, we can only insert all possible combinations of $\frac{\partial}{\partial k_i^\mu} k_j^\mu$ into the integrals. This results in the general relation [45]

$$\begin{aligned} 0 &= \delta_{ij} D \cdot I(c_1, \dots, c_F; T_1', \dots, T_N'; a_1, \dots, a_N) \\ &\quad - t^F \left(\prod_{f=1}^{F} \int_0^1 \mathrm{d}u_f \, u_f^{c_f} \right) \int_{k_1,\dots,k_L} \frac{\exp[-t(T_1' q_1^2 + \dots + T_N' q_N^2)]}{P_1^{a_1} \cdots P_N^{a_N}} \sum_{n=1}^{N} \left[\left(\frac{a_n}{P_n} + t T_n' \right) k_j^\mu \frac{\partial q_n^2}{\partial k_i^\mu} \right]. \end{aligned} \tag{3.2}$$

The emerging scalar products of the form $k_i \cdot k_j$ can be absorbed by the propagators P_n by completing the square, effectively reducing the power of the corresponding propagator by one. Then, the sum consists of integrals where the indices a_n and c_f are shifted by ± 1. Obviously, IBP relations neither alter the number of flow-time integrations nor the exponential functions.

We may apply an analogous strategy for the flow-time parameters though. Inserting a derivative w.r.t. one of the flow-time integration variables, one arrives at the sum of two integrals with fewer flow-time integrations and altered exponentials,

$$\int_0^{t_f^{\mathrm{up}}} \mathrm{d}t_f \frac{\partial}{\partial t_f} f(t_f, \dots) = f(t_f^{\mathrm{up}}, \dots) - f(0, \dots). \tag{3.3}$$

On the other hand, explicit evaluation of the derivative at the integrand level either reduces one of the indices c_f or one of the indices a_n by one. When taking the derivative w.r.t. $u_{f'}$, the general relation reads [45]

$$\begin{aligned} 0 &= t \cdot I(c_1, \dots, c_{f'-1}, c_{f'+1}, \dots c_F; T_1', \dots, T_N'; a_1, \dots, a_N)\big|_{u_{f'}=1} \\ &\quad - t \cdot I(c_1, \dots, c_{f'-1}, c_{f'+1}, \dots c_F; T_1', \dots, T_N'; a_1, \dots, a_N)\big|_{u_{f'}=0} \\ &\quad - c_{f'} \cdot I(c_1, \dots, c_{f'} - 1, \dots c_F; T_1', \dots, T_N'; a_1, \dots, a_N) \\ &\quad + t^{F+1} \left(\prod_{f=1}^{F} \int_0^1 \mathrm{d}u_f \, u_f^{c_f} \right) \int_{k_1,\dots,k_L} \frac{\exp[-t(T_1' q_1^2 + \dots + T_N' q_N^2)]}{P_1^{a_1} \cdots P_N^{a_N}} \sum_{j=n}^{N} \frac{\partial T_n'}{\partial u_{f'}} q_n^2. \end{aligned} \tag{3.4}$$

One therefore arrives at linear relations among integrals with a different number of flow-time integrations F and different exponentials.

In addition to the relations described above, we also employ symmetry relations, which are obtained by shifting or renaming loop momenta, or by renaming flow-time variables. Since they are simple one-to-one relations, we exploit them as much as possible to reduce the set of distinct integrals before performing the reduction described in the next sections.

3.2 REDUCTION STRATEGIES

All of the relations introduced in the previous section can be expressed as linear equations of the form

$$0 = \sum_i C_i I_i, \tag{3.5}$$

which we collectively call IBP relations in the following. The different integrals are denoted as I_i, indicating that at least one of the indices a_n, c_f, the number of flow-time integrations, or the exponential is different from all other integrals in the equation. The coefficients C_i are rational functions with small degrees in D, the masses m_n, kinematical invariants of the external momenta p_n, and the flow time t of the operator insertion. Of course, they also depend on the a_n and c_f. Since the linear IBP equations are homogeneous, one can only express the integrals by a smaller set of *master integrals*, which have to be solved by other means. This procedure is called *integral reduction*. For the standard Feynman integrals of Eq. (2.74) it was proven that the number of master integrals is finite [51]. Of course, the choice of the basis of master integrals is not unique and depends on the ordering criterium of the integrals, cf. Section 2.5. The obvious choice is of course a basis with master integrals that are the easiest to evaluate.

Currently, there exist two different reduction strategies in the literature. The first tries to combine the IBP relations to recursion relations which express an integral through easier integrals. Recursively applying these relations then reduces all integrals to the master integrals. At the three-loop level, this approach has been successfully applied to massless propagator type diagrams [33, 52, 53], massive tadpoles [54, 55], and on-shell propagators [56–58]. At the four-loop level, it has been successfully applied to massless propagator type diagrams [59]. However, the recursion relations usually have to be derived manually which makes this procedure unfeasible for multi-loop calculations with other topologies. In Refs. [60, 61], Lee published an algorithm and the program `LiteRed` for the automated construction of recursion formulas. Although elegant, both the construction and application of the formulas tend to become too slow for state-of-the-art reductions.

In Ref. [62], it was attempted to construct an algorithm based on recursion formulas for the massless vacuum gradient flow integrals given by Eq. (2.77). While succeeding for two-loop vacuum integrals, it suffers from the fact that most of the different exponentials require a special treatment. This makes it unfeasible, especially at the three-loop level, where only two cases without flow-time integrations have been worked out.

Instead, we employ the second strategy called *Laporta algorithm* [44]. By inserting integer values for the a_n into Eq. (3.5), one obtains a system of equations for the integrals. These *seeds* are usually restricted by the requirements $r \leq r_{\max}$ and $s \leq s_{\max}$, with r and s defined in Eq. (2.78) and $r_{\max}$, and $s_{\max}$ chosen large enough to cover all relevant integrals in the reduction process, but usually no larger. Again, this can be easily generalized to the gradient flow by inserting different values for c_f, while demanding $c \leq c_{\max}$, cf. Eq. (2.79). This system of equations can then systematically be solved with a Gauss-type elimination algorithm. The Laporta algorithm has been implemented in the public codes `AIR` [63], `FIRE` [64–67], `Reduze` [68, 69], and `Kira` [70]. Since none of these programs natively supports gradient flow integrals, we generate the system with a separate `Mathematica` [71] code developed in Ref. [45] and then solve this system with `Kira` employing the feature to reduce user-defined systems.

However, integral reductions with the Laporta algorithm for state-of-the-art problems are usually very expensive in terms of both CPU time and main memory usage. This is due to the huge number of equations in the system to solve, the growth of intermediate

expressions while solving the system, and the size of the rational functions that appear as coefficients of master integrals. In particular, the coefficients of intermediate results are typically more complicated than those appearing in the final result. Simplifying those coefficients by algebraic means, e.g. with `Fermat` [72], is very time consuming and memory intensive. This can even be illustrated with the univariate three-loop reductions of gradient flow integrals: For one reduction performed for this thesis, monomials with at least degree 508 in D appeared at intermediate steps, even though the final result only had a maximum degree of 34.[1] None of the public implementations of the Laporta algorithm available was able to complete the desired reductions so that we had to resort to the rather new techniques over finite fields discussed in the next section.

3.3 THE LAPORTA ALGORITHM OVER FINITE FIELDS

The problems of the Laporta algorithm can be mitigated by solving the system over finite fields [34]. In practice, one uses prime fields $\mathbb{Z}_p$ with characteristic p, where p is the defining prime. Importantly, the multiplicative inverse is uniquely defined in $\mathbb{Z}_p$ and can be computed with the extended Euclidean algorithm [73]. Due to the 64-bit architecture of modern CPUs, p is usually chosen to be a large 63-bit prime so that the sum of two elements of $\mathbb{Z}_p$ still fits into 64 bits. One can then replace all variables in the system by integers in $\mathbb{Z}_p$ and perform all operations modulo p. This way, all coefficients are mapped to 64-bit integers, independent of the size of the original rational functions. On one hand this reduces the memory needed for the coefficients, and on the other hand, arithmetic operations on $\mathbb{Z}_p$ are performed in constant time, independent of the size of the original coefficients, utilizing the CPU's native integer operations.

These methods can be used to eliminate linearly dependent equations from the system [35]. This reduces the size of the system which has to be solved algebraically and already leads to significant performance improvements. Furthermore, if a list of integrals is provided that should be reduced, the information gathered in this step can be used to select only those equations which are needed to reduce the integrals from this list. In `Kira`, this procedure is implemented in the software component `pyRed` [70]. Once the selection of the equations is done, the system is solved analytically, employing algebraic simplifications of the rational functions.

However, it is also possible to avoid the algebraic solution altogether and reconstruct the analytic result from the solutions over finite fields by combining *interpolation algorithms over finite fields*, the *Chinese remainder theorem* (CRT), and *rational reconstruction* (RR) *algorithms* as it is done for the computation of greatest common divisors of polynomials, see e.g. Refs. [74–76]. In the context of IBP reductions this has been suggested in Refs. [34, 36] and further worked out in Ref. [37], albeit the latter reference focuses on the related strategy of integrand reduction via generalized unitarity.

Since the IBP relations are linear, the solution strategies only involve the addition, subtraction, multiplication, and division of rational functions. Therefore, the coefficients

1 We know this because we had to change the `Fermat` [72] settings to support higher degrees when attempting the reduction with `Kira 1.1`.

of the master integrals are also rational functions. Efficient algorithms for the interpolation of polynomials and rational functions from their images in a finite field have been studied in computer science for several decades, see e.g. Refs. [76–83]. The variables of the rational function are replaced by elements of the finite field and the function is evaluated at this point, i.e. for each tuple of values for the variables one obtains the image of the rational function at this point. These evaluations are called *probes*. The rational function is then interpolated by processing a sufficient number of probes so that one obtains the rational function over the chosen prime field. Note that all coefficients in the numerator and denominator polynomials are, of course, mapped to the finite field.

The rational function with rational numbers in $\mathbb{Q}$ as coefficients can be reconstructed with the help of RR algorithms [84, 85]. Based on the image of the rational number in $\mathbb{Z}_p$ and the prime number p of the field, these algorithms can "guess" the rational number in $\mathbb{Q}$. They only succeed if both numerator and denominator of the rational number are significantly smaller than p. However, this guess is unique if they succeed. The limit on the size can be circumvented by combining the images over several prime fields with the help of the CRT [73]. It combines the images of a rational number over two coprime numbers to a new image over the product of both coprimes. Thus, the upper limit in the RR is increased.

It is important to note that most of the mentioned algorithms are probabilistic, i.e. there is a chance that they fail or provide a wrong result. Most of the failures are triggered by hitting accidental zeros with a probability based on the DeMillo-Lipton-Schwartz–Zippel lemma [77, 86, 87]. The probability of obtaining a wrong result can be reduced by performing additional checks after the termination of the algorithms.

The general strategy over finite fields applied to the Laporta algorithm can be summarized as follows.[2] The system of equations is repeatedly solved over a prime field. Each solution results in a probe for each master integral coefficient. These are then handed to a rational function interpolation algorithm. This procedure is repeated until all rational functions have been interpolated over the prime field. Their coefficients are then passed to a RR algorithm to obtain the rational functions with coefficients in $\mathbb{Q}$. If the RR did not succeed, the same process is repeated over additional distinct prime fields, and the results are combined with the help of the CRT until the RR succeeds.

While the algebraic simplification of rational functions can be performed in parallel to some degree, limited by their interdependencies, the evaluations of probes in a finite field are completely independent, opening the possibility for massive parallelization on many CPU cores and even nodes of a computer cluster.

`FIRE6` was the first public program implementing this strategy [67]. However, it is currently limited to problems with D and two scales, of which one has to be set to one. It uses a factorization strategy which still has to be generalized to more scales. Very recently, the framework Caravel was published, which provides algorithms to calculate multi-loop scattering amplitudes based on generalized unitarity and the techniques outlined in this section [88].

2 Of course, it can be applied to many other problems as well.

As part of this thesis, we codeveloped the public open-source C++ library FireFly [46, 47] which implements the interpolation and RR algorithms. To our knowledge, it was the first open-source library for these tasks. Shortly after, the similar library FiniteFlow was published [89], which in addition provides many building blocks to assemble physical calculations. FireFly allowed us to implement the reduction strategy described above into version 2.0 of the public program Kira [48] as follows: FireFly requests pyRed to solve the system of equations repeatedly over the finite fields for different tuples of values of the variables and then processes the resulting probes until the master integral coefficients are successfully reconstructed over $\mathbb{Q}$. The input system is the same system as for the algebraic reduction. Particularly, it is already trimmed of the linearly dependent equations and of the equations which are not relevant for the selected integrals. Exactly as in the algebraic reduction, the system is trimmed again after the forward elimination, i.e. the equations which are no longer relevant are dropped. However, in contrast to the algebraic reduction, we only select the relevant master integral coefficients after the back substitution. Hence, the interpolation of irrelevant (but potentially difficult) rational functions is avoided. This selection does not offer any advantage in the algebraic reduction because all intermediate coefficients need to be known in order to calculate the final result.

In Kira, the forward elimination is usually the dominant part of a reduction over a finite field, whereas in the algebraic solution it is usually the other way round. Hence, we implemented a second strategy which first performs the forward elimination using algebraic simplifications for the coefficients, and then performs the back substitution over the finite field, reconstructing the result with FireFly.

In Section 3.3.1, we describe the interpolation of rational functions in more detail and emphasize the new ideas published in Refs. [46, 47]. Similarly, we proceed for the RR in Section 3.3.2. We also discuss the role of polynomial factors in Section 3.3.3 and some performance critical technical features like parallelization and overhead reduction in Section 3.3.4. In Section 3.3.5, we present selected benchmarks to quantify the performance improvements. For more details and benchmarks we refer to Refs. [46–48].

Most of the algorithms in FireFly [46, 47] were implemented by Jonas Klappert, who also developed some parts of the overhead reduction and of the user interface, most notably the executable ff_insert, which can be used to perform replacements in mathematical expressions with the help of FireFly. Sven Yannick Klein implemented the Ben-Or/Tiwari algorithm [78] as well as the polynomial racing algorithm of Refs. [81, 82] in the course of his Bachelor's thesis [90]. I implemented a few algorithms and some parts of the user interface as well as most of the interface to Kira. Most of the parallelization as well as its interplay with the overhead reduction has been developed by me.

In Kira 2.0 [48] most of the interface to FireFly was implemented by me. Beyond the standard options, this includes the features specifically designed for the combination with FireFly. Jonas Klappert also developed some parts of the interface to FireFly. In addition, I participated in improving the reduction of user-defined systems, which we then applied to the reductions of the gradient flow integrals for this thesis. Philipp

Maierhöfer and Johann Usovitsch implemented most of the other new features not directly related to `FireFly`.

3.3.1 *Interpolation of Rational Functions*

In this section we explain the basic ideas behind the interpolation of rational functions just from their evaluations, the probes. This problem class is known as *black-box* interpolation problem in computer science. Additionally, we outline the new ideas of the algorithms implemented in `FireFly` [46, 47].

To fix the notation, we start by defining multivariate polynomials as follows. Given a set of n variables $\vec{z} = (z_1, \ldots, z_n)$ and an n-dimensional multi-index $\alpha = (\alpha[1], \ldots, \alpha[n])$ containing integers $\alpha[i] \geq 0$, we define a monomial $\vec{z}^{\,\alpha}$ as

$$\vec{z}^{\,\alpha} \equiv \prod_{i=1}^{n} z_i^{\alpha[i]} \tag{3.6}$$

with a degree

$$d = \sum_{i=1}^{n} \alpha[i]. \tag{3.7}$$

A polynomial f, which is an element of the polynomial ring $\mathbb{Z}_p[\vec{z}]$ in the variables $\vec{z}$, is defined as

$$f(\vec{z}) = \sum_{j=1}^{T} c_{\alpha_j} \vec{z}^{\,\alpha_j}, \tag{3.8}$$

where T is the number of non-zero terms. The total degree D is defined as the maximum of all individual d of the monomials. The coefficients c_{α_j} are elements of $\mathbb{Z}_p$ corresponding to different multi-indices α_j.

Rational functions can be constructed by combining two polynomials. Given two polynomials $P, Q \in \mathbb{Z}_p[\vec{z}]$, we define a rational function $f \in \mathbb{Z}_p(\vec{z})$, where $\mathbb{Z}_p(\vec{z})$ is the field of rational functions in the variables $\vec{z}$, as the ratio of P and Q:

$$f(\vec{z}) = \frac{P(\vec{z})}{Q(\vec{z})} = \frac{\sum_{i=1}^{T_\mathrm{n}} n_{\alpha_i} \vec{z}^{\,\alpha_i}}{\sum_{j=1}^{T_\mathrm{d}} d_{\beta_j} \vec{z}^{\,\beta_j}}. \tag{3.9}$$

In order to provide a unique representation, we define the lowest degree coefficient in the denominator to be equal to one. If several monomials contribute to the lowest degree d_min, we choose to define that coefficient of the monomial $\vec{z}^{\,\alpha}$ to be equal to one whose multi-index α is the smallest in a colexicographical ordering, e.g.

$$(1,1,0) < (1,0,1) < (0,1,1), \tag{3.10}$$

for $d = 2$ with three variables.

In the univariate case, a rational function can be expressed as a continued fraction through Thiele's formula [91]

$$\tau(t) = b_0 + (t - t_1) \left(b_1 + (t - t_2) \left(b_2 + (t - t_3) \left(\cdots + \frac{t - t_N}{b_N} \right)^{-1} \right)^{-1} \right)^{-1}, \tag{3.11}$$

with $t_1, \ldots, t_{N+1}$ being distinct elements of $\mathbb{Z}_p$. The coefficients $b_0 \ldots, b_N$ can be obtained recursively from the probes of the rational function $f(t)$ at $t_1, \ldots, t_{N+1}$,

$$b_i \equiv b_{i,i}, \qquad b_{i,j} = \frac{t_{i+1} - t_j}{b_{i,j-1} - b_{j-1}}, \qquad b_{i,0} = f(t_{i+1}). \tag{3.12}$$

With each probe $f(t_i)$ the interpolated function $\tau(t)$ describes the full function $f(t)$ better and better. If one finds agreement between $f(t_i)$ and $\tau(t_i)$, the interpolation can be terminated since the full functional dependence is known with high probability. Thiele's interpolation formula can be extended to the multivariate case, but it scales abysmal with the number of variables.

Another univariate interpolation strategy is based on the extended Euclidean algorithm [73].

At this point, it is useful to introduce the notions of *dense* and *sparse*: A polynomial of n variables and a total degree D can have up to $\binom{n+D}{D}$ terms. We call a polynomial, or a rational function, *sparse* if most of the monomial coefficients c_{α_j} vanish, and *dense* otherwise. Extending this notion to the interpolation algorithms, we call an algorithm which performs well for dense functions dense and one which performs well for sparse functions sparse. In this sense, the univariate interpolation with Thiele's formula is a dense algorithm because it requires $2D$ or $2D + 1$ probes, depending on whether the maximum degree term is in the numerator or denominator, plus additional probes to check for termination, while the actual number of terms T does not affect the scaling.

Our algorithm for the interpolation of multivariate rational functions implemented in `FireFly` is based on the sparse algorithm of Cuyt and Lee [83]. There are other algorithms, both dense and sparse, in the literature, see e.g. [76, 92–97], but we found that the algorithm of Cuyt and Lee performs best in our applications.

The idea of the algorithm of Cuyt and Lee is to perform the multivariate rational function interpolation with a univariate rational function interpolation and embedded multivariate polynomial interpolations. First, one introduces a *homogenization* variable t and defines the auxiliary function [98]

$$\tilde{f}(t\vec{z}) = f(tz_1, \ldots, tz_n). \tag{3.13}$$

$\tilde{f}$ can be interpreted as univariate rational function in the variable t, whose coefficients are multivariate polynomials in $\vec{z}$. By interpolating $\tilde{f}$ univariately in t at different values for $\vec{z}$, one thus obtains probes which can be used for multivariate polynomial interpolations of the polynomial coefficients. As optimization, one can set $z_1 = 1$ and reconstruct its power by homogenizing w.r.t. the corresponding power of t, after the dependence of all other variables has been successfully interpolated. However, the algorithm requires a constant term in either numerator or denominator to fix the normalization of the rational function. By introducing a variable shift $\vec{s} = (s_1, \ldots, s_n)$, one can ensure that

$$\tilde{f}(t\vec{z}) \to \hat{f}(t, \vec{z}, \vec{s}) \equiv \tilde{f}(t\vec{z} + \vec{s}) = \tilde{f}(t + s_1, tz_2 + s_2, \ldots, tz_n + s_n) \tag{3.14}$$

has a constant term. However, the shift introduces many additional terms so that $\hat{f}$ is usually much denser than $\tilde{f}$. The maximum degree terms in t are not affected by the shift

though and retain their sparsity. Thus, one first interpolates these polynomials and stores the probes for all lower degree polynomial coefficients for later use. After termination of these interpolations, one knows how these terms affect the lower degree terms through the shift. By subtracting the shift-induced terms, the next-to-highest degree terms are no longer affected by the shift and can be interpolated sparsely, preferably by using the probes already stored while interpolating the higher degree terms and only computing new probes if those are not sufficient. By repeating this procedure from the highest to the lowest degrees, the whole rational function can be interpolated without interpolating the artificial terms introduced by the shift.

We identified three areas to improve this algorithm: First, removing the shift requires to subtract the additional terms for every probe, which becomes very expensive for many variables or high degrees. Secondly, the univariate interpolation with Thiele's formula (3.11) is dense and does not take into account that most of the terms will be known at intermediate stages of the interpolation. Thirdly, the lower degree terms can be interpolated with very few probes even if they are completely dense. This is especially relevant for dense rational functions, where this sparse algorithm requires much more probes than a dense algorithm because the high degree terms are interpolated first.

To address the first point, we perform a scan before the actual interpolation. By checking different shift configurations, we can choose the one which shifts the minimum amount of variables while still generating a constant term. The number of probes required for this scan is negligible compared to the number of probes for most multivariate interpolations, but it avoids some expensive subtraction steps and saves some probes, especially in physical applications. It also works well together with our second and third suggestion.

Secondly, we only perform the interpolation with Thiele's formula once. Afterwards, we know all the nonvanishing polynomial coefficients of the rational function with high probability. This allows us to construct equations of the form

$$\sum_i n_{\mathrm{u},i}(\vec{z},\vec{s})t^i - \hat{f}(t,\vec{z},\vec{s})\sum_j d_{\mathrm{u},j}(\vec{z},\vec{s})t^j = \hat{f}(t,\vec{z},\vec{s})\sum_j d_{\mathrm{s},j}(\vec{z},\vec{s})t^j - \sum_i n_{\mathrm{s},i}(\vec{z},\vec{s})t^i, \qquad (3.15)$$

where the subscripts s and u denote the solved and unsolved coefficients, respectively. In this notation the normalizing coefficient is included in the solved subset. Each of the solved coefficients can be computed by evaluating the corresponding multivariate polynomial. Instead of interpolating the function with Thiele's formula, we can thus construct and solve a system of equations which requires less probes, because we can *prune* the system, i.e. remove all known coefficients. This is inspired by the *temporary pruning* idea of Refs. [81, 82].

Thirdly, instead of only interpolating the highest degree unsolved terms sparsely, we additionally interpolate all lower degree terms densely. Due to their small degrees, the low degree terms can be interpolated with few probes, which allows us to prune the system earlier. If for some degree the dense interpolation is still running while all higher degree terms have been interpolated, we abort the dense interpolation and restart it sparsely while reusing the probes. The effect of the shift on the terms interpolated densely is subtracted after the interpolation of the whole rational function terminated.

Based on the third idea, we call our algorithm *hybrid racer*, because it races a dense against a sparse interpolation. It is applicable for both dense and sparse rational functions and avoids the oversampling of the algorithm of Cuyt and Lee for dense functions, while still maintaining a good performance for sparse functions. The hybrid racer is described in Ref. [47] in detail, while the other two improvements are described in Ref. [46]. This includes examples as well as benchmarks.

Let us briefly mention the polynomial interpolation algorithm implemented in `FireFly`. We employ the multivariate Zippel algorithm [77, 80] which interpolates one variable after the other. Each univariate interpolation is performed with the racing algorithm of Refs. [81, 82] which races the dense Newton algorithm [91] against the sparse Ben-Or/Tiwari algorithm [78]. We describe our implementation of the Zippel algorithm in Ref. [46] and the racing algorithm in Ref. [47].

All of the mentioned algorithms have a probability of failing. Usually, this probability can be related to the DeMillo-Lipton-Schwartz–Zippel lemma [77, 86, 87]. It states that the probability that a polynomial f of total degree D over a field $\mathbb{F}$ evaluates to zero when selecting $\vec{y}$ independently and uniformly randomly from a subset S of $\mathbb{F}$ is bounded by[3]

$$\Pr[f(\vec{y}) = 0] \leq \frac{D}{|S|}. \tag{3.16}$$

For example, while recursively constructing the rational function with Thiele's formula, one can hit a zero in the denominator of Eq. (3.12) which leads to the failure of the algorithm. Similarly, Zippel proved that his algorithm fails at the interpolation of a polynomial with n variables, total degree D, and T non-zero terms over $\mathbb{Z}_p$ with a probability less than

$$\frac{nD^2T^2}{p} \tag{3.17}$$

if the variables are chosen uniformly randomly from $\mathbb{Z}_p$ [80].[4] The probability of the univariate Newton algorithm yielding a wrong result after interpolating a polynomial with total degree D over a field $\mathbb{F}$ and checking its termination criterium $\eta > 0$ times with uniformly randomly chosen points from a subset S of $\mathbb{F}$ is less than [81, 82]

$$\eta D \left(\frac{D}{|S|}\right)^{\eta}. \tag{3.18}$$

Lastly, the probability of the Ben-Or/Tiwari algorithm terminating wrongly is less than

$$\frac{T(T+1)(2T+1)D}{6|S|} \tag{3.19}$$

for a polynomial with total degree D and T nonzero terms over a field $\mathbb{F}$ when selecting the interpolation points uniformly randomly from a subset S of $\mathbb{F}$ [81, 82]. All of these probabilities are inversely proportional to the characteristic prime number of the prime

3 The bound when selecting of the entirety of a finite field was already proved by Ore in 1922 [99].

4 Actually, the *anchor points* have to be chosen uniformly randomly from $\mathbb{Z}_p$. We did not introduce this term in this thesis because it is only relevant for some of the polynomial subalgorithms.

fields $\mathbb{Z}_p$ used in `FireFly`. Since we use large 63-bit prime numbers, these probabilities are small enough that they should not concern us at the moment. Nonetheless, one should keep in mind that the algorithms are probabilistic.

3.3.2 *Rational Reconstruction*

With the algorithms discussed in the previous section, one obtains the image of the rational function in $\mathbb{Z}_p(\vec{z})$, i.e. all monomial coefficients are integers in $\mathbb{Z}_p$. While there is no inversion from $\mathbb{Z}_p(\vec{z})$ to the field of rational functions over rational numbers $\mathbb{Q}(\vec{z})$, one can employ *rational reconstruction* (RR) algorithms. They are based on the extended Euclidean algorithm [73] and the first algorithm was published by Wang in 1981 [84].

His algorithm leads to a guess for a rational number $a = n/d$ from its image

$$e = a \bmod m, \tag{3.20}$$

where n, d, and $m > e \geq 0$ are integers. If $|n|, |d| \leq \sqrt{m/2}$, it succeeds and yields a unique a as was proven in Ref. [100]. However, a still might not be the correct rational number in $\mathbb{Q}$, because the unique guess may differ for different moduli m. Moreover, the bound of $\sqrt{m/2}$ leads to failures of Wang's algorithm for large n and d if m is restricted to machine-size integers.

Both problems can be solved with the help of the *Chinese remainder theorem* (CRT) [73]: The theorem states that for pairwise coprime moduli $m_1, \ldots, m_k$ and integers $e_1, \ldots, e_k$ fulfilling $0 \leq e_i < m_i$ one can find exactly one integer x such that $0 \leq x < M \equiv m_1 \cdot m_2 \cdots m_k$ and

$$\begin{aligned} e_1 &= x \bmod m_1, \\ &\vdots \\ e_k &= x \bmod m_k. \end{aligned} \tag{3.21}$$

Thus, if the RR fails, one can interpolate the rational function over different prime fields $\mathbb{Z}_{p_i}$ and apply the CRT to the images of the coefficients to obtain new unique images $x = a \bmod p_1 \cdot p_2 \cdots$. Repeating this several times, one effectively increases the modulus which in turn increases the bound of the RR. If the RR succeeds with the same rational number a for two consecutive prime fields, we consider the guess as correct. This procedure is applied to all monomial coefficients of the rational function until we obtained probably correct guesses for all of them. Afterwards, we check if the resulting rational function coincides with the probes over another prime field. If this check succeeds as well, we finally terminate the whole procedure and return the rational function in $\mathbb{Q}(\vec{z})$.

Wang's RR algorithm is not optimal for arbitrary n and d because it only succeeds if both $|n|$ and $|d|$ are smaller than $\sqrt{m/2}$. In the worst case they differ by many orders in magnitude and only one of them fails the bound. In Ref. [85] it was observed that the guess of the rational number comes together with a huge quotient in the Euclidean algorithm. Based on this observation, a modified version of Wang's algorithm called

maximal quotient rational reconstruction was proposed. It can only be proven that it returns a unique solution if $|n||d| \leq \sqrt{m}/3$. However, it performs much better in the average case because large quotients from random input are rare.

Instead of deciding on one of the algorithms, we race both against each other to reap the advantages of both. Hence, we run both algorithms and consider a guess a as correct if either of the two algorithms reconstructs the same number in two consecutive prime fields. More details of our implementation in `FireFly` can be found in Ref. [46].

3.3.3 *Factors*

The rational functions appearing in physical calculations usually include polynomial factors. Once these factors are found, they lead to simpler results and can be divided out to reduce the number of probes required for the interpolations. Recently, algorithms and tools have been published that make it possible to determine the denominators of all coefficients in the result of an IBP reduction without performing the full reduction [101, 102]. Our improvements in this direction are twofold.

On the one hand, we implemented a feature into `Kira` which allows the user to provide factors of the master integral coefficients, for example obtained by the tools mentioned above. During the interpolation with `FireFly`, the results of the reductions over finite fields are divided by these factors so that only simpler functions have to be interpolated. In the optimal case, this not only reduces the number of terms but also removes all denominators so that no shift is required. In the final result, all factors are restored. This feature is described in Ref. [48] in detail.

On the other hand, we proposed a general algorithm to search for univariate factors in Ref. [47]. For each variable, it performs a univariate interpolation while setting all other variables to fixed random values. The resulting univariate rational function is then factorized. By performing another univariate interpolation and factorization with different random values for the other variables in the same prime field, one can identify univariate polynomial factors. These steps are then repeated over additional prime fields until all monomial coefficients are reconstructed over $\mathbb{Q}$ as described in Section 3.3.2. We implemented this algorithm into `FireFly` and divide out the detected factors to simplify the interpolation. Of course, they are restored in the final result. We refer to Ref. [47] for a detailed discussion as well as some benchmarks.

3.3.4 *Parallelization and Overhead Reduction*

`FireFly` offers the `Reconstructor` class as an interface between the user and the lower-level algorithms. The user just has to provide an implementation of the black-box functions which shall be interpolated. The `Reconstructor` class then handles the whole interpolation process. It offers a parallelization based on the thread-pool pattern, i.e. most computational tasks are queued and the threads of the thread pool work their way through the queue. This ensures that the threads are occupied as long as there are

enough tasks. The two main classes of tasks are the evaluation of the probes and the interpolations. In most cases, the former require almost all of the computation time.

We thus implemented an additional parallelization with `MPI` [103] to utilize several nodes on a computer cluster. While the main node handles the whole interpolation procedure, the evaluation of the probes can be distributed to the additional worker nodes. While `MPI` support was originally implemented into `FireFly`, we also extended it to `Kira`.

Another possibility to speed up the evaluation of the probes is to perform the individual computational operations on vectors instead of scalars inspired by the vectorization of modern CPUs. For example, instead of solving a system of equations multiple times for different input values, one can combine the input values to an array and only solve it once by performing each operation on the entries of the array. This reduces the overhead of the calculation for some problems, most notably when solving systems of equations. However, one pays with an increased memory footprint. `FireFly` allows the user to set the maximum size of these arrays, called *bunches*, and the `Reconstructor` then dynamically handles the size depending on the current workload. We favor parallelism over overhead reduction.

Both features are described in Refs. [47, 48] with more details as well as benchmarks.

3.3.5 *Selected Benchmarks*

In this section we briefly present some selected benchmarks to quantify the performance improvements gained through the combination of `Kira` and `FireFly`.

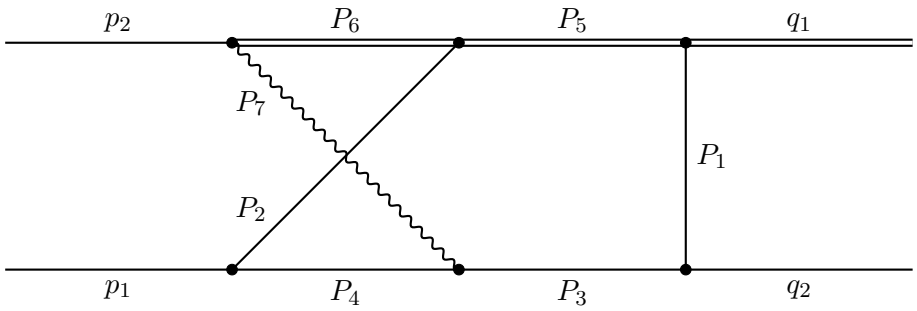

Figure 3.1: A non-planar double box which occurs, e.g., in virtual corrections to single top production at NNLO. Both the double line and the wiggly line represent massive lines with masses m_1 and m_2, respectively, cf. Eqs. (3.22) and (3.23).

The first benchmark is the reduction of the two-loop double-box topology shown in Fig. 3.1 with the propagators

$$\begin{aligned} P_1 = k_1^2, \quad P_2 = k_2^2, \quad P_3 = (q_2 - k_1)^2, \quad P_4 = (p_1 - k_2)^2, \\ P_5 = (q_1 + k_1)^2 - m_1^2, \quad P_6 = (q_1 + k_1 - k_2)^2 - m_1^2, \\ P_7 = (q_1 - p_2 + k_1 - k_2)^2 - m_2^2, \quad P_8 = (k_1 - p_1)^2, \quad P_9 = (k_2 - q_2 - p_2)^2, \end{aligned} \tag{3.22}$$

where P_8 and P_9 are auxiliary propagators. The scalar products of the external momenta can be expressed through the kinematical invariants by

$$\begin{aligned} p_1^2 = p_2^2 = q_2^2 = 0, \quad q_1^2 = m_2^2, \quad (p_1 + p_2)^2 = s, \\ (q_2 - p_1)^2 = t, \quad (q_2 - p_2)^2 = m_1^2 - s - t. \end{aligned} \tag{3.23}$$

We perform the reduction with $r_{\max} = 7$ and $s_{\max} = 4$, which is sufficient for the virtual NNLO corrections to the amplitude of single top production. This results in about 1.6 million probes in total over four prime fields to complete the reduction. The calculations were performed on cluster nodes equipped with two Intel Xeon Platinum 8160 processors with 24 cores each and 192 GiB of RAM in total with hyper-threading disabled. Table 3.1 shows the runtime of `Kira` ⊕ `FireFly` in comparison to `Kira` ⊕ `Fermat`, i.e. the algebraic reduction utilizing `Fermat` [72] to process the coefficients. Not

Table 3.1: Reduction of the double box in Fig. 3.1 with $r_{\max} = 7$, $s_{\max} = 4$ utilizing `FireFly` and the overhead reduction with bunches described in Section 3.3.4. As a comparison we present the algebraic reduction with `Kira` and `Fermat`.

maximum bunch size	Runtime	Memory	CPU time per probe
1	18 h	40 GiB	1.73 s
2	14 h	41 GiB	1.30 s
4	11 h	46 GiB	1.00 s
8	10 h 15 min	51 GiB	0.91 s
16	9 h 45 min	63 GiB	0.85 s
32	9 h 30 min	82 GiB	0.84 s
64	9 h 30 min	116 GiB	0.83 s
`Kira` ⊕ `Fermat`	82 h	147 GiB	-

only is the runtime faster by a factor of four, also the memory footprint reduces by more than a factor of three. The free memory can be traded against an even better performance when increasing the bunch size to reduce the overhead of solving the system of equations. This however reaches a plateau at bunch size 32 while costing more and more memory.

Table 3.2 shows the same reduction while utilizing multiple nodes of the cluster. The performance increases significantly, but again, at some point the gain through additional nodes reaches a plateau.

The most impressive benchmark is the reduction of the double-pentagon topology that appears in the amplitude of five-light-parton scattering at the two-loop level illustrated in Fig. 3.2. There are five external momenta $p_1, \ldots, p_5$ fulfilling $p_i^2 = 0$. All p_i are assumed

Table 3.2: Reduction of the double box in Fig. 3.1 with $r_{\max} = 7$, $s_{\max} = 4$ utilizing `FireFly` and multiple nodes with `MPI`. As a comparison we present the algebraic reduction with `Kira` and `Fermat`.

# nodes	Runtime	Speed-up
1	18 h	1.0
2	10 h 15 min	1.8
3	7 h 15 min	2.5
4	5 h 45 min	3.1
5	5 h 30 min	3.3
`Kira` ⊕ `Fermat`	82 h	-

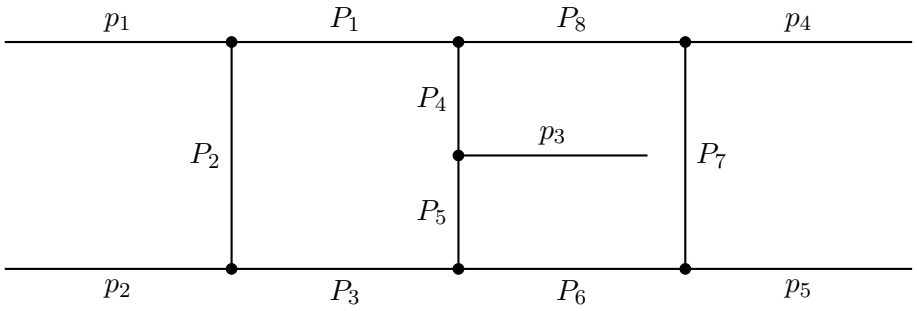

Figure 3.2: The double-pentagon topology for five-light-parton scattering.

to be incoming, i.e. $\sum_i p_i = 0$. The kinematical invariants are defined by

$$\begin{aligned} s_{12} = (p_1 + p_2)^2, \quad s_{23} = (p_2 + p_3)^2, \quad s_{34} = (p_3 + p_4)^2, \\ s_{45} = (p_4 + p_5)^2, \quad s_{51} = (p_5 + p_1)^2. \end{aligned} \tag{3.24}$$

Including D, the reduction of the double-pentagon topology is a six variable problem. By setting $s_{12} = 1$ and restoring its dependence by dimensional analysis after the reduction, it can be reduced to a five variable problem. The set of denominators describing the topology depicted in Fig. 3.2 is chosen as

$$\begin{aligned} P_1 = l_1^2, \quad P_2 = (l_1 + p_1)^2, \quad P_3 = (l_1 + p_1 + p_2)^2, \quad P_4 = l_2^2, \\ P_5 = (l_2 + p_3)^2, \quad P_6 = (l_1 + l_2 + p_1 + p_2 + p_3)^2, \quad P_7 = (l_1 + l_2 - p_4)^2, \\ P_8 = (l_1 + l_2)^2, \quad P_9 = (l_2 + p_1)^2, \quad P_{10} = (l_2 + p_2)^2, \quad P_{11} = (l_2 + p_4)^2, \end{aligned} \tag{3.25}$$

where the last three entries are auxiliary denominators. The system of equations used in this reduction is taken from Ref. [104], which provides it in block-triangular form. This form is much better suited for the reduction than a naive IBP system as generated, e.g., by `Kira`. Additionally, we used `FireFly` to transform the coefficients in the system

to the Horner form for faster evaluations. We benchmark the reduction of all integrals including five scalar products. The reductions are performed on a machine with two Intel Xeon Gold 6138 with 20 cores each and 768 GiB of RAM in total with hyperthreading enabled. The results of this benchmark are shown in Table 3.3. The most complicated

Table 3.3: Reduction of all integrals with five scalar products in the double-pentagon topology.

Runtime	Memory	Probes
12 d	540 GiB	38278000

master integral coefficient has a maximum degree in the numerator of 87 and in the denominator of 50 thus yielding a dense bound of roughly $5.46 \cdot 10^7$ possible non-zero monomials. Fortunately, many of these are zero such that only about 10^7 monomials contribute. Without the scan for factors, the maximum degree of the denominator of the most complicated coefficient rises to 85. The database of the reduction occupies 25 GiB of disk space.

These and more benchmarks are studied in detail in Refs. [47, 48], displaying the impact of many options offered by `Kira` and `FireFly`.

3.3.6 *Conclusions*

We described the ideas behind the interpolation and RR techniques and how they can be applied to IBP reductions over finite fields. Additionally, we developed some improved algorithms as well as some technical advancements, which are implemented in our public general-purpose `C++` library `FireFly` [46, 47]. Moreover, we integrated support for `FireFly` into the public IBP reduction program `Kira` [48], which reduces the memory footprint and runtime of many reduction problems significantly. Of course, finite field and interpolation techniques are not limited to IBP reductions. We thus hope that these tools can be used to finish some of the challenging calculations on the forefront of high-energy physics as well as other fields.

3.4 REDUCTION OF GRADIENT FLOW INTEGRALS

After describing the new techniques and tools, we now turn back to the gradient flow. As mentioned before, we generate the system of equations based on the relations introduced in Section 3.1 with a `Mathematica` [71] code developed in Ref. [45] and then solve this system with `Kira` $\oplus$ `FireFly` employing the feature to reduce user-defined systems. Since t is the only dimensionful scale and can thus be factored out, the coefficients of the integrals in the linear system are simply rational functions in D. However, even with these improvements, the whole system required for the higher-order terms in the expansion of the quark masses at the three-loop level did not fit in our main memory of 768 GiB before removing the linearly dependent equations. We thus had to divide the

system into 24 subsystems, solve them one after each other, and finally perform another reduction for the temporary master integrals to arrive at the final basis. The largest of the subsystems consisted of more than 14 million linearly independent equations with more than 145 million terms in total. Solving this subsystem once over a finite field takes more than half an hour and more than 35 GiB of RAM so that we could only solve a few in parallel. Luckily, we only required a few hundred probes per subsystem since this is a univariate problem in D and the maximum degrees in the master integral coefficients are at most 51. Thus, we were able to finish the whole reduction in less than two weeks.

Finally, we found one master integral at one-loop level, six at two-loop level, and 216 at three-loop level. However, these numbers may not be absolute because there might exist additional master integrals which are not required for the integrals we encountered. In the next section, we discuss how these master integrals can be solved.

4 CALCULATION OF THE MASTER INTEGRALS

In this chapter we discuss methods to calculate the master integrals. The simplest master integrals can be solved analytically to all orders in ϵ by direct integrations described in Section 4.1. However, many master integrals are too complicated for this strategy to succeed. In Section 4.2, we describe how the integrands can be expanded in ϵ despite their singularities and integrated afterwards, but also this method has its limitations. The most general method is a numerical integration following the *sector decomposition* strategy [105, 106], which works well for all gradient flow integrals. The application to gradient flow integrals was worked out by Tobias Neumann in his PhD thesis [107]. Therefore, we only discuss the main ideas in Section 4.3.

Let us briefly comment on other common techniques for the calculation of master integrals. Since there is only the flow time t as sole mass scale after the expansion in the quark masses, we cannot use *differential equations* [108–111], because they only produce trivial relations. *Dimensional recurrence relations* [112, 113] on the other hand yield nontrivial difference equations, which can be used to determine the master integrals up to periodic functions. However, these have to be fixed by knowing the solution of the integrals in some limit. We did not find an exploitable limit and thus abandoned this approach for now. Finally, we also explored the *Mellin-Barnes representation* [114, 115]. In Ref. [45], we developed a procedure to construct Mellin-Barnes representations of gradient flow integrals based on the *modified method of brackets* [116]. The obtained representations are quite high dimensional though so that the speed of convergence in the numerical evaluation with `MB` [117] or `MBresolve.m` [118] is outclassed by the sector decomposition based method by orders of magnitude. Hence, we did not attempt an analytic solution of these representations.

All analytical results for the master integrals in this thesis were calculated by myself: a subset of simple master integrals employing direct integration as part of my Master's thesis [45] and the remainder as part of this thesis. Tobias Neumann calculated all numerical results. Section 4.3 is thus based on the compact discussion of Ref. [41].

4.1 DIRECT INTEGRATION

The simplest method to calculate the master integrals is to solve the momentum integrals with the help of the Gaußian integral

$$\int_q \mathrm{e}^{-sq^2} (q^2)^{-\alpha} = \frac{s^\alpha}{(4\pi s)^{D/2}} \frac{\Gamma(D/2-\alpha)}{\Gamma(D/2)}, \tag{4.1}$$

where $\Gamma(x)$ is the well-known gamma function. However, starting at two-loop level, there are multiple momentum integrations which are interconnected in general. By introducing Schwinger parameters x_i as

$$\frac{1}{(q^2)^a} = \frac{1}{\Gamma(a)} \int_0^\infty \mathrm{d}x\, x^{a-1} \mathrm{e}^{-xq^2} \tag{4.2}$$

one can rewrite some or all of the propagators as exponential functions. By completing the square in the loop momenta, one can then again apply Eq. (4.1) so that only integrals over the flow-time and Schwinger parameters remain. These can be solved with the help of `Mathematica` [71] for all master integrals up to two-loop order and the simplest three-loop master integrals. Often, this results in hypergeometric functions which can be expanded with the package `HypExp` [119, 120].

4.2 INTEGRAND EXPANSION

When the integrations of the Schwinger and flow-time parameters proof too difficult to be integrated with the exact dependence in D, one can simplify the integrands by expanding in ϵ, which would be done at a later stage anyway. However, one cannot perform a naive expansion as long as there are divergences in the integration region. Usually, they are encountered at the integration boundaries. Ref. [121] introduced a strategy to both detect and extract the singularities so that the finite integrand can be expanded. We briefly summarize it in the following.

To unify the integration variables, we substitute the flow-time parameters by $u = \frac{x}{1+x}$ to map them from $u \in [0,1]$ to $x \in [0,\infty)$ and denote all Schwinger-like parameters as x_i. One can compute the *degree of vanishing* $\deg_J^K(F)$ of an integrand F by

$$F_{x_j \to \lambda x_j \ \forall j \in J \text{ and } x_k \to \lambda^{-1} x_k \ \forall k \in K} \propto \lambda^{\deg_J^K(F)} \quad \text{for} \quad \lambda \to 0, \tag{4.3}$$

where all x_j in the set J tend to zero and all x_k in the set K to infinity. The *degree of divergence* is then defined as

$$\omega_J^K(F) \equiv |J| - |K| + \deg_J^K(F). \tag{4.4}$$

If $\omega_J^K(F) > 0$ for all disjoint sets J and K, the integral is absolutely convergent.[1] Furthermore, it was shown in Ref. [121] that the operators

$$\mathcal{D}_J^K \equiv 1 - \frac{1}{\omega_J^K} \left[\sum_{j \in J} \frac{\partial}{\partial x_j} x_j - \sum_{k \in K} \frac{\partial}{\partial x_k} x_k \right] \tag{4.5}$$

fulfill

$$\left[\prod_{i=1}^E \int_0^\infty \mathrm{d}x_i \right] F = \left[\prod_{i=1}^E \int_0^\infty \mathrm{d}x_i \right] \mathcal{D}_J^K F \tag{4.6}$$

1 This assumes that there are no divergences inside the integration domain.

and improve the degree of divergence. By applying such operators a finite number of times, one can turn all integrals absolutely convergent. Of course, there are still poles in ϵ after this procedure, but they are explicit and can be factored out of the integrals.

As an example, let us discuss the two-loop master integral

$$\begin{aligned}\int_0^1 \mathrm{d}u \int_{p,k} \mathrm{e}^{-(2-u)p^2-uk^2-u(p-k)^2} &= \frac{1}{(4\pi)^D}\int_0^1 \mathrm{d}u\,(4u-u^2)^{-\frac{D}{2}} \\ &= \frac{1}{(4\pi)^D}\int_0^\infty \mathrm{d}x\,(1+x)^{2-2\epsilon}\,(3x^2+4x)^{\epsilon-2} \equiv \frac{1}{(4\pi)^D}\int_0^\infty \mathrm{d}x\,F.\end{aligned} \tag{4.7}$$

It is immediately clear that the integral diverges at $\epsilon \to 0$ for $x \to 0$ and is finite for $x \to \infty$, which can also be read off from

$$\omega^{\{x\}}(F) = 1, \qquad \omega_{\{x\}}(F) = \epsilon - 1. \tag{4.8}$$

Applying the operator of Eq. (4.5) to F, we obtain

$$\left[1 - \frac{1}{\epsilon-1}\frac{\partial}{\partial x}x\right] F = \frac{((3x+5)\,\epsilon-2)\,(1+x)^{1-2\epsilon}}{(\epsilon-1)\,x^{1-\epsilon}\,(3x+4)^{3-\epsilon}} \equiv \tilde{F} \tag{4.9}$$

and find that the degrees of divergence improved to

$$\omega^{\{x\}}(\tilde{F}) = 1, \qquad \omega_{\{x\}}(\tilde{F}) = \epsilon. \tag{4.10}$$

Repeating this step with

$$\left[1 - \frac{1}{\epsilon}\frac{\partial}{\partial x}x\right] \tilde{F} = \frac{9x^\epsilon\left(\left(x+\frac{5}{3}\right)^2\epsilon^2 + \left(x^2+2x+\frac{1}{3}\right)\epsilon - \frac{4}{3}x - \frac{10}{9}\right)}{\epsilon\,(\epsilon-1)\,(1+x)^{2\epsilon}\,(3x+4)^{4-\epsilon}} \equiv \hat{F}, \tag{4.11}$$

the degrees of divergence improve again to

$$\omega^{\{x\}}(\hat{F}) = 1, \qquad \omega_{\{x\}}(\hat{F}) = 1 + \epsilon. \tag{4.12}$$

Hence, the integral $\int_0^\infty \mathrm{d}x\,\hat{F}$ converges absolutely and one can safely expand the integrand in ϵ to the desired order. Note that the pole in $1/\epsilon$ is now explicit.

The `Maple` [122] package `HyperInt` [123] provides the convenient functions to compute the degrees of divergence in Eq. (4.4) for all sets of variables and to apply the operator in Eq. (4.5) to the integrand. For integrals with more than one variable, there are usually several variable sets with negative degrees of divergence and, thus, several operators could be applied. Quite often, applying one operator directed towards a specific degree of divergence improves others as well. Hence, we test several possible operators and application orders to obtain the smallest integrand which is absolutely convergent. After expanding the integrands to the desired order in ϵ, we use `HyperInt` to solve the integrals in terms of *hyperlogarithms*[2]. Conveniently, `HyperInt` can also convert them to multiple polylogarithms [125, 126]

$$\mathrm{Li}_{n_1,\ldots,n_r}(z_1,\ldots,z_r) = \sum_{0<k_1<\cdots<k_r} \frac{z_1^{k_1}\cdots z_r^{k_r}}{k_1^{n_1}\cdots k_r^{n_r}}, \tag{4.13}$$

which we prefer in this thesis.

2 Hyperlogarithms have already been studied in the 19th century. For an overview of their properties and application to Feynman integrals we refer to Ref. [124].

4.3 SECTOR DECOMPOSITION

In this section, we briefly describe the numerical approach based on the sector decomposition algorithm [105, 106]. For the gradient flow integrals, it was worked out in Ref. [107] and we refer to this reference for details.

As a first step of the numerical evaluation of the gradient flow integrals given by Eq. (2.77), we express the propagators through Schwinger parameter integrals and map them from $x \in [0, \infty)$ to $y \in [0, 1]$ using the simple transformation $x = \frac{y}{1-y}$. Momentum integrations are performed as D-dimensional Gaußian integrals after a diagonalization, cf. Section 4.1. The overall result is an integral over a unit hypercube.

The integrand typically involves a number of (overlapping) singularities, which we factorize using `FIESTA` [127–129], an implementation of the sector decomposition algorithm. As opposed to regular Feynman integrals where sector decomposition is typically employed in combination with Feynman parameterization, it appears that we cannot restrict the singularities to the lower integration bound only. To identify cases where singularities appear at the upper bound, we determine the degree of divergence for each subset of integration variables at the level of the Schwinger parameterization as already discussed in Section 4.2. If an integral involves singularities both at the lower and the upper bound, we split all integration intervals in the middle, and map the singularities to the lower bound by an appropriate change of variable.

The sector decomposed integrals obtained from `FIESTA` are then integrated with our implementation of fully symmetric integration rules of order 13 [21, 107, 130], which can handle integrable logarithmic-like singularities at the integration boundaries very well. We perform all arithmetic with 256-bit precision using the `MPFR` library [131], and use a local adaptive bisection in the direction of the largest fourth difference. A high precision arithmetic turns out to be necessary to achieve a relative numerical accuracy of 10^{-10} or better. The integration uncertainty is estimated by the difference between the integration results of rules of order 13 and 11.

5

VACUUM EXPECTATION VALUES AT NEXT-TO-NEXT-TO-LEADING ORDER

Using the methods described in Chapters 2 to 4 and Appendix C, we can calculate the VEVs of $E(t,x)$, $S(t,x)$, and $R(t,x)$ defined in Section 2.4 through three loops, i.e. NNLO in perturbation theory. Sample diagrams for these quantities are shown in Fig. 5.1. The number of diagrams in each case is given in Table 5.1. Note that it takes the re-writing of the four-gluon vertex into trilinear vertices as described in Appendix C into account. Not

Table 5.1: The number of Feynman diagrams contributing to the quantities computed in this chapter. At three-loop level, the number for "quenched QCD" (marked as $T_R = 0$) is shown separately.

#loops	1	2	3	3 ($T_R = 0$)
$\langle E(t) \rangle$	1	11	232	211
$\langle S(t) \rangle$	1	8	210	202
$\langle R(t) \rangle$	1	11	311	300

included in this number are diagrams with closed flow-line loops, but integrals with scale-less sub-loops are counted in.

Since $\langle E(t) \rangle$, $\langle S(t) \rangle$, and $\langle R(t) \rangle$ are gauge independent, we are free to choose Feynman gauge for the QCD gauge parameter ($\xi = 1$) and $\kappa = 1$ for the gradient flow gauge parameter for the evaluation of the results presented in the following sections, which facilitates the actual calculation significantly. However, we also checked gauge invariance explicitly for the leading terms in the quark masses: At two-loop level, we computed the result with general gauge parameter ξ and its dependence vanishes in the final results. Keeping the gauge parameter fully general at three-loop level unfortunately leads to intermediate expressions which exceed our available computing resources. Nonetheless, we were able to evaluate the terms with the highest power in the gauge parameter ξ, i.e. ξ^4 for $\langle E(t) \rangle$ and ξ^3 for $\langle S(t) \rangle$ and $\langle R(t) \rangle$, and show that their coefficients vanish. This already happens algebraically after the reduction to master integrals, even before their numerical values are inserted.

As further check, we computed the numerical expressions for all integrals at vanishing quark masses before the reduction to master integrals and checked that they lead to the same results within their (larger) uncertainties.

The results for $\langle E(t) \rangle$, $\langle \mathring{R}(t) \rangle$, and $\langle \mathring{S}(t) \rangle$ are presented and discussed in Sections 5.1 to 5.3.

We are also interested in the quark mass effects of $\mathcal{O}(m^2 t)$ on $\langle E(t) \rangle$ and $\langle \mathring{R}(t) \rangle$. They can be calculated by a naive expansion in the bare masses before the loop integrations,

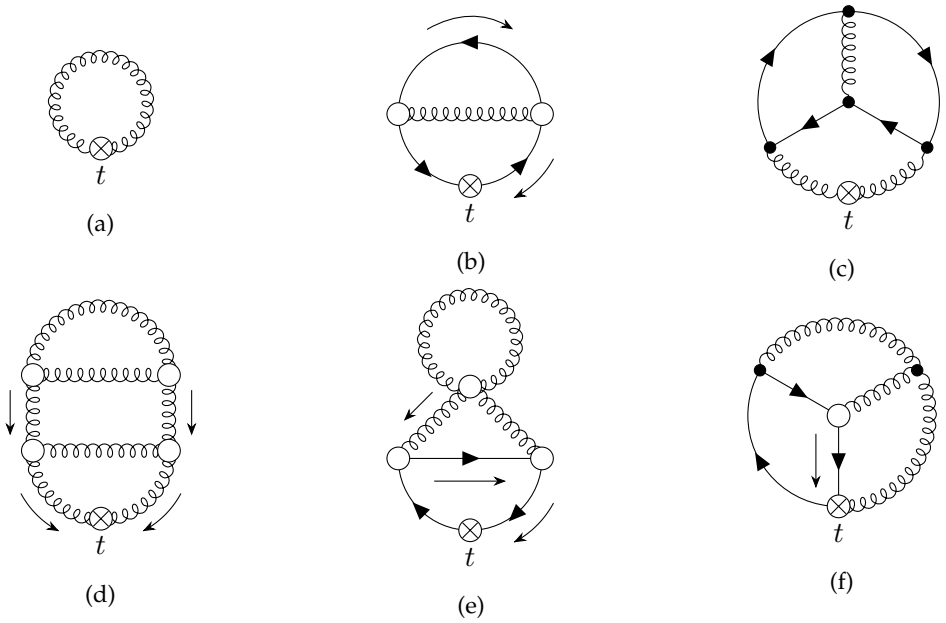

Figure 5.1: (a) The only diagram contributing to $\langle E(t)\rangle$ at one loop; (b) a two-loop diagram for $\langle S(t)\rangle$ and $\langle R(t)\rangle$; and four three-loop diagrams: (c,d) two diagrams for $\langle E(t)\rangle$; (e) one diagram for $\langle S(t)\rangle$ and $\langle R(t)\rangle$; (f) and one diagram for $\langle R(t)\rangle$.

while higher orders require a more sophisticated treatment. For the calculation in Chapter 7, we additionally require the naive terms to $\mathcal{O}(m_B^4 t)$. Quark masses only appear in form of (flowed) quark propagators, see Eq. (B.2), which we expand as

$$\frac{-i\not{p} + m_B}{p^2 + m_B^2} = \frac{-i\not{p} + m_B}{p^2} - \frac{-i\not{p} m_B^2 + m_B^3}{p^4} + \frac{-i\not{p} m_B^4}{p^6} + \mathcal{O}(m_B^5). \tag{5.1}$$

Therefore, m_B becomes a multiplicative factor, which can pulled out of the integrals, and we again end up with massless integrals of the form in Eq. (2.77). Terms of higher orders in m_B produced by the multiplication of multiple propagators are immediately discarded. Additionally, it is enlightening to split the n_f quarks into n_l massless quarks and n_h degenerate massive quarks with mass m (and bare mass m_B). The quark mass effects are discussed in Section 5.4.

Finally, our results can be used to introduce a *gradient flow coupling* and a *gradient flow mass* in Section 5.5.

This chapter is based on parts of Ref. [41], where I was mainly responsible for the calculation of the VEVs and for collecting the final results. The two color factors $T_R^2 n_f^2$ and $C_F T_R n_f$ for $\langle E(t)\rangle$ were already computed in my Master's thesis [45]. The discussion of the quark mass effects is new, even though the results can already be extracted from Ref. [132].

5.1 RESULTS FOR THE GLUON ACTION DENSITY

We write the perturbative result for the gluon action density as

$$\langle E(t)\rangle = \frac{3\alpha_s}{4\pi t^2}\frac{N_A}{8}\left[1+\frac{\alpha_s}{4\pi}e_1(\mu^2 t)+\left(\frac{\alpha_s}{4\pi}\right)^2 e_2(\mu^2 t)+\mathcal{O}(\alpha_s^3)\right]+E^m(t,m), \tag{5.2}$$

where $\alpha_s = \alpha_s(\mu)$, with μ the renormalization scale. $E^m(t,m)$ captures the quark mass effects which are studied to $\mathcal{O}(m^2 t)$ in Section 5.4. Without masses, the e_i depend only on the product $z \equiv \mu^2 t$. It is convenient to parameterize this dependence in terms of

$$L(z) \equiv \ln(2z) + \gamma_E, \tag{5.3}$$

which is motivated by the product of the typical factor $(8\pi t)^\epsilon$ occurring in flow-time integrals [4] and the usual definition of the renormalization scale in the $\overline{\text{MS}}$ scheme, see Eq. (A.8): $(8\pi t)^\epsilon(\mu^2 e^{\gamma_E}/(4\pi))^\epsilon = 1+\epsilon\, L(\mu^2 t)+\mathcal{O}(\epsilon^2)$. A natural choice for the renormalization scale is defined by the inverse smearing radius $q_8 \equiv 1/\sqrt{8t}$ of the gradient flow, cf. Eq. (2.31). However, from explicit higher order calculations, we find that the slightly larger value

$$\mu_0 = \frac{e^{-\gamma_E/2}}{\sqrt{2t}} \approx 1.5\, q_8, \tag{5.4}$$

corresponding to $L(\mu_0^2 t) = 0$, improves the stability of the perturbative corrections both for the VEVs computed in this chapter as well as for the EMT in Chapter 6 (see also Ref. [21]). This was corroborated by the behavior of the $t \to 0$ extrapolation for thermodynamical quantities evaluated in Ref. [133] using the two-loop results of Chapter 6, which are published in Ref. [43].

We thus write the coefficients of Eq. (5.2) as

$$\begin{aligned} e_1(z) &= e_{1,0} + \beta_0\, L(z), \\ e_2(z) &= e_{2,0} + (2\beta_0\, e_{1,0} + \beta_1)\, L(z) + \beta_0^2\, L^2(z), \end{aligned} \tag{5.5}$$

with β_0, β_1 from Eq. (A.10). For the coefficients $e_{i,j}$, we find

$$e_{0,0} = 1, \qquad e_{1,0} = \left(\frac{52}{9}+\frac{22}{3}\ln 2 - 3\ln 3\right)C_A - \frac{8}{9}T_R n_f \tag{5.6}$$

$$e_{2,0} = 27.9784\, C_A^2 - (31.5652\ldots)\, C_A T_R n_f + \left(16\zeta(3)-\frac{43}{3}\right)C_F T_R n_f + \left(\frac{8\pi^2}{27}-\frac{80}{81}\right)T_R^2 n_f^2,$$

where $\zeta(z)$ is Riemann's ζ function with $\zeta(3) = 1.20206\ldots$. The three dots in the coefficient of $C_A T_R n_f$ indicate that we were able to obtain the expression in analytical, albeit cumbersome, form:

$$\begin{aligned}
-(31.5652\ldots) = \frac{2}{81}\Bigg(& -108\,\mathrm{Li}_3\left(-\frac{1}{3}\right) - 792\,\mathrm{Li}_2\left(\frac{3}{4}\right) + 216\,\mathrm{Li}_2\left(-\frac{1}{3}\right) \\
& + 108\,\mathrm{Li}_{1,2}\left(-3,-\frac{1}{3}\right) - 216\,\mathrm{Li}_{1,2}\left(1,-\frac{1}{3}\right) + 216\,\mathrm{Li}_{2,1}\left(-3,-\frac{1}{3}\right) \\
& - 216\,\mathrm{Li}_{2,1}\left(1,-\frac{1}{3}\right) + 216\,\mathrm{Li}_{1,1,1}\left(-1,-3,-\frac{1}{3}\right) \\
& - 864\,\mathrm{Li}_{1,1,1}\left(-1,3,-\frac{1}{3}\right) + 216\,\mathrm{Li}_{1,1,1}\left(1,3,-\frac{1}{3}\right) \\
& + 432\,\mathrm{Li}_{1,1,1}\left(3,1,-\frac{1}{3}\right) - 1134\zeta(3) + 90\pi^2 - 641 - 54\ln^3 3 \\
& + 324\ln^3 2 + 324\ln 2\ln^2 3 + 270\ln^2 3 - 648\ln^2 2\ln 3 - 2232\ln^2 2 \\
& + 504\ln 2\ln 3 - 18\pi^2\ln 3 + 1890\ln 3 + 108\pi^2\ln 2 - 2148\ln 2\Bigg),
\end{aligned} \tag{5.7}$$

with the multiple polylogarithms Li defined in Eq. (4.13). Only four decimal places of the numerical result for the C_A^2 coefficient are displayed here, while our estimate of the numerical accuracy, obtained by propagating the uncertainty of the individual integrals to the final result, is at least six digits beyond that. This estimate matches the observed differences between the numerical and analytical results in the cases where the latter have been computed. The same statements hold for the other observables listed below. The NLO coefficient e_1 was first evaluated in Ref. [4]. Setting $\mu = q_8$, one finds that the NNLO result agrees with Ref. [21] at the sub-percent level.[1]

The logarithmic terms $e_{n,k}L^k(z)$ obey the all-order recursion formula ($1 \le k \le n$)

$$k\,e_{n,k} = \sum_{l=0}^{n-1}(n-l)e_{n-l-1,k-1}\beta_l, \tag{5.8}$$

which follows from renormalization-group invariance, i.e.

$$\mu^2\frac{\mathrm{d}^2}{\mathrm{d}\mu^2}\langle E(t)\rangle = 0 \tag{5.9}$$

and Eq. (A.7). This provides a welcome check of our calculation.

Even though $\langle E(t)\rangle$ is formally independent of the renormalization scale μ, we introduce a residual scale dependence by truncating the series. We study this dependence by varying μ around different central scales μ_0. The running of α_s is evaluated with the help

1 To be precise, all color coefficients of Ref. [21] are compatible with our new calculation, except for the C_A^2 term, for which "only" the first three digits agree, corresponding to an overly optimistic uncertainty estimate of Ref. [21] for that term. The effect for any practical application should be irrelevant.

Table 5.2: Settings for the different renormalization scales. Additionally, we display the corresponding size of t on the lattice in the last column.

μ_0	n_f	$\alpha_\mathrm{s}^{(n_\mathrm{f})}(\mu_0)$	t
3 GeV	3	0.248	$(0.03\,\mathrm{fm})^2$
10 GeV	5	0.178	$(0.01\,\mathrm{fm})^2$
130 GeV	5	0.112	$(8 \cdot 10^{-4}\,\mathrm{fm})^2$

RunDec [134, 135] at the corresponding loop order, i.e. we apply one-loop running for the LO result, two-loop running for the NLO result, and three-loop running for the NNLO result. The number of fermion flavors n_f is fixed during the running and no decoupling is performed. Table 5.2 shows the chosen values for n_f as well as the value $\alpha_\mathrm{s}^{(n_\mathrm{f})}(\mu_0)$ for the coupling at the central scale. The residual dependence on μ is shown in Fig. 5.2. For large values of μ, the renormalization scale dependence drops significantly when

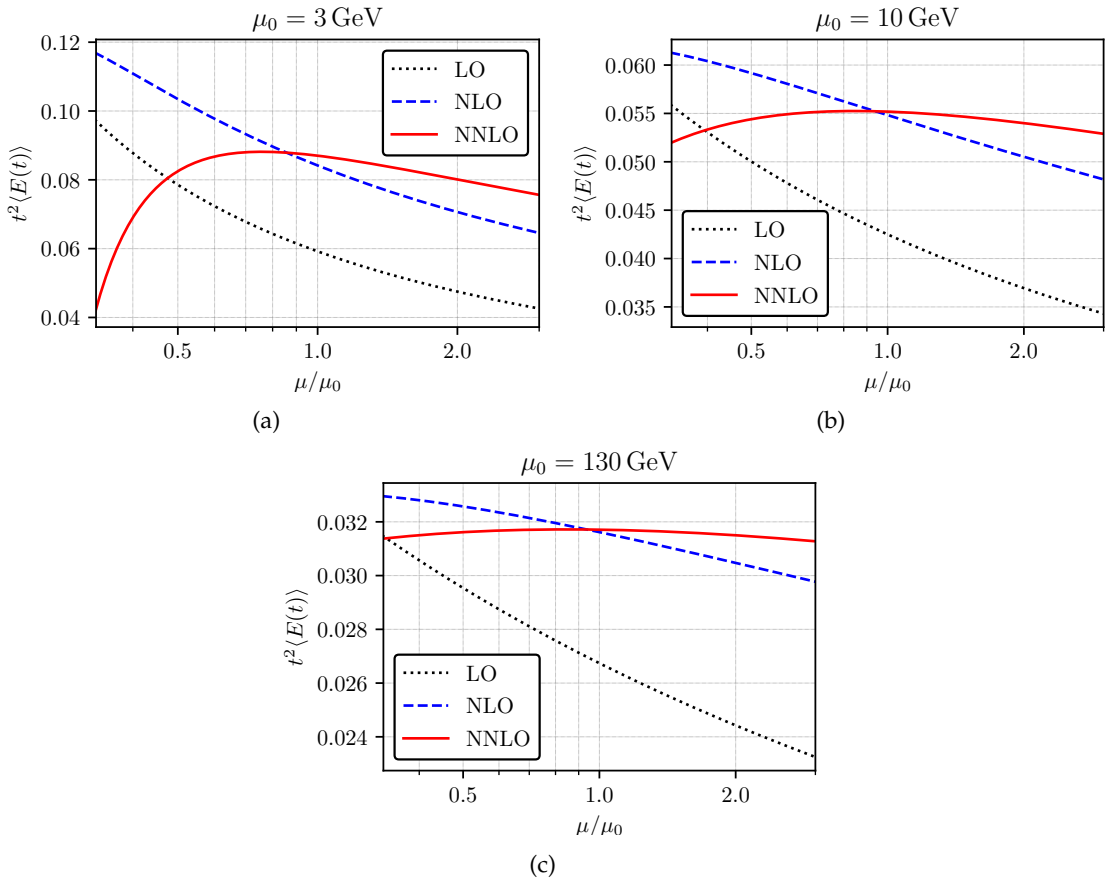

Figure 5.2: Renormalization scale dependence of $t^2\langle E(t)\rangle$ in QCD for three different values of the central scale $\mu_0 = e^{-\gamma_\mathrm{E}/2}/\sqrt{2t}$. The detailed settings are given in Table 5.2.

going to higher order results. This improvement diminishes when reducing the scale towards the non-perturbative regime. Especially, the perturbative expansion seems to break down at around $1 - 1.5\,\mathrm{GeV}$. Taking the variation of μ by a factor of two around the central scale as an estimate of the uncertainty due to missing higher orders, one finds that the NLO and NNLO uncertainties overlap nicely for all three values of μ_0: The NNLO corrections amount to 3.4 % at 3 GeV, 0.68 % at 10 GeV, and 0.29 % at 130 GeV, whereas the NLO uncertainty estimates with 19 %, 7.9 %, and 3.3 %, respectively, are significantly larger. Therefore, we also expect the NNLO uncertainty estimates of 6.6 %, 1.8 %, and 0.48 % to be extremely conservative. Probably, this can be mainly attributed to the choice of μ_0, which is particularly well suited for this observable. The same study was performed in Ref. [21] more thoroughly with similar conclusion.

5.2 RESULTS FOR THE VACUUM EXPECTATION VALUE OF THE QUARK KINETIC OPERATOR

Due to Eq. (2.62), $\langle \mathring{R}(t) \rangle$ is already fixed to all orders in perturbation theory neglecting quark masses, cf. Eq. (2.67). However, we have to compute $\langle R(t) \rangle|_{m=0}$ to obtain $\mathring{Z}_\chi(t,\mu)$ as renormalization constant for the ringed scheme. For the conversion factor from $\overline{\text{MS}}$ to the ringed scheme, defined in Eq. (2.65), we find

$$\begin{aligned}\zeta_\chi(t,\mu) = 1 &+ \frac{\alpha_s}{4\pi}\left(\gamma_{\chi,0} L(\mu^2 t) - 3C_F \ln 3 - 4C_F \ln 2\right) \\ &+ \left(\frac{\alpha_s}{4\pi}\right)^2 \left\{ \frac{\gamma_{\chi,0}}{2}\left(\beta_0 + \gamma_{\chi,0}\right) L^2(\mu^2 t) + \Big[\gamma_{\chi,1} - \gamma_{\chi,0}\left(\beta_0 + \gamma_{\chi,0}\right)\ln 3 \right. \\ &\left. - \frac{4}{3}\gamma_{\chi,0}\left(\beta_0 + \gamma_{\chi,0}\right)\ln 2\Big] L(\mu^2 t) + c_\chi^{(2)} \right\} + \mathcal{O}(\alpha_s^3),\end{aligned} \tag{5.10}$$

with

$$c_\chi^{(2)} = -23.7947\, C_A C_F + 30.3914\, C_F^2 - (3.92255\ldots) C_F T_R n_f. \tag{5.11}$$

Again, we only keep the six leading digits even though our uncertainty is at least six digits beyond that. As indicated by the three dots, the coefficient of $C_F T_R n_f$ was obtained in analytical form:

$$\begin{aligned}-(3.92255\ldots) = \frac{1}{18}\Bigg(&48\,\mathrm{Li}_2\left(\frac{1}{9}\right) - 2400\,\mathrm{Li}_2\left(\frac{1}{3}\right) + 672\,\mathrm{Li}_2\left(\frac{3}{4}\right) - 131 + 46\pi^2 \\ &+ 960\ln^2 2 - 1068\ln^2 3 + 1888\ln 2 - 1032\ln 3 + 624\ln 2\ln 3\Bigg).\end{aligned} \tag{5.12}$$

The NLO result has been obtained in Ref. [11] and we computed the NNLO terms as part of this thesis. An important consistency check is that $\langle R(t) \rangle|_{m=0}$ can be renormalized with the flowed-quark field renormalization constant Z_χ in Eq. (2.59).

Additionally, there are quark mass corrections $R^m(t,m)$ following

$$\langle \mathring{R}(t) \rangle = -\frac{2N_C n_f}{(4\pi t)^2} + \mathring{R}^m(t,m) \tag{5.13}$$

which are studied to $\mathcal{O}(m^2 t)$ in Section 5.4.

5.3 RESULTS FOR THE QUARK CONDENSATE

Let us now turn to the quark condensate $\langle \mathring{S}(t) \rangle$. Since it vanishes in the chiral limit $m_f = 0$, we compute the leading coefficient of the expansion in the quark masses m_f,

$$\langle \zeta_\chi S(t) \rangle \equiv \langle \mathring{S}(t) \rangle = \sum_{f=1}^{n_f} s_f(t) + \mathcal{O}(m^2 t), \qquad s_f(t) \equiv m_f \frac{\mathrm{d}\langle \mathring{S}(t) \rangle}{\mathrm{d}m_f}\bigg|_{m=0}, \tag{5.14}$$

where it is understood that *all* quark masses are set to zero after taking the derivative. We thus write

$$s_f(t) = -\frac{N_C m_f}{8\pi^2 t}\left[1 + \frac{\alpha_s}{4\pi} s_1(z) + \left(\frac{\alpha_s}{4\pi}\right)^2 s_2(z) + \mathcal{O}(\alpha_s^3)\right]. \tag{5.15}$$

Renormalizing the quark masses in the $\overline{\text{MS}}$ scheme according to Eq. (A.13), we find

$$\begin{aligned} s_1(z) &= s_{1,0} + \gamma_{m,0}\, L(z), \\ s_2(z) &= s_{2,0} + \left[(\gamma_{m,0} + \beta_0)\, s_{1,0} + \gamma_{m,1}\right] L(z) + \frac{1}{2}(\gamma_{m,0} + \beta_0)\gamma_{m,0}\, L^2(z), \end{aligned} \tag{5.16}$$

with $z = \mu^2 t$ and the $\gamma_{m,i}$ and β_i from Eqs. (A.10) and (A.12). The non-logarithmic terms are given by

$$\begin{aligned} s_{0,0} &= 1, \qquad s_{1,0} = (4 + 4\ln 2 - 3\ln 3) C_F, \\ s_{2,0} &= 19.6422\, C_F^2 + 41.3897\, C_F C_A - (15.7975\ldots)\, C_F T_R n_f, \end{aligned} \tag{5.17}$$

where again the $C_F T_R n_f$ term is known analytically, as indicated by the three dots:

$$\begin{aligned} -(15.7975\ldots) = \frac{16}{3}\,\mathrm{Li}_2\left(\frac{1}{9}\right) - \frac{800}{3}\,\mathrm{Li}_2\left(\frac{1}{3}\right) + 104\,\mathrm{Li}_2\left(\frac{3}{4}\right) - \frac{71}{6} + \frac{23\pi^2}{9} \\ + 192\ln^2 2 - \frac{362}{3}\ln^2 3 + \frac{544}{9}\ln 2 - \frac{100}{3}\ln 3 + \frac{56}{3}\ln 2 \ln 3. \end{aligned} \tag{5.18}$$

The NLO term has been obtained in Refs. [11, 136][2], the NNLO term is new. Again, only four decimal places are displayed and our uncertainty estimate for the numerical integration is several digits beyond that. An important consistency check is that $\langle S(t) \rangle$ can be renormalized with the flowed-quark field renormalization constant Z_χ in Eq. (2.59) such that both $\langle S(t) \rangle$ and $\langle \mathring{S}(t) \rangle$ are finite.

The logarithmic terms $s_{n,k} L^k(z)$ obey the all-order recursion formula ($1 \le k \le n$)

$$k\, s_{n,k} = \sum_{l=0}^{n-1} \left[\gamma_{m,l} + (n - l - 1)\beta_l\right] s_{n-l-1,k-1}, \tag{5.19}$$

2 To be more precise, it was computed in the arXiv version v2 of Ref. [11].

which follows from RG invariance, i.e.

$$\mu^2 \frac{\mathrm{d}^2}{\mathrm{d}\mu^2} s_f(t) = 0 \tag{5.20}$$

and the RG equations for α_s and m_f given in Eqs. (A.7) and (A.11). This again provides a welcome check of our calculation. The residual dependence on μ can be used as probe of the perturbative behavior. It is displayed in Fig. 5.3 for three values of the central energy scale $\mu_0 = (2te^{\gamma_E})^{-1/2}$, see Eq. (5.4). The curves are normalized to the LO result at the

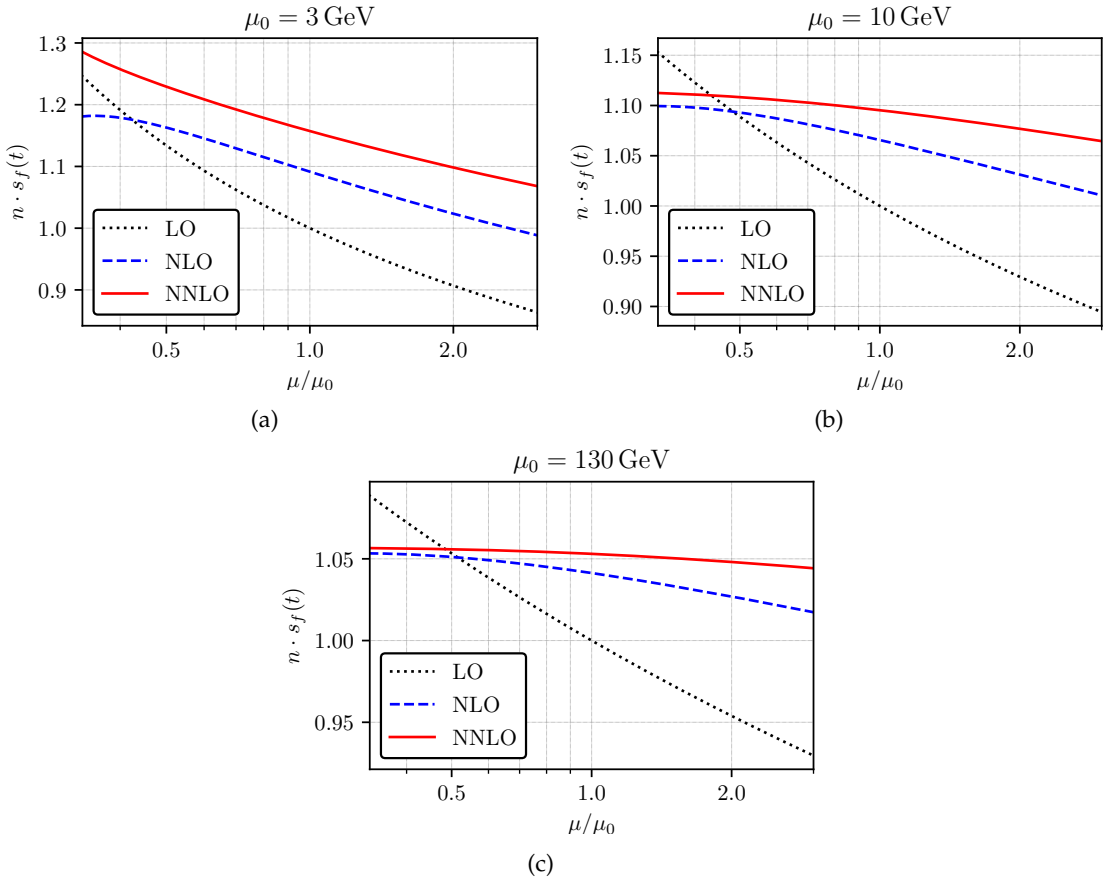

Figure 5.3: Renormalization scale dependence of $n \cdot s_f(t)$ in QCD for three different values of the central scale $\mu_0 = e^{-\gamma_E/2}/\sqrt{2t}$. The curves are normalized to the LO result, cf. Eq. (5.21). The detailed settings are given in Table 5.2.

central scale μ_0, i.e.

$$n = -\frac{8\pi^2 t}{N_C m_f(\mu_0)}. \tag{5.21}$$

We observe a qualitatively similar behavior as was found for $\langle t^2 E(t) \rangle$ in Section 5.1. While for large μ_0, the reduction of the renormalization scale dependence with increasing perturbative order is quite significant, this improvement reduces as μ_0 gets closer to the non-perturbative regime. Taking the variation of μ by a factor of two around the central

scale as an estimate of the uncertainty due to missing higher orders, one finds that they overlap between successive perturbative orders for all three values of μ_0: The NNLO corrections amount to 6.0 % at 3 GeV, 2.8 % at 10 GeV, and 1.1 % at 130 GeV, and the NLO uncertainty estimates with 6.4 %, 2.9 %, and 1.2 %, respectively, are almost of the same size. Hence, we also expect the NNLO uncertainty estimates of 5.7 %, 1.4 %, and 0.37 % to be reliable. However, the trend of the curves does not explicitly support μ_0 as the central scale in this case, but seems to favor a slightly smaller scale.

5.4 QUARK MASS EFFECTS TO $\mathcal{O}(m^2t)$

As described in the beginning of this chapter, we split the n_f quarks into n_l massless quarks and n_h degenerate massive quarks with mass m. The naive expansion in Eq. (5.1) is sufficient to calculate the quark mass effects to $\mathcal{O}(m^2t)$. Of course, the bare masses in the calculation have to be renormalized in the $\overline{\text{MS}}$ scheme according to Eq. (A.13) in addition to the renormalization in the previous sections.

For the quark mass effects for the gluon action density $\langle E(t)\rangle$, cf. in Eq. (5.2), we write

$$E^m(t,m) = m^2 t E^{(2)}(t) + \mathcal{O}(m^4t^2). \tag{5.22}$$

For the $\mathcal{O}(m^2t)$ term we find

$$E^{(2)}(t) = \frac{3\alpha_s}{4\pi t^2}\frac{N_A}{8}\cdot\frac{\alpha_s}{4\pi}16T_R n_h\left[1+\frac{\alpha_s}{4\pi}e_2^{(2)}(\mu^2 t)+\mathcal{O}(\alpha_s^3)\right] \tag{5.23}$$

with

$$e_2^{(2)}(z) = e_{2,0}^{(2)} + 2(\gamma_{m,0}+\beta_0)L(z) \tag{5.24}$$

and the non-logarithmic terms

$$e_{1,0}^{(2)} = 1, \qquad e_{2,0}^{(2)} = 29.7516\,C_A + 8\,C_F - \frac{40}{9}T_R n_f. \tag{5.25}$$

Since quark loops appear only at the two-loop level, $E^m(t,m)$ starts at $\mathcal{O}(\alpha_s^2)$. The term $e_{1,0}^{(2)}$ coincides with the limit of the exact quark mass effects at $\mathcal{O}(\alpha_s^2)$ which have been computed in Ref. [21], while the NNLO term $e_{2,0}^{(2)}$ is new. Once again, we only write the six leading digits of the numerical result even though our numerical precision is at least six order of magnitude beyond that. The logarithmic terms $e_{n,k}^{(2)}L^k(z)$ obey the all-order recursion formula ($1 \le k \le n-1$)

$$k\,e_{n,k}^{(2)} = \sum_{l=0}^{n-2}\left[2\gamma_{m,l}+(n-l)\beta_l\right]e_{n-l-1,k-1}^{(2)}, \tag{5.26}$$

which is again derived from RG invariance following Eq. (5.9) and serves as a check of our calculation.

In Fig. 5.4, we show the size of the mass effects presented above for a single heavy quark, $n_h = 1$, relative to $\langle E(t)\rangle|_{m=0}$ slightly above the charm and bottom thresholds. In addition, we show the exact mass dependence at NLO computed in Ref. [21]. The

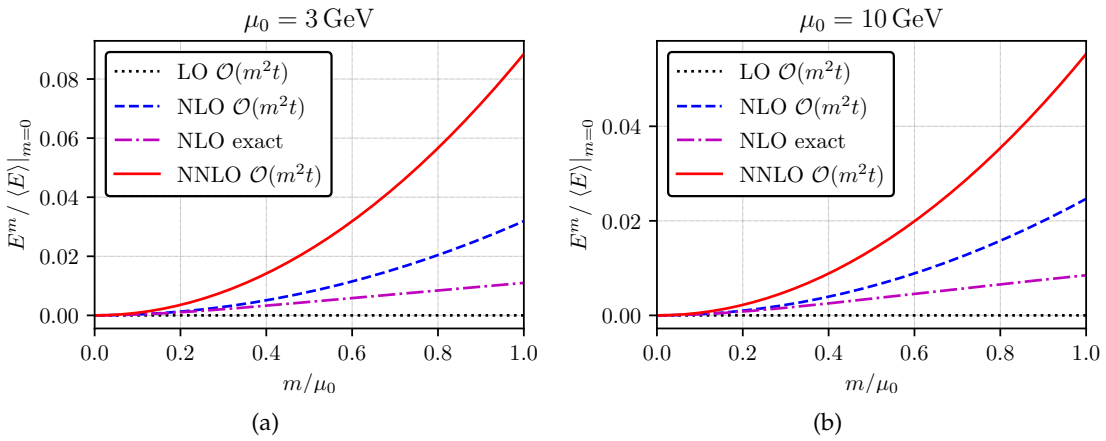

Figure 5.4: Relative size of the mass effects for $\langle E(t) \rangle$ for a single heavy quark, $n_\mathrm{h} = 1$, compared to the massless result at different orders in α_s. We use $n_\mathrm{f} = 4$ and $\alpha_\mathrm{s}^{(4)}(3\,\mathrm{GeV}) = 0.254$ at $\mu_0 = 3\,\mathrm{GeV}$ and $n_\mathrm{f} = 5$ and $\alpha_\mathrm{s}^{(5)}(10\,\mathrm{GeV}) = 0.178$ at $\mu_0 = 10\,\mathrm{GeV}$. The exact result at NLO is taken from Ref. [21].

expansion variable m^2t is rewritten as

$$m^2t = \left(\frac{m}{\sqrt{2}e^{\gamma_\mathrm{E}/2}\mu_0}\right)^2 \approx \left(\frac{m}{1.88736\,\mu_0}\right)^2. \tag{5.27}$$

The quark mass effects are negligible for small ratios m/μ_0 but reach the percent level when m and μ_0 are of a similar size. For $\mu_0 = 3\,\mathrm{GeV}$, the effect of the charm mass of $m_\mathrm{c} \approx 0.63\,\mathrm{GeV}$ corresponds to corrections of 0.14 % at NLO with $\mathcal{O}(m^2t)$ terms, 0.11 % with the exact NLO result, and 0.39 % at NNLO with $\mathcal{O}(m^2t)$. The effect of the bottom mass of $m_\mathrm{b} \approx 3.5\,\mathrm{GeV}$ at $\mu_0 = 10\,\mathrm{GeV}$ amounts to 0.30 %, 0.21 %, and 0.68 %, respectively. Interestingly, the relative size of the mass effects at $\mathcal{O}(m^2t)$ increases significantly at NNLO compared to NLO in α_s. While the mass effects are still smaller than the uncertainty estimates at NNLO in Section 5.1 for the two examples, they certainly become relevant when a smaller central renormalization scale is chosen. However, around the ratio $m/\mu_0 \approx 0.3$ the $\mathcal{O}(m^2t)$ approximation at NLO starts to significantly deviate from the exact correction. The form of the exact curve at NLO might indicate that the $\mathcal{O}(m^2t)$ results at NNLO exaggerate the exact mass effects.

The quark mass effects for $\langle \mathring{R}(t) \rangle$, cf. in Eq. (5.13), can be expressed as

$$\mathring{R}^m(t, m) = m^2 t \mathring{R}^{(2)}(t) + \mathcal{O}(m^4t^2), \tag{5.28}$$

where the NNLO result of $\mathring{R}^{(2)}(t)$ reads

$$\mathring{R}^{(2)}(t) = -\frac{2N_\mathrm{C}n_\mathrm{h}}{(4\pi t)^2} \cdot (-2)\left[1 + \frac{\alpha_\mathrm{s}}{4\pi} r_1^{(2)}(\mu^2 t) + \left(\frac{\alpha_\mathrm{s}}{4\pi}\right)^2 r_2^{(2)}(\mu^2 t) + \mathcal{O}(\alpha_\mathrm{s}^3)\right]. \tag{5.29}$$

Note that $\mathring{R}^m(t,m)$ is only proportional to the number of massive quarks n_h in contrast to $\langle\mathring{R}(t)\rangle\big|_{m=0}$ which is proportional to n_f. The coefficients read

$$\begin{aligned} r_1^{(2)}(z) &= r_{1,0}^{(2)} + 2\gamma_{m,0}\,L(z), \\ r_2^{(2)}(z) &= r_{2,0}^{(2)} + \Big[(2\gamma_{m,0}+\beta_0)r_{1,0}^{(2)} + 2\gamma_{m,1}\Big]L(z) + (2\gamma_{m,0}+\beta_0)\gamma_{m,0}\,L^2(z) \end{aligned} \tag{5.30}$$

and the non-logarithmic terms are given by

$$\begin{aligned} r_{0,0}^{(2)} &= 1, \qquad r_{1,0}^{(2)} = (7-3\ln 3)C_\mathrm{F}, \\ r_{2,0}^{(2)} &= 32.8252\,C_\mathrm{F}^2 + 33.7424\,C_\mathrm{F}C_\mathrm{A} - 4.30254\,C_\mathrm{F}T_\mathrm{R}n_\mathrm{f}. \end{aligned} \tag{5.31}$$

The logarithmic terms $r_{n,k}^{(2)}L^k(z)$ obey $(1 \le k \le n)$

$$k\,r_{n,k}^{(2)} = \sum_{l=0}^{n-1}\left[2\gamma_{m,l} + (n-l-1)\beta_l\right] r_{n-l-1,k-1}^{(2)} \tag{5.32}$$

due to RG invariance, which provides a check for our calculation.

In Fig. 5.5 we again show the relative size of the quadratic mass effects compared to $\langle\mathring{R}(t)\rangle\big|_{m=0}$. In comparison to the gluon action density, the mass effects are larger:

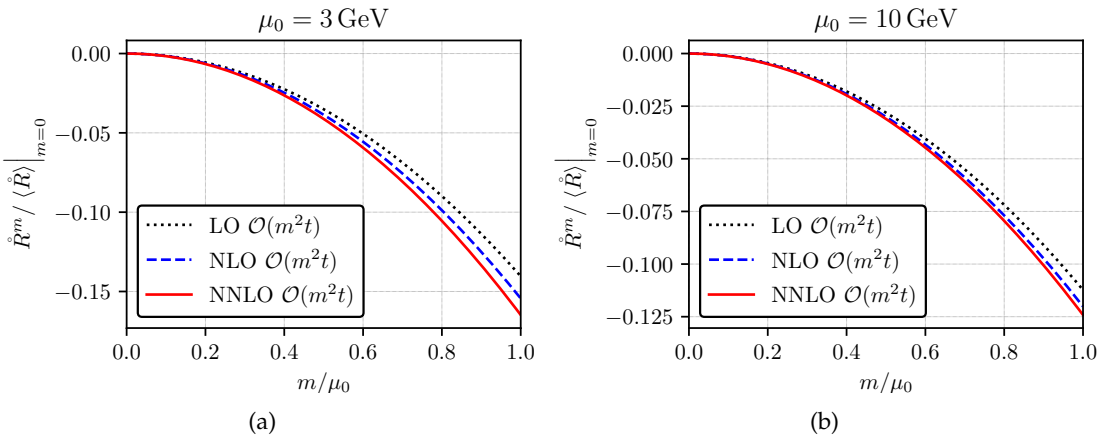

Figure 5.5: Relative size of the mass effects for $\langle\mathring{R}(t)\rangle$ for a single heavy quark, $n_\mathrm{h} = 1$ compared to the massless result at different orders in α_s. We use $n_\mathrm{f} = 4$ and $\alpha_\mathrm{s}^{(4)}(3\,\mathrm{GeV}) = 0.254$ at $\mu_0 = 3\,\mathrm{GeV}$ and $n_\mathrm{f} = 5$ and $\alpha_\mathrm{s}^{(5)}(10\,\mathrm{GeV}) = 0.178$ at $\mu_0 = 10\,\mathrm{GeV}$.

For example, for the charm mass effects at $\mu_0 = 3\,\mathrm{GeV}$, they amount to 0.62 % at LO, 0.68 % at NLO, and 0.73 % at NNLO, and for the bottom mass effects at $\mu_0 = 10\,\mathrm{GeV}$ to 1.4 % at LO, 1.5 % at NLO, and 1.5 % at NNLO, respectively. Since $\langle\mathring{R}(t)\rangle\big|_{m=0}$ is known to all orders, the mass effects constitute the main uncertainty which becomes quite sizeable when going to smaller renormalization scales due to the quadratic growth in our approximation. On the other hand, the differences between the different orders in perturbation theory are much smaller than for $\langle E(t)\rangle$. Thus, calculating the quark mass effects to higher orders in m^2t might be more relevant than to higher orders in α_s.

Higher order effects in the quark masses for the observables considered in this chapter require more sophisticated methods. On the one hand, one can perform an *expansion by regions* [137–139] to obtain results also from regions other than the "naive" region considered in this section. Luckily, those regions do not contribute up to $\mathcal{O}(m^2 t)$ in our case, but they are necessary to calculate higher order effects. On the other hand, one can perform an OPE, cf. Chapter 7, and compute the relevant operator mixing to obtain the desired quark mass effects. We leave this for future work.

5.5 GRADIENT FLOW COUPLING AND MASS

5.5.1 *Gradient Flow Coupling*

The RG invariance of $\langle E(t)\rangle$ allows us to fix a scale $\mu = \sqrt{\rho/t}$ with constant $\rho \in \mathbb{R}$, and its proportionality to α_s suggests to define a *gradient flow coupling*

$$\hat{\alpha}_\rho(\mu) \equiv \frac{32\pi\rho^2}{3N_A\mu^4}\,\langle E(\rho/\mu^2)\rangle|_{m=0} \equiv \alpha_s(\mu)\left[1+\sum_{n=1}^{\infty}\left(\frac{\alpha_s(\mu)}{4\pi}\right)^n e_n(\rho)\right]. \tag{5.33}$$

For the usual definition of the gradient flow coupling [4], ρ is set to $1/8 = 0.125$, while $\rho = \frac{1}{2e^{\gamma_E}} = 0.281\ldots$ appears to be more suitable from a perturbative point of view (cf. Eq. (5.4)).

Perturbatively solving Eq. (5.2) for α_s results in

$$\alpha_s = \hat{\alpha}_\rho\left[1-\frac{\hat{\alpha}_\rho}{4\pi}e_1(\rho)+\left(\frac{\hat{\alpha}_\rho}{4\pi}\right)^2(2e_1^2(\rho)-e_2(\rho))+\ldots\right], \tag{5.34}$$

with the coefficients $e_n(\rho)$ given in Eq. (5.5). Such a transformation between mass-independent renormalization schemes leaves the first two coefficients of the β function invariant, i.e.

$$\begin{aligned}\mu^2\frac{\mathrm{d}}{\mathrm{d}\mu^2}\hat{\alpha}_\rho(\mu) &= \hat{\alpha}_\rho(\mu)\hat{\beta}_\rho(\hat{\alpha}_\rho),\\ \hat{\beta}_\rho(\hat{\alpha}_\rho) = -\sum_{n=0}^{\infty}\left(\frac{\hat{\alpha}_\rho}{4\pi}\right)^{n+1}\hat{\beta}_{\rho,n} &= -\frac{\hat{\alpha}_\rho}{4\pi}\beta_0-\left(\frac{\hat{\alpha}_\rho}{4\pi}\right)^2\beta_1-\sum_{n=2}^{\infty}\left(\frac{\hat{\alpha}_\rho}{4\pi}\right)^{n+1}\hat{\beta}_{\rho,n}.\end{aligned} \tag{5.35}$$

The third coefficient is given by

$$\hat{\beta}_{\rho,2} = \beta_2 - e_1(\rho)\,\beta_1 + (e_2(\rho)-e_1^2(\rho))\,\beta_0, \tag{5.36}$$

with the $\overline{\text{MS}}$ coefficients β_i from Eq. (A.10).

5.5.2 *Gradient Flow Mass*

Similarly, we may define a *gradient flow quark mass* as

$$\hat{m}_f^{(\rho)}(\mu) = -\frac{8\pi^2\rho}{N_C\mu^2}m_f\frac{\mathrm{d}\langle\mathring{S}(\rho/\mu^2)\rangle}{\mathrm{d}m_f}\Big|_{m=0} = m_f(\mu)\left[1+\sum_{n=1}^{\infty}\left(\frac{\hat{\alpha}_\rho(\mu)}{4\pi}\right)^n\hat{s}_n(\rho)\right], \tag{5.37}$$

where

$$\hat{s}_1(\rho) = s_1(\rho), \qquad \hat{s}_2(\rho) = s_2(\rho) - s_1(\rho)\, e_1(\rho), \tag{5.38}$$

with the s_n and e_1 given in Eqs. (5.5) and (5.16). The inverse relation is

$$m_f = \hat{m}_f^{(\rho)} \left[1 - \frac{\hat{\alpha}_\rho}{4\pi}\, \hat{s}_1(\rho) + \left(\frac{\hat{\alpha}_\rho}{4\pi} \right)^2 (\hat{s}_1^2(\rho) - \hat{s}_2(\rho)) + \dots \right]. \tag{5.39}$$

The new mass obeys the RG equation

$$\mu^2 \frac{\mathrm{d}^2}{\mathrm{d}\mu^2} \hat{m}_f^{(\rho)}(\mu) = \hat{\gamma}_m^{(\rho)}(\hat{\alpha}_\rho)\, \hat{m}_f^{(\rho)}(\mu) \equiv -\hat{m}_f^{(\rho)}(\mu) \sum_{n=0}^{\infty} \left(\frac{\hat{\alpha}_\rho(\mu)}{4\pi} \right)^{n+1} \hat{\gamma}_{m,n}^{(\rho)} \tag{5.40}$$

where

$$\begin{aligned} \hat{\gamma}_{m,0}^{(\rho)} &= \gamma_{m,0}, \qquad \hat{\gamma}_{m,1}^{(\rho)} = \gamma_{m,1} - \gamma_{m,0}\, e_1(\rho) + \beta_0\, \hat{s}_1(\rho), \\ \hat{\gamma}_{m,2}^{(\rho)} &= \gamma_{m,2} - 2\,\gamma_{m,1}\, e_1(\rho) + \gamma_{m,0} \left[2\, e_1^2(\rho) - e_2(\rho) \right] \\ &\quad + \beta_1 \hat{s}_1(\rho) + \beta_0 \left(2\, \hat{s}_2(\rho) - \hat{s}_1^2(\rho) \right), \end{aligned} \tag{5.41}$$

with β_0, β_1, $\gamma_{m,0}$, $\gamma_{m,1}$, and $\gamma_{m,2}$ given in Eqs. (A.10) and (A.12).

5.6 CONCLUSIONS

To demonstrate the viability of our setup described in Chapters 2 to 4 and Appendix C, we reproduced and improved the three-loop result for the gluon action density of an earlier calculation, which was based on explicit field-theoretic calculations at the level of Wick contractions [21].

We then evaluated the three-loop approximations to the quark condensate and the conversion factor from $\overline{\mathrm{MS}}$ renormalized to ringed quark fields, both of which are new results. Checks on gauge parameter independence, RG invariance, as well as alternative calculational approaches (with and without reduction to master integrals) convinced us of the correctness of these results.

In addition, we studied the quark mass effects of $\mathcal{O}(m^2 t)$ on the gluon action density and the VEV of the quark kinetic operator. While they can be safely neglected as long as the quark masses are well below the scale set by the flow time t, they already become relevant sources of uncertainties for the examples slightly above the charm and bottom quark thresholds. For both observables higher orders in $m^2 t$ seem desirable.

The gluon action density and the quark condensate lend themselves for straightforward definitions of a gradient flow gauge coupling and a gradient flow quark mass, for which we derive the three-loop matching relations to the $\overline{\mathrm{MS}}$ scheme. Provided that sufficiently accurate lattice results for these quantities become available, the conversion factors evaluated in this chapter should allow for precise first-principle determinations of the gauge coupling,[3] and possibly also quark masses.

While focusing on the calculation of vacuum matrix elements in this chapter, we demonstrated that our setup is ready to be applied to other perturbative calculations in the gradient flow formalism such as those in the following chapters.

3 First steps in this direction have been taken in Ref. [140].

6

THE ENERGY-MOMENTUM TENSOR WITHIN THE GRADIENT FLOW FORMALISM

The *energy-momentum tensor* (EMT) as Noether current of the translational symmetry is a central object of every Quantum Field Theory. Especially, it contains thermodynamical information like the energy density or the pressure. Since calculations at finite temperature are hardly accessible by perturbative approaches, the lattice seems to be the ideal tool for these computations. However, the lattice breaks the translational invariance to a discretized version with severe consequences: The EMT is no longer finite and, thus, ill-defined. Refs. [141, 142] developed a strategy to construct it on the lattice, which however requires the calculation of renormalization constants. These have been calculated perturbatively to one-loop order in Refs. [143–146]. The transition to a non-perturbative definition of the EMT was not clear though.

As discussed in Section 2.4, composite operators at finite flow time t do not require UV renormalization beyond the one of the involved parameters and fields. This means that the operators do not mix under RG running, which makes it particularly simple to combine results from different regularization schemes, e.g. lattice and perturbative schemes. A particularly powerful way to exhibit this possible interplay is obtained by considering the expansion of composite operators in the limit of small flow time, which expresses flowed operators in terms of QCD operators at $t = 0$, with t-dependent Wilson coefficients [8]. This method has been used by Makino and Suzuki [10, 11] to derive a regularization-independent formula for the EMT $T_{\mu\nu}$ which has already led to promising thermodynamical results like the energy density and pressure of QCD [12–16].

Shortly after, Refs. [147, 148] presented another method to define the EMT on the lattice non-perturbatively without employing the gradient flow formalism. Nonetheless, we follow the gradient flow based approach of Refs. [10, 11] in this chapter.

In Section 6.1 we introduce the EMT of QCD as well as its flowed version with the help of the small-flow-time expansion. The universal Wilson coefficients that occur in the formula of Ref. [11] for the EMT have been calculated through NLO in perturbation theory [10, 11]. This corresponds to a one-loop calculation in the sense that it involves integrals over a single D-dimensional momentum. In this chapter, we will carry this calculation to the next perturbative order using the setup described in Chapters 2 to 4 and Appendix C. Additionally, we introduce the *method of projectors* [149, 150] in Section 6.2 to compute the Wilson coefficients. This method also plays an important role for the following chapters of this thesis.

We present our NNLO results of the Wilson coefficients of the EMT in Section 6.3. By suitable renormalization, they can be defined in such a way that they are formally renormalization scale independent. Based on the form of the analytical result, we again argue for the specific choice of μ_0 in Eq. (5.4) as renormalization scale. Our numerical study shows that the higher-order terms indeed lead to an appreciable reduction of the

μ-variation. However, by comparison of the successive higher-order terms, it appears that the uncertainty estimate from a variation within $\mu \in [\mu_0/2, 2\mu_0]$, as it is common practice in regular perturbative QCD calculation, might be too optimistic.

As pointed out in Ref. [11], the trace anomaly of the EMT allows for a welcome check of the calculation; we briefly describe the derivation of the resulting relations among the coefficient functions in Section 6.4.

While the NNLO expressions for the Wilson coefficients of the EMT are the main result of this chapter, we additionally compute the matrix of anomalous dimensions for the set of operators which form the EMT in regular QCD through NNLO in Section 6.5.

This chapter is based on Ref. [43] which itself is based on Yannick Kluth's Master's thesis [151]. Since I only had a supporting role in this project, the chapter stays close to Ref. [43] whereas Ref. [151] describes much more details. In the original publication of Ref. [43], the computation of the anomalous dimension and mixing matrices in Section 6.5 was only performed while summing the quark flavors. The same calculation distinguishing the flavors was later added as additional ancillary files to Ref. [43] as part of this thesis.

6.1 ENERGY-MOMENTUM TENSOR

In a continuous D-dimensional space-time, the gauge invariant part of the EMT reads

$$T_{\mu\nu}(x) \equiv \frac{1}{g_{\mathrm{B}}^2}\left[\mathcal{O}_{1,\mu\nu}(x) - \frac{1}{4}\mathcal{O}_{2,\mu\nu}(x)\right] + \frac{1}{4}\mathcal{O}_{3,\mu\nu}(x) - \frac{1}{2}\mathcal{O}_{4,\mu\nu}(x) - \mathcal{O}_{5,\mu\nu}(x), \tag{6.1}$$

where g_{B} is the bare coupling constant of QCD. The operators are defined as

$$\begin{aligned}
\mathcal{O}_{1,\mu\nu}(x) &\equiv F^a_{\mu\rho}(x)F^a_{\nu\rho}(x),\\
\mathcal{O}_{2,\mu\nu}(x) &\equiv \delta_{\mu\nu}F^a_{\rho\sigma}(x)F^a_{\rho\sigma}(x),\\
\mathcal{O}_{3_f,\mu\nu}(x) &\equiv \bar\psi_f(x)\left(\gamma_\mu \overleftrightarrow{D}^{\mathrm{F}}_\nu + \gamma_\nu \overleftrightarrow{D}^{\mathrm{F}}_\mu\right)\psi_f(x),\\
\mathcal{O}_{4_f,\mu\nu}(x) &\equiv \delta_{\mu\nu}\bar\psi_f(x)\overleftrightarrow{\not{D}}^{\mathrm{F}}\psi_f(x),\\
\mathcal{O}_{5_f,\mu\nu}(x) &\equiv \delta_{\mu\nu}m_{f,\mathrm{B}}\bar\psi_f(x)\psi_f(x),\\
\mathcal{O}_{i,\mu\nu}(x) &= \sum_{f=1}^{n_{\mathrm{f}}}\mathcal{O}_{i_f,\mu\nu}(x)\,, \qquad i\in\{3,4,5\},
\end{aligned} \tag{6.2}$$

where f labels the n_{f} different quark flavors, $m_{f,\mathrm{B}}$ is the bare quark mass, and

$$\overleftrightarrow{D}^{\mathrm{F}}_\mu = D^{\mathrm{F}}_\mu - \overleftarrow{D}^{\mathrm{F}}_\mu \qquad \text{with} \qquad \overleftarrow{D}^{\mathrm{F}} = \overleftarrow{\partial}_\mu - A^a_\mu T^a. \tag{6.3}$$

The notation $i_f \in \{i_1, \ldots, i_{n_{\mathrm{f}}}\}$ for the indices which label different flavors will be useful later on in this chapter. In general, $T_{\mu\nu}$ may contain gauge-dependent operators which vanish when evaluating physical matrix elements [152]. Here and in what follows, we implicitly assume that the vacuum expectations values of all composite operators have been subtracted[1] so that $\langle\mathcal{O}_{i,\mu\nu}(x)\rangle \equiv 0\ \forall i$.

1 In other words, the precise definition of $\mathcal{O}_{1,\mu\nu}$, for example, would be given by $F^a_{\mu\rho}F^a_{\rho\nu} - \langle F^a_{\mu\rho}F^a_{\rho\nu}\rangle$.

In this chapter, we will focus on the case where physical matrix elements of the EMT itself are considered, i.e. no other operator multiplies the EMT at the same space-time point. In this case, the *equations of motion* (EOM) render the set of operators in Eq. (6.2) redundant because all Green's functions including EOM vanish through the Schwinger-Dyson equations [11]. In particular, the EOM for the quark fields in regular QCD implies

$$0 = \mathcal{O}_{4,\mu\nu}(x) + 2\,\mathcal{O}_{5,\mu\nu}(x), \tag{6.4}$$

which allows us to eliminate $\mathcal{O}_{5,\mu\nu}$ from the set of operators in Eq. (6.2). Note that due to this relation, the last two terms in Eq. (6.1) cancel.

We will further assume all quark masses to be equal to each other

$$m_{f,\mathrm{B}} = m_{\mathrm{B}}, \qquad f = 1, \ldots, n_{\mathrm{f}}. \tag{6.5}$$

Therefore, the different quarks are indistinguishable and the mixing between two different quark flavors cannot depend on the flavors.

Defining the analogous operators of Eq. (6.2) for flowed fields, we write

$$\begin{aligned}
\tilde{\mathcal{O}}_{1,\mu\nu}(t,x) &\equiv G^a_{\mu\rho}(t,x)G^a_{\nu\rho}(t,x),\\
\tilde{\mathcal{O}}_{2,\mu\nu}(t,x) &\equiv \delta_{\mu\nu}G^a_{\rho\sigma}(t,x)G^a_{\rho\sigma}(t,x),\\
\tilde{\mathcal{O}}_{3_f,\mu\nu}(t,x) &\equiv Z_{\chi_f}\bar{\chi}_f(t,x)\left(\gamma_\mu \overleftrightarrow{\mathcal{D}}^{\mathrm{F}}_{\nu} + \gamma_\nu \overleftrightarrow{\mathcal{D}}^{\mathrm{F}}_{\mu}\right)\chi_f(t,x),\\
\tilde{\mathcal{O}}_{4_f,\mu\nu}(t,x) &\equiv Z_{\chi_f}\delta_{\mu\nu}\bar{\chi}_f(t,x)\overleftrightarrow{\not{\mathcal{D}}}^{\mathrm{F}}\chi_f(t,x),\\
\tilde{\mathcal{O}}_{i,\mu\nu} &= \sum_{f=1}^{n_{\mathrm{f}}}\tilde{\mathcal{O}}_{i_f,\mu\nu}, \qquad i \in \{3,4\},
\end{aligned} \tag{6.6}$$

where $Z_{\chi_f} \equiv Z_\chi$ is the renormalization constant for the flowed quark fields given in Eq. (2.59). Since we have eliminated $\mathcal{O}_{5,\mu\nu}$ from the set of operators by using Eq. (6.4), we do not need to include a flowed version of this operator in Eq. (6.6). Similar to the composite operators of regular QCD, we assume that the VEVs of the flowed composite operators have been subtracted, i.e. $\langle\tilde{\mathcal{O}}_{i,\mu\nu}(t,x)\rangle \equiv 0\ \forall i$.

We can now use the expansion in small flow time [8]

$$\tilde{\mathcal{O}}_{i,\mu\nu}(t,x) = \zeta_{ij}(t)\mathcal{O}_{j,\mu\nu}(x) + O(t), \tag{6.7}$$

to get a relation between flowed and regular QCD operators. In Eq. (6.7), and similarly in what follows, a sum $\sum_{j=1}^{4}$ is understood. The higher order terms that vanish as $t \to 0$ will be neglected throughout this thesis. As discussed above, matrix elements of the l.h.s. of this equation are finite after renormalization of the QCD parameters, while those of the regular QCD operators on the r.h.s. are in general divergent. The mixing matrix $\zeta_{ij}(t)$ will therefore be divergent as well.

Inverting Eq. (6.7) and using it to re-express the regular QCD operators in the EMT in terms of flowed fields, one arrives at

$$T_{\mu\nu}(x) = c_i(t)\tilde{\mathcal{O}}_{i,\mu\nu}(t,x), \tag{6.8}$$

where

$$c_i(t) \equiv \frac{1}{g_{\mathrm{B}}^2}\left(\zeta_{1i}^{-1}(t) - \frac{1}{4}\zeta_{2i}^{-1}(t)\right) + \frac{1}{4}\zeta_{3i}^{-1}(t), \qquad i = 1,\dots,4\,. \tag{6.9}$$

Since matrix elements of the $\tilde{\mathcal{O}}_i$ as well as the EMT itself are finite (after mass and charge renormalization), the universal coefficients $c_i(t)$ of Eq. (6.9) are finite as well. However, due to the quark-field renormalization Z_χ, the individual factors on the r.h.s. are renormalization scheme dependent. By employing ringed quark fields as discussed in Section 2.4 they become RG invariant.

As pointed out in Ref. [11], the small flow-time expansion, which is used to express the EMT in terms of flowed fields, only holds if there is no other operator contribution at the same space-time point as the EMT. Therefore we have to require that the EMT is separated from all other operators and hence we can always use EOM to arrive at Eq. (6.9), which would contain additional terms otherwise.

In Ref. [11], the coefficients $c_i(t)$ have been calculated in perturbation theory through NLO QCD. The goal of the current thesis is to evaluate them through NNLO QCD.

6.2 THE METHOD OF PROJECTORS

To compute the elements $\zeta_{ij}(t)$ of the mixing matrix we use the so-called *method of projectors* [138, 149, 150], which consists of constructing external states $|k\rangle$ and differential operators D_k such that

$$P_k[\mathcal{O}_i(x)] \equiv D_k\langle 0|\mathcal{O}_i(x)|k\rangle = \delta_{ik}, \tag{6.10}$$

where we have dropped the Lorentz indices for convenience, and we define the matrix element to include only diagrams which are *one-particle irreducible* (1PI) w.r.t. QCD particles. Applying P_k on both sides of Eq. (6.7), one obtains

$$P_k[\tilde{\mathcal{O}}_i(t,x)] = \zeta_{ij}(t)P_k[\mathcal{O}_j(x)]. \tag{6.11}$$

Since the $\zeta_{ij}(t)$ only depend on the flow time t and the renormalization scale μ, we can choose arbitrary values for all other dimensional parameters in this equation. Setting them to zero turns all higher-order corrections on the r.h.s. into massless tadpoles so that Eq. (6.10) resembles an all order equation for the regular operators. One thus obtains

$$\zeta_{ij}(t) = P_j[\tilde{\mathcal{O}}_i(t,x)]\Big|_{p=m=0}, \tag{6.12}$$

where p and m collectively denote all masses and external momenta. The r.h.s. thus results in vacuum diagrams whose only dimensional scale is t.

In order to find suitable projectors, we first derive the Feynman rules for the operators. In the case of $\mathcal{O}_{1,\mu\nu}$ this leads to the two-point vertex

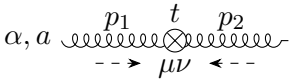

$$= g_{\mathrm{B}}^2\delta^{ab}\big[-p_{1,\mu}p_{2,\nu}\delta_{\alpha\beta} + p_{1,\beta}p_{2,\mu}\delta_{\alpha\nu} + p_{1,\nu}p_{2,\alpha}\delta_{\beta\mu} - (p_1\cdot p_2)\delta_{\alpha\nu}\delta_{\beta\mu} + (\mu\leftrightarrow\nu)\big] \tag{6.13}$$

as well as the three- and the four-point vertex in Eqs. (B.24) and (B.25) in Appendix B.3. Instead of mentioning all occurring Feynman rules for all of the following operators, we refer to Appendix B.3. The first term of Eq. (6.13) suggests to use the projector

$$P_1[X] = -\frac{\delta^{ab}}{g_{\mathrm{B}}^2 N_{\mathrm{A}}} P_{\alpha\beta|\rho\mu|\sigma\nu} \left[\frac{\partial}{\partial p_{1,\rho}} \frac{\partial}{\partial p_{2,\sigma}} \langle 0|\hat{A}^a_\alpha(p_1)\hat{A}^b_\beta(p_2)X_{\mu\nu}|0\rangle \right]_{p=m=0}, \tag{6.14}$$

where the hats on the fields denote that they are external fields. Their open indices in the matrix elements emphasize that the polarization vectors are removed from the matrix element and the indices are instead contracted with the Lorentz structure of the projector. The same holds true for all other indices of the external fields, in particular spinors when quarks are used as external state. The projector onto the Lorentz structure is defined by

$$P_{\alpha_1\beta_1|\cdots|\alpha_n\beta_n} T_{\alpha_1\beta_1\cdots\alpha_n\beta_n} = \begin{cases} 1 & \text{for } T_{\alpha_1\beta_1\cdots\alpha_n\beta_n} = \delta_{\alpha_1\beta_1}\cdots\delta_{\alpha_n\beta_n}, \\ 0 & \text{for any other linearly} \\ & \text{independent Lorentz tensor.} \end{cases} \tag{6.15}$$

It ensures that only the first term contributes at LO because all other terms have a different Lorentz structure. Since this definition does not simply contract the Lorentz indices, we have to perform a tensor reduction of the matrix elements. Using the Gram-Schmidt process, one can construct a basis of generalized, symmetric metric tensors with up to six indices, which are the only objects allowed after setting all external momenta to zero and employing symmetry arguments. This allows us to express all tensor integrals in terms of this basis and apply Eq. (6.15). We refer to Ref. [151] for more details on the tensor reduction.

Similarly, for $\mathcal{O}_{2,\mu\nu}$ with the two-point vertex

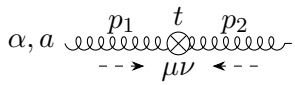

$$= g_{\mathrm{B}}^2 \delta^{ab} \delta_{\mu\nu} \left[-4(p_1 \cdot p_2)\delta_{\alpha\beta} + 4p_{1,\beta}p_{2,\alpha} \right] \tag{6.16}$$

we construct the projector

$$P_2[X] = -\frac{\delta^{ab}}{4 g_{\mathrm{B}}^2 N_{\mathrm{A}}} P_{\alpha\beta|\mu\nu|\rho\sigma} \left[\frac{\partial}{\partial p_{1,\rho}} \frac{\partial}{\partial p_{2,\sigma}} \langle 0|\hat{A}^a_\alpha(p_1)\hat{A}^b_\beta(p_2)X_{\mu\nu}|0\rangle \right]_{p=m=0}. \tag{6.17}$$

The different Lorentz structures ensure that $P_{1/2}[\mathcal{O}_{2/1}] = 0$.

The remaining operators consist of quark fields. We choose to distinguish the different quark flavors during the calculation and, hence, the two-point vertex of $\mathcal{O}_{3_f,\mu\nu}$ represented by

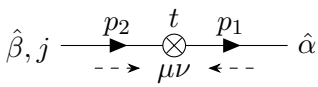

$$= \mathrm{i}\delta_{ij} \left[(p_{1,\nu} - p_{2,\nu})\gamma_\mu + (p_{1,\mu} - p_{2,\mu})\gamma_\nu \right]_{\hat{\alpha}\hat{\beta}} \tag{6.18}$$

exists once for every flavor. Therefore, we use an external state with quarks of the same flavor f for the projector

$$P_{3_f}[X] = \mathrm{i}\frac{\delta^{ij}}{4N_\mathrm{C}} P_{\rho\mu|\sigma\nu}\gamma^{\rho}_{\hat{\beta}\hat{\alpha}} \left[\frac{\partial}{\partial p_{2,\sigma}} \langle 0|\hat{\psi}^{j}_{f,\hat{\beta}}(p_2)\hat{\bar{\psi}}^{i}_{f,\hat{\alpha}}(p_1)X_{\mu\nu}|0\rangle\right]_{p=m=0}, \tag{6.19}$$

where we project onto the second term of the Feynman rule. The open spinor indices of the external quarks in the matrix element are contracted with the Dirac matrix in the projector. The ensuing trace helps to remove unwanted terms because the matrices

$$\Gamma^a = \{\mathbf{1}, \gamma_\mu, \gamma_5, \gamma_\mu\gamma_5, \sigma_{\mu\nu}\} \tag{6.20}$$

form a basis in spinor space, i.e.

$$\mathrm{Tr}[\Gamma^a\Gamma^b] \propto \delta^{ab}. \tag{6.21}$$

Similarly, for $\mathcal{O}_{4_f,\mu\nu}$ we project onto the two-point vertex

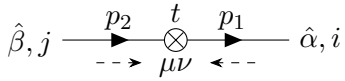

$$= \mathrm{i}\delta_{ij}\delta_{\mu\nu}\left(\not{p}_1 - \not{p}_2\right)_{\hat{\alpha}\hat{\beta}} \tag{6.22}$$

with

$$\begin{aligned} P_{4_f}[X] = \mathrm{i}\frac{\delta^{ij}}{4N_\mathrm{C}} P_{\mu\nu|\sigma\rho}\gamma^{\rho}_{\hat{\beta}\hat{\alpha}} \left[\frac{\partial}{\partial p_{2,\sigma}} \langle 0|\hat{\psi}^{j}_{f,\hat{\beta}}(p_2)\hat{\bar{\psi}}^{i}_{f,\hat{\alpha}}(p_1)X_{\mu\nu}|0\rangle\right]_{p=m=0} \\ - \frac{1}{2}\frac{\delta^{ij}}{4N_\mathrm{C}} P_{\mu\nu}\delta_{\hat{\beta}\hat{\alpha}} \left[\frac{\partial}{\partial m_\mathrm{B}} \langle 0|\hat{\psi}^{j}_{f,\hat{\beta}}(p_2)\hat{\bar{\psi}}^{i}_{f,\hat{\alpha}}(p_1)X_{\mu\nu}|0\rangle\right]_{p=m=0}. \end{aligned} \tag{6.23}$$

The second term corresponds to a projector onto $\mathcal{O}_{5_f,\mu\nu}$ with the Feynman rule

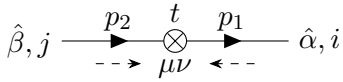

$$= \delta_{ij}\delta_{\hat{\alpha}\hat{\beta}}\delta_{\mu\nu} m_\mathrm{B} \tag{6.24}$$

so that

$$P_{4_f}[\mathcal{O}_4 + 2\mathcal{O}_5] = 0 \tag{6.25}$$

in order to ensure that only those fermionic operators are taken into account which do not vanish according to the EOM, see Eq. (6.4). If P_{4_f} is constructed this way, one does not have to include $\mathcal{O}_{5_f,\mu\nu}$ in the calculation.

With this procedure, we get a mixing matrix which distinguishes between different quark flavors. To avoid confusion with $\zeta_{ij}(t)$, which is the mixing matrix between operators summed over all flavors, we will call it $\Omega_{ij}(t)$. This matrix is then defined by

$$\tilde{\mathcal{O}}_{i,\mu\nu}(t,x) = \Omega_{ij}(t)\mathcal{O}_{j,\mu\nu}(x), \tag{6.26}$$

where double indices in this expression are summed over $\{1, 2, 3_1, \ldots, 3_{n_f}, 4_1, \ldots, 4_{n_f}\}$ (see Eq. (6.2)), in contrast to Eq. (6.8), where double indices are summed over $\{1, 2, 3, 4\}$. Its general structure is given by

$$\Omega = \begin{pmatrix} \Omega_{11} & \Omega_{12} & \underline{\Omega_{13}}^T & \underline{\Omega_{14}}^T \\ \Omega_{21} & \Omega_{22} & \underline{\Omega_{23}}^T & \underline{\Omega_{24}}^T \\ \underline{\Omega_{31}} & \underline{\Omega_{32}} & \underline{\underline{\Omega_{33}}} & \underline{\underline{\Omega_{34}}} \\ \underline{\Omega_{41}} & \underline{\Omega_{42}} & \underline{\underline{\Omega_{43}}} & \underline{\underline{\Omega_{44}}} \end{pmatrix}, \tag{6.27}$$

where an element Ω_{ij} represents the mixing between $\mathcal{O}_i$ and $\tilde{\mathcal{O}}_j$, taking into account individual flavors. Therefore, an underlined and a double underlined element denotes an n_f-dimensional vector and an $n_f \times n_f$ dimensional matrix, respectively. Their elements describe the mixing between different flavors. As the quarks are indistinguishable, the n_f and n_f^2 dimensional objects appearing in Eq. (6.27) can each be described by the two independent parameters ω_{ij} and $\overline{\omega}_{ij}$:

$$\begin{aligned} \Omega_{ij} &= \omega_{ij} \quad \text{for} \quad i, j < 3, \\ \underline{\Omega_{ij}} &= \omega_{ij} \begin{pmatrix} 1 \\ \vdots \\ 1 \end{pmatrix} \quad \text{for} \quad i < 3,\ j > 2 \quad \text{or} \quad i > 2,\ j < 3, \\ \underline{\underline{\Omega_{ij}}} &= \begin{pmatrix} \omega_{ij} & \overline{\omega}_{ij} & \overline{\omega}_{ij} & \ldots & \overline{\omega}_{ij} \\ \overline{\omega}_{ij} & \omega_{ij} & \overline{\omega}_{ij} & \ldots & \overline{\omega}_{ij} \\ \overline{\omega}_{ij} & \overline{\omega}_{ij} & \omega_{ij} & \ldots & \overline{\omega}_{ij} \\ \vdots & \vdots & \vdots & \ddots & \vdots \\ \overline{\omega}_{ij} & \overline{\omega}_{ij} & \overline{\omega}_{ij} & \ldots & \omega_{ij} \end{pmatrix} \quad \text{for} \quad i, j > 2. \end{aligned} \tag{6.28}$$

Summing over the different flavors occurring in Eq. (6.27), the relation between $\Omega(t)$ and $\zeta(t)$ can be easily established by

$$\begin{aligned} \zeta_{ij} &= \omega_{ij} && \text{for} \quad i < 3, \\ \zeta_{ij} &= n_f\, \omega_{ij} && \text{for} \quad i > 2,\ j < 3, \\ \zeta_{ij} &= \omega_{ij} + (n_f - 1)\, \overline{\omega}_{ij} && \text{for} \quad i > 2,\ j > 2. \end{aligned} \tag{6.29}$$

6.3 COEFFICIENT FUNCTIONS THROUGH NEXT-TO-NEXT-TO-LEADING ORDER

We can now compute the mixing matrices $\Omega(t)$ and $\zeta(t)$ and from them the Wilson coefficients c_i by employing the setup described in Chapters 2 to 4 and Appendix C to calculate matrix elements and then applying the projectors introduced in the previous section. The strong coupling and the quark mass require the regular QCD renormalization according to Eqs. (A.8) and (A.13) and the flowed quark fields require the renormalization with Z_χ given in Eq. (2.59), thus leading to the factor Z_χ in the definition of the operators $\tilde{\mathcal{O}}_{3,4}$ in Eq. (6.6). The finiteness of our results provides a valuable consistency check of both this calculation and our whole setup in general.[2]

2 Note that since $c_4 = 0$ at LO, this coefficient only requires NLO renormalization.

This allows us to evaluate the coefficients of the EMT in the $\overline{\text{MS}}$ scheme through NNLO QCD:

$$
\begin{aligned}
c_1(t) = \frac{1}{4\pi\alpha_\text{s}}\Bigg\{ & 1 + \frac{\alpha_\text{s}}{4\pi}\left[-\frac{7}{3}C_\text{A} + \frac{3}{2}T_\text{R}n_\text{f} - \beta_0\, L(\mu^2 t)\right] \\
& + \left(\frac{\alpha_\text{s}}{4\pi}\right)^2\Bigg[- \beta_1\, L(\mu^2 t) + C_\text{A}^2\left(-\frac{14482}{405} - \frac{16546}{135}\ln 2 + \frac{1187}{10}\ln 3\right) \\
& \quad + C_\text{A}T_\text{R}n_\text{f}\left(\frac{59}{9}\text{Li}_2\left(\frac{1}{4}\right) + \frac{10873}{810} + \frac{73}{54}\pi^2 - \frac{2773}{135}\ln 2 + \frac{302}{45}\ln 3\right) \\
& \quad + C_\text{F}T_\text{R}n_\text{f}\left(-\frac{256}{9}\text{Li}_2\left(\frac{1}{4}\right) + \frac{2587}{108} - \frac{7}{9}\pi^2 - \frac{106}{9}\ln 2 - \frac{161}{18}\ln 3\right)\Bigg] \\
& + \mathcal{O}(\alpha_\text{s}^3)\Bigg\},
\end{aligned}
\tag{6.30a}
$$

$$
\begin{aligned}
c_2(t) = \frac{1}{16\pi\alpha_\text{s}}\Bigg\{ & -1 + \frac{\alpha_\text{s}}{4\pi}\left[\frac{25}{6}C_\text{A} - 3T_\text{R}n_\text{f} + \beta_0\, L(\mu^2 t)\right] \\
& + \left(\frac{\alpha_\text{s}}{4\pi}\right)^2\Bigg[\beta_1\, L(\mu^2 t) + C_\text{A}^2\left(\frac{56713}{1620} - \frac{1187}{10}\ln 3 + \frac{16546}{135}\ln 2\right) \\
& \quad + C_\text{A}T_\text{R}n_\text{f}\left(-\frac{59}{9}\text{Li}_2\left(\frac{1}{4}\right) - \frac{6071}{405} - \frac{73}{54}\pi^2 + \frac{2287}{135}\ln 2 - \frac{361}{90}\ln 3\right) \\
& \quad + C_\text{F}T_\text{R}n_\text{f}\left(\frac{220}{9}\text{Li}_2\left(\frac{1}{4}\right) - \frac{1757}{54} + \frac{10}{9}\pi^2 - \frac{164}{9}\ln 2 + \frac{247}{9}\ln 3\right)\Bigg] \\
& + \mathcal{O}(\alpha_\text{s}^3)\Bigg\},
\end{aligned}
\tag{6.30b}
$$

$$
\begin{aligned}
c_3(t) = \frac{1}{4}\Bigg\{ & 1 + \frac{\alpha_\text{s}}{4\pi}\left(\frac{3}{2}C_\text{F} + \gamma_{\chi,0} L(\mu^2 t)\right) \\
& + \left(\frac{\alpha_\text{s}}{4\pi}\right)^2\Bigg[\frac{\gamma_{\chi,0}}{2}\left(\beta_0 + \gamma_{\chi,0}\right)\left(L^2(\mu^2 t) + L(\mu^2 t)\right) + \gamma_{\chi,1} L(\mu^2 t) \\
& \quad + C_\text{F}^2\left(-\frac{137}{9}\text{Li}_2\left(\frac{1}{4}\right) - \frac{559}{216} + \frac{103}{108}\pi^2 - \frac{1736}{27}\ln 2 + \frac{122}{3}\ln 3 - 4\ln^2 2\right) \\
& \quad + C_\text{F}T_\text{R}n_\text{f}\left(-\frac{136}{9}\text{Li}_2\left(\frac{1}{4}\right) - \frac{3377}{810} - \frac{7}{9}\pi^2 + \frac{1232}{135}\ln 2 - \frac{136}{15}\ln 3\right) \\
& \quad + C_\text{A}C_\text{F}\left(-\frac{365}{9}\text{Li}_2\left(\frac{1}{4}\right) + \frac{261829}{3240} + \frac{77}{108}\pi^2 + \frac{5788}{45}\ln 2\right.
\end{aligned}
\tag{6.30c}
$$

$$
\begin{aligned}
&\quad - \frac{2102}{15}\ln 3 - 4\ln^2 2\Big)\Big] \\
&\quad + \mathcal{O}(\alpha_s^3)\Big\},
\end{aligned}
$$

$$
\begin{aligned}
c_4(t) = \frac{C_F}{2}\Bigg\{ &\frac{\alpha_s}{4\pi} + \left(\frac{\alpha_s}{4\pi}\right)^2 \Bigg[(\beta_0 + \gamma_{\chi,0})\, L(\mu^2 t) \\
&+ C_F\left(-\frac{161}{18}\mathrm{Li}_2\left(\frac{1}{4}\right) - \frac{41}{54} - \frac{55}{108}\pi^2 - \frac{1105}{27}\ln 2 + \frac{101}{6}\ln 3\right) \\
&+ T_R n_f\left(\frac{25}{9}\mathrm{Li}_2\left(\frac{1}{4}\right) - \frac{20573}{1620} + \frac{5}{18}\pi^2 + \frac{6559}{135}\ln 2 - \frac{679}{30}\ln 3\right) \\
&+ C_A\left(\frac{257}{36}\mathrm{Li}_2\left(\frac{1}{4}\right) - \frac{137}{405} + \frac{11}{216}\pi^2 - \frac{419}{90}\ln 2 + \frac{1157}{60}\ln 3\right)\Bigg] \\
&+ \mathcal{O}(\alpha_s^3)\Bigg\},
\end{aligned}
\tag{6.30d}
$$

with $L(\mu^2 t)$ defined in Eq. (5.3). Through NLO, these results are in full agreement with those of Ref. [10, 11]. We have carried out the calculation in the general R_ξ gauge of regular QCD; the fact that the gauge-parameter dependence cancels in the final result serves as another welcome check. The gauge parameter κ of Eq. (2.2) has been set to 1.

While the EMT $T_{\mu\nu}(x)$ is renormalization-scheme independent, this is not necessarily the case for the operators $\tilde{\mathcal{O}}_{i,\mu\nu}(t,x)$ and the coefficient functions $c_i(t)$. Since $\tilde{\mathcal{O}}_{1,\mu\nu}$ and $\tilde{\mathcal{O}}_{2,\mu\nu}$ do not require operator renormalization, their matrix elements as well as the coefficient function are indeed renormalization-scheme independent. On the other hand, using the quark-field renormalization Z_χ of Eq. (2.59) in the $\overline{\text{MS}}$ scheme, matrix elements of $\tilde{\mathcal{O}}_{i,\mu\nu}$ and coefficient functions $c_i(t)$ become explicitly dependent on the renormalization scale μ for $i \in \{3,4\}$.

However, this renormalization-scheme dependence can be avoided by introducing the ringed quark fields as discussed in Section 2.4. This corresponds to replacing Z_χ in Eq. (6.6) by $\mathring{Z}_\chi$ defined in Eq. (2.62) by multiplying with ζ_χ, cf. Eq. (2.65). Indeed, dividing $c_3(t)$ and $c_4(t)$ by ζ_χ found in Eq. (5.10) renders them μ-independent up to higher order terms. This again provides a welcome consistency check.

Hence, the set of coefficients

$$
\{c_1, c_2, \mathring{c}_3, \mathring{c}_4\} \quad \text{with} \quad \mathring{c}_i \equiv \zeta_\chi^{-1} c_i \tag{6.31}
$$

is formally μ-independent, i.e.

$$
\mu^2 \frac{\mathrm{d}^2}{\mathrm{d}\mu^2}\{c_1, c_2, \mathring{c}_3, \mathring{c}_4\} = 0. \tag{6.32}
$$

As in any perturbative calculation, the μ-independence only holds up to higher orders in α_s. The decrease of the residual μ-dependence is thus commonly used as a qualitative

check of the perturbation expansion for the specific observable under consideration. We thus study the μ-dependence of the four coefficients in Eq. (6.31) by fixing a characteristic value for the flow time t and varying the renormalization scale μ around the central value μ_0 given in Eq. (5.4), i.e. $L(\mu_0^2 t) = 0$. Figs. 6.1 and 6.2 show the LO, NLO, and the NNLO approximation of c_1, c_2, $\mathring{c}_3$, and $\mathring{c}_4$ as functions of the renormalization scale for two different values of the flow time t, corresponding to $\mu_0 = 3\,\text{GeV}$ and $n_f = 3$ as well as $\mu_0 = 130\,\text{GeV}$ and $n_f = 5$, respectively.[3] The running of the coupling around the central

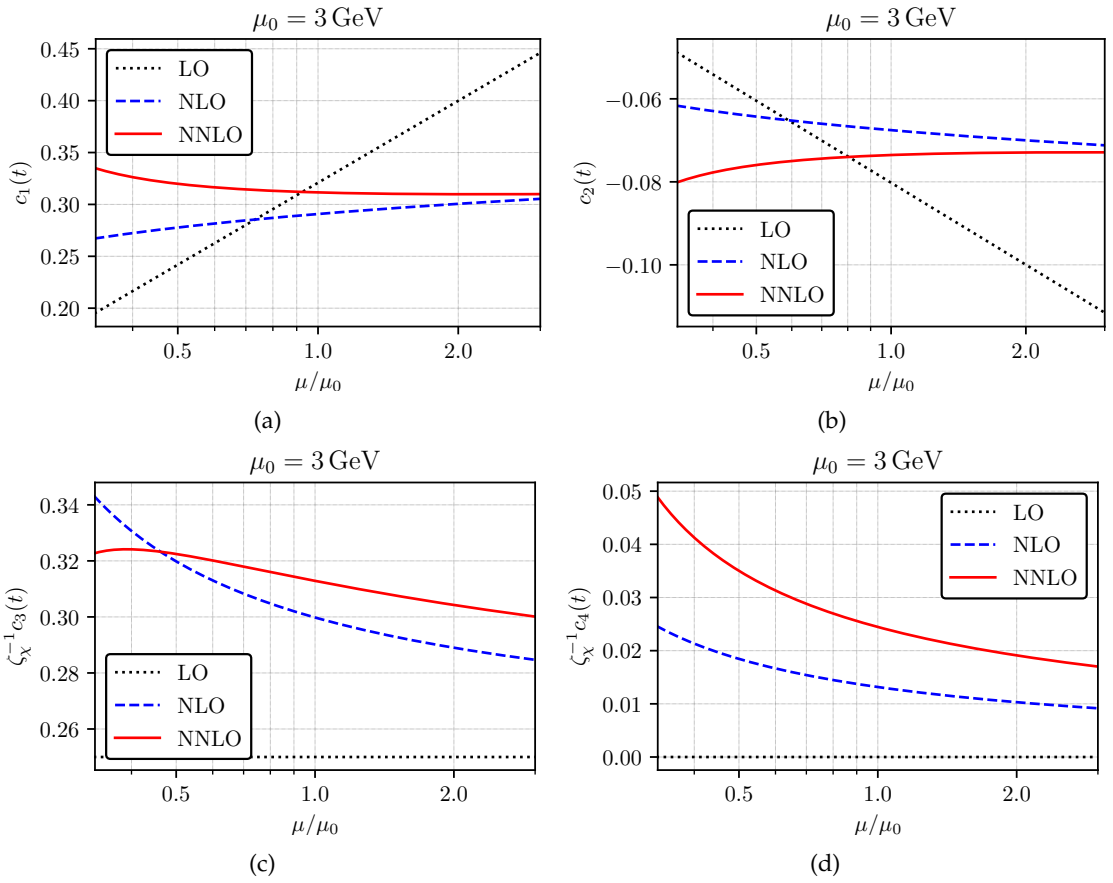

Figure 6.1: Renormalization scale dependence of the coefficients c_1, c_2, $\mathring{c}_3 = \zeta_\chi^{-1} c_3$, $\mathring{c}_4 = \zeta_\chi^{-1} c_4$ in QCD at the central scale $\mu_0 = 3\,\text{GeV}$. The detailed settings are given in Table 5.2.

values in Table 5.2 is again evaluated with the help of `RunDec` [134, 135] at one-, two-, and three-loop order for the LO, NLO, and NNLO curve, respectively. At $\mu_0 = 3\,\text{GeV}$, the NNLO corrections increase the modulus of the coefficients c_1 and c_2 by 7.1 % and 8.9 % relative to NLO, respectively. This is within twice the NLO uncertainty due to missing higher-order effects as estimated by varying μ/μ_0 between $1/2$ and 2, where one finds 3.9 % for c_1, and 4.2 % for c_2. We are therefore confident that the NNLO uncertainty

3 There is a mistake in the running for the 3 GeV plots of Ref. [43] which exaggerates the breakdown of perturbation theory for small values of μ/μ_0. Hence, the uncertainties at 3 GeV were overestimated. This is corrected in this thesis.

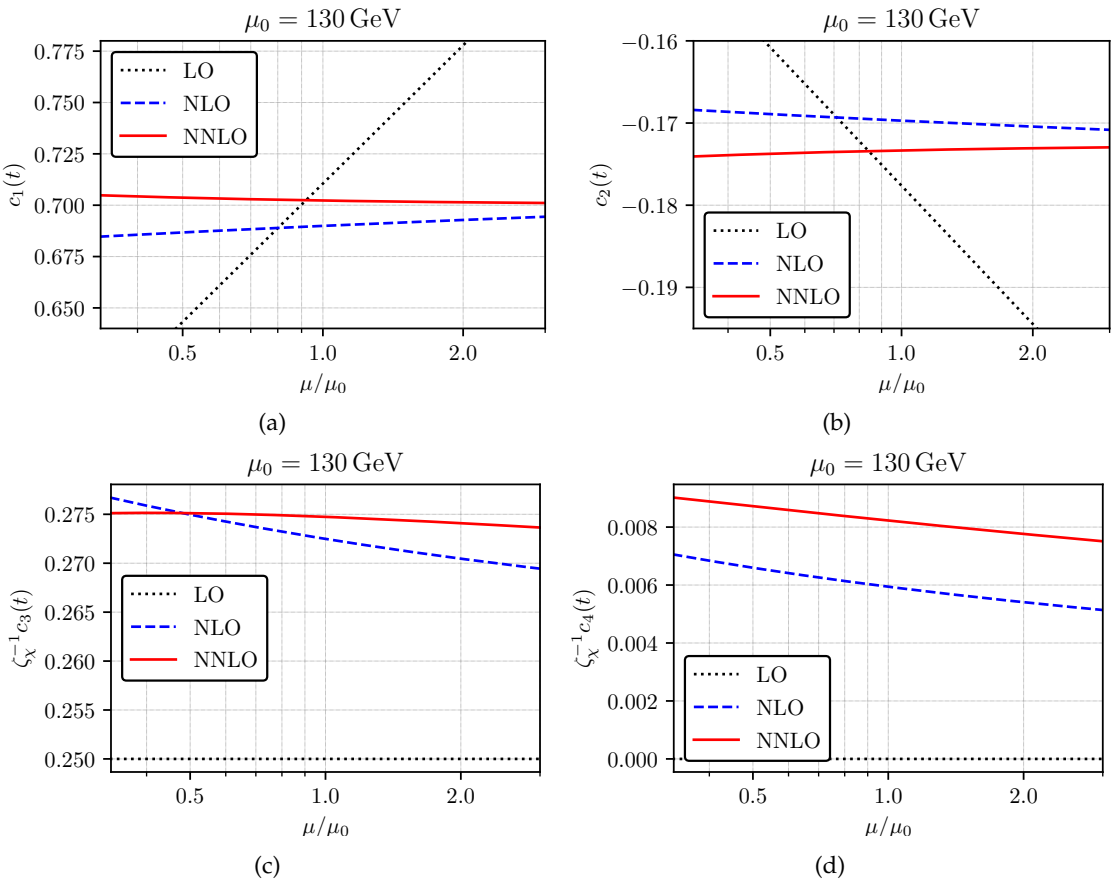

Figure 6.2: Renormalization scale dependence of the coefficients c_1, c_2, $\mathring{c}_3 = \zeta_\chi^{-1} c_3$, $\mathring{c}_4 = \zeta_\chi^{-1} c_4$ in QCD at the central scale $\mu_0 = 130\,\mathrm{GeV}$. The detailed settings are given in Table 5.2.

estimated in the same way is rather reliable: it is given by 1.6 % for c_1 and 2.0 % for c_2. Note that the dominant contribution to these numbers comes from the downward variation of μ, where $\alpha_s(\mu)$ starts to become sensitive to the non-perturbative region.

As opposed to the gluonic coefficients c_1 and c_2, the coefficients of the fermionic operators c_3 and c_4 exhibit a residual scale dependence only from the NLO term onwards. One therefore expects a stronger μ-dependence at NNLO for these terms. Nevertheless, for $\mathring{c}_3$, the estimate of the theory uncertainty due to scale variation still decreases from 5.1 % to 2.9 %. The increase of the result due to the NNLO effects is 4.4 % relative to the NLO result at $\mu = \mu_0$.

The behavior of $\mathring{c}_4$, on the other hand, is less satisfactory at $\mu_0 = 3\,\mathrm{GeV}$. The NNLO effects nearly double the NLO result in this case, and the uncertainty estimate due to scale variation actually *increases* from 31 % to 33 % when going from NLO to NNLO. Note, however, that $c_4 = 0$ at LO, which means that this coefficient is numerically sub-dominant.

As one would expect, for $\mu_0 = 130\,\mathrm{GeV}$, the perturbative behavior of all coefficients is significantly improved, cf. Fig. 6.2. For c_1, c_2, and $\mathring{c}_3$, the scale uncertainty is at the

sub-percent level already at NLO; at NNLO, it amounts to less than 0.2 % in all three cases. The effect of the NNLO corrections relative to the NLO result is 1.8 % for c_1, 2.1 % for c_2, and 0.83 % for $\mathring{c}_3$. Also for $\mathring{c}_4$, the situation improves significantly: the NNLO terms add 38 % to the NLO result, and the uncertainty goes down from 10 % at NLO to 5.8 % at NNLO.

It is also worth pointing out that the choice of the central scale μ_0 as defined in Eq. (5.4) seems justified by the behavior of the successively higher orders. In almost all cases, the NLO and the NNLO corrections are *both* relatively small at $\mu = \mu_0$. At the same time, the NNLO corrections relative to the NLO result are always smaller than the NLO corrections compared to the LO result. The only exception to this is $\mathring{c}_4$ at $\mu_0 = 3\,\text{GeV}$, where, however, no choice of μ seems to stand out over any other.

However, the NLO and NNLO uncertainty bands, derived from scale variation as described above, do not always overlap. Since the proximity of the non-perturbative region in the case $\mu_0 = 3\,\text{GeV}$ leads to a relatively large NNLO uncertainty band, this effect is less pronounced in this case compared to the situation for $\mu_0 = 130\,\text{GeV}$. In the latter case, the distance between the uncertainty intervals suggests a more conservative error estimate of at least twice the one obtained from varying μ/μ_0 within $[1/2, 2]$.

In summary, we conclude that the NNLO terms lead to a significant improvement of the perturbative accuracy of the Wilson coefficients. The perturbative behavior, however, makes it desirable to aim for the next order in perturbation theory, in order to firmly pin down the remaining uncertainty.

6.4 TRACE ANOMALY

As a test of our result, we use the trace anomaly of the EMT. As suggested in Ref. [152], a simple derivation consists of taking the trace of the EMT in $D = 4 - 2\epsilon$ dimensions. By use of the EOM, this gives for the gauge invariant part

$$T_{\mu\mu} = \frac{\epsilon}{2g_{\text{B}}^2} F^a_{\rho\sigma} F^a_{\rho\sigma} - \sum_{f=1}^{n_{\text{f}}} m_{f,\text{B}} \bar{\psi}_f \psi_f = \frac{1}{2D} \left(\frac{\epsilon}{g_{\text{B}}^2} \mathcal{O}_{2,\mu\mu} + \mathcal{O}_{4,\mu\mu} \right), \tag{6.33}$$

where we have used Eq. (6.4) in the last step. At LO in perturbation theory, the first term of Eq. (6.33) vanishes in four dimensions. However, since the operators in this expression are understood as bare, it generates finite terms at higher orders. Using the mixing matrix $\zeta_{ij}(t)$, we can rewrite this in terms of flowed operators:

$$T_{\mu\mu} = \bar{c}_i(t) \tilde{\mathcal{O}}_{i,\mu\mu}(t,x), \qquad \bar{c}_i(t) = \frac{1}{2D} \left(\frac{\epsilon}{g_{\text{B}}^2} \zeta_{2i}^{-1}(t) + \zeta_{4i}^{-1}(t) \right). \tag{6.34}$$

Note that $\bar{c}_1(t) = \bar{c}_3(t) = 0$, as $\tilde{\mathcal{O}}_{1,\mu\nu}(t,x)$ and $\tilde{\mathcal{O}}_{3,\mu\nu}(t,x)$ have a non-trivial index structure and therefore $\mathcal{O}_{2,\mu\nu}(x)$ and $\mathcal{O}_{4,\mu\nu}(x)$ cannot mix with them. Since $\tilde{\mathcal{O}}_{2,\mu\mu} = D\tilde{\mathcal{O}}_{1,\mu\mu}$ and $2\tilde{\mathcal{O}}_{4,\mu\mu} = D\tilde{\mathcal{O}}_{3,\mu\mu}$, we cannot equate coefficients with Eq. (6.8) for all i individually. Instead, only the weaker conditions

$$c_1(t) + Dc_2(t) = D\bar{c}_2(t), \qquad 2c_3(t) + Dc_4(t) = D\bar{c}_4(t). \tag{6.35}$$

can be derived. We checked that these equations are indeed fulfilled by our result.

6.5 OPERATOR RENORMALIZATION

Using the fact that flowed operators are finite after mass and field renormalization, we can also compute the renormalization matrix for the regular QCD operators $\{\mathcal{O}_{1,\mu\nu}(x), \mathcal{O}_{2,\mu\nu}(x), \mathcal{O}_{3_f,\mu\nu}(x), \mathcal{O}_{4_f,\mu\nu}(x)\}$ where $f = 1, \ldots, n_\mathrm{f}$ labels the quark flavor, i.e. the indices in this section run over $\{1, 2, 3_1, \ldots, 3_{n_\mathrm{f}}, 4_1, \ldots, 4_{n_\mathrm{f}}\}$. Thus, in contrast to the set of operators in Eq. (6.2) we distinguish quark flavors in this section. The original publication of Ref. [43] only considered the flavor summed operators and the discussion for the non-summed operators was later added as an ancillary file to the arXiv version.

Similar to $\Omega_{ij}(t)$, cf. Eqs. (6.26) to (6.28), the matrices in this section which distinguish the quark flavor can be expressed as

$$M_\mathrm{F} = \begin{pmatrix} M_{\mathrm{F},11} & M_{\mathrm{F},12} & \underline{M_{\mathrm{F},13}}^\mathrm{T} & \underline{M_{\mathrm{F},14}}^\mathrm{T} \\ M_{\mathrm{F},21} & M_{\mathrm{F},22} & \underline{M_{\mathrm{F},23}}^\mathrm{T} & \underline{M_{\mathrm{F},24}}^\mathrm{T} \\ \underline{M_{\mathrm{F},31}} & \underline{M_{\mathrm{F},32}} & \underline{\underline{M_{\mathrm{F},33}}} & \underline{\underline{M_{\mathrm{F},34}}} \\ \underline{M_{\mathrm{F},41}} & \underline{M_{\mathrm{F},42}} & \underline{\underline{M_{\mathrm{F},43}}} & \underline{\underline{M_{\mathrm{F},44}}} \end{pmatrix} \tag{6.36}$$

with

$$\begin{aligned} M_{\mathrm{F},ij} &= m_{\mathrm{F},ij} \quad \text{for} \quad i,j < 3, \\ \underline{M_{\mathrm{F},ij}} &= m_{\mathrm{F},ij} \begin{pmatrix} 1 \\ \vdots \\ 1 \end{pmatrix} \quad \text{for} \quad i < 3,\ j > 2 \quad \text{or} \quad i > 2,\ j < 3, \\ \underline{\underline{M_{\mathrm{F},ij}}} &= \begin{pmatrix} m_{\mathrm{F},ij} & \overline{m}_{\mathrm{F},ij} & \overline{m}_{\mathrm{F},ij} & \ldots & \overline{m}_{\mathrm{F},ij} \\ \overline{m}_{\mathrm{F},ij} & m_{\mathrm{F},ij} & \overline{m}_{\mathrm{F},ij} & \ldots & \overline{m}_{\mathrm{F},ij} \\ \overline{m}_{\mathrm{F},ij} & \overline{m}_{\mathrm{F},ij} & m_{\mathrm{F},ij} & \ldots & \overline{m}_{\mathrm{F},ij} \\ \vdots & \vdots & \vdots & \ddots & \vdots \\ \overline{m}_{\mathrm{F},ij} & \overline{m}_{\mathrm{F},ij} & \overline{m}_{\mathrm{F},ij} & \ldots & m_{\mathrm{F},ij} \end{pmatrix} \quad \text{for} \quad i,j > 2. \end{aligned} \tag{6.37}$$

They are related to the matrices which are summed over the flavor by

$$\begin{aligned} M_{ij} &= m_{\mathrm{F},ij} && \text{for} \quad i < 3, \\ M_{ij} &= n_\mathrm{f}\, m_{\mathrm{F},ij} && \text{for} \quad i > 2,\ j < 3, \\ M_{ij} &= m_{\mathrm{F},ij} + (n_\mathrm{f} - 1)\, \overline{m}_{\mathrm{F},ij} && \text{for} \quad i > 2,\ j > 2. \end{aligned} \tag{6.38}$$

These are the same relations as for $\zeta \leftrightarrow \Omega$ in Eq. (6.29).

It is convenient to define an equivalent set of operators as

$$\hat{\mathcal{O}}_{i,\mu\nu}(x) = H_{\mathrm{F},ij}\mathcal{O}_{j,\mu\nu}(x), \qquad \text{where} \quad H_{\mathrm{F},ij} = \begin{cases} 1/g_\mathrm{B}^2 & \text{for } i = j \in \{1,2\}, \\ 1 & \text{for } i = j \in \{3_f, 4_f\}, \\ 0 & \text{for } i \neq j, \end{cases} \tag{6.39}$$

where the subscript F indicates that the quark flavors are distinguished as described above in contrast to the equivalent matrix in Ref. [43]. This multiplication of $\mathcal{O}_{1,\mu\nu}$ and

$\mathcal{O}_{2,\mu\nu}$ by $1/g_{\mathrm{B}}^2$ ensures that the mass dimension of all operators $\hat{\mathcal{O}}_{i,\mu\nu}$ is equal to D. A similar redefinition of the flowed operators is appropriate:

$$\mathring{\mathcal{O}}_{i,\mu\nu}(t,x) = \tilde{H}_{\mathrm{F},ij}\tilde{\mathcal{O}}_{j,\mu\nu}(t,x), \qquad \text{where} \quad \tilde{H}_{\mathrm{F},ij} = \begin{cases} 1/(\hat{\mu}^{\epsilon}g)^2 & \text{for } i=j\in\{1,2\}, \\ \zeta_\chi & \text{for } i=j\in\{3_f,4_f\}, \\ 0 & \text{for } i\neq j, \end{cases} \tag{6.40}$$

where the multiplication of $\tilde{\mathcal{O}}_{3_f,\mu\nu}$ and $\tilde{\mathcal{O}}_{4_f,\mu\nu}$ by ζ_χ ensures that they are RG invariant, cf. Section 2.4. Keeping track of the non-integer mass dimension of $\mathring{\mathcal{O}}_{1,\mu\nu}$ and $\mathring{\mathcal{O}}_{2,\mu\nu}$ becomes relevant in Chapter 7. The renormalization matrix for the regular operators is then defined as

$$\{\hat{\mathcal{O}}_{i,\mu\nu}\}_{\mathrm{R}}(x) = Z_{\mathrm{F},ij}\hat{\mathcal{O}}_{j,\mu\nu}(x). \tag{6.41}$$

Expressing the $\hat{\mathcal{O}}_{i,\mu\nu}(x)$ in terms of flowed operators $\mathring{\mathcal{O}}_{i,\mu\nu}(t,x)$, one can determine its entries in the $\overline{\mathrm{MS}}$ scheme by demanding that

$$\{\hat{\mathcal{O}}_{i,\mu\nu}\}_{\mathrm{R}}(x) = Z_{\mathrm{F},ij}\,H_{\mathrm{F},jk}\,\Omega^{-1}_{kl}(t)\,\tilde{H}^{-1}_{\mathrm{F},lm}\,\mathring{\mathcal{O}}_{m,\mu\nu}(t,x) \equiv M_{\mathrm{F},im}(t)\,\mathring{\mathcal{O}}_{m,\mu\nu}(t,x) \tag{6.42}$$

be finite, where Ω_{kl} was defined in Eq. (6.26) and $M_{\mathrm{F},il}(t)$ is the mixing matrix between the renormalized regular and ringed flowed operators.

In analogy to Eqs. (2.59) and (A.13), we write

$$Z_{\mathrm{F},ij} = \delta_{ij} - \frac{\alpha_{\mathrm{s}}}{4\pi}\frac{\Gamma_{\mathrm{F},0,ij}}{\epsilon} + \left(\frac{\alpha_{\mathrm{s}}}{4\pi}\right)^2\left[\frac{1}{2\epsilon^2}\left(\Gamma_{\mathrm{F},0,ik}\Gamma_{\mathrm{F},0,kj} + \beta_0\Gamma_{\mathrm{F},0,ij}\right) - \frac{\Gamma_{\mathrm{F},1,ij}}{2\epsilon}\right] + \mathcal{O}(\alpha_{\mathrm{s}}^3), \tag{6.43}$$

where the anomalous dimension matrices $\Gamma_{\mathrm{F},n}$ also have the form in Eqs. (6.36) and (6.37). For the individual matrix elements at NLO we find

$$\begin{aligned}
&\gamma_{\mathrm{F},0,11} = -\frac{4}{3}T_{\mathrm{R}}n_{\mathrm{f}}, && \gamma_{\mathrm{F},0,12} = \frac{11}{12}C_{\mathrm{A}}, && \gamma_{\mathrm{F},0,13} = \frac{2}{3}C_{\mathrm{F}}, && \gamma_{\mathrm{F},0,14} = \frac{7}{6}C_{\mathrm{F}}, \\
&\gamma_{\mathrm{F},0,21} = 0, && \gamma_{\mathrm{F},0,22} = \frac{11}{3}C_{\mathrm{A}} - \frac{4}{3}T_{\mathrm{R}}n_{\mathrm{f}}, && \gamma_{\mathrm{F},0,23} = 0, && \gamma_{\mathrm{F},0,24} = 6C_{\mathrm{F}}, \\
&\gamma_{\mathrm{F},0,31} = \frac{16}{3}T_{\mathrm{R}}, && \gamma_{\mathrm{F},0,32} = -\frac{4}{3}T_{\mathrm{R}}, && \gamma_{\mathrm{F},0,33} = -\frac{8}{3}C_{\mathrm{F}}, && \gamma_{\mathrm{F},0,34} = \frac{4}{3}C_{\mathrm{F}}, \\
&\gamma_{\mathrm{F},0,41} = 0, && \gamma_{\mathrm{F},0,42} = 0, && \gamma_{\mathrm{F},0,43} = 0, && \gamma_{\mathrm{F},0,44} = 0.
\end{aligned} \tag{6.44}$$

and

$$\overline{\gamma}_{\mathrm{F},0,ij} = 0 \quad \forall\, i,j, \tag{6.45}$$

which is in agreement with Ref. [11] when Eq. (6.38) is used. At NNLO, we find

$$\begin{aligned}
\gamma_{\mathrm{F},1,11} &= -\frac{70}{27}C_\mathrm{A}T_\mathrm{R}n_\mathrm{f} - \frac{148}{27}C_\mathrm{F}T_\mathrm{R}n_\mathrm{f}, & \gamma_{\mathrm{F},1,12} &= \frac{17}{3}C_\mathrm{A}^2 - \frac{56}{27}C_\mathrm{A}T_\mathrm{R}n_\mathrm{f} - \frac{5}{27}C_\mathrm{F}T_\mathrm{R}n_\mathrm{f}, \\
\gamma_{\mathrm{F},1,13} &= \frac{94}{27}C_\mathrm{A}C_\mathrm{F} - \frac{28}{27}C_\mathrm{F}^2 - \frac{52}{27}C_\mathrm{F}T_\mathrm{R}n_\mathrm{f}, & \gamma_{\mathrm{F},1,14} &= \frac{406}{27}C_\mathrm{A}C_\mathrm{F} + \frac{85}{54}C_\mathrm{F}^2 - \frac{22}{27}C_\mathrm{F}T_\mathrm{R}n_\mathrm{f}, \\
\gamma_{\mathrm{F},1,21} &= 0, & \gamma_{\mathrm{F},1,22} &= \frac{68}{3}C_\mathrm{A}^2 - \frac{40}{3}C_\mathrm{A}T_\mathrm{R}n_\mathrm{f} - 8C_\mathrm{F}T_\mathrm{R}n_\mathrm{f}, \\
\gamma_{\mathrm{F},1,23} &= 0, & \gamma_{\mathrm{F},1,24} &= \frac{194}{3}C_\mathrm{A}C_\mathrm{F} + 6C_\mathrm{F}^2 - \frac{40}{3}C_\mathrm{F}T_\mathrm{R}n_\mathrm{f}, \\
\gamma_{\mathrm{F},1,31} &= \frac{280}{27}C_\mathrm{A}T_\mathrm{R} + \frac{592}{27}C_\mathrm{F}T_\mathrm{R}, & \gamma_{\mathrm{F},1,32} &= -\frac{136}{27}C_\mathrm{A}T_\mathrm{R} - \frac{196}{27}C_\mathrm{F}T_\mathrm{R}, \\
\gamma_{\mathrm{F},1,33} &= -\frac{376}{27}C_\mathrm{A}C_\mathrm{F} + \frac{112}{27}C_\mathrm{F}^2 + \frac{80}{27}C_\mathrm{F}T_\mathrm{R} + \frac{128}{27}C_\mathrm{F}T_\mathrm{R}n_\mathrm{f}, & & \\
\gamma_{\mathrm{F},1,34} &= \frac{122}{27}C_\mathrm{A}C_\mathrm{F} - \frac{8}{27}C_\mathrm{F}^2 - \frac{232}{27}C_\mathrm{F}T_\mathrm{R} - \frac{40}{27}C_\mathrm{F}T_\mathrm{R}n_\mathrm{f}, & & \\
\gamma_{\mathrm{F},1,41} &= \gamma_{\mathrm{F},1,42} = \gamma_{\mathrm{F},1,43} = \gamma_{\mathrm{F},1,44} = 0. & &
\end{aligned} \tag{6.46}$$

and

$$\overline{\gamma}_{\mathrm{F},1,33} = \frac{80}{27}C_\mathrm{F}T_\mathrm{R}, \quad \overline{\gamma}_{\mathrm{F},1,34} = -\frac{232}{27}C_\mathrm{F}T_\mathrm{R}, \quad \overline{\gamma}_{\mathrm{F},1,ij} = 0 \quad \text{for all other } i,j. \tag{6.47}$$

Utilizing Eq. (6.38), this agrees with our flavor summed matrix in Ref. [43].

Of course, Eq. (6.42) also allows us to express the renormalized regular operators through their flowed counterparts. Expanding it in terms of the individual operators, we find

$$\begin{aligned}
\{\hat{\mathcal{O}}_{i,\mu\nu}\}_\mathrm{R}(x) = {} & m_{\mathrm{F},i1}(t)\,\mathring{\mathcal{O}}_{1,\mu\nu}(t,x) + m_{\mathrm{F},i2}(t)\,\mathring{\mathcal{O}}_{2,\mu\nu}(t,x) \\
& + m_{\mathrm{F},i3}(t)\,\mathring{\mathcal{O}}_{3,\mu\nu}(t,x) + m_{\mathrm{F},i4}(t)\,\mathring{\mathcal{O}}_{4,\mu\nu}(t,x) \quad \text{for} \quad i = 1,2,
\end{aligned} \tag{6.48}$$

where

$$\mathring{\mathcal{O}}_{i,\mu\nu} = \sum_{f=1}^{n_\mathrm{f}} \mathring{\mathcal{O}}_{i_f,\mu\nu} \quad \text{for} \quad i = 3,4, \tag{6.49}$$

and

$$\begin{aligned}
\{\hat{\mathcal{O}}_{i_f,\mu\nu}\}_\mathrm{R}(x) = {} & m_{\mathrm{F},i1}(t)\,\mathring{\mathcal{O}}_{1,\mu\nu}(t,x) + m_{\mathrm{F},i2}(t)\,\mathring{\mathcal{O}}_{2,\mu\nu}(t,x) \\
& + m_{\mathrm{F},i3}(t)\,\mathring{\mathcal{O}}_{3_f,\mu\nu}(t,x) + m_{\mathrm{F},i4}(t)\,\mathring{\mathcal{O}}_{4_f,\mu\nu}(t,x) \\
& + \sum_{f'\neq f}\left[\overline{m}_{\mathrm{F},i3}(t)\,\mathring{\mathcal{O}}_{3_{f'},\mu\nu}(t,x) + \overline{m}_{\mathrm{F},i4}(t)\,\mathring{\mathcal{O}}_{4_{f'},\mu\nu}(t,x)\right] \quad \text{for} \quad i = 3,4.
\end{aligned} \tag{6.50}$$

For example, the gluonic energy-density operator can be expressed through

$$
\begin{aligned}
\left\{\frac{1}{g_{\mathrm{B}}^2}F_{\mu\nu}(x)F_{\mu\nu}(x)\right\}_{\mathrm{R}} &= \frac{1}{D}\left[m_{\mathrm{F},22}(t)\,\mathring{\mathcal{O}}_{2,\mu\mu}(t,x)+m_{\mathrm{F},24}(t)\,\mathring{\mathcal{O}}_{4,\mu\mu}\right]\\
&= \frac{1}{4\pi\alpha_{\mathrm{s}}}G_{\mu\nu}(t,x)G_{\mu\nu}(t,x)\Bigg\{1-\frac{7}{2}C_{\mathrm{A}}\frac{\alpha_{\mathrm{s}}}{4\pi}\\
&\quad+\left(\frac{\alpha_{\mathrm{s}}}{4\pi}\right)^2\Bigg[\left(-\frac{3}{2}\,C_{\mathrm{A}}^2-2\,C_{\mathrm{A}}T_{\mathrm{R}}n_{\mathrm{f}}-14\,C_{\mathrm{F}}T_{\mathrm{R}}n_{\mathrm{f}}\right)L(\mu^2t)\\
&\qquad+C_{\mathrm{A}}^2\left(-\frac{1427}{180}+\frac{87}{5}\ln 2-\frac{54}{5}\ln 3\right)+\frac{8}{9}\,C_{\mathrm{A}}T_{\mathrm{R}}n_{\mathrm{f}}-\frac{34}{3}\,C_{\mathrm{F}}T_{\mathrm{R}}n_{\mathrm{f}}\Bigg]+\mathcal{O}(\alpha_{\mathrm{s}}^3)\Bigg\}\\
&\quad+\mathring{Z}_\chi\sum_{f=1}^{n_{\mathrm{f}}}\bar{\chi}_f(t,x)\overleftrightarrow{\mathcal{D}}^{\mathrm{F}}\chi_f(t,x)\Bigg\{\frac{\alpha_{\mathrm{s}}}{4\pi}\left(5C_{\mathrm{F}}+2\gamma_{\chi,0}L(\mu^2t)\right)\\
&\quad+\left(\frac{\alpha_{\mathrm{s}}}{4\pi}\right)^2\Bigg[2\gamma_{\chi,0}\beta_0L^2(\mu^2t)\\
&\qquad+\left(\frac{304}{3}\,C_{\mathrm{A}}C_{\mathrm{F}}+C_{\mathrm{F}}^2\,(3+24\ln 2+18\ln 3)-\frac{80}{3}\,C_{\mathrm{F}}T_{\mathrm{R}}n_{\mathrm{f}}\right)L(\mu^2t)\\
&\qquad+C_{\mathrm{A}}C_{\mathrm{F}}\left(-2\,\mathrm{Li}_2\left(\frac{1}{4}\right)+\frac{2923}{30}-\frac{4}{3}\pi^2+\frac{8546}{15}\ln 2-\frac{2139}{5}\ln 3\right)\\
&\qquad+C_{\mathrm{F}}^2\,(6+20\ln 2+15\ln 3)-C_{\mathrm{F}}T_{\mathrm{R}}n_{\mathrm{f}}\left(30+\frac{4}{3}\pi^2\right)\Bigg]+\mathcal{O}(\alpha_{\mathrm{s}}^3)\Bigg\}.
\end{aligned}
\tag{6.51}
$$

Through NLO, this result agrees with Refs. [11, 153]. For the quark kinetic operator we find

$$
\begin{aligned}
\left\{\bar{\psi}_f(x)\overleftrightarrow{\not{D}}^{\mathrm{F}}\psi_f(x)\right\}_{\mathrm{R}} &= \frac{1}{D}\left[m_{\mathrm{F},42}(t)\mathring{\mathcal{O}}_{2,\mu\mu}(t,x)+m_{\mathrm{F},44}(t)\mathring{\mathcal{O}}_{4_f,\mu\mu}+\overline{m}_{\mathrm{F},44}(t)\sum_{f'\neq f}\mathring{\mathcal{O}}_{4_{f'},\mu\mu}(t,x)\right]\\
&= \frac{1}{4\pi\alpha_{\mathrm{s}}}G_{\mu\nu}(t,x)G_{\mu\nu}(t,x)\Bigg\{-\frac{5}{3}T_{\mathrm{R}}\frac{\alpha_{\mathrm{s}}}{4\pi}\\
&\quad+\left(\frac{\alpha_{\mathrm{s}}}{4\pi}\right)^2\Bigg[C_{\mathrm{A}}T_{\mathrm{R}}\left(-\frac{17}{15}-\frac{36}{5}\ln 2+\frac{27}{5}\ln 3\right)+C_{\mathrm{F}}T_{\mathrm{R}}\Bigg(8\,\mathrm{Li}_2\left(\frac{3}{4}\right)-\frac{19}{6}-\frac{2}{3}\pi^2\\
&\qquad-60\ln 2+37\ln 3+32\ln^2 2-16\ln 2\ln 3\Bigg)\Bigg]+\mathcal{O}(\alpha_{\mathrm{s}}^3)\Bigg\}\\
&\quad+Z_\chi\bar{\chi}_f(t,x)\overleftrightarrow{\not{D}}^{\mathrm{F}}\chi_f(t,x)\Bigg\{1+\frac{\alpha_{\mathrm{s}}}{4\pi}C_{\mathrm{F}}\left(-\frac{1}{2}+4\ln 2+3\ln 3\right)\\
&\quad+\left(\frac{\alpha_{\mathrm{s}}}{4\pi}\right)^2\Bigg[\Bigg(C_{\mathrm{A}}C_{\mathrm{F}}\Bigg(-\frac{11}{6}+\frac{44}{3}\ln 2+11\ln 3\Bigg)
\end{aligned}
$$

$$+ C_F T_R n_f \left(\frac{2}{3} - \frac{16}{3}\ln 2 - 4\ln 3\right)\Bigg) L(\mu^2 t) \tag{6.52}$$
$$+ C_F^2 \left(51\,\mathrm{Li}_2\left(\frac{3}{4}\right) - \frac{45}{8} - \frac{115}{12}\pi^2 - 230\ln 2 + \frac{213}{2}\ln 3 + 216\ln^2 2 + 9\ln^2 3 \right.$$
$$\left. - 78\ln 2\ln 3\right) + C_F C_A \left(12\,\mathrm{Li}_2\left(\frac{3}{4}\right) + \frac{691}{24} - \frac{13}{12}\pi^2 + 110\ln 2 - 63\ln 3 \right.$$
$$\left. + 44\ln^2 2 - 24\ln 2\ln 3\right) + C_F T_R \left(4\,\mathrm{Li}_2\left(\frac{3}{4}\right) - \frac{179}{5} + \frac{3052}{15}\ln 2 - \frac{498}{5}\ln 3 \right.$$
$$\left. + 16\ln^2 2 - 8\ln 2\ln 3\right) + C_F T_R n_f \left(-\frac{\pi^2}{3} - \frac{35}{6}\right) - c_\chi^{(2)}\Bigg] + \mathcal{O}(\alpha_s^3)\Bigg\}$$
$$+ Z_\chi \sum_{f'\neq f} \bar{\chi}_{f'}(t,x) \overleftrightarrow{\not{D}}^F \chi_{f'}(t,x) \Bigg\{ \left(\frac{\alpha_s}{4\pi}\right)^2 C_F T_R \left(4\,\mathrm{Li}_2\left(\frac{3}{4}\right) - \frac{179}{5} \right.$$
$$\left. + \frac{3052}{15}\ln 2 - \frac{498}{5}\ln 3 + 16\ln^2 2 - 8\ln 2\ln 3\right) + \mathcal{O}(\alpha_s^3)\Bigg\}$$

These mixings are relevant for Chapter 7. Equivalent expressions for the other two operators can be extracted from the mixing matrices in the ancillary files of Ref. [43].

6.6 CONCLUSIONS

We have presented the universal Wilson coefficients for the gradient flow definition of the EMT through NNLO QCD. The NNLO corrections modify the three numerically dominant coefficients c_1, c_2, $\mathring{c}_3$ at the level of 10 % ($1 - 2$ %) for a central scale of $\mu_0 = 3\,\mathrm{GeV}$ ($\mu_0 = 130\,\mathrm{GeV}$), where μ_0 is related to the flow time t according to Eq. (5.4). We observe a reduction of the theoretical uncertainty relative to the NLO result as derived from varying the renormalization scale by a factor of two around its central value. The behavior of the fourth coefficient $\mathring{c}_4$ is less satisfactory, but its impact is expected to be numerically suppressed. Moreover, we observed that the uncertainty estimate from a variation within $\mu \in [\mu_0/2, 2\mu_0]$ might be too optimistic.

Our results were published in Ref. [43] and have already been used in Refs. [133, 154–156] to study thermodynamics on the lattice with the help of the gradient flow. In Ref. [133] it was shown that our NNLO coefficients significantly decrease systematic uncertainties for energy density and pressure, especially in the $t \to 0$ extrapolation. The choice of μ_0 as the central scale decreases them further compared to the traditional choice $q_8 = 1/\sqrt{8t}$. Additionally, the N^{3}LO result of the Wilson coefficient c_2 has been computed by exploiting the trace anomaly in quenched QCD. However, it appears that the EOM suffer from large discretization errors on the lattice, which then lead to discrepancies for observables affected by the EOM, e.g. the trace anomaly beyond the quenched approximation [155]. We also computed the Wilson coefficients without exploiting the EOM, but it turns out that they are divergent and, moreover, the divergences depend

on the gauge parameter ξ (see also Ref. [151]). Therefore, it is not clear how to proceed when the EOM play a role.

Aside from the Wilson coefficients as main outcome, we computed the anomalous dimension matrix for the regular QCD operators which make up the EMT and the mixing matrix between the renormalized regular operators with the flowed operators.

7 HADRONIC VACUUM POLARIZATION USING GRADIENT FLOW

The *vacuum polarization function* (VPF) for (axial-)vector and (pseudo-)scalar particles are among the most important objects when studying QCD. On the one hand, this is because their imaginary part is directly related to physical observables such as the decay rates of the Z- or the Higgs boson, or the hadronic R-ratio. If the characteristic energy scale is far above the QCD scale, a perturbative evaluation of the polarization functions is sufficient in these cases to arrive at high-precision results (see, e.g., Ref. [157]).

But VPFs also contribute indirectly to physical observables such as anomalous magnetic moments [38, 39], the definition of short-distance quark masses [158], or hadronic contributions to the coupling of *Quantum Electrodynamics* (QED) [159, 160]. These applications involve an integration of the VPFs over the non-perturbative regime, which is typically achieved with the help of experimental data and dispersion relations. Only very recently, first-principle lattice calculations have become competitive with these dispersive approaches. In the case of the hadronic vacuum polarization contribution to the muon's anomalous magnetic moment, the two approaches turn out to lead to incompatible results [40][1]. It would therefore be highly desirable to have additional independent first-principle calculations of the VPF.

Utilizing the small-flow-time expansion in Eq. (6.7), we present the flowed OPE for the time-ordered product of two currents through NNLO QCD in this chapter. Taking the VEV leads to the VPF. This should thus allow for an alternative first-principle evaluation of VPFs on the lattice. Section 7.1 introduces the regular OPE of current-current correlators with operators up to mass dimension four. This includes the renormalization of these operators as well as an overview of the literature which provides the corresponding perturbative Wilson coefficients. The transition to the flowed OPE is presented in Section 7.2. Section 7.3 describes the calculation of the mixing matrix between regular and flowed operators in the small-flow-time limit. While a large part of this mixing matrix is already known by reusing the results obtained in Chapters 5 and 6, the missing components require the naive expansion of the VEVs of the flowed dimension-four operators to $\mathcal{O}(m_B^4 t^2)$ and a sophisticated renormalization with the help of the vacuum-energy renormalization constant. These results complete the ingredients required for the flowed OPE of the VPF through NNLO.

In addition, we derive a general logarithmic flow-time evolution equation for flowed operators in Section 7.4, which resembles the RG equation of regular operators.

This chapter is based on Ref. [132]. My main responsibility in this project was the computation of the VEVs and the higher order terms in ϵ for the mixing matrix of the EMT operators. I also checked the flow-time evolution in Section 7.4.

1 The lattice calculation of the light-by-light contribution to $(g-2)_\mu$ is in agreement with other determinations though [161, 162].

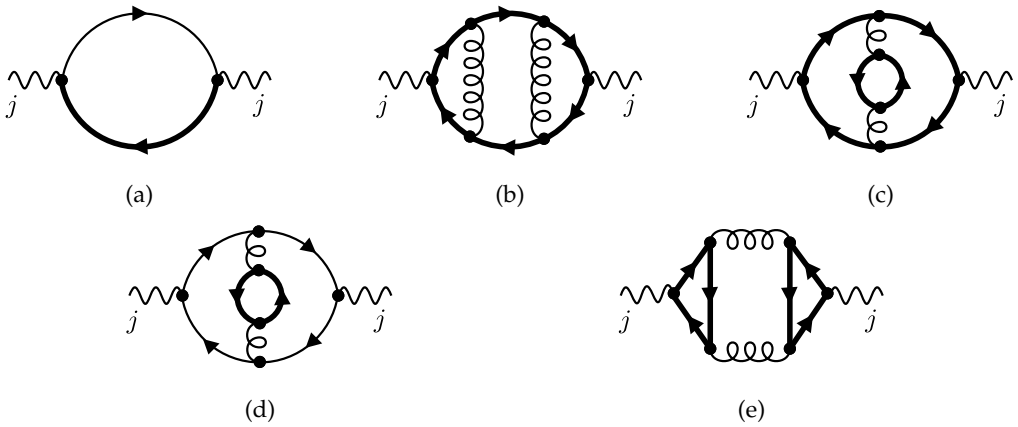

Figure 7.1: Sample diagrams contributing to the perturbative calculation of the VPF, i.e., the l.h.s. of Eq. (7.1). The currents are symbolized by wavy lines, gluons by spirals. We consider the case where n_l quarks are massless (thin straight lines), and n_h quarks are degenerate with mass m (thick straight lines). (a) One-loop contribution for non-diagonal currents; (b-e) sample three-loop diagrams for diagonal currents. In (d), the currents couple to massless quarks. (e) is a "singlet" diagram.

7.1 CURRENT-CURRENT CORRELATORS

7.1.1 *Operator Product Expansion*

The role of the perturbative and the non-perturbative regime of VPFs can be made most explicit through the OPE (see, e.g., Ref. [163]):

$$T(Q) \equiv \int \mathrm{d}^4x\, e^{\mathrm{i}Qx} \langle T j(x) j(0) \rangle \overset{Q^2\to\infty}{\sim} \sum_{k,n} C_n^{(k),\mathrm{B}}(Q) \langle \mathcal{O}_n^{(k)}(x=0) \rangle, \tag{7.1}$$

where $j(x)$ generically stands for a scalar, pseudo-scalar, vector, axial-vector, or tensor current, and k labels the mass dimension. Fig. 7.1 shows sample Feynman diagrams which arise from the perturbative evaluation of the current correlator in Eq. (7.1). In the following, we only consider the so-called non-singlet diagrams, where the currents are connected by a common quark line. An example for a singlet-diagram, on the other hand, is shown in Fig. 7.1(e).

The coefficients $C_n^{(k),\mathrm{B}}$ on the r.h.s. of Eq. (7.1) depend on the quantum numbers of the currents and may thus carry Lorentz indices. We suppress these indices throughout this chapter. We furthermore assume that, upon transition from the left- to the right-hand side, possible global divergences are subtracted off of $T(Q)$.

Up to mass dimension two, the only operators of QCD which contribute to physical matrix elements are proportional to unity, i.e.,

$$\mathcal{O}_1^{(0)} \equiv \mathcal{O}^{(0)} = \mathbb{1}, \qquad \mathcal{O}_1^{(2)} \equiv \mathcal{O}^{(2)} = m_\mathrm{B}^2\, \mathbb{1}, \tag{7.2}$$

where m_B is the bare mass of the n_h degenerate massive quarks. This means that

$$C_1^{(0)} \equiv C^{(0)} \equiv C^{(0),\mathrm{B}}, \qquad C_1^{(2)} \equiv C^{(2)} \equiv Z_m^2 C^{(2),\mathrm{B}} \tag{7.3}$$

are UV-finite, where Z_m is the renormalization constant of the quark mass defined in Eq. (A.13).

At mass dimension four, we choose the following basis of operators (the space-time argument is suppressed in most of what follows):

$$\begin{aligned} \mathcal{O}_1^{(4)} &\equiv \mathcal{O}_1 = \frac{1}{g_{\mathrm{B}}^2} F_{\mu\nu}^a F_{\mu\nu}^a, \\ \mathcal{O}_2^{(4)} &\equiv \mathcal{O}_2 = \sum_{f=1}^{n_{\mathrm{f}}} \bar{\psi}_f \overleftrightarrow{\not{D}}^{\mathrm{F}} \psi_f, \\ \mathcal{O}_3^{(4)} &\equiv \mathcal{O}_3 = m_{\mathrm{B}}^4. \end{aligned} \tag{7.4}$$

In D space-time dimensions the mass dimensions of $\mathcal{O}_1$ and $\mathcal{O}_2$ are actually equal to D, while that of $\mathcal{O}_3$ is equal to 4. Higher dimensional operators are neglected in the following.

The set in Eq. (7.4) does not contain gauge dependent operators or operators that vanish due to the EOM when acting on physical states, since they are irrelevant for the scope of this chapter. In fact, in this respect the upper limit of the sum over f in $\mathcal{O}_2$ could be replaced by n_{h}, because the terms with massless quarks vanish on-shell. For the same reason, one could use $\mathcal{O}_2' \equiv -2m_{\mathrm{B}} \sum_{f=1}^{n_{\mathrm{h}}} \bar{\psi}_f \psi_f$ instead of $\mathcal{O}_2$ in the definition of the operator basis (7.4). Other choices are possible as well, but the basis in Eq. (7.4) is particularly suitable for our purposes, because it is most directly related to the operators used in Chapters 5 and 6.

Matrix elements of the dimension-four operators are divergent in general. However, one may define renormalized operators $\mathcal{O}_n^{\mathrm{R}}$ as linear combinations among them, for which physical matrix elements become finite:

$$\mathcal{O}_n^{\mathrm{R}} = \sum_k Z_{nk}\, \mathcal{O}_k \,. \tag{7.5}$$

Analogously, one defines renormalized coefficient functions through the condition

$$\sum_n C_n^{\mathrm{B}} \mathcal{O}_n \stackrel{!}{=} \sum_n C_n \mathcal{O}_n^{\mathrm{R}} \quad \Rightarrow \quad C_n = \sum_m C_m^{\mathrm{B}} (Z^{-1})_{mn}, \tag{7.6}$$

where $C_n^{\mathrm{B}} \equiv C_n^{(4),\mathrm{B}}$, cf. Eqs. (7.1) and (7.4). It is well known that, since the operators of Eq. (7.4) are part of the QCD Lagrangian, the renormalization matrix Z can be expressed in terms of the anomalous dimensions of QCD [164, 165]:

$$\begin{aligned} Z = \begin{pmatrix} Z_{2\times 2} & \vec{Z}_3 \\ \vec{0}^{\,\mathrm{T}} & Z_m^{-4} \end{pmatrix}, \quad \text{where} \quad Z_{2\times 2} &= \begin{pmatrix} -\epsilon/\beta_\epsilon & -2\gamma_m/\beta_\epsilon \\ 0 & 1 \end{pmatrix}, \\ \vec{Z}_3 &= 4\hat{\mu}^{-2\epsilon} Z_m^{-4} \begin{pmatrix} \alpha_{\mathrm{s}} \frac{\partial}{\partial \alpha_{\mathrm{s}}} Z_0 \\ 2\, Z_0 \end{pmatrix}. \end{aligned} \tag{7.7}$$

β_ϵ, γ_m, Z_m, and $\hat{\mu}$ are defined in Appendix A.2. The 't Hooft mass μ ensures that each renormalized operator $\mathcal{O}_n^{\mathrm{R}}$ in Eq. (7.5) has the same mass dimension as the corresponding

bare one, and $\hat{\mu}$ appears in the $\overline{\text{MS}}$ scheme by default. Z_0 is the $\overline{\text{MS}}$ renormalization constant for the vacuum energy [165]. It is related to the corresponding anomalous dimension γ_0 through

$$\gamma_0(\alpha_s) = [4\gamma_m(\alpha_s) - \epsilon]\, Z_0(\alpha_s) + \beta_\epsilon(\alpha_s)\alpha_s \frac{\partial}{\partial \alpha_s} Z_0(\alpha_s) \equiv -\frac{N_C n_h}{(4\pi)^2} \sum_{n\geq 0} \left(\frac{\alpha_s}{4\pi}\right)^n \gamma_{0,n}, \tag{7.8}$$

which leads to

$$\begin{aligned} Z_0(\alpha_s) = \frac{N_C n_h}{(4\pi)^2 \epsilon} \Bigg\{ 1 + \frac{\alpha_s}{4\pi}\left(\frac{\gamma_{0,1}}{2} - \frac{2\gamma_{m,0}}{\epsilon}\right) + \left(\frac{\alpha_s}{4\pi}\right)^2 \Big[\frac{2}{3\epsilon^2}\left(\beta_0\, \gamma_{m,0} + 4\,\gamma_{m,0}^2\right) \\ - \frac{1}{6\epsilon}\left(\beta_0\, \gamma_{0,1} + 4\,\gamma_{0,1}\gamma_{m,0} + 8\,\gamma_{m,1}\right) + \frac{1}{3}\gamma_{0,2} \Big] \Bigg\} + \mathcal{O}(\alpha_s^3). \end{aligned} \tag{7.9}$$

The first three perturbative coefficients are given by [165, 166][2]

$$\begin{aligned} &\gamma_{0,0} = 1, \qquad \gamma_{0,1} = 4C_F, \\ &\gamma_{0,2} = -C_F^2\left(\frac{131}{2} - 48\,\zeta(3)\right) - C_F C_A\left(-\frac{109}{2} + 24\,\zeta(3)\right) - C_F T_R\left(10 n_f + 48 n_h\right). \end{aligned} \tag{7.10}$$

7.1.2 *Coefficient Functions*

The OPE form of the current correlators is usually inconvenient for their perturbative evaluation. Instead, one rather evaluates the l.h.s. of Eq. (7.1) directly by calculating the relevant two-point functions to the appropriate order. The exact analytical result for general quark masses is known at the two-loop level [168–171], while higher orders up to the four-loop level have been reconstructed by combining various kinematical limits [172–182], or through integral reduction and subsequent numerical evaluation of the resulting master integrals [183].

Since the dimension-zero and -two operators in Eq. (7.1) are proportional to unity, the coefficients $C^{(0)}$ and $C^{(2)}$ are immediately determined from the small-mass expansion of these perturbative results for the VPF. They are thus known up to the four-loop level at the moment [184–192].[3]

The Wilson coefficients C_n of the dimension-four operators, on the other hand, require a dedicated calculation which keeps track of the contributions from the individual operators. This has been done through $\mathcal{O}(\alpha_s^3)$ for C_1 and C_2, and through $\mathcal{O}(\alpha_s^2)$ for C_3 in Refs. [166, 197–199]. For the purpose of this chapter, only the $\mathcal{O}(\alpha_s^2)$ results are required.

7.2 FLOWED OPERATOR PRODUCT EXPANSION

Having introduced the setup in the regular theory, we now translate this to the flowed OPE for the current correlators.

2 Higher orders have been computed in Ref. [167].

3 The imaginary parts of the VPFs are known even at the five-loop level in the phenomenologically most relevant cases [193–196].

7.2.1 *Flowed Operators*

We introduce the flowed operators as

$$\begin{aligned}
\tilde{\mathcal{O}}_1(t,x) &= \frac{Z_\mathrm{s}}{g_\mathrm{B}^2} G^a_{\mu\nu}(t,x) G^a_{\mu\nu}(t,x) = \frac{1}{\hat{\mu}^{2\epsilon} g^2} G^a_{\mu\nu}(t,x) G^a_{\mu\nu}(t,x) = \frac{4}{\hat{\mu}^{2\epsilon} g^2} E(t,x), \\
\tilde{\mathcal{O}}_2(t,x) &= \mathring{Z}_\chi \sum_{f=1}^{n_\mathrm{f}} \bar{\chi}_f(t,x) \overleftrightarrow{\mathcal{D}}^\mathrm{F}(t,x) \chi_f(t,x) = \mathring{R}(t,x), \\
\tilde{\mathcal{O}}_3(t,x) &= m^4,
\end{aligned} \tag{7.11}$$

where $E(t,x)$ and $\mathring{R}(t,x)$ are the composite operators already introduced in Section 2.4. Compared to $E(t,x)$, we divide $\tilde{\mathcal{O}}_1(t,x)$ by g_B^2 to have the same normalization as in Section 6.5 which allows us to reuse the results for the operator mixing. The strong coupling renormalization constant Z_s then ensures that matrix elements of $\tilde{\mathcal{O}}_1(t)$ are finite. The reason for keeping track of the non-integer mass dimension of $\tilde{\mathcal{O}}_1(t)$ is clarified later.

Similar to the regular operators in Eq. (7.4), one could trade the flowed operator $\tilde{\mathcal{O}}_2(t)$ for $\tilde{\mathcal{O}}'_2(t) = -2m\mathring{Z}_\chi \sum_{f=1}^{n_\mathrm{f}} \bar{\chi}_f(t)\chi_f(t)$. However, in this case the final results to be derived below would be different, because the EOM for the flowed operators relate $\tilde{\mathcal{O}}'_2(t)$ to both $\tilde{\mathcal{O}}_2(t)$ and $\tilde{\mathcal{O}}_1(t)$ (see Section 6.1). A transformation of the results in this chapter to $\tilde{\mathcal{O}}'_2(t)$ is straightforward though.

7.2.2 *Small-Flow-Time Expansion*

The small-flow-time expansion in Eq. (6.7) allows us to relate the regular QCD operators and coefficients with their flowed counterparts as follows:

$$\begin{aligned}
\tilde{\mathcal{O}}_n(t) &= \zeta_n^{(0)}(t)\mathbb{1} + \zeta_n^{(2),\mathrm{B}}(t)\, m_\mathrm{B}^2 \mathbb{1} + \sum_k \zeta_{nk}^\mathrm{B}(t) \mathcal{O}_k + \dots \\
&\equiv \zeta_n^{(0)}(t)\mathbb{1} + \zeta_n^{(2)}(t)\, m^2 \mathbb{1} + \sum_k \zeta_{nk}(t) \mathcal{O}_k^\mathrm{R} + \dots,
\end{aligned} \tag{7.12}$$

where the ellipsis denotes terms that vanish as $t \to 0$, and

$$\zeta_n^{(2)}(t) = \zeta_n^{(2),\mathrm{B}}(t)\, Z_m^2, \qquad \zeta_{nk}(t) = \sum_l \zeta_{nl}^\mathrm{B}(t)\, Z_{lk}^{-1} \tag{7.13}$$

are the renormalized, finite mixing coefficients. Inversion of Eq. (7.12) gives

$$\begin{aligned}
\mathcal{O}_n^\mathrm{R} &= \sum_k \zeta_{nk}^{-1}(t)\, \bar{\mathcal{O}}_k(t) + \dots, \\
\bar{\mathcal{O}}_n(t) &\equiv \tilde{\mathcal{O}}_n(t) - \zeta_n^{(0)}(t)\mathbb{1} - \zeta_n^{(2)}(t) m^2 \mathbb{1}.
\end{aligned} \tag{7.14}$$

This lets one define the "flowed OPE" for the current correlator:

$$T(Q) \overset{Q^2\to\infty}{\sim} \tilde{C}^{(0)}(Q^2,t)\mathbb{1} + \tilde{C}^{(2)}(Q^2,t) m^2 \mathbb{1} + \sum_n \tilde{C}_n(Q^2,t) \tilde{\mathcal{O}}_n(t) + \dots \tag{7.15}$$

where the corresponding coefficient functions are related to the regular Wilson coefficients through

$$\begin{aligned}\tilde{C}_n(Q^2,t) &= \sum_k C_k(Q^2)\zeta^{-1}_{kn}(t),\\ \tilde{C}^{(0,2)}(Q^2,t) &= C^{(0,2)}(Q^2) - \sum_n \tilde{C}_n(Q^2,t)\,\zeta_n^{(0,2)}(t).\end{aligned} \tag{7.16}$$

The regular QCD coefficients $C^{(0)}$ and $C^{(2)}$ are given by the first two terms in m^2/Q^2 of the large-Q^2 expansion of the VPFs. Through the required order, they can be found in Ref. [188] for vector-, in Ref. [190] for axial-vector-, and in Ref. [189] for scalar- and pseudo-scalar currents, for example. The dimension-four coefficients can be found in Refs. [197, 199].[4]

7.3 CALCULATION OF THE MIXING MATRIX

We now determine the mixing matrix ζ in a perturbative calculation through NNLO. By using the known results for the regular Wilson coefficients, one can determine the flowed coefficients of Eq. (7.16) to the same order. Together with an evaluation of the flowed operator matrix elements on the lattice, the VPFs can be extracted and used in the determination of various physical quantities.

The bare mixing matrix ζ^{B} can be determined with the help of the method of projectors introduced in Section 6.2:

$$\zeta_n^{(0,2),\mathrm{B}}(t) = P^{(0,2)}[\tilde{\mathcal{O}}_n(t)], \qquad \zeta^{\mathrm{B}}_{nk}(t) = P_k^{(4)}[\tilde{\mathcal{O}}_n(t)], \tag{7.17}$$

where we construct $P^{(n)}$ such that

$$P^{(n)}[\mathcal{O}^{(m)}] = \delta_{nm}, \qquad P^{(n)}[\mathcal{O}_k] = P_k^{(4)}[\mathcal{O}^{(n)}] = 0, \qquad P_k^{(4)}[\mathcal{O}_l] = \delta_{kl}, \tag{7.18}$$

for $n,m \in \{0,2\}$ and $k,l \in \{1,2,3\}$.

Specifically, the projectors onto $\mathbb{1}$, $m_{\mathrm{B}}^2\mathbb{1}$, and $\mathcal{O}_3^{\mathrm{B}}$ are given by derivatives of vacuum matrix elements w.r.t. m_{B}:

$$\begin{aligned}\zeta_n^{(0)}(t) &= P^{(0)}[\tilde{\mathcal{O}}_n(t)] \equiv \langle\tilde{\mathcal{O}}_n(t)\rangle\Big|_{m_{\mathrm{B}}=0},\\ \zeta_n^{(2)}(t) &= Z_m^2\,P^{(2)}[\tilde{\mathcal{O}}_n(t)] \equiv Z_m^2\frac{1}{2!}\frac{\partial^2}{\partial m_{\mathrm{B}}^2}\langle\tilde{\mathcal{O}}_n(t)\rangle\Big|_{m_{\mathrm{B}}=0},\\ \zeta^{\mathrm{B}}_{n3}(t) &= P_3^{(4)}[\tilde{\mathcal{O}}_n(t)] \equiv \frac{1}{4!}\frac{\partial^4}{\partial m_{\mathrm{B}}^4}\langle\tilde{\mathcal{O}}_n(t)\rangle\Big|_{m_{\mathrm{B}}=0}.\end{aligned} \tag{7.19}$$

A crucial point of the method of projectors is that the derivatives and limits are taken *before* loop integration [149, 150]. This guarantees that all loop contributions of projections on the r.h.s. of Eq. (7.12) lead to scaleless integrals and thus vanish in dimensional regularization. On the other hand, it implies that the projections on the l.h.s. of Eq. (7.12)

4 Since the latter reference is only available in German, they have also been included in Ref. [132].

can be divergent, even though physical matrix elements of $\tilde{\mathcal{O}}_n(t)$ are finite. This is why we need to carefully account for a possible non-integer mass dimension of these operators, see Eq. (7.11).

We directly obtain

$$\zeta_{33}^{\mathrm{B}} = \frac{1}{4!}\frac{\partial^4}{\partial m_{\mathrm{B}}^4} m^4 = Z_m^{-4}, \qquad \zeta_3^{(0),\mathrm{B}} = \zeta_3^{(2),\mathrm{B}} = 0, \qquad \zeta_{31}^{\mathrm{B}} = \zeta_{32}^{\mathrm{B}} = 0, \tag{7.20}$$

where the third set of equations follows from $\tilde{\mathcal{O}}_3(t) = m^4 = \mathcal{O}_3$ and the projector property $P_1^{(4)}[\mathcal{O}_3] = P_2^{(4)}[\mathcal{O}_3] = 0$, see Eq. (7.18).

The bare and renormalized mixing matrices for the dimension-four operators thus take the form

$$\zeta^{\mathrm{B}} = \begin{pmatrix} \zeta_{2\times 2}^{\mathrm{B}} & \vec{\zeta}_3^{\mathrm{B}} \\ \vec{0}^T & Z_m^{-4} \end{pmatrix}, \qquad \zeta = \begin{pmatrix} \zeta_{2\times 2} & \vec{\zeta}_3 \\ \vec{0}^T & 1 \end{pmatrix}, \tag{7.21}$$

where $\vec{0}^{\,\mathrm{T}} = (0,0)$, and

$$\begin{aligned} \zeta_{2\times 2}^{\mathrm{B}} &= \begin{pmatrix} \zeta_{11}^{\mathrm{B}} & \zeta_{12}^{\mathrm{B}} \\ \zeta_{21}^{\mathrm{B}} & \zeta_{22}^{\mathrm{B}} \end{pmatrix}, & \zeta_{2\times 2} &= \zeta_{2\times 2}^{\mathrm{B}} Z_{2\times 2}^{-1}, \\ \vec{\zeta}_3^{\mathrm{B}} &= \left(\zeta_{13}^{\mathrm{B}}, \zeta_{23}^{\mathrm{B}}\right)^{\mathrm{T}}, & \vec{\zeta}_3 &= (\vec{\zeta}_3^{\mathrm{B}} - \zeta_{2\times 2}\vec{Z}_3) Z_m^4. \end{aligned} \tag{7.22}$$

$\zeta_{2\times 2}$ can be obtained from the mixing matrix of the operators occurring in the EMT. This is easily derived from the relation between the operators $\mathcal{O}_i$ defined in Eq. (7.4) and the $\hat{\mathcal{O}}_{i,\mu\nu}$ defined in Eq. (6.39),

$$\begin{pmatrix} \mathcal{O}_1 \\ \mathcal{O}_2 \end{pmatrix} \delta_{\mu\nu} = \begin{pmatrix} \hat{\mathcal{O}}_{2,\mu\nu} \\ \hat{\mathcal{O}}_{4,\mu\nu} \end{pmatrix}, \tag{7.23}$$

as well as the equivalent relation

$$\begin{pmatrix} \tilde{\mathcal{O}}_1 \\ \tilde{\mathcal{O}}_2 \end{pmatrix} \delta_{\mu\nu} = \begin{pmatrix} \mathring{\mathcal{O}}_{2,\mu\nu} \\ \mathring{\mathcal{O}}_{4,\mu\nu} \end{pmatrix} \tag{7.24}$$

for the flowed operators $\tilde{\mathcal{O}}_i$ defined in Eq. (7.11) and the flowed EMT operators $\mathring{\mathcal{O}}_{i,\mu\nu}$ in Eq. (6.40). Note that $\mathring{\mathcal{O}}_{4,\mu\nu} = \sum_f^{n_{\mathrm{f}}} \mathring{\mathcal{O}}_{4_f,\mu\nu}$. Following Eqs. (6.38) and (6.42), we thus find

$$\zeta_{2\times 2}^{-1} = \begin{pmatrix} m_{\mathrm{F},22} & m_{\mathrm{F},24} \\ n_{\mathrm{f}} m_{\mathrm{F},42} & m_{\mathrm{F},44} + (n_{\mathrm{f}} - 1)\overline{m}_{\mathrm{F},44} \end{pmatrix} \tag{7.25}$$

with the NNLO mixing matrix elements from Eqs. (6.51) and (6.52).

The coefficients $\zeta_n^{(0)}$ are simply the VEVs of $\tilde{\mathcal{O}}_n(t)$ for $m = 0$. Thus, we can reuse the results obtained in Chapter 5 and we have

$$\begin{aligned} \zeta_1^{(0)}(t) &= \langle \tilde{\mathcal{O}}_1(t) \rangle\big|_{m=0} = \frac{1}{\hat{\mu}^{2\epsilon}\pi\alpha_{\mathrm{s}}} \langle E(t) \rangle\big|_{m=0}, \\ \zeta_2^{(0)}(t) &= \langle \tilde{\mathcal{O}}_2(t) \rangle\big|_{m=0} = \langle \mathring{R}(t) \rangle\big|_{m=0} = -\frac{2N_{\mathrm{C}} n_{\mathrm{f}}}{(4\pi t)^2}, \end{aligned} \tag{7.26}$$

where the latter all-order result follows from the definition of the ringed scheme in Eq. (2.62), cf. Eq. (2.67). For $\tilde{\mathcal{O}}_1(t)$ the VEV has been calculated through NNLO in Eqs. (5.2) and (5.5) to (5.7).

The renormalized expressions for $\zeta_n^{(2)}$ correspond to the mass effects calculated in Section 5.4 and we directly find

$$\begin{aligned}\zeta_1^{(2)}(t) &= Z_m^2 \frac{1}{2!}\frac{\partial^2}{\partial m_\mathrm{B}^2}\langle\tilde{\mathcal{O}}_1(t)\rangle\Big|_{m_\mathrm{B}=0} = \frac{t}{\hat{\mu}^{2\epsilon}\pi\alpha_\mathrm{s}}E^{(2)}(t),\\ \zeta_2^{(2)}(t) &= Z_m^2 \frac{1}{2!}\frac{\partial^2}{\partial m_\mathrm{B}^2}\langle\tilde{\mathcal{O}}_2(t)\rangle\Big|_{m_\mathrm{B}=0} = t\mathring{R}^{(2)}(t),\end{aligned} \tag{7.27}$$

with $E^{(2)}(t)$ given through Eqs. (5.23) to (5.25) and $\mathring{R}^{(2)}(t)$ through Eqs. (5.29) to (5.31).

ζ_{13} and ζ_{23} require the naive expansion of the VEVs to $\mathcal{O}(m_\mathrm{B}^4 t^2)$, which did not suffice to obtain the mass effects to $\mathcal{O}(m^4t^2)$ in Section 5.4 because other regions contribute at this order. Hence, we only present the results for ζ_{13} and ζ_{23} after the sophisticated renormalization given in Eq. (7.22). It is important here to work consistently in D space-time dimensions. Since $\vec{Z}_3$ contains a $1/\epsilon$ pole already at $\mathcal{O}(\alpha_\mathrm{s}^0)$, we need to keep the $\mathcal{O}(\epsilon^2)$ terms of $\zeta_{2\times2}$ at NLO, and the $\mathcal{O}(\epsilon)$ terms at NNLO. We did not include these terms in Eqs. (6.51) and (6.52) and instead refer to the ancillary file of Ref. [132]. Using the identity $N_\mathrm{A}T_\mathrm{R} = N_\mathrm{C}C_\mathrm{F}$ [200], our final result for $\vec{\zeta}_3$ reads

$$\begin{aligned}\zeta_{13}(t) = \frac{n_\mathrm{h}N_\mathrm{C}C_\mathrm{F}}{16\pi^2}\frac{\alpha_\mathrm{s}}{\pi}\Bigg\{&5 - 6\,\zeta(2) - 6\,L(\mu^2t) - 6\,L^2(\mu^2t)\\ &+ \frac{\alpha_\mathrm{s}}{\pi}\Bigg[-3.31445\,C_\mathrm{A} - 27.5707\,C_\mathrm{F} - 15.0886\,T_\mathrm{R}n_\mathrm{h} + 19.5780\,T_\mathrm{R}n_\mathrm{l}\\ &\quad + L(\mu^2t)\left(-5.68293\,C_\mathrm{A} - 32.7594\,C_\mathrm{F} - 4.17386\,T_\mathrm{R}n_\mathrm{h} + 19.8261\,T_\mathrm{R}n_\mathrm{l}\right)\\ &\quad + L^2(\mu^2t)\left(-\frac{433}{12}\,C_\mathrm{A} - \frac{33}{2}\,C_\mathrm{F} + \frac{26}{3}\,T_\mathrm{R}n_\mathrm{f}\right)\\ &\quad + L^3(\mu^2t)\left(-\frac{22}{3}\,C_\mathrm{A} - 6\,C_\mathrm{F} + \frac{8}{3}\,T_\mathrm{R}n_\mathrm{f}\right)\Bigg]\Bigg\} + \mathcal{O}(\alpha_\mathrm{s}^3),\end{aligned} \tag{7.28a}$$

$$\begin{aligned}\zeta_{23}(t) = \frac{N_\mathrm{C}n_\mathrm{h}}{2\pi^2}\Bigg\{&1 + L(\mu^2t) + \frac{\alpha_\mathrm{s}}{\pi}C_\mathrm{F}\left[\frac{67}{16} + \frac{13}{2}\,\ln 2 - \frac{15}{2}\,\ln 3 - \frac{9}{4}\,\mathrm{Li}_2\left(\frac{1}{4}\right)\right.\\ &\quad\left. + \left(\frac{33}{8} - \ln 2 - \frac{3}{4}\,\ln 3\right)L(\mu^2t) + \frac{3}{2}\,L^2(\mu^2t)\right]\\ &+ \left(\frac{\alpha_\mathrm{s}}{\pi}\right)^2 C_\mathrm{F}\Bigg[-0.710509\,C_\mathrm{A} + 6.97943\,C_\mathrm{F} - 6.43804\,T_\mathrm{R}n_\mathrm{h} - 2.87689\,T_\mathrm{R}n_\mathrm{l}\\ &\quad + L(\mu^2t)\left(1.53754\,C_\mathrm{A} + 4.22899\,C_\mathrm{F} - 4.47865\,T_\mathrm{R}n_\mathrm{h} - 1.47865\,T_\mathrm{R}n_\mathrm{l}\right)\\ &\quad + L^2(\mu^2t)\left(2.57807\,C_\mathrm{A} + 4.09934\,C_\mathrm{F} - 0.931798\,T_\mathrm{R}n_\mathrm{f}\right)\\ &\quad + L^3(\mu^2t)\left(\frac{11}{24}\,C_\mathrm{A} + \frac{3}{2}\,C_\mathrm{F} - \frac{1}{6}\,T_\mathrm{R}n_\mathrm{f}\right)\Bigg]\Bigg\} + \mathcal{O}(\alpha_\mathrm{s}^3),\end{aligned} \tag{7.28b}$$

where we only display the six leading digits of the numerical results. Similar to the results in Chapter 5, our numerical uncertainty is about six orders of magnitude beyond that. The logarithmic terms at $\mathcal{O}(\alpha_s^n)$ are determined by the RG equation derived in the next section. Thus, they are in principle available analytically. However, for all practical purposes we consider these numerical numbers as equivalent.

This completes the results for the small-flow-time coefficients of the OPE up to dimension four of Eq. (7.15). They are available with higher accuracy in the ancillary file of Ref. [132].

7.4 FLOW-TIME EVOLUTION

In the final section of this chapter we derive a general flow-time evolution equation for flowed operators. It resembles the RG equation for regular operators but with a "flowed anomalous dimension matrix". While studies of the relation between the RG and the flow-time evolution have also been performed elsewhere in the literature (see, e.g., Refs. [136, 201–208]), to our knowledge the treatment described here has not been discussed before.

Let us return to the small-flow-time expansion of the operators $\bar{\mathcal{O}}$ defined in Eqs. (7.12) and (7.14), employing a matrix rather than component-wise notation for the sake of clarity:

$$\bar{\mathcal{O}}(t) = \zeta^{\mathrm{B}}(t)\mathcal{O} = \zeta(t)\mathcal{O}^{\mathrm{R}}. \tag{7.29}$$

Since we work in the small-flow-time limit, the dependence of $\zeta(t)$ on t can be only through $L(\mu^2 t)$, defined in Eq. (5.3). Taking the logarithmic derivative w.r.t. t of Eq. (7.29), one thus obtains

$$t\partial_t\bar{\mathcal{O}}(t) = (t\partial_t\zeta(t))\mathcal{O}^{\mathrm{R}}. \tag{7.30}$$

Using Eq. (7.29) to eliminate the regular operators $\mathcal{O}^{\mathrm{R}}$, we find the flow-equation for flowed composite operators

$$t\partial_t\bar{\mathcal{O}}(t) = \gamma^{\mathrm{f}}(t)\,\bar{\mathcal{O}}(t), \quad \text{where} \quad \gamma^{\mathrm{f}}(t) \equiv (t\partial_t\zeta(t))\zeta^{-1}(t). \tag{7.31}$$

So far the discussion is general and holds for any flowed OPE. Specializing to our case of the QCD dimension-four operators, we can write the "flowed anomalous dimension" matrix as

$$\begin{aligned} \gamma^{\mathrm{f}} = \begin{pmatrix} \gamma^{\mathrm{f}}_{2\times2} & \vec{\gamma}^{\mathrm{f}}_3 \\ 0 & 0 \end{pmatrix}, \qquad \gamma^{\mathrm{f}}_{2\times2}(t) &= (t\partial_t\zeta_{2\times2}(t))\,\zeta^{-1}_{2\times2}(t), \\ \vec{\gamma}^{\mathrm{f}}_3(t) &= -\gamma^{\mathrm{f}}_{2\times2}(t)\vec{\zeta}_3(t) + t\partial_t\vec{\zeta}_3(t). \end{aligned} \tag{7.32}$$

Through $\mathcal{O}(\alpha_s^2)$, the result can be directly evaluated from Eqs. (7.25) and (7.28). A consistency check is obtained by noting that $\zeta(t)$ depends on t only through $L(\mu^2 t)$:

$$t\partial_t\zeta(t) = \mu^2\frac{\partial}{\partial\mu^2}\zeta(t) = \mu^2\frac{\mathrm{d}}{\mathrm{d}\mu^2}\zeta(t) - \alpha_s\beta\frac{\partial}{\partial\alpha_s}\zeta(t). \tag{7.33}$$

On the other hand, we know that $\alpha_s\tilde{\mathcal{O}}_1(t)$ and $\tilde{\mathcal{O}}_2(t)$ are RG invariant [4, 8, 11] and therefore, with Eq. (7.12),

$$\begin{aligned}\begin{pmatrix}0\\0\\4m^4\gamma_m\end{pmatrix} &= \mu^2\frac{\mathrm{d}}{\mathrm{d}\mu^2}H^{-1}(\alpha_s)\tilde{\mathcal{O}}(t)\\ &= \mu^2\frac{\mathrm{d}}{\mathrm{d}\mu^2}H^{-1}(\alpha_s)\left(\zeta^{(0)}(t)\mathbb{1}+\zeta^{(2)}(t)m^2\mathbb{1}+\zeta(t)\mathcal{O}^{\mathrm{R}}\right),\end{aligned} \tag{7.34}$$

where

$$H(x) = \begin{pmatrix}H_{2\times2}(x) & \vec{0}\\ \vec{0}^T & 1\end{pmatrix}, \quad \text{with} \quad H_{2\times2}(x) = \begin{pmatrix}(4\pi x)^{-1} & 0\\ 0 & 1\end{pmatrix}. \tag{7.35}$$

Since operators of different mass dimensions do not mix under RG evolution and $\zeta_3^{(0,2)}(t) = 0$, we can drop the first two terms in the brackets on the r.h.s. of Eq. (7.34).[5] We thus arrive at

$$\mu^2\frac{\mathrm{d}}{\mathrm{d}\mu^2}\zeta(t) = \begin{pmatrix}0&0&0\\0&0&0\\0&0&4\gamma_m\end{pmatrix} - \begin{pmatrix}\beta&0&0\\0&0&0\\0&0&0\end{pmatrix}\zeta(t) - \zeta(t)\gamma^{\mathcal{O}}, \tag{7.36}$$

where $\gamma^{\mathcal{O}}$ is the anomalous dimension of the operators $\mathcal{O}^{\mathrm{R}}$, defined through

$$\mu^2\frac{\mathrm{d}}{\mathrm{d}\mu^2}\mathcal{O}^{\mathrm{R}} = \gamma^{\mathcal{O}}(\alpha_s)\mathcal{O}^{\mathrm{R}}. \tag{7.37}$$

It can be written as

$$\gamma^{\mathcal{O}} = \left(\mu^2\frac{\mathrm{d}}{\mathrm{d}\mu^2}Z\right)Z^{-1} = \begin{pmatrix}\gamma^{\mathcal{O}}_{2\times2} & \vec{\gamma}_3^{\mathcal{O}}\\ \vec{0}^T & 4\gamma_m\end{pmatrix}, \tag{7.38}$$

with Z from Eq. (7.7). Using the expressions of Section 7.1.1, one derives [164, 165]

$$\begin{aligned}\gamma^{\mathcal{O}}_{2\times2} &= \left(\mu^2\frac{\mathrm{d}}{\mathrm{d}\mu^2}Z_{2\times2}\right)Z^{-1}_{2\times2} = \begin{pmatrix}-\alpha_s\frac{\partial}{\partial\alpha_s}\beta & -2\,\alpha_s\frac{\partial}{\partial\alpha_s}\gamma_m\\ 0 & 0\end{pmatrix},\\ \vec{\gamma}_3^{\mathcal{O}} &= Z_m^4\left(\mu^2\frac{\mathrm{d}}{\mathrm{d}\mu^2}\vec{Z}_3 - \gamma^{\mathcal{O}}_{2\times2}\vec{Z}_3\right) = \begin{pmatrix}4\alpha_s\frac{\partial}{\partial\alpha_s}\gamma_0\\ 8\gamma_0\end{pmatrix}.\end{aligned} \tag{7.39}$$

The QCD RG functions β and γ_m are defined in Eqs. (A.9) and (A.11), respectively. Since they are of $\mathcal{O}(\alpha_s)$, the explicit μ-dependence of $\zeta_{2\times2}(t)$ can be derived through $\mathcal{O}(\alpha_s^3)$ from the results of Section 6.5. Thus, for $\gamma^{\mathrm{f}}_{2\times2}$, Eq. (7.33) is not just a consistency check,

5 This can also be seen by noting that these two terms, multiplied by $H^{-1}(\alpha_s)$, are $\alpha_s\langle\tilde{\mathcal{O}}_1(t)\rangle$ and $\langle\tilde{\mathcal{O}}_2(t)\rangle$, expanded through order m^2.

but a means to derive higher order terms. In our case, we can obtain the result through $\mathcal{O}(\alpha_s^3)$:

$$\begin{aligned}
\gamma_{11}^{\mathrm{f}} &= \left(\frac{\alpha_s}{\pi}\right)^2 \left[\frac{3}{32} C_A^2 + \frac{1}{8} C_A T_R n_f + \frac{7}{8} C_F T_R n_f\right] + \left(\frac{\alpha_s}{\pi}\right)^3 \left[-\frac{7}{48} C_A T_R^2 n_f^2\right. \\
&\quad - \frac{35}{36} C_F T_R^2 n_f^2 + C_A C_F T_R n_f \left(\frac{11891}{2880} + \frac{27}{40} \ln 2 - \frac{81}{160} \ln 3\right) \\
&\quad + C_A^2 T_R n_f \left(\frac{1687}{2880} + \frac{29}{40} \ln 2 - \frac{9}{20} \ln 3\right) + C_A^3 \left(\frac{6643}{11520} - \frac{319}{160} \ln 2 + \frac{99}{80} \ln 3\right) \\
&\quad + C_F^2 T_R n_f \left(\frac{25}{64} + \frac{45}{8} \ln 2 - \frac{111}{32} \ln 3 + \frac{3}{4} \mathrm{Li}_2\left(\frac{1}{4}\right) - \frac{3}{8} \zeta(2)\right) \qquad (7.40a) \\
&\quad \left. + \left(\frac{1}{6} C_A^2 T_R n_f + \frac{11}{64} C_A^3 + \frac{77}{48} C_A C_F T_R n_f - \frac{1}{12} C_A T_R^2 n_f^2 - \frac{7}{12} C_F T_R^2 n_f^2\right) L(\mu^2 t)\right] \\
&\quad + \mathcal{O}(\alpha_s^4), \\
\gamma_{12}^{\mathrm{f}} &= -\frac{3}{2} \frac{\alpha_s}{\pi} C_F + \left(\frac{\alpha_s}{\pi}\right)^2 \left\{-\frac{367}{48} C_A C_F + \frac{5}{3} C_F T_R n_f + C_F^2 \left[-\frac{3}{16} - \frac{3}{2} \ln 2 - \frac{9}{8} \ln 3\right]\right. \\
&\quad \left. + \left[-\frac{11}{4} C_A C_F + C_F T_R n_f\right] L(\mu^2 t)\right\} \\
&\quad + \left(\frac{\alpha_s}{\pi}\right)^3 \left\{C_F^2 C_A \left[-\frac{391}{768} - \frac{431}{24} \ln 2 + \frac{3}{8} \ln^2 2 + \frac{11}{64} \ln 3 + \frac{9}{8} \mathrm{Li}_2\left(\frac{1}{4}\right) - \frac{33}{64} \zeta(2)\right]\right. \\
&\quad + C_F T_R^2 n_f^2 \left[-\frac{25}{18} - \frac{1}{2} \zeta(2)\right] + C_F^3 \left[-\frac{1401}{256} + \frac{339}{16} \ln 2 - \frac{9}{8} \ln^2 2\right. \\
&\quad \left. - \frac{657}{64} \ln 3 - \frac{9}{4} \ln 2 \ln 3 - \frac{27}{32} \ln^2 3 + \frac{153}{32} \mathrm{Li}_2\left(\frac{1}{4}\right) + \frac{39}{64} \zeta(2)\right] \\
&\quad + C_A^2 C_F \left[-\frac{5291}{144} - \frac{2311}{24} \ln 2 + \frac{4641}{64} \ln 3 + \frac{11}{32} \mathrm{Li}_2\left(\frac{1}{4}\right) + \frac{11}{8} \zeta(2)\right] \qquad (7.40b) \\
&\quad + C_F^2 T_R n_f \left[\frac{8827}{960} - \frac{2089}{120} \ln 2 + \frac{847}{80} \ln 3 + \frac{3}{8} \mathrm{Li}_2\left(\frac{1}{4}\right) - \frac{3}{16} \zeta(2) - \frac{9}{2} \zeta(3)\right] \\
&\quad + C_A C_F T_R n_f \left[\frac{5861}{360} + \frac{4273}{120} \ln 2 - \frac{2139}{80} \ln 3 - \frac{1}{8} \mathrm{Li}_2\left(\frac{1}{4}\right) + \frac{7}{8} \zeta(2) + \frac{9}{2} \zeta(3)\right] \\
&\quad + \frac{3}{32} C_F c_\chi^{(2)} + \left[-\frac{4445}{192} C_A^2 C_F + \frac{647}{48} C_A C_F T_R n_f - \frac{5}{3} C_F T_R^2 n_f^2\right. \\
&\quad \left. + C_F^2 C_A \left(-\frac{33}{64} - \frac{33}{8} \ln 2 - \frac{99}{32} \ln 3\right) + C_F^2 T_R n_f \left(\frac{15}{16} + \frac{3}{2} \ln 2 + \frac{9}{8} \ln 3\right)\right] L(\mu^2 t) \\
&\quad \left. + \left[-\frac{121}{32} C_A^2 C_F + \frac{11}{4} C_A C_F T_R n_f - \frac{1}{2} C_F T_R^2 n_f^2\right] L^2(\mu^2 t)\right\} + \mathcal{O}(\alpha_s^4), \\
\gamma_{21}^{\mathrm{f}} &= \left(\frac{\alpha_s}{\pi}\right)^3 \left[C_A^2 T_R n_f \left(\frac{599}{5760} + \frac{33}{80} \ln 2 - \frac{99}{320} \ln 3\right) + C_A T_R^2 n_f^2 \left(\frac{41}{1440}\right.\right.
\end{aligned}$$

$$
\begin{aligned}
&- \frac{3}{20}\ln 2 + \frac{9}{80}\ln 3\Big) + C_A C_F T_R n_f \Big(\frac{209}{1152} + \frac{55}{16}\ln 2 - \frac{407}{192}\ln 3 \\
&+ \frac{11}{24}\mathrm{Li}_2\Big(\frac{1}{4}\Big) - \frac{11}{48}\zeta(2)\Big) + C_F T_R^2 n_f^2 \Big(\frac{43}{144} - \frac{5}{4}\ln 2 + \frac{37}{48}\ln 3 \\
&- \frac{1}{6}\mathrm{Li}_2\Big(\frac{1}{4}\Big) + \frac{1}{12}\zeta(2)\Big)\Big] + \mathcal{O}(\alpha_s^4),
\end{aligned} \tag{7.40c}
$$

$$
\begin{aligned}
\gamma_{22}^f = &\Big(\frac{\alpha_s}{\pi}\Big)^2 \Big[C_A C_F \Big(\frac{11}{96} - \frac{11}{12}\ln 2 - \frac{11}{16}\ln 3\Big) + C_F T_R n_f \Big(-\frac{2}{3} + \frac{1}{3}\ln 2 \\
&+ \frac{1}{4}\ln 3\Big)\Big] + \Big(\frac{\alpha_s}{\pi}\Big)^3 \Big\{C_A C_F T_R n_f \Big[\frac{2521}{960} - \frac{1709}{90}\ln 2 - \frac{1}{6}\ln^2 2 \\
&+ \frac{1537}{160}\ln 3 - \frac{1}{24}\mathrm{Li}_2\Big(\frac{1}{4}\Big)\Big] + C_A^2 C_F \Big[-\frac{7397}{2304} - \frac{213}{16}\ln 2 + \frac{11}{24}\ln^2 2 \\
&+ \frac{107}{16}\ln 3 + \frac{11}{8}\mathrm{Li}_2\Big(\frac{1}{4}\Big) - \frac{121}{192}\zeta(2)\Big] + C_F T_R^2 n_f^2 \Big[-\frac{749}{720} + \frac{763}{90}\ln 2 \\
&- \frac{83}{20}\ln 3 - \frac{1}{6}\mathrm{Li}_2\Big(\frac{1}{4}\Big) + \frac{1}{12}\zeta(2)\Big] + C_F^2 T_R n_f \Big[-\frac{139}{192} - \frac{119}{8}\ln 2 \\
&+ \frac{1}{6}\ln^2 2 + \frac{261}{32}\ln 3 + \frac{1}{2}\ln 2\ln 3 + \frac{3}{16}\ln^2 3 - \frac{23}{8}\mathrm{Li}_2\Big(\frac{1}{4}\Big) + \frac{5}{48}\zeta(2)\Big] \\
&+ C_F^2 C_A \Big[\frac{253}{384} + \frac{209}{8}\ln 2 - \frac{11}{24}\ln^2 2 - \frac{99}{8}\ln 3 - \frac{11}{8}\ln 2\ln 3 - \frac{33}{64}\ln^2 3 \\
&+ \frac{187}{32}\mathrm{Li}_2\Big(\frac{1}{4}\Big) + \frac{143}{192}\zeta(2)\Big] + \Big(\frac{11}{96}C_A - \frac{1}{24}T_R n_f\Big) c_\chi^{(2)} \\
&+ \Big[C_A^2 C_F \Big(\frac{121}{576} - \frac{121}{72}\ln 2 - \frac{121}{96}\ln 3\Big) + C_F T_R^2 n_f^2 \Big(\frac{4}{9} - \frac{2}{9}\ln 2 - \frac{1}{6}\ln 3\Big) \\
&+ C_A C_F T_R n_f \Big(-\frac{187}{144} + \frac{11}{9}\ln 2 + \frac{11}{12}\ln 3\Big)\Big] L(\mu^2 t)\Big\} + \mathcal{O}(\alpha_s^4).
\end{aligned} \tag{7.40d}
$$

We verified that this agrees through $\mathcal{O}(\alpha_s^2)$ with the result which is obtained by directly inserting Eq. (7.25) into Eq. (7.32). Due to the factor of $1/g^2$ in $\tilde{\mathcal{O}}_1$ (see Eq. (7.11)), $\gamma_{2\times 2}^f$ is not RG invariant, while $H_{2\times 2}^{-1}\gamma_{2\times 2}^f H_{2\times 2}$ is. It may be useful to note that, by subtracting the VEVs off of $\tilde{\mathcal{O}}_1$ and $\tilde{\mathcal{O}}_2$,

$$
\begin{aligned}
\tilde{\mathcal{O}}_{1,\mathrm{sub}}(t,x) &= \tilde{\mathcal{O}}_1(t,x) - \langle\tilde{\mathcal{O}}_1(t,x)\rangle, \\
\tilde{\mathcal{O}}_{2,\mathrm{sub}}(t,x) &= \tilde{\mathcal{O}}_2(t,x) - \langle\tilde{\mathcal{O}}_2(t,x)\rangle,
\end{aligned} \tag{7.41}
$$

the resulting operators do not mix with $\tilde{\mathcal{O}}_3$ under t-evolution. Rather, their logarithmic t-evolution is fully governed by $\gamma_{2\times 2}^f$ and thus known through $\mathcal{O}(\alpha_s^3)$.

Eq. (7.36) does not analogously allow one to derive the $\mathcal{O}(\alpha_s^3)$ terms of $\vec{\gamma}_3^{\,f}$, because it involves γ_0 which, in contrast to β and γ_m, starts at $\mathcal{O}(\alpha_s^0)$ rather than $\mathcal{O}(\alpha_s)$, see Eq. (7.8). Therefore, we can only give the result through $\mathcal{O}(\alpha_s^2)$ for $\vec{\gamma}_3^{\,f}$:

$$\gamma_{13}^f = \frac{3N_C n_h}{8\pi^2}\frac{\alpha_s}{\pi}C_F\Bigg\{1+\frac{\alpha_s}{\pi}\Bigg[9.24729\,C_A - 2.47340\,C_F - 2.91787\,T_R n_h + 1.08213\,T_R n_l + L(\mu^2 t)\left(\frac{11}{6}\,C_A + 3\,C_F - \frac{2}{3}\,T_R n_f\right)\Bigg]\Bigg\} + \mathcal{O}(\alpha_s^3), \tag{7.42a}$$

$$\gamma_{23}^f = \frac{N_C n_h}{2\pi^2}\Bigg\{1+\frac{\alpha_s}{\pi}C_F\left[\frac{33}{8} - \ln 2 - \frac{3}{4}\ln 3 + 3\,L(\mu^2 t)\right] + \left(\frac{\alpha_s}{\pi}\right)^2 C_F\Bigg[2.81363\,C_A + 4.22899\,C_F - 4.31769\,T_R n_h - 1.31769\,T_R n_l + L(\mu^2 t)\Bigg(6.43224\,C_A + 8.19868\,C_F - 1.70263\,T_R n_f\Bigg) + L^2(\mu^2 t)\left(\frac{11}{8}\,C_A + \frac{9}{2}\,C_F - \frac{1}{2}\,T_R n_f\right)\Bigg]\Bigg\} + \mathcal{O}(\alpha_s^3). \tag{7.42b}$$

We checked, of course, that Eq. (7.36) is consistent with the results for ζ_{13} and ζ_{23} of Eq. (7.28).

7.5 CONCLUSIONS

We presented the flowed OPE for general current-current correlators and its matching to regular QCD through NNLO in the strong coupling α_s and through mass dimension four by using the small-flow-time expansion. Our calculation is based on the renormalization procedure for the regular QCD dimension-four operators worked out in Ref. [164, 165], the mixing matrix between flowed and regular EMT operators derived in Section 6.5, the method of projectors described in Section 6.2, and the results for the VEVs presented in Chapter 5.

Overall, our results allow to combine the known perturbative results for the regular QCD current-current correlators from the literature to gradient flow lattice calculations. This lays out the path for an alternative determination of hadronic contributions to observables such as the anomalous magnetic moment of the muon. In addition, we derived a general logarithmic flow-time evolution equation for flowed operators and presented its explicit form for the dimension-four operators considered in this chapter.

8

THE ELECTROWEAK HAMILTONIAN IN THE GRADIENT FLOW FORMALISM

Flavor observables play an important role in the verification of the Standard Model. For example, neutral kaon oscillations provide an insight into indirect *charge conjugation parity* (CP) violation. Calculations of such flavor observables are usually performed in the effective theory of weak interactions described by an effective Hamiltonian. In its generic form, it reads

$$\mathcal{H}_{\text{eff}} = -\frac{4G_{\text{F}}}{\sqrt{2}} V_{\text{CKM}} \sum_i Q_i C_i, \tag{8.1}$$

where G_{F} denotes the Fermi constant, V_{CKM} is the relevant *Cabibbo-Kobayashi-Maskawa* (CKM) element for the operators Q_i, and C_i are the corresponding Wilson coefficients [209]. This OPE separates the perturbative UV from non-perturbative infrared contributions. The perturbative electroweak effects are captured in the Wilson coefficients. Due to the small scale of hadronic physics, calculations of the matrix elements with insertions of the operators Q_i require non-perturbative treatment. The full result of the effective theory is then obtained by combining the perturbative Wilson coefficients with lattice determinations of the hadronic matrix elements [210]. These matrix elements are often expressed as so-called *bag* parameters. However, while the perturbative Wilson coefficients are usually computed in the $\overline{\text{MS}}$ scheme, the bag parameters are usually obtained in some scheme related to the lattice. The necessary perturbative matching of the schemes is one of the dominant sources of uncertainties for theoretical predictions of kaon mixing [210].

As already discussed in Section 2.4, flowed composite operators do not require renormalization beyond coupling and field renormalization. In particular, they do not mix under RG running so that they can simply be transferred between different regularization schemes. Applying this to the operators of the electroweak Hamiltonian might thus help to avoid the scheme matching of the perturbative and the lattice calculations.

We introduce the relevant operators for $\Delta F = 2$ transitions, e.g. kaon or B meson mixing, in Section 8.1. Since those operators include γ_5, we discuss its treatment in dimensional regularization as well as the appearing evanescent operators. Employing the small-flow-time expansion of Eq. (6.7), we then express the regular operators through their flowed counterparts with the help of a mixing matrix in Section 8.2. In the same section, we also discuss the renormalization of the regular operators and its impact on the mixing matrix. In Section 8.3, we outline our calculation of the mixing matrix based on the method of projectors already introduced in Section 6.2 and discuss some of the delicate aspects of the calculation. Section 8.4 then presents our preliminary results, while we discuss possible next steps of the project in Section 8.5.

8.1 OPERATOR BASIS

The operator basis of the Hamiltonian for weak interactions in Eq. (8.1) up to mass dimension six consists of 18 operators, which can be divided into five classes: Current-current operators, QCD penguin operators, electroweak penguin operators, magnetic penguin operators, and semileptonic operators [209]. All operators are of dimension six except for the magnetic penguin operators which are of dimension five. In addition, Ref. [209] shows a sixth class for $\Delta F = 2$ operators. In the effective theory they are essentially current-current operators just with a different quark content, which are generated by different diagrams in the Standard Model. Since we are only interested in the operator basis of the effective theory and not their source, we also call them current-current operators.

Not all of the 18 operators contribute to all problems. In this thesis, we focus on a pure QCD calculation and can directly neglect all electroweak and semileptonic operators. Moreover, we require no penguin operators by restricting us to the case that no quark-antiquark pair has the same flavor. This can be simply understood by the fact that pure QCD corrections cannot generate penguin diagrams in this case because it conserves flavor. Fig. 8.1 shows the eponymous penguin diagram in the Standard Model as well as penguin diagrams in the effective theory.

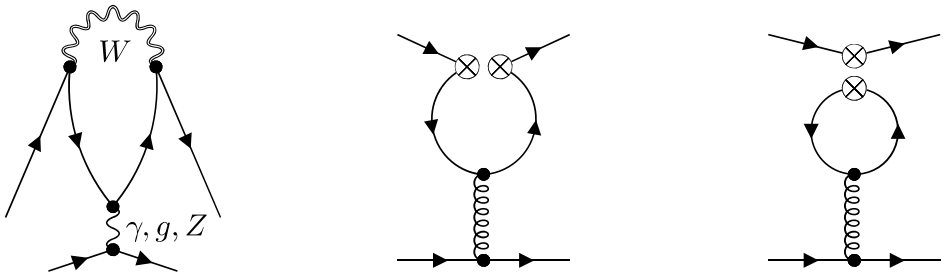

(a) (b) (c)

Figure 8.1: (a) The eponymous penguin diagram in the Standard Model, (b) and (c) penguin diagrams in the effective theory.

We choose the two current-current operators as [211]

$$\begin{aligned} \mathcal{O}_1 &= -\left(\bar{\psi}_{1,\mathrm{L}}\gamma_\mu T^a \psi_{2,\mathrm{L}}\right)\left(\bar{\psi}_{3,\mathrm{L}}\gamma_\mu T^a \psi_{4,\mathrm{L}}\right), \\ \mathcal{O}_2 &= \left(\bar{\psi}_{1,\mathrm{L}}\gamma_\mu \psi_{2,\mathrm{L}}\right)\left(\bar{\psi}_{3,\mathrm{L}}\gamma_\mu \psi_{4,\mathrm{L}}\right), \end{aligned} \tag{8.2}$$

where the subscript L denotes the left-handed component of the spinors

$$\psi_{\mathrm{R/L}} = P_\pm \psi = \tfrac{1}{2}(1 \pm \gamma_5)\psi. \tag{8.3}$$

Note that the sign difference in $\mathcal{O}_1$ compared to Ref. [211] is induced by the different conventions for the color matrices T^a, cf. Appendix A.1.

Similar operators with ψ_2 and ψ_4 exchanged can be eliminated by the Fierz identities. Moreover, color non-singlet operators like

$$\left(\bar{\psi}_{1,\mathrm{L},i}\gamma_\mu \psi_{2,\mathrm{L},j}\right)\left(\bar{\psi}_{3,\mathrm{L},j}\gamma_\mu \psi_{4,\mathrm{L},i}\right) \tag{8.4}$$

can be eliminated by employing the relation

$$T^a_{ij}T^a_{kl} = T_R\left(\delta_{il}\delta_{jk} - \tfrac{1}{N}\delta_{ij}\delta_{kl}\right) \tag{8.5}$$

which is only valid in the fundamental representation of SU(N) [212]. Hence, if the color non-singlet operators are eliminated through Eq. (8.5), any calculation in the remaining basis is no longer independent of the gauge group.

We restrict ourselves to the case of four different flavors throughout this chapter, which allows us to easily compare with the literature. Penguin operators do not appear due to $\psi_2 \neq \psi_1 \neq \psi_4$ and $\psi_2 \neq \psi_3 \neq \psi_4$. For $\Delta F = 2$, i.e. $\psi_1 = \psi_3$ or $\psi_2 = \psi_4$, the two operators in Eq. (8.2) are related by a Fierz identity and, thus, are no longer linearly independent. However, the physical $\Delta F = 2$ mixing matrix can be obtained from the result in the basis of Eq. (8.2) by transforming to a basis in which one of the operators vanishes algebraically due to the Fierz identity.

Naturally, the basis choice is not unique and one can construct linear combinations or add nonphysical or vanishing operators. For example, the current-current operators in Eq. (8.2) differ from the corresponding operators in the *standard basis* introduced in Ref. [213]. However, there are different preferences of these two operators even in the standard basis, e.g. comparing Ref. [213] and Ref. [214]. Of course, all these operators are related through the Fierz identities and Eq. (8.5). Instead, the advantage of the basis introduced in Ref. [211], from now on abbreviated as *Chetyrkin-Misiak-Münz* (CMM) basis, concerns the QCD penguin operators and the treatment of γ_5.

In dimensional regularization the anticommutativity of γ_5 with the other γ matrices

$$\{\gamma_\mu, \gamma_5\} = 0 \tag{8.6}$$

is incompatible with the trace requirement

$$\mathrm{Tr}(\gamma_\mu\gamma_\nu\gamma_\rho\gamma_\sigma\gamma_5) \neq 0 \underset{D\to 4}{\longrightarrow} 4\mathrm{i}\epsilon_{\mu\nu\rho\sigma}, \tag{8.7}$$

which is needed for a meaningful transition to four dimensions [215]. There are many schemes on how to deal with this problem, but we will just mention the two most prominent. The 't Hooft-Veltman scheme splits the D-dimensional Lorentz space into a four- and a -2ϵ-dimensional subspace [216]. γ_5 only anticommutes with the γ matrices of the four-dimensional subspace. However, this violates gauge invariance and introduces anomalies [215]. Moreover, the 't Hooft-Veltman scheme leads to tedious calculations, especially at higher orders in perturbation theory. On the other hand, the naive dimensional regularization scheme drops the requirement (8.7) and just uses a fully anticommuting γ_5. This makes calculations much simpler, but still forces one to adopt some prescription for treating traces with γ_5 in D dimensions if they appear. Then, one also has to carefully check that spurious anomalies cancel [215]. Recently, Zerf performed a sophisticated analysis on the treatment of traces with γ_5 and developed an algorithm to obtain unambiguous results in D dimensions in Ref. [217]. Although it is applicable to traces with an arbitrary number of γ matrices, a central ingredient is still missing for traces with more than ten γ matrices.

The advantage of the CMM basis over the standard basis in perturbative calculations can be illustrated by the one-loop diagram in Fig. 8.1(c) with the insertion of a penguin operator. For example, in the standard basis one of the penguin operators is chosen as

$$\mathcal{O}_{3,\mathrm{SB}} = \left(\bar{\psi}_{1,\mathrm{L}}\gamma_\mu\psi_{2,\mathrm{L}}\right)\sum_f\left(\bar{\psi}_{f,\mathrm{L}}\gamma_\mu\psi_{f,\mathrm{L}}\right), \tag{8.8}$$

where the sum runs over the different quark flavors. The corresponding operator in the CMM basis reads

$$\mathcal{O}_{3,\mathrm{CMM}} = \left(\bar{\psi}_{1,\mathrm{L}}\gamma_\mu\psi_{2,\mathrm{L}}\right)\sum_f\left(\bar{\psi}_f\gamma_\mu\psi_f\right). \tag{8.9}$$

The fermion loop in Fig. 8.1(c) and with it the trace contains γ_5 in the standard basis. In the CMM basis, on the other hand, there is no γ_5 in the loop and, thus, the trace is free of γ_5. Instead, γ_5 only appears on the fermion lines which are connected to the external fields. Hence, one can unambiguously use an anticommuting γ_5, because one does not have to specify how γ_5 shall be treated in traces. Since we aim to extend our calculation to the QCD penguin operators in the future, we choose the CMM basis over the standard basis.

However, there is a further complication for four-fermion operators: Each order in perturbation theory introduces additional operators [218]. These operators are called *evanescent*, because they vanish for $D = 4$, i.e. algebraically they are of $O(\epsilon)$. Nonetheless, they mix with the physical operators in dimensional regularization and are necessary to remove all UV divergences. On the other hand, one can prevent the physical operators from mixing into the evanescent operators by a finite renormalization such that all Green's functions of evanescent operators vanish [218–220].

Also for the evanescent operators we follow Ref. [211] and choose

$$\begin{aligned} E_1^{(1)} &= -\left(\bar{\psi}_{1,\mathrm{L}}\gamma_{\mu_1\mu_2\mu_3}T^a\psi_{2,\mathrm{L}}\right)\left(\bar{\psi}_{3,\mathrm{L}}\gamma_{\mu_1\mu_2\mu_3}T^a\psi_{4,\mathrm{L}}\right) - 16\mathcal{O}_1, \\ E_2^{(1)} &= \left(\bar{\psi}_{1,\mathrm{L}}\gamma_{\mu_1\mu_2\mu_3}\psi_{2,\mathrm{L}}\right)\left(\bar{\psi}_{3,\mathrm{L}}\gamma_{\mu_1\mu_2\mu_3}\psi_{4,\mathrm{L}}\right) - 16\mathcal{O}_2 \end{aligned} \tag{8.10}$$

with $\gamma_{\mu_1\cdots\mu_n} \equiv \gamma_{\mu_1}\cdots\gamma_{\mu_n}$ as the evanescent operators at NLO, as denoted by the superscript (1). At NNLO, we additionally require

$$\begin{aligned} E_1^{(2)} &= -\left(\bar{\psi}_{1,\mathrm{L}}\gamma_{\mu_1\mu_2\mu_3\mu_4\mu_5}T^a\psi_{2,\mathrm{L}}\right)\left(\bar{\psi}_{3,\mathrm{L}}\gamma_{\mu_1\mu_2\mu_3\mu_4\mu_5}T^a\psi_{4,\mathrm{L}}\right) - 20E_1^{(1)} - 256\mathcal{O}_1, \\ E_2^{(2)} &= \left(\bar{\psi}_{1,\mathrm{L}}\gamma_{\mu_1\mu_2\mu_3\mu_4\mu_5}\psi_{2,\mathrm{L}}\right)\left(\bar{\psi}_{3,\mathrm{L}}\gamma_{\mu_1\mu_2\mu_3\mu_4\mu_5}\psi_{4,\mathrm{L}}\right) - 20E_2^{(1)} - 256\mathcal{O}_2. \end{aligned} \tag{8.11}$$

Ref. [211] also introduces an operator which vanishes by the EOM. It cannot mix into the operators introduced above as long as we can discard the penguin operators.

8.2 SMALL-FLOW-TIME EXPANSION AND RENORMALIZATION

We now want to express the physical current-current operators in Eq. (8.2) through the corresponding flowed operators

$$\begin{aligned} \tilde{\mathcal{O}}_1 &= -\mathring{Z}_\chi^2\left(\bar{\chi}_{1,\mathrm{L}}\gamma_\mu T^a\chi_{2,\mathrm{L}}\right)\left(\bar{\chi}_{3,\mathrm{L}}\gamma_\mu T^a\chi_{4,\mathrm{L}}\right), \\ \tilde{\mathcal{O}}_2 &= \mathring{Z}_\chi^2\left(\bar{\chi}_{1,\mathrm{L}}\gamma_\mu\chi_{2,\mathrm{L}}\right)\left(\bar{\chi}_{3,\mathrm{L}}\gamma_\mu\chi_{4,\mathrm{L}}\right) \end{aligned} \tag{8.12}$$

with the help of the small-flow-time expansion, cf. Eq. (6.7). $\mathring{Z}_\chi$ denotes the field renormalization constant for ringed quarks defined in Eq. (2.62). Due to the operator mixing described in Section 8.1, we also have to include the flowed evanescent operators

$$\begin{aligned}
\tilde{E}_1^{(1)} &= -\mathring{Z}_\chi^2 \left(\bar{\chi}_{1,\mathrm{L}} \gamma_{\mu_1\mu_2\mu_3} T^a \chi_{2,\mathrm{L}}\right) \left(\bar{\chi}_{3,\mathrm{L}} \gamma_{\mu_1\mu_2\mu_3} T^a \chi_{4,\mathrm{L}}\right) - 16\tilde{\mathcal{O}}_1, \\
\tilde{E}_2^{(1)} &= \mathring{Z}_\chi^2 \left(\bar{\chi}_{1,\mathrm{L}} \gamma_{\mu_1\mu_2\mu_3} \chi_{2,\mathrm{L}}\right) \left(\bar{\chi}_{3,\mathrm{L}} \gamma_{\mu_1\mu_2\mu_3} \chi_{4,\mathrm{L}}\right) - 16\tilde{\mathcal{O}}_2,
\end{aligned} \tag{8.13}$$

$$\begin{aligned}
\tilde{E}_1^{(2)} &= -\mathring{Z}_\chi^2 \left(\bar{\chi}_{1,\mathrm{L}} \gamma_{\mu_1\mu_2\mu_3\mu_4\mu_5} T^a \chi_{2,\mathrm{L}}\right) \left(\bar{\chi}_{3,\mathrm{L}} \gamma_{\mu_1\mu_2\mu_3\mu_4\mu_5} T^a \chi_{4,\mathrm{L}}\right) - 20\tilde{E}_1^{(1)} - 256\tilde{\mathcal{O}}_1, \\
\tilde{E}_2^{(2)} &= \mathring{Z}_\chi^2 \left(\bar{\chi}_{1,\mathrm{L}} \gamma_{\mu_1\mu_2\mu_3\mu_4\mu_5} \chi_{2,\mathrm{L}}\right) \left(\bar{\chi}_{3,\mathrm{L}} \gamma_{\mu_1\mu_2\mu_3\mu_4\mu_5} \chi_{4,\mathrm{L}}\right) - 20\tilde{E}_2^{(1)} - 256\tilde{\mathcal{O}}_2
\end{aligned} \tag{8.14}$$

at NLO and NNLO, respectively. By inverting the small-flow-time expansion and neglecting the $O(t)$ terms, we find

$$\begin{pmatrix} \vec{\mathcal{O}} \\ \vec{E} \end{pmatrix} = \zeta^{-1} \begin{pmatrix} \vec{\tilde{\mathcal{O}}} \\ \vec{\tilde{E}} \end{pmatrix} \equiv \begin{pmatrix} \zeta_{\mathrm{PP}}^{-1} & \zeta_{\mathrm{PE}}^{-1} \\ \zeta_{\mathrm{EP}}^{-1} & \zeta_{\mathrm{EE}}^{-1} \end{pmatrix} \begin{pmatrix} \vec{\tilde{\mathcal{O}}} \\ \vec{\tilde{E}} \end{pmatrix}, \tag{8.15}$$

where $\vec{\mathcal{O}}^{\mathrm{T}} = (\mathcal{O}_1, \mathcal{O}_2)^{\mathrm{T}}$ and $\vec{E}^{\mathrm{T}} = (E_1^{(1)}, E_2^{(1)})^{\mathrm{T}}$ at NLO and $\vec{E}^{\mathrm{T}} = (E_1^{(1)}, E_2^{(1)}, E_1^{(2)}, E_2^{(2)})^{\mathrm{T}}$ at NNLO, respectively. $\vec{\tilde{\mathcal{O}}}$ and $\vec{\tilde{E}}$ are defined equivalently. The subscripts P and E in the submatrices of ζ^{-1} denote the mixing of the two sets, e.g. ζ_{PE}^{-1} describes the mixing of the flowed evanescent operators (E) into the regular physical operators (P).

Even though the flowed operators do not require renormalization apart from the field and coupling renormalization, the regular operators have to be renormalized with the renormalization matrix Z according to [209]

$$\begin{Bmatrix} \vec{\mathcal{O}} \\ \vec{E} \end{Bmatrix}_{\mathrm{R}} = Z \begin{pmatrix} \vec{\mathcal{O}} \\ \vec{E} \end{pmatrix} \equiv \begin{pmatrix} Z_{\mathrm{PP}} & Z_{\mathrm{PE}} \\ Z_{\mathrm{EP}} & Z_{\mathrm{EE}} \end{pmatrix} \begin{pmatrix} \vec{\mathcal{O}} \\ \vec{E} \end{pmatrix}. \tag{8.16}$$

Accordingly, the Wilson coefficients in Eq. (8.1) are renormalized by $\vec{C}_{\mathrm{B}} = Z^{\mathrm{T}} \vec{C}$. Each matrix element Z_{ij} can be expanded as the power series

$$Z_{ij} = \delta_{ij} + \sum_{k=1}^{\infty} \left(\frac{\alpha_{\mathrm{s}}}{4\pi}\right)^k Z_{ij}^{(k)} \quad \text{with} \quad Z_{ij}^{(k)} = \sum_{l=0}^{k} \frac{1}{\epsilon^l} Z_{ij}^{(k,l)}. \tag{8.17}$$

In the $\overline{\mathrm{MS}}$ scheme, Z_{PP}, Z_{PE}, and Z_{EE} are given by pure $1/\epsilon^l$ poles, while Z_{EP} contains finite terms [218–220]. The anomalous dimension γ_{ij} is defined by

$$\mu^2 \frac{\mathrm{d}^2 C_i(\mu)}{\mathrm{d}\mu^2} \equiv \gamma_{ji} C_j(\mu) = \left[\sum_{k=0}^{\infty} \left(\frac{\alpha_{\mathrm{s}}}{4\pi}\right)^{k+1} \gamma_{k,ji}\right] C_j(\mu). \tag{8.18}$$

In Refs. [219, 220] it was shown that γ possesses an upper-block-triangular form, i.e. $\gamma_{\mathrm{EP}} = 0$. Since in any mass independent renormalization scheme the only μ-dependence of Z_{ij} resides in α_{s}, we obtain the relation

$$\gamma_{ij} = \alpha_{\mathrm{s}} \beta_\epsilon Z_{ik} \frac{\partial Z_{kj}^{-1}}{\partial \alpha_{\mathrm{s}}}, \tag{8.19}$$

which allows us to express some of the coefficients $Z_{ij}^{(k,l)}$ of the renormalization matrix through the coefficients $\gamma_{n,ij}$ of the anomalous dimension. Through NNLO we can write the renormalization matrix as [211, 221]

$$\begin{aligned} Z_{ij} = \delta_{ij} + \frac{\alpha_s}{4\pi}\left[\frac{\gamma_{0,ij}}{\epsilon} + Z_{ij}^{(1,0)}\right] + \left(\frac{\alpha_s}{4\pi}\right)^2 \Bigg[\frac{1}{2\epsilon^2}\left(\gamma_{0,ik}\gamma_{0,kj} - \beta_0\gamma_{0,ij}\right) \\ + \frac{1}{2\epsilon}\left(\gamma_{1,ij} + \gamma_{0,ik}Z_{kj}^{(1,0)} + Z_{ik}^{(1,0)}\gamma_{0,kj} - \beta_0 Z_{ij}^{(1,0)}\right) + Z_{ij}^{(2,0)}\Bigg] + \mathcal{O}(\alpha_s^3). \end{aligned} \tag{8.20}$$

By inserting Eq. (8.16) into Eq. (8.15), we arrive at

$$\begin{aligned} \begin{Bmatrix} \vec{\mathcal{O}} \\ \vec{E} \end{Bmatrix}_R &= Z\zeta^{-1}\begin{pmatrix} \vec{\mathcal{O}} \\ \vec{E} \end{pmatrix} = \begin{pmatrix} Z_{PP} & Z_{PE} \\ Z_{EP} & Z_{EE} \end{pmatrix}\begin{pmatrix} \zeta_{PP}^{-1} & \zeta_{PE}^{-1} \\ \zeta_{EP}^{-1} & \zeta_{EE}^{-1} \end{pmatrix}\begin{pmatrix} \vec{\mathcal{O}} \\ \vec{E} \end{pmatrix} \\ &\equiv \zeta_R^{-1}\begin{pmatrix} \vec{\mathcal{O}} \\ \vec{E} \end{pmatrix} = \begin{pmatrix} \zeta_{R,PP}^{-1} & \zeta_{R,PE}^{-1} \\ \zeta_{R,EP}^{-1} & \zeta_{R,EE}^{-1} \end{pmatrix}\begin{pmatrix} \vec{\mathcal{O}} \\ \vec{E} \end{pmatrix}, \end{aligned} \tag{8.21}$$

where ζ_R^{-1} is the renormalized (inverse) mixing matrix. Of course, we are only interested in the physical submatrix $\zeta_{R,PP}^{-1}$, i.e. the mixing of the flowed physical operators into the regular physical operators. Especially, we do not want any contributions from the flowed evanescent operators to the regular physical operators through the submatrix $\zeta_{R,PE}^{-1}$. If $\zeta_{R,PE}^{-1}$ is finite after renormalization, this requirement is trivially fulfilled, because the evanescent operators only contribute with $O(\epsilon)$ terms which vanish for $D = 4$. More importantly, the regular evanescent operators must not receive any contributions from flowed physical operators through $\zeta_{R,EP}^{-1}$ in order for their Green's functions to vanish. Therefore, we have to demand $\zeta_{R,EP}^{-1} \overset{!}{=} O(\epsilon)$, i.e. the finite renormalization through Z_{EP} has to subtract all finite terms in this submatrix. The mixing of the evanescent operators with themselves described by $\zeta_{R,EE}^{-1}$ is irrelevant for us as long as it is finite.

8.3 CALCULATION OF THE MIXING MATRIX

For the calculation of the mixing matrix ζ we again use the method of projectors introduced in Section 6.2. The Feynman rules for the operators can simply be read off from Eqs. (8.2), (8.10), and (8.11) and we find

$$\begin{aligned} \mathcal{O}_{1,ijkl,\hat{\alpha}\hat{\beta}\hat{\gamma}\hat{\delta}} &= -T_{ij}^a T_{kl}^a \{P_+\gamma_\mu P_-\}_{\hat{\alpha}\hat{\beta}}\{P_+\gamma_\mu P_-\}_{\hat{\gamma}\hat{\delta}}, \\ \mathcal{O}_{2,ijkl,\hat{\alpha}\hat{\beta}\hat{\gamma}\hat{\delta}} &= \delta_{ij}\delta_{kl}\{P_+\gamma_\mu P_-\}_{\hat{\alpha}\hat{\beta}}\{P_+\gamma_\mu P_-\}_{\hat{\gamma}\hat{\delta}}, \\ E_{1,ijkl,\hat{\alpha}\hat{\beta}\hat{\gamma}\hat{\delta}}^{(1)} &= -T_{ij}^a T_{kl}^a \{P_+\gamma_{\mu_1\mu_2\mu_3} P_-\}_{\hat{\alpha}\hat{\beta}}\{P_+\gamma_{\mu_1\mu_2\mu_3} P_-\}_{\hat{\gamma}\hat{\delta}} - 16\,\mathcal{O}_{1,ijkl,\hat{\alpha}\hat{\beta}\hat{\gamma}\hat{\delta}}, \\ E_{2,ijkl,\hat{\alpha}\hat{\beta}\hat{\gamma}\hat{\delta}}^{(1)} &= \delta_{ij}\delta_{kl}\{P_+\gamma_{\mu_1\mu_2\mu_3} P_-\}_{\hat{\alpha}\hat{\beta}}\{P_+\gamma_{\mu_1\mu_2\mu_3} P_-\}_{\hat{\gamma}\hat{\delta}} - 16\,\mathcal{O}_{2,ijkl,\hat{\alpha}\hat{\beta}\hat{\gamma}\hat{\delta}}, \\ E_{1,ijkl,\hat{\alpha}\hat{\beta}\hat{\gamma}\hat{\delta}}^{(2)} &= -T_{ij}^a T_{kl}^a \{P_+\gamma_{\mu_1\mu_2\mu_3\mu_4\mu_5} P_-\}_{\hat{\alpha}\hat{\beta}}\{P_+\gamma_{\mu_1\mu_2\mu_3\mu_4\mu_5} P_-\}_{\hat{\gamma}\hat{\delta}} - 20\,E_{1,ijkl,\hat{\alpha}\hat{\beta}\hat{\gamma}\hat{\delta}}^{(1)} \\ &\quad - 256\,\mathcal{O}_{1,ijkl,\hat{\alpha}\hat{\beta}\hat{\gamma}\hat{\delta}}, \end{aligned} \tag{8.22}$$

$$E^{(2)}_{2,ijkl,\hat{\alpha}\hat{\beta}\hat{\gamma}\hat{\delta}} = \delta_{ij}\delta_{kl}\{P_+\gamma_{\mu_1\mu_2\mu_3\mu_4\mu_5}P_-\}_{\hat{\alpha}\hat{\beta}}\{P_+\gamma_{\mu_1\mu_2\mu_3\mu_4\mu_5}P_-\}_{\hat{\gamma}\hat{\delta}} - 20\,E^{(1)}_{2,ijkl,\hat{\alpha}\hat{\beta}\hat{\gamma}\hat{\delta}} - 256\,\mathcal{O}_{2,ijkl,\hat{\alpha}\hat{\beta}\hat{\gamma}\hat{\delta}}.$$

The flowed operators defined in Eqs. (8.12) to (8.14) have the same Feynman rules except that they are multiplied by $\mathring{Z}_\chi^2$ and that the incoming propagators can be flow lines. Hence, we depict them by the same graphical Feynman rule

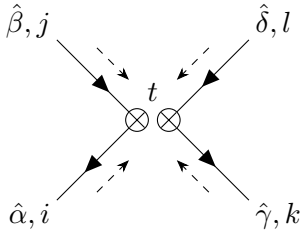

(8.23)

and easily differentiate between them by the flow time assigned to the vertex, i.e. flow time 0 corresponds to a regular QCD operator. Then, all flow-line contributions trivially vanish for the regular operators. Moreover, all operators have the same field content and, thus, their graphical Feynman rule is exactly the same.

This means that we can use the same external state for all projectors. However, while it is trivial to construct diagonal projectors for the two color structures of the operators, their spinor structure is heavily intertwined. For example, we can choose

$$\begin{aligned}\hat{P}_1[\mathcal{O}] &= -\frac{T^b_{ji}T^b_{lk}}{T_R^2 N_A}\,\{\gamma_\nu\}_{\hat{\beta}\hat{\alpha}}\{\gamma_\nu\}_{\hat{\delta}\hat{\gamma}}\,\langle 0|\hat{\psi}_{4,L,\hat{\delta},l}\hat{\bar{\psi}}_{3,L,\hat{\gamma},k}\hat{\psi}_{2,L,\hat{\beta},j}\hat{\bar{\psi}}_{1,L,\hat{\alpha},i}\mathcal{O}|0\rangle\Big|_{p=m=0},\\ \hat{P}_2[\mathcal{O}] &= \frac{\delta_{ji}\delta_{lk}}{N_C^2}\,\{\gamma_\nu\}_{\hat{\beta}\hat{\alpha}}\{\gamma_\nu\}_{\hat{\delta}\hat{\gamma}}\,\langle 0|\hat{\psi}_{4,L,\hat{\delta},l}\hat{\bar{\psi}}_{3,L,\hat{\gamma},k}\hat{\psi}_{2,L,\hat{\beta},j}\hat{\bar{\psi}}_{1,L,\hat{\alpha},i}\mathcal{O}|0\rangle\Big|_{p=m=0},\end{aligned} \tag{8.24}$$

which fulfill $\hat{P}_i[\mathcal{O}_j] \propto \delta_{ij}$ for $\mathcal{O}_1$ and $\mathcal{O}_2$ due to

$$\hat{P}_1[\mathcal{O}_2] \propto \hat{P}_2[\mathcal{O}_1] \propto \delta_{ij}\delta_{kl}T^b_{ji}T^b_{lk} = 0. \tag{8.25}$$

However, at NLO we have to include the evanescent operators $E_1^{(1)}$ and $E_2^{(1)}$ and, thus, have to compute additional zero-loop diagrams with insertions of the new operators. It is immediately clear that

$$\hat{P}_1[E_1^{(1)}] \neq 0 \tag{8.26}$$

already at zero-loop order, which means that the projectors are no longer diagonal. Hence, not only do we have to construct new projectors for the new operators, we also have to construct new projectors for $\mathcal{O}_1$ and $\mathcal{O}_2$. In general, for each additional order in perturbation theory additional evanescent operators have to be included. Their spinor structure is not diagonal w.r.t. the projectors constructed at lower orders already for the new zero-loop contributions. Since there is an infinite tower of evanescent operators, it is impossible to construct projectors which are diagonal to all orders in perturbation theory. Instead, we use projectors which are only diagonalized and normalized in color

space but not in spinor space and construct diagonal linear combinations of them after computing the matrix elements. In our calculation up to NNLO, we choose the projectors in Eq. (8.24) and additionally

$$\begin{aligned}
\hat{P}_3[\mathcal{O}] &= -\frac{T^b_{ji}T^b_{lk}}{T_R^2 N_A}\,\{\gamma_{\nu_1\nu_2\nu_3}\}_{\hat{\beta}\hat{\alpha}}\{\gamma_{\nu_1\nu_2\nu_3}\}_{\hat{\delta}\hat{\gamma}}\,\langle 0|\hat{\psi}_{4,\mathrm{L},\hat{\delta},l}\hat{\bar{\psi}}_{3,\mathrm{L},\hat{\gamma},k}\hat{\psi}_{2,\mathrm{L},\hat{\beta},j}\hat{\bar{\psi}}_{1,\mathrm{L},\hat{\alpha},i}\mathcal{O}|0\rangle\Big|_{p=m=0}\,,\\
\hat{P}_4[\mathcal{O}] &= \frac{\delta_{ji}\delta_{lk}}{N_C^2}\,\{\gamma_{\nu_1\nu_2\nu_3}\}_{\hat{\beta}\hat{\alpha}}\{\gamma_{\nu_1\nu_2\nu_3}\}_{\hat{\delta}\hat{\gamma}}\,\langle 0|\hat{\psi}_{4,\mathrm{L},\hat{\delta},l}\hat{\bar{\psi}}_{3,\mathrm{L},\hat{\gamma},k}\hat{\psi}_{2,\mathrm{L},\hat{\beta},j}\hat{\bar{\psi}}_{1,\mathrm{L},\hat{\alpha},i}\mathcal{O}|0\rangle\Big|_{p=m=0}\,,\\
\hat{P}_5[\mathcal{O}] &= -\frac{T^b_{ji}T^b_{lk}}{T_R^2 N_A}\,\{\gamma_{\nu_1\nu_2\nu_3\nu_4\nu_5}\}_{\hat{\beta}\hat{\alpha}}\{\gamma_{\nu_1\nu_2\nu_3\nu_4\nu_5}\}_{\hat{\delta}\hat{\gamma}}\,\langle 0|\hat{\psi}_{4,\mathrm{L},\hat{\delta},l}\hat{\bar{\psi}}_{3,\mathrm{L},\hat{\gamma},k}\hat{\psi}_{2,\mathrm{L},\hat{\beta},j}\hat{\bar{\psi}}_{1,\mathrm{L},\hat{\alpha},i}\mathcal{O}|0\rangle\Big|_{p=m=0}\,,\\
\hat{P}_6[\mathcal{O}] &= \frac{\delta_{ji}\delta_{lk}}{N_C^2}\,\{\gamma_{\nu_1\nu_2\nu_3\nu_4\nu_5}\}_{\hat{\beta}\hat{\alpha}}\{\gamma_{\nu_1\nu_2\nu_3\nu_4\nu_5}\}_{\hat{\delta}\hat{\gamma}}\,\langle 0|\hat{\psi}_{4,\mathrm{L},\hat{\delta},l}\hat{\bar{\psi}}_{3,\mathrm{L},\hat{\gamma},k}\hat{\psi}_{2,\mathrm{L},\hat{\beta},j}\hat{\bar{\psi}}_{1,\mathrm{L},\hat{\alpha},i}\mathcal{O}|0\rangle\Big|_{p=m=0}\,.
\end{aligned} \tag{8.27}$$

After calculating all these basis elements, we construct the linear combinations

$$P_i[\mathcal{O}] = c_{i,j}\hat{P}_j[\mathcal{O}] \tag{8.28}$$

and fix the coefficients by demanding $P_i[\mathcal{O}_j] = \delta_{ij}$ at zero-loop level. Due to their color structure, we immediately find that $c_{i,j} = 0$ if i is odd (even) and j is even (odd). Moreover, the coefficients $c_{i,k}$ obey $c_{1,k} = c_{2,k+1}$, $c_{3,k} = c_{4,k+1}$, …, because the Dirac structure of each set of operators is the same.

In particular, this strategy allows us to reuse the results obtained at lower orders in perturbation theory by simply adjusting the coefficients of the linear combinations. For example, if we are only interested in the LO result, it is sufficient to only include $\mathcal{O}_1$ and $\mathcal{O}_2$ and we can set $c_{i,k} = 0\ \forall k > 2$. For the NLO result, we have to include $E_1^{(1)}$ and $E_2^{(1)}$ as well as the corresponding projectors $\hat{P}_3$ and $\hat{P}_4$ in the linear combinations. However, the known results for $\hat{P}_{1/2}[\mathcal{O}_{1/2}]$ at zero-loop level do not have to be recomputed. Thus, for the NLO result, we have to compute the one-loop corrections to $\hat{P}_{1/2}[\mathcal{O}_{1/2}]$ as well as all zero- and one-loop results for $\hat{P}_{1/2}[E_{1/2}^{(1)}]$ and $\hat{P}_{3/4}[\mathcal{O}_{1/2}/E_{1/2}^{(1)}]$.

Strictly speaking, this procedure is not necessary for the physical operators, because $\hat{P}_{1/2}[E] = \mathcal{O}(\epsilon)$ at zero-loop level for all evanescent operators. Hence, all their nondiagonal mixing matrix elements vanish automatically for $\epsilon \to 0$ at zero-loop level and this submatrix is effectively diagonal. However, this no longer holds for the nondiagonal mixing matrix elements of the evanescent operators with themselves and we have to perform the procedure introduced above for their mixing at NNLO at the latest.

The subscript L in the external states of the matrix elements of the projectors indicates that we remove the left-handed spinors $u_\mathrm{L} = P_- u$. By using a strictly anticommuting γ_5, all appearances of γ_5 through $P_\pm$ in the Feynman rules can be commuted to the external spinors where they combine with them through $P_\pm^2 = P_\pm$. The Feynman rules, with the exception of the operator insertions, always introduce an even number of γ matrices, which means that no term vanishes through $P_+P_- = 0$. By removing u_L, no γ_5 is left in the traces obtained by contracting the spinor indices of the external spinors and the γ matrices in the projectors. As discussed in Section 8.1, the choice of the operator basis additionally prevents traces with γ_5 appearing through loop corrections. Hence,

no traces with γ_5 appear in our calculation and we are allowed to consistently use an anticommuting γ_5.

As described in Section 6.2, we set all external momenta and masses to zero to significantly simplify the calculation. Again, all loop corrections on the r.h.s. of Eq. (6.11) trivially vanish in dimensional regularization because scaleless loop integrals vanish. However, for the gradient flow integrals one might be concerned whether one has to perform a sophisticated expansion or whether one is allowed to directly set all external momenta and masses to zero, which corresponds to a naive expansion to LO. Of course, one is allowed to set all external momenta and masses to zero if no denominator in the diagram vanishes through this procedure. The only Feynman rules introducing denominators in the momenta and masses are the propagators, see Appendix B. Flow lines and vertices are free of them. Only propagators outside of loops possess problematic denominators of the form $\frac{1}{p_i^2}$ or $\frac{1}{p_i^2+m_j^2}$. Thus, they only appear in one-particle-reducible diagrams. All other propagators contain an additional loop momentum such that $\frac{1}{(k+p_i)^2} \xrightarrow[p_i \to 0]{} \frac{1}{k^2}$. The external fermions have to be connected to the corresponding fermions of the operators through continuous fermion lines, because they cannot annihilate and create new pairs through QCD alone, cf. the discussion on penguin operators in Section 8.1. Thus, only fermion propagators can connect the subdiagrams of the one-particle-reducible diagrams other than tadpoles. Then, at least one of the two subdiagrams has to be a correction to one of the external legs, while the other subdiagram contains the operator insertion or is another correction to the external leg. Furthermore, the vertex in the former subdiagram connected by the propagator cannot be a flow vertex, because those require a flow line flowing towards the operator insertion instead of a normal propagator. Thereby, the outer subdiagram contains a loop without a flow time scale solely produced by the Feynman rules of regular QCD. The simplest example is shown in Fig. 8.2(a). But this subdiagram also appears in the loop corrections of the regular operators and,

(a) (b)

Figure 8.2: (a) A pure regular QCD correction to one of the external legs, (b) a correction induced by the flowed Lagrangian.

by performing a suitable tensor reduction, can always be reduced to a scaleless scalar integral which vanishes in dimensional regularization. Therefore, the whole diagram can safely be set to zero, e.g. by naively setting the external momenta and masses in the numerator of the propagator to zero and neglecting the denominator. On the other hand, similar subdiagrams connected by flow lines do not vanish in general, but do not contain

problematic denominators either. The corresponding example is shown in Fig. 8.2(b). Thus, we are allowed to naively set all external momenta and masses to zero, first in the numerator and, if the diagram does not vanish, also in the denominator. However, this argument only holds for our calculation with just the current-current operators. It breaks down when penguin-type corrections are included, because at least one fermion flavor is allowed to annihilate in this case and the problematic propagators also appear beyond corrections to the external legs, cf. Figs. 8.1(b) and 8.1(c).

Let us conclude this section by discussing the effect of quarks or antiquarks with the same flavor in the operator, i.e. $\psi_1 = \psi_3$ and/or $\psi_2 = \psi_4$, on the diagrammatic level, ignoring the fact that four-fermion operators become linearly dependent on the operator level as discussed in Section 8.1. Compared to the case with four different flavors, new diagrams contribute, in which the external lines for the fermions with the same flavor are crossed, effectively doubling or quadrupling *all* diagrams. Since this applies to both the regular and the flowed side of Eq. (6.11), the mixing matrix stays the same.

8.4 PRELIMINARY RESULTS FOR THE MIXING MATRIX

In this section we present our preliminary results. Since we applied Eq. (8.5) to reduce the operator basis, they are only valid in SU(N). This translates to the fact that we have to utilize the relations in Eq. (A.4) *and* set $T_R = 1/2$ to cancel the $1/\epsilon^2$ poles at NNLO (at least partially, see below). We do not understand the restriction to $T_R = 1/2$ yet.

If we include all operators in Eqs. (8.2), (8.10), and (8.11), the coefficients of the projectors in Eq. (8.28) read

$$
\begin{aligned}
c_{1,1} = c_{2,2} &= \frac{432 - 900D + 364D^2 - 35D^3}{128D(1-D)(6-5D+D^2)}, \quad c_{1,3} = c_{2,4} = \frac{136 - 78D + 7D^2}{64D(1-D)(6-5D+D^2)}, \\
c_{1,5} = c_{2,6} &= \frac{10 - D}{128D(1-D)(6-5D+D^2)}, \quad c_{3,1} = c_{4,2} = \frac{12 - 24D + 7D^2}{64D(1-D)(6-5D+D^2)}, \\
c_{3,3} = c_{4,4} &= \frac{13 - 6D}{96D(1-D)(6-5D+D^2)}, \quad c_{3,5} = c_{4,6} = \frac{1}{192D(1-D)(6-5D+D^2)}, \\
c_{5,1} = c_{6,2} &= \frac{24 - 50D + 15D^2}{1920D(12-7D+D^2)(2-3D+D^2)}, \\
c_{5,3} = c_{6,4} &= \frac{1}{192D(1-D)(12-7D+D^2)}, \\
c_{5,5} = c_{6,6} &= \frac{1}{1920D(12-7D+D^2)(2-3D+D^2)}, \quad c_{i,j} = 0 \quad \text{for all other } i,j.
\end{aligned}
\tag{8.29}
$$

For the anomalous dimension at NLO we find

$$
\gamma_{0,\mathrm{PP}} = \begin{pmatrix} \frac{-6}{N_C} & \frac{-3}{2N_C^2} + \frac{3}{2} \\ 6 & 0 \end{pmatrix}, \quad \gamma_{0,\mathrm{PE}} = \begin{pmatrix} \frac{-1}{N_C} + \frac{N_C}{4} & \frac{-1}{4N_C^2} + \frac{1}{4} & 0 & 0 \\ 1 & 0 & 0 & 0 \end{pmatrix},
$$

$$\gamma_{0,\mathrm{EE}} = \begin{pmatrix} \frac{6}{N_C} - 3N_C & \frac{3}{2N_C^2} - \frac{3}{2} & \frac{-1}{N_C} + \frac{N_C}{4} & \frac{-1}{4N_C^2} + \frac{1}{4} \\ -6 & 0 & 1 & 0 \\ 0 & 0 & \left[\frac{8}{N_C} + \frac{5N_C}{2}\right] & [0] \\ 0 & 0 & [0] & \frac{8}{N_C} - 8N_C \end{pmatrix}, \tag{8.30}$$

and for the finite renormalization

$$Z_{\mathrm{EP}}^{(1,0)} = \begin{pmatrix} \frac{-24}{N_C} + 24N_C & \frac{-12}{N_C^2} + 12 \\ 48 & \frac{24}{N_C} - 24N_C \\ \left[\frac{2760}{N_C} + 390N_C\right] & \left[\frac{330}{N_C^2} - 330\right] \\ [-1320] & \frac{1440}{N_C} - 1440N_C \end{pmatrix}, \tag{8.31}$$

where we remind that $\gamma_{\mathrm{EP}} = Z_{\mathrm{PP}}^{(i,0)} = Z_{\mathrm{PE}}^{(i,0)} = Z_{\mathrm{EE}}^{(i,0)} = 0$. Everything except those elements marked by square brackets coincides with the results from Refs. [211, 221, 222]. At NNLO we find

$$\gamma_{1,\mathrm{PP}} = \begin{pmatrix} -\frac{135}{4N_C^2} + \frac{151}{12} - \frac{11N_C^2}{3} - \frac{2n_f}{3}\left(\frac{5}{N_C} - N_C\right) & -\frac{39}{4N_C^3} + \frac{377}{24N_C} - \frac{143N_C}{24} - \frac{5n_f}{6}\left(\frac{1}{N_C^2} - 1\right) \\ \frac{39}{N_C} - \frac{71N_C}{6} + \frac{10n_f}{3} & \frac{21}{4N_C^2} - \frac{21}{4} \end{pmatrix},$$

$$\gamma_{1,\mathrm{PE}^{(1)}} = \begin{pmatrix} -\frac{1}{N_C^2} - \frac{49}{9} + \frac{259N_C^2}{144} + \frac{n_f}{36}\left(\frac{4}{N_C} - N_C\right) & \frac{1}{4N_C^3} - \frac{77}{288N_C} + \frac{5N_C}{288} + \frac{n_f}{36}\left(\frac{1}{N_C^2} - 1\right) \\ -\frac{1}{N_C} + \frac{365N_C}{72} - \frac{n_f}{9} & -\frac{2}{N_C^2} + 2 \end{pmatrix},$$

$$\gamma_{1,\mathrm{PE}^{(2)}} = \begin{pmatrix} -\frac{21}{32N_C^2} + \frac{7}{32} - \frac{N_C^2}{64} & -\frac{7}{32N_C^3} + \frac{35}{128N_C} - \frac{7N_C}{128} \\ \frac{7}{8N_C} - \frac{7N_C}{32} & \frac{7}{32N_C^2} - \frac{7}{32} \end{pmatrix},$$

$$\gamma_{1,\mathrm{EE}^{(1)}} = \begin{pmatrix} \left[-\frac{931}{4N_C^2} + \frac{499}{12} - \frac{85N_C^2}{6} - \frac{11n_f}{3}\left(\frac{2}{N_C} - N_C\right)\right] & \left[-\frac{263}{4N_C^3} + \frac{251}{2N_C} - \frac{239N_C}{4} - \frac{5n_f}{2}\left(\frac{1}{N_C^2} - 1\right)\right] \\ \left[\frac{263}{N_C} - 23N_C + 10n_f\right] & \left[\frac{121}{4N_C^2} - \frac{539}{12} + \frac{44N_C^2}{3} + \frac{8n_f}{3}\left(\frac{1}{N_C} - N_C\right)\right] \\ \left\{\frac{1930}{N_C^2} + \frac{50}{3} + \frac{1235N_C^2}{6} + \frac{n_f}{3}\left(\frac{520}{N_C} + 110N_C\right)\right\} & \left\{\frac{230}{N_C^3} - \frac{1340}{3N_C} + \frac{650N_C}{3} + \frac{50n_f}{3}\left(\frac{1}{N_C^2} - 1\right)\right\} \\ \left\{-\frac{920}{N_C} + \frac{980N_C}{3} - \frac{200n_f}{3}\right\} & \left\{\frac{1010}{N_C^2} - \frac{8630}{3} + \frac{5600N_C^2}{3} + \frac{320n_f}{3}\left(\frac{1}{N_C} - N_C\right)\right\} \end{pmatrix}, \tag{8.32}$$

$$\gamma_{1,\mathrm{EE}^{(2)}} = \begin{pmatrix} \left[-\frac{393}{16N_C^2} + \frac{539}{144} - \frac{283N_C^2}{288} + \frac{n_f}{36}\left(\frac{4}{N_C} - N_C\right)\right] & \left[-\frac{127}{16N_C^3} + \frac{5381}{576N_C} - \frac{809N_C}{576} + \frac{n_f}{36}\left(\frac{1}{N_C^2} - 1\right)\right] \\ \left[\frac{127}{4N_C} - \frac{89N_C}{144} - \frac{n_f}{9}\right] & \left[\frac{115}{16N_C^2} - \frac{115}{16}\right] \\ \times & \times \\ \times & \times \end{pmatrix},$$

$$Z_{\mathrm{EP}}^{(2,0)} = \begin{pmatrix} \left[-\frac{6207}{8N_C^2} + \frac{3295}{24} - \frac{3809N_C^2}{48} - \frac{20n_f}{3}\left(\frac{1}{N_C} - N_C\right)\right] & \left[-\frac{1989}{8N_C^3} + \frac{25787}{96N_C} - \frac{1919N_C}{96} - \frac{10n_f}{3}\left(\frac{1}{N_C^2} - 1\right)\right] \\ \left[\frac{1989}{2N_C} - \frac{767N_C}{24} + \frac{40n_f}{3}\right] & \left[\frac{1749}{8N_C^2} - \frac{4447}{24} - \frac{100N_C^2}{3} + \frac{20n_f}{3}\left(\frac{1}{N_C} - N_C\right)\right] \\ \times & \times \\ \times & \times \end{pmatrix},$$

where we split $\gamma_{1,\mathrm{XE}} = \begin{pmatrix} \gamma_{1,\mathrm{XE}^{(1)}} & \gamma_{1,\mathrm{XE}^{(2)}} \end{pmatrix}$ so that the matrices fit the page width. In addition to elements that do not agree with the results from Refs. [211, 221, 222],

we marked those elements which we did not find in the literature by curly brackets. Moreover, ✗ denotes those elements that require further careful treatment: In the case of $\gamma_{1,\mathrm{EE}^{(2)}}$ the $1/\epsilon^2$ poles do not cancel and in the case of $Z^{(2,0)}_{\mathrm{EP}}$ the corresponding elements of $\gamma_{1,\mathrm{EP}}$ do not vanish. While this is certainly a severe problem, it only affects the physical results beyond NNLO.

Concerning the elements differing from the literature, one might wonder whether this is at least partially an effect of the choice of evanescent operators, because these elements are all unphysical. After all, it is well known that even the physical anomalous dimension, except for the first term $\gamma_{0,\mathrm{PP}}$, depends not only on the basis of physical operators but also on both the renormalization scheme *and* the choice of evanescent operators [218–220].

If we only consider NLO and discard the evanescent operators $E^{(2)}$, which corresponds to the coefficients

$$\begin{aligned} c_{1,1} &= c_{2,2} = \frac{5D^2-26D+16}{32D\,(D^2-3D+2)}, \quad c_{1,3} = c_{2,4} = \frac{6-D}{32D\,(D^2-3D+2)}, \\ c_{3,1} &= c_{4,2} = \frac{2-3D}{96D\,(D^2-3D+2)}, \quad c_{3,3} = c_{4,4} = \frac{1}{96D\,(D^2-3D+2)}, \\ c_{i,j} &= 0 \quad \text{for all other } i,j, \end{aligned} \tag{8.33}$$

for the projectors in Eq. (8.28), we observe that the elements of the anomalous dimension do not change except for the fact that we remove those entries concerning $E^{(2)}$. However, the finite renormalization now reads

$$Z^{(1,0)}_{\mathrm{EP}} = \begin{pmatrix} \left[\frac{156}{N_\mathrm{C}} - 21N_\mathrm{C}\right] & \left[\frac{33}{N_\mathrm{C}^2} - 33\right] \\ [-132] & \frac{24}{N_\mathrm{C}} - 24N_\mathrm{C} \end{pmatrix} \tag{8.34}$$

and thus differs from Eq. (8.31). This also affects the unphysical mixing $\zeta^{-1}_{\mathrm{R,EE}}$, which differs at $\mathcal{O}(\alpha_\mathrm{s})$. On the other hand, both $\zeta^{-1}_{\mathrm{R,PP}}$ and $\zeta^{-1}_{\mathrm{R,PE}}$ yield exactly the same result at $\mathcal{O}(\alpha_\mathrm{s})$ as in the case including $E^{(2)}$.

Since we only consider operators with four different flavors, our operator basis in Eqs. (8.2), (8.10), and (8.11) differs from those in Refs. [211, 221, 222]. These bases not only include additional physical operators but also the associated additional evanescent operators. Even though these evanescent operators cannot mix with our basis, the simple fact that there are more of them might cause some differences in the unphysical terms.

On the other hand, both the physical mixing matrix $\zeta^{-1}_{\mathrm{R,PP}}$ as well as $\zeta^{-1}_{\mathrm{R,PE}}$ can be renormalized with the anomalous dimension found in the literature through NNLO. Hence, the mixing into the regular physical operators seems to be under control. Moreover, *all* our results, including the problematic non-physical elements discussed before, are independent of the QCD gauge parameter ξ, which we kept general throughout the calculation. In fact, all dependence on ξ already drops out before constructing the

diagonal projectors, cf. Eq. (8.28). Thus, our physically relevant result might very well be correct already. Through NNLO we find

$$
\begin{aligned}
\bar{\zeta}^{-1}_{\mathrm{R,PP},11} &= 1 + \frac{\alpha_\mathrm{s}}{4\pi}\left\{\frac{31}{2N_\mathrm{C}} - \frac{3N_\mathrm{C}}{2} + 3\,L(\mu^2 t)\left(\frac{1}{N_\mathrm{C}} + N_\mathrm{C}\right)\right\} \\
&\quad + \left(\frac{\alpha_\mathrm{s}}{4\pi}\right)^2\left\{\frac{1}{N_\mathrm{C}^2}\left[-56\,\mathrm{Li}_2\left(\frac{1}{4}\right) + 82\,\mathrm{Li}_2\left(\frac{3}{4}\right) + \frac{405}{2} - \frac{85\pi^2}{6} + 326\ln^2 2\right.\right. \\
&\quad \left. - 80\ln 2 + 54\ln 3 - 164\ln 2\ln 3\right] + 10\,\mathrm{Li}_2\left(\frac{1}{4}\right) - 26\,\mathrm{Li}_2\left(\frac{3}{4}\right) + \frac{1381}{72} \\
&\quad + \frac{91\pi^2}{24} - 96\ln^2 2 + 54\ln 2 - 27\ln 3 + 52\ln 2\ln 3 + N_\mathrm{C}^2\left[-14\,\mathrm{Li}_2\left(\frac{1}{4}\right)\right. \\
&\quad \left. + 19\,\mathrm{Li}_2\left(\frac{3}{4}\right) + \frac{2441}{72} - \frac{61\pi^2}{24} + 70\ln^2 2 + 48\ln 2 - 54\ln 3 - 38\ln 2\ln 3\right] \\
&\quad + n_\mathrm{f}\left[-\frac{\pi^2 N_\mathrm{C}}{6} - \frac{115N_\mathrm{C}}{36} - \frac{\pi^2}{6N_\mathrm{C}} - \frac{185}{36N_\mathrm{C}}\right] + L(\mu^2 t)\left[-\frac{4\ln 2}{N_\mathrm{C}^2} + \frac{877}{12}\right. \\
&\quad \left. + 16\ln 2 + \frac{361N_\mathrm{C}^2}{12} + \frac{57}{N_\mathrm{C}^2} - 12N_\mathrm{C}^2\ln 2 + n_\mathrm{f}\left(-\frac{10}{3N_\mathrm{C}} - \frac{10N_\mathrm{C}}{3}\right)\right] \qquad (8.35a) \\
&\quad + L^2(\mu^2 t)\left[19 + 10N_\mathrm{C}^2 - n_\mathrm{f}\left(\frac{1}{N_\mathrm{C}} + N_\mathrm{C}\right)\right]\Bigg\} + \mathcal{O}(\alpha_\mathrm{s}^3), \\
\bar{\zeta}^{-1}_{\mathrm{R,PP},12} &= \frac{\alpha_\mathrm{s}}{4\pi}\left\{\frac{15}{4N_\mathrm{C}^2} - \frac{15}{4} + L(\mu^2 t)\left(\frac{3}{2N_\mathrm{C}^2} - \frac{3}{2}\right)\right\} \\
&\quad + \left(\frac{\alpha_\mathrm{s}}{4\pi}\right)^2\left\{\frac{1}{N_\mathrm{C}^3}\left[-17\,\mathrm{Li}_2\left(\frac{1}{4}\right) + \frac{47}{2}\,\mathrm{Li}_2\left(\frac{3}{4}\right) + \frac{493}{8} - \frac{101\pi^2}{24} + 94\ln^2 2\right.\right. \\
&\quad \left. - 19\ln 2 + \frac{27}{2}\ln 3 - 47\ln 2\ln 3\right] + \frac{1}{N_\mathrm{C}}\left[19\,\mathrm{Li}_2\left(\frac{1}{4}\right) - \frac{113}{4}\,\mathrm{Li}_2\left(\frac{3}{4}\right) - \frac{4217}{72}\right. \\
&\quad \left. + \frac{83\pi^2}{16} - 113\ln^2 2 + \frac{87}{2}\ln 2 - \frac{135}{4}\ln 3 + \frac{113}{2}\ln 2\ln 3\right] + N_\mathrm{C}\left[-2\,\mathrm{Li}_2\left(\frac{1}{4}\right)\right. \\
&\quad \left. + \frac{19}{4}\,\mathrm{Li}_2\left(\frac{3}{4}\right) - \frac{55}{18} - \frac{47\pi^2}{48} + 19\ln^2 2 - \frac{49}{2}\ln 2 + \frac{81}{4}\ln 3 - \frac{19}{2}\ln 2\ln 3\right] \\
&\quad + n_\mathrm{f}\left[-\frac{\pi^2}{12N_\mathrm{C}^2} - \frac{145}{72N_\mathrm{C}^2} + \frac{\pi^2}{12} + \frac{145}{72}\right] + L(\mu^2 t)\left[\frac{87}{4N_\mathrm{C}^3} - \frac{83}{24N_\mathrm{C}} - \frac{439N_\mathrm{C}}{24}\right. \\
&\quad \left. + n_\mathrm{f}\left(-\frac{5}{3N_\mathrm{C}^2} + \frac{5}{3}\right)\right] + L^2(\mu^2 t)\left[\frac{29}{4N_\mathrm{C}} - \frac{29N_\mathrm{C}}{4} + n_\mathrm{f}\left(-\frac{1}{2N_\mathrm{C}^2} + \frac{1}{2}\right)\right]\Bigg\} \\
&\quad + \mathcal{O}(\alpha_\mathrm{s}^3), \qquad (8.35b) \\
\bar{\zeta}^{-1}_{\mathrm{R,PP},21} &= \frac{\alpha_\mathrm{s}}{4\pi}\left\{-15 - 6\,L(\mu^2 t)\right\}
\end{aligned}
$$

$$
\begin{aligned}
&+\left(\frac{\alpha_s}{4\pi}\right)^2\left\{\frac{1}{N_C}\left[68\,\mathrm{Li}_2\left(\frac{1}{4}\right)-94\,\mathrm{Li}_2\left(\frac{3}{4}\right)-\frac{493}{2}+\frac{101\pi^2}{6}-376\ln^2 2+76\ln 2\right.\right.\\
&\left.-54\ln 3+188\ln 2\ln 3\right]+N_C\left[-8\,\mathrm{Li}_2\left(\frac{1}{4}\right)+19\,\mathrm{Li}_2\left(\frac{3}{4}\right)-\frac{245}{9}-\frac{47\pi^2}{12}\right.\\
&\left.+76\ln^2 2-98\ln 2+81\ln 3-38\ln 2\ln 3\right]+n_f\left[\frac{145}{18}+\frac{\pi^2}{3}\right] \qquad (8.35c)\\
&\left.+L(\mu^2 t)\left[-\frac{87}{N_C}-\frac{475N_C}{6}+\frac{20n_f}{3}\right]+L^2(\mu^2 t)\left[-29N_C+2n_f\right]\right\}+\mathcal{O}(\alpha_s^3),
\end{aligned}
$$

$$
\begin{aligned}
\bar{\zeta}^{-1}_{\mathrm{R,PP,22}} &= 1+\frac{\alpha_s}{4\pi}\left\{\frac{1}{2N_C}-\frac{N_C}{2}+3\,L(\mu^2 t)\left(-\frac{1}{N_C}+N_C\right)\right\}\\
&+\left(\frac{\alpha_s}{4\pi}\right)^2\left\{\frac{1}{N_C^2}\left[12\,\mathrm{Li}_2\left(\frac{1}{4}\right)-12\,\mathrm{Li}_2\left(\frac{3}{4}\right)-44+\frac{8\pi^2}{3}-50\ln^2 2-4\ln 2\right.\right.\\
&\left.+24\ln 2\ln 3\right]+2\,\mathrm{Li}_2\left(\frac{1}{4}\right)-7\,\mathrm{Li}_2\left(\frac{3}{4}\right)+\frac{227}{24}-\frac{\pi^2}{8}-20\ln^2 2-44\ln 2\\
&+54\ln 3+14\ln 2\ln 3+N_C^2\left[-14\,\mathrm{Li}_2\left(\frac{1}{4}\right)+19\,\mathrm{Li}_2\left(\frac{3}{4}\right)+\frac{829}{24}-\frac{61\pi^2}{24}\right.\\
&\left.+70\ln^2 2+48\ln 2-54\ln 3-38\ln 2\ln 3\right]+n_f\left[\frac{\pi^2}{6N_C}+\frac{35}{12N_C}-\frac{\pi^2 N_C}{6}\right.\\
&\left.-\frac{35N_C}{12}\right]+L(\mu^2 t)\left[-\frac{30}{N_C^2}-\frac{4\ln 2}{N_C^2}-\frac{37}{12}+16\ln 2+\frac{397N_C^2}{12}-12N_C^2\ln 2\right.\\
&\left.\left.+n_f\left(\frac{10}{3N_C}-\frac{10N_C}{3}\right)\right]+L^2(\mu^2 t)\left[-10+10N_C^2+n_f\left(\frac{1}{N_C}-N_C\right)\right]\right\}\\
&+\mathcal{O}(\alpha_s^3), \qquad (8.35d)
\end{aligned}
$$

where $\bar{\zeta}_R^{-1}=\zeta_R^{-1}\zeta_\chi^2$ is renormalized in the $\overline{\mathrm{MS}}$ instead of the ringed-quark scheme to minimize the error sources until the issues are resolved. $\zeta^{-1}_{\mathrm{R,PE}}$ is finite and thus irrelevant, because matrix elements of the evanescent operators vanish in $D=4$ dimensions, cf. Section 8.2.

8.5 OUTLOOK

We obtained preliminary results for the mixing matrix of the regular current-current operators with their flowed counterparts, which together with the known Wilson coefficients yield the flowed OPE for the electroweak Hamiltonian in Eq. (8.1). However, there are some unresolved issues: We cannot cancel all $1/\epsilon^2$ poles in the evanescent-evanescent mixing matrix and our anomalous dimension does not preserve its block-triangular form at NNLO. In addition, we still have to understand why we have to demand $T_R=1/2$ to cancel the other $1/\epsilon^2$ poles. Moreover, while the physical submatrices of the anomalous dimension coincide with the results from the literature, some of the evanescent subma-

trices as well as the finite renormalization disagree. Some of this might be explained by the fact that the literature considers an increased operator basis with both more physical and more evanescent operators.

While the physical mixing matrix might not be affected by these problems through NNLO in QCD, we cannot completely trust our results until these issues are resolved. Afterwards, one has to perform a transformation to a basis in which one of the two operators becomes Fierz evanescent. The coefficient of the remaining $\Delta F = 2$ operator can then be used to combine the lattice determination of the bag parameters for Kaon and B meson mixing with the perturbative Wilson coefficients, hopefully reducing the uncertainty of the overall predictions of the effective electroweak theory.

While working on this project, Ref. [223] was published. In this reference, the same calculation was performed to NLO accuracy in a different operator basis and with the dimensional reduction scheme for γ_5. Thus, the two results cannot directly be compared but require a sophisticated basis and scheme transformation. We leave this for future work.

Afterwards, our calculation can be extended to the $\Delta F = 1$ basis, i.e. including penguin operators.

9 CONCLUSIONS

In this thesis, we developed a framework for the calculation of correlation functions in the perturbative gradient flow formalism. It employs tools and techniques from standard perturbative QCD calculations, in particular Feynman diagrams and rules. The calculation of correlations functions is fully automatized. For the calculation of the ensuing Feynman integrals we employ IBP reductions generalized to the perturbative gradient flow and a subsequent calculation of the master integrals.

The IBP reductions of three-loop gradient flow integrals proved to be beyond the capabilities of existing programs so that we had to resort to finite-field and interpolation techniques which seeped into the field of precision calculations over the last decade. Since no public implementation of these algorithms was available, we participated in the development of the open source `C++` library `FireFly` implementing these algorithms. It can be applied to many problems due to its general nature. Moreover, we integrated support for `FireFly` into the public IBP reduction program `Kira`.

With these newly developed tools, we were able to complete the three-loop reduction for the calculation of VEVs to check the validity of our whole gradient flow setup. Not only did we improve on the accuracy of the previous result for the gluon action density of Ref. [21], we also extended the calculation to the quark condensate and the VEV of the quark kinetic operator. Moreover, we calculated the mass effects to second order. The gluon action density and the quark condensate allow for a straightforward definition of a gradient flow coupling and a gradient flow mass as well as a subsequent extraction of the gauge coupling and the quark masses as soon as corresponding lattice results become available.

We then employed our setup and the method of projectors to calculate the Wilson coefficients of the gradient flow definition of the EMT through NNLO. These results have already been used in Refs. [133, 154–156] to study thermodynamics on the lattice. However, it turned out that operators affected by the EOM suffer from large discretization errors on the lattice [155].

The results and techniques of the preceding chapters were then assembled to the flowed OPE for current-current correlators. It allows to combine the known perturbative results for the Wilson coefficients of regular QCD with lattice determinations of the flowed operators through the OPE. This might pave the way for an alternative determination of the hadronic corrections to the anomalous magnetic moment as well as other observables. Moreover, we derived a general flow-time evolution equation for flowed operators.

Finally, we applied these methods to the current-current operators of the electroweak Hamiltonian and computed the mixing matrix between the regular and the flowed operators through NNLO. While there are some unresolved issues within our calculation, our physical result might already be correct. Apart from solving these problems, the non-trivial comparison with the NLO results from Ref. [223] seems desirable. After a

basis transformation, our results can then be used to extract the bag parameters of Kaon and B meson mixing from lattice QCD and the extension to penguin operators can be pursued.

Moreover, our methods can be applied to similar problems like CP violating operators relevant for the nucleon electric dipole moment [224] to higher orders in perturbation theory.

Part II

APPENDICES

A

CONVENTIONS

In this chapter we summarize our conventions for the gauge group and its invariants as well as the QCD RG functions. Moreover, we often use the short-hand notation

$$\int_p \equiv \int \frac{\mathrm{d}^D p}{(2\pi)^D}, \qquad \int_x \equiv \int \mathrm{d}^D x \tag{A.1}$$

for integrals throughout this thesis, where it should be clear from the context whether an integration variable is in position $(x, y, z, \ldots)$ or momentum space $(p, k, q, \ldots)$.

A.1 GAUGE GROUP

Throughout this thesis we perform calculations for a general non-Abelian gauge theory based on a simple compact Lie group with n_f quark fields $\psi_1, \ldots, \psi_{n_\mathrm{f}}$ in the fundamental representation, of which the first n_h are degenerate with mass m, while the remaining n_l are massless. The generators T^a of the fundamental representation obey the commutation relation

$$[T^a, T^b] = f^{abc} T^c, \tag{A.2}$$

where f^{abc} are the structure constants. Traces over the generators are normalized to

$$\mathrm{Tr}(T^a T^b) = -T_\mathrm{R} \delta^{ab} \tag{A.3}$$

with $T_\mathrm{R} > 0$. The dimensions of the fundamental and the adjoint representation are N_C and N_A, respectively, and their quadratic Casimir eigenvalues are denoted by C_F and C_A. While these numbers are usually sufficient to display all results, we additionally encounter the two contractions $d_{\mathrm{V},33}$ and $d_{\mathrm{V},44}$ in the fundamental vector representation in Chapter 8. For the gauge group $\mathrm{SU}(N_\mathrm{C})$, the invariants can be expressed through [200]

$$\begin{aligned}
N_\mathrm{A} &= N_\mathrm{C}^2 - 1 && \overset{N_\mathrm{C}=3,\, T_\mathrm{R}=1/2}{=} && 8, \\
C_\mathrm{F} &= T_\mathrm{R} \frac{N_\mathrm{C}^2 - 1}{N_\mathrm{C}} && \overset{N_\mathrm{C}=3,\, T_\mathrm{R}=1/2}{=} && \frac{4}{3}, \\
C_\mathrm{A} &= 2 T_\mathrm{R} N_\mathrm{C} && \overset{N_\mathrm{C}=3,\, T_\mathrm{R}=1/2}{=} && 3, \\
d_{\mathrm{V},33} &= \frac{T_\mathrm{R}^3}{2} \frac{(N_\mathrm{C}^2 - 1)(N_\mathrm{C}^2 - 4)}{N_\mathrm{C}} && \overset{N_\mathrm{C}=3,\, T_\mathrm{R}=1/2}{=} && \frac{5}{6}, \\
d_{\mathrm{V},44} &= \frac{T_\mathrm{R}^4}{6} \frac{(N_\mathrm{C}^2 - 1)(N_\mathrm{C}^4 - 6N_\mathrm{C}^2 + 18)}{N_\mathrm{C}^2} && \overset{N_\mathrm{C}=3,\, T_\mathrm{R}=1/2}{=} && \frac{5}{12},
\end{aligned} \tag{A.4}$$

where we show the numerical results for QCD with $N_\mathrm{C} = 3$ and $T_\mathrm{R} = 1/2$ in the third column. For brevity, we often use QCD also to refer to the more general gauge group in this thesis.

Note that our convention for the generators and structure constants in Eqs. (A.2) and (A.3) deviates from the more common convention

$$\begin{aligned}[\hat{T}^a, \hat{T}^b] &= \mathrm{i}\hat{f}^{abc}\hat{T}^c, \\ \mathrm{Tr}(\hat{T}^a\hat{T}^b) &= T_\mathrm{R}\delta^{ab},\end{aligned} \tag{A.5}$$

where the hat distinguishes the two conventions. This convention is for example implemented in the package `color` [200], which we employ to evaluate the color factors within `FORM` [225, 226], cf. Appendix C. The transformation from the convention in Eqs. (A.2) and (A.3) to the one in Eq. (A.5) is simply given by

$$T^a = \mathrm{i}\hat{T}^a, \qquad f^{abc} = -\hat{f}^{abc}. \tag{A.6}$$

A.2 RENORMALIZATION GROUP FUNCTIONS

The D-dimensional beta function of the QCD coupling is defined as

$$\mu^2\frac{\mathrm{d}}{\mathrm{d}\mu^2}\alpha_\mathrm{s}(\mu) = \alpha_\mathrm{s}(\mu)\beta_\epsilon(\alpha_\mathrm{s}(\mu)), \tag{A.7}$$

where $\alpha_\mathrm{s} \equiv g^2/(4\pi)$. The renormalized coupling $g = g(\mu)$ is related to the bare one through

$$g_\mathrm{B} \equiv \hat{\mu}^\epsilon Z_\mathrm{s}^{1/2}(\alpha_\mathrm{s}(\mu))\, g(\mu) \quad \text{with} \quad \hat{\mu} \equiv \frac{\mu \mathrm{e}^{\gamma_\mathrm{E}/2}}{\sqrt{4\pi}}, \tag{A.8}$$

where Z_s is the $\overline{\mathrm{MS}}$ renormalization constant, μ the renormalization scale, and $\gamma_\mathrm{E} = 0.5772\ldots$ the Euler-Mascheroni constant. From this follow the relations

$$\begin{aligned}\beta_\epsilon(\alpha_\mathrm{s}) &= -\epsilon\left(1 + \alpha_\mathrm{s}\frac{\partial}{\partial\alpha_\mathrm{s}}\ln Z_\mathrm{s}(\alpha_\mathrm{s})\right)^{-1} = -\epsilon + \beta(\alpha_\mathrm{s}) \equiv -\epsilon - \sum_{n\geq 0}\left(\frac{\alpha_\mathrm{s}}{4\pi}\right)^{n+1}\beta_n, \\ Z_\mathrm{s}(\alpha_\mathrm{s}) &= 1 - \frac{\alpha_\mathrm{s}}{4\pi}\frac{\beta_0}{\epsilon} + \left(\frac{\alpha_\mathrm{s}}{4\pi}\right)^2\left(\frac{\beta_0^2}{\epsilon^2} - \frac{\beta_1}{2\epsilon}\right) + \mathcal{O}(\alpha_\mathrm{s}^3).\end{aligned} \tag{A.9}$$

Throughout this thesis we only need the first two perturbative coefficients for the renormalization of all results, while β_2 is required in order to define the β function of the gradient flow coupling to $\mathcal{O}(\alpha_\mathrm{s}^3)$ in Section 5.5.1 and to derive the $\mathcal{O}(\alpha_\mathrm{s}^3)$ terms of γ^f in Section 7.4:

$$\begin{aligned}\beta_0 &= \frac{11}{3}C_\mathrm{A} - \frac{4}{3}T_\mathrm{R}n_\mathrm{f}, \qquad \beta_1 = \frac{34}{3}C_\mathrm{A}^2 - 4C_\mathrm{F}T_\mathrm{R}n_\mathrm{f} - \frac{20}{3}C_\mathrm{A}T_\mathrm{R}n_\mathrm{f}, \\ \beta_2 &= \frac{2857}{54}C_\mathrm{A}^3 + 2C_\mathrm{F}^2T_\mathrm{R}n_\mathrm{f} - \frac{205}{9}C_\mathrm{F}C_\mathrm{A}T_\mathrm{R}n_\mathrm{f} - \frac{1415}{27}C_\mathrm{A}^2T_\mathrm{R}n_\mathrm{f} \\ &\quad + \frac{44}{9}C_\mathrm{F}T_\mathrm{R}^2n_\mathrm{f}^2 + \frac{158}{27}C_\mathrm{A}T_\mathrm{R}^2n_\mathrm{f}^2.\end{aligned} \tag{A.10}$$

The anomalous dimension of the quark mass is defined through

$$\begin{aligned}\mu^2\frac{\mathrm{d}}{\mathrm{d}\mu^2}m(\mu) &= m\gamma_m(\alpha_\mathrm{s}), \\ \gamma_m(\alpha_\mathrm{s}) &= -\alpha_\mathrm{s}\beta_\epsilon(\alpha_\mathrm{s})\frac{\partial}{\partial\alpha_\mathrm{s}}\ln Z_m(\alpha_\mathrm{s}) \equiv -\sum_{n\geq 0}\left(\frac{\alpha_\mathrm{s}}{4\pi}\right)^{n+1}\gamma_{m,n},\end{aligned} \tag{A.11}$$

with the first three perturbative coefficients given by

$$\begin{aligned}\gamma_{m,0} &= 3C_F, \qquad \gamma_{m,1} = \frac{3}{2}C_F^2 + \frac{97}{6}C_A C_F - \frac{10}{3}C_F T_R n_f, \\ \gamma_{m,2} &= \frac{129}{2}C_F^3 - \frac{129}{4}C_F^2 C_A + \frac{11413}{108}C_F C_A^2 + C_F^2 T_R n_f(-46 + 48\zeta(3)) \\ &\quad + C_F C_A T_R n_f\left(-\frac{556}{27} - 48\zeta(3)\right) - \frac{140}{27}C_F T_R^2 n_f^2.\end{aligned} \tag{A.12}$$

It determines the $\overline{\text{MS}}$ renormalized mass m through

$$m_B = Z_m\, m, \qquad Z_m = 1 - \frac{\alpha_s}{4\pi}\frac{\gamma_{m,0}}{\epsilon} + \left(\frac{\alpha_s}{4\pi}\right)^2\left[\frac{\gamma_{m,0}}{2\epsilon^2}\left(\gamma_{m,0} + \beta_0\right) - \frac{\gamma_{m,1}}{2\epsilon}\right] + \mathcal{O}(\alpha_s^3). \tag{A.13}$$

Similarly to β_ϵ, the third coefficient $\gamma_{m,2}$ is needed only in Sections 5.5.2 and 7.4.

B

FEYNMAN RULES

In this chapter we list all the Feynman rules appearing in this thesis. The first section lists all general gradient flow Feynman rules and the following sections the Feynman rules for the operator insertions of the different problems considered in this thesis.

A few general rules apply to all Feynman rules: All momenta are considered to be outgoing. Lines with a solid arrow are flow lines and lines with a dashed arrow can be both flow lines or flowed propagators. The regular QCD vertices denoted by black dots are always defined at flow time 0. The symbols p, q, r denote Euclidean four-momenta, s, t real-valued flow-time variables, $\mu, \nu, \rho, \ldots$ D-dimensional Lorentz indices, $\hat{\alpha}, \hat{\beta}, \hat{\gamma}, \ldots$ spinor indices, $a, b, c, \ldots$ color indices of the adjoint representation, and, finally, $i, j, k, \ldots$ color indices of the fundamental representation. ξ is the usual QCD gauge parameter and κ the additional gradient flow gauge parameter introduced by the flow equations (2.2).

All Feynman rules are given in their *bare* form. To obtain renormalized results, the gauge coupling g_B and the quark mass m_B have to be renormalized according to Eqs. (A.8) and (A.13), respectively, and the Feynman rules for the composite operators have to be multiplied by $Z_\chi^{1/2}$ or $\mathring{Z}_\chi^{1/2}$ for each (anti-)quark field in the operator, cf. Eqs. (2.59) and (2.62).

B.1 GENERAL GRADIENT FLOW FEYNMAN RULES

The following Feynman rules are derived from the Lagrangian in Eq. (2.10) as discussed in Section 2.3 and are relevant for all perturbative calculations in the gradient flow formalism.

Propagators and flow lines

- gluon propagator:

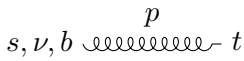

$$= \delta^{ab}\frac{1}{p^2}\left[\left(\delta_{\mu\nu}-\frac{p_\mu p_\nu}{p^2}\right)e^{-(t+s)p^2} + \xi\frac{p_\mu p_\nu}{p^2}e^{-\kappa(t+s)p^2}\right] \tag{B.1}$$

- (anti)quark propagator:

$$= \delta_{ij}\frac{(-\mathrm{i}\not{p}+m_\mathrm{B})_{\hat{\alpha}\hat{\beta}}}{p^2+m_\mathrm{B}^2}\,e^{-(t+s)p^2} \tag{B.2}$$

- ghost propagator:

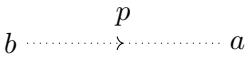

$$= \quad \delta^{ab}\frac{1}{p^2} \tag{B.3}$$

- gluon flow line:

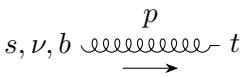

$$= \quad \delta^{ab}\,\theta(t-s)\left[\left(\delta_{\mu\nu}-\frac{p_\mu p_\nu}{p^2}\right)e^{-(t-s)p^2} + \frac{p_\mu p_\nu}{p^2}\,e^{-\kappa(t-s)p^2}\right] \tag{B.4}$$

- quark flow line:

$$= \quad \delta_{ij}\delta_{\hat{\alpha}\hat{\beta}}\,\theta(t-s)\,e^{-(t-s)p^2} \tag{B.5}$$

- antiquark flow line:

$$= \quad \delta_{ij}\delta_{\hat{\alpha}\hat{\beta}}\,\theta(t-s)\,e^{-(t-s)p^2} \tag{B.6}$$

Vertices

- three-gluon vertex:

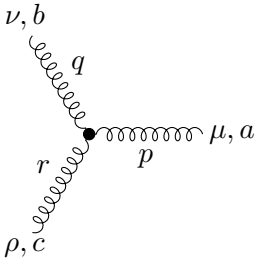

$$= \quad \mathrm{i}g_{\mathrm{B}}f^{abc}\left[\delta_{\mu\nu}(p-q)_\rho+\delta_{\nu\rho}(q-r)_\mu+\delta_{\rho\mu}(r-p)_\nu\right] \tag{B.7}$$

- four-gluon vertex:

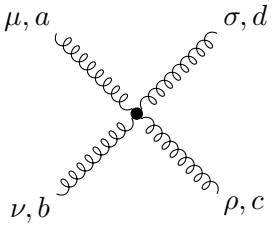

$$= \quad -g_{\mathrm{B}}^2\left[f^{abe}f^{cde}(\delta_{\mu\rho}\delta_{\nu\sigma}-\delta_{\mu\sigma}\delta_{\nu\rho}) + f^{ace}f^{bde}(\delta_{\mu\nu}\delta_{\rho\sigma}-\delta_{\mu\sigma}\delta_{\nu\rho}) + f^{ade}f^{bce}(\delta_{\mu\nu}\delta_{\rho\sigma}-\delta_{\mu\rho}\delta_{\nu\sigma})\right] \tag{B.8}$$

- ghost-gluon vertex:

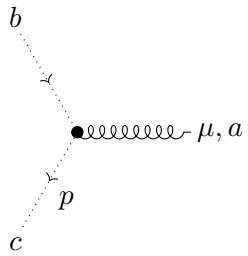

$$= \quad -\mathrm{i}g_{\mathrm{B}} f^{abc}\, p_\mu \tag{B.9}$$

- quark-gluon vertex:

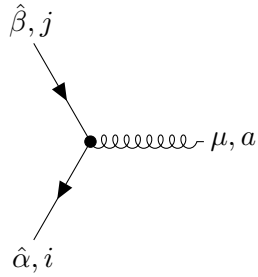

$$= \quad g_{\mathrm{B}}\, T^a_{ij}\, (\gamma_\mu)_{\hat{\alpha}\hat{\beta}} \tag{B.10}$$

- two-plus-one gluon flow vertex:

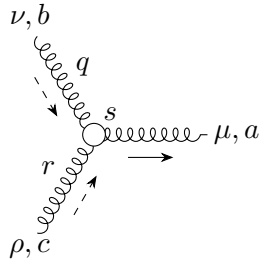

$$= \quad -\mathrm{i}g_{\mathrm{B}} f^{abc} \int_0^\infty \mathrm{d}s \big[\delta_{\nu\rho}(r-q)_\mu + 2\delta_{\mu\nu} q_\rho - 2\delta_{\mu\rho} r_\nu + (\kappa - 1)(\delta_{\mu\rho} q_\nu - \delta_{\mu\nu} r_\rho)\big] \tag{B.11}$$

- three-plus-one gluon flow vertex:

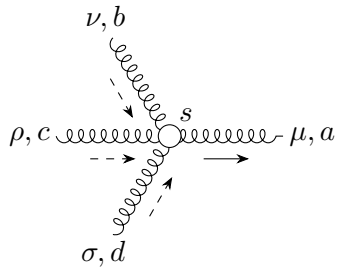

$$= \quad -g_{\mathrm{B}}^2 \int_0^\infty \mathrm{d}s \big[f^{abe} f^{cde} (\delta_{\mu\rho}\delta_{\nu\sigma} - \delta_{\mu\sigma}\delta_{\nu\rho}) + f^{ace} f^{bde} (\delta_{\mu\nu}\delta_{\rho\sigma} - \delta_{\mu\sigma}\delta_{\nu\rho}) + f^{ade} f^{bce} (\delta_{\mu\nu}\delta_{\rho\sigma} - \delta_{\mu\rho}\delta_{\nu\sigma})\big] \tag{B.12}$$

- quark-one-gluon flow vertex:

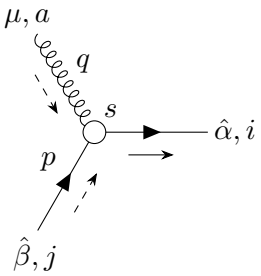

$$= \quad \mathrm{i} g_{\mathrm{B}} \, \delta_{\hat{\alpha}\hat{\beta}} T^a_{ij} \int_0^\infty \mathrm{d}s \left[2p_\mu + (1-\kappa) q_\mu \right] \tag{B.13}$$

- antiquark-one-gluon flow vertex:

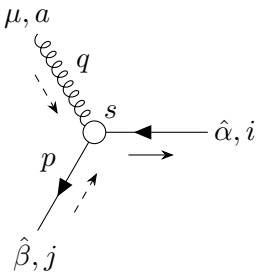

$$= \quad -\mathrm{i} g_{\mathrm{B}} \, \delta_{\hat{\alpha}\hat{\beta}} T^a_{ji} \int_0^\infty \mathrm{d}s \left[2p_\mu + (1-\kappa) q_\mu \right] \tag{B.14}$$

- quark-two-gluons flow vertex:

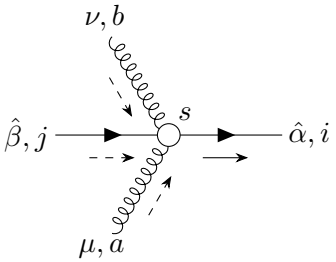

$$= \quad g^2_{\mathrm{B}} \delta_{\hat{\alpha}\hat{\beta}} \delta_{\mu\nu} \left\{ T^a, T^b \right\}_{ij} \int_0^\infty \mathrm{d}s \tag{B.15}$$

- antiquark-two-gluons flow vertex:

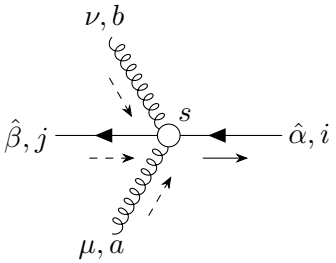

$$= \quad g^2_{\mathrm{B}} \delta_{\hat{\alpha}\hat{\beta}} \delta_{\mu\nu} \left\{ T^a, T^b \right\}_{ji} \int_0^\infty \mathrm{d}s \tag{B.16}$$

B.2 OPERATORS FOR THE VACUUM EXPECTATION VALUES

The composite operators introduced in Section 2.4 have the following Feynman rules:

- $E(t,x) \equiv \frac{1}{4} G^a_{\mu\nu}(t,x) G^a_{\mu\nu}(t,x)$:
  - two-gluon vertex:

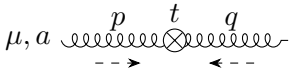

$$= \quad -g_B^2 \delta^{ab} \left(\delta_{\mu\nu} p \cdot q - p_\mu q_\nu \right) \tag{B.17}$$

  - three-gluon vertex:

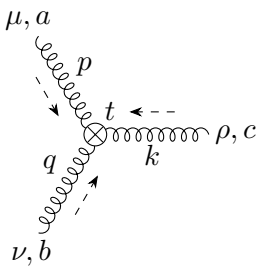

$$= \quad \begin{aligned} & i g_B^3 f^{abc} \left[\delta_{\mu\nu} (q-p)_\rho + \delta_{\nu\rho} (k-q)_\mu \right. \\ & \left. \quad + \delta_{\mu\rho} (p-k)_\nu \right] \end{aligned} \tag{B.18}$$

  - four-gluon vertex:

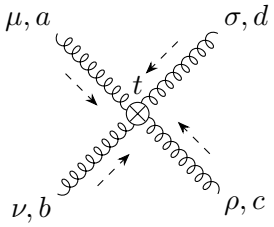

$$= \quad \begin{aligned} & g_B^4 \left[f^{abe} f^{cde} (\delta_{\mu\rho}\delta_{\nu\sigma} - \delta_{\mu\sigma}\delta_{\nu\rho}) \right. \\ & \quad + f^{ace} f^{bde} (\delta_{\mu\nu}\delta_{\rho\sigma} - \delta_{\mu\sigma}\delta_{\nu\rho}) \\ & \left. \quad + f^{ade} f^{bce} (\delta_{\mu\nu}\delta_{\rho\sigma} - \delta_{\mu\rho}\delta_{\nu\sigma}) \right] \end{aligned} \tag{B.19}$$

- $S(t,x) \equiv \bar{\chi}(t,x) \chi(t,x)$:

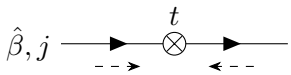

$$= \quad \delta_{ij} \delta_{\hat{\alpha}\hat{\beta}} \tag{B.20}$$

- $R(t,x) \equiv \bar{\chi}(t,x) \overleftrightarrow{\not{D}}^{\mathrm{F}} \chi(t,x)$:
  - quark-antiquark vertex:

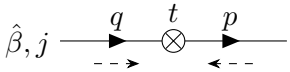

$$= \quad i \delta_{ij} (\not{p} - \not{q})_{\hat{\alpha}\hat{\beta}} \tag{B.21}$$

– quark-antiquark-gluon vertex:

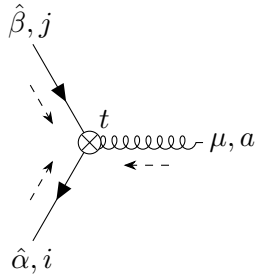

$$= \quad -2g_{\mathrm{B}} T^a_{ij} (\gamma_\mu)_{\hat{\alpha}\hat{\beta}} \tag{B.22}$$

B.3 OPERATORS COMPOSING THE ENERGY-MOMENTUM TENSOR

In this section we list all Feynman rules for the flowed operators in Eq. (6.6) composing the EMT discussed in Section 6.1.

- $\tilde{\mathcal{O}}_{1,\mu\nu}(t,x) \equiv G^a_{\mu\rho}(t,x) G^a_{\nu\rho}(t,x)$:
  - two-gluon vertex:

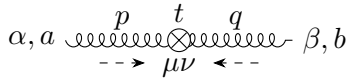

$$= \quad \begin{aligned} g_{\mathrm{B}}^2 \delta^{ab} \big[& -q_\mu p_\nu \delta_{\alpha\beta} + q_\mu p_\beta \delta_{\alpha\nu} \\ & + q_\alpha p_\nu \delta_{\beta\mu} - (q\cdot p)\delta_{\alpha\nu}\delta_{\beta\mu} \\ & + (\mu \leftrightarrow \nu) \big] \end{aligned} \tag{B.23}$$

  - three-gluon vertex:

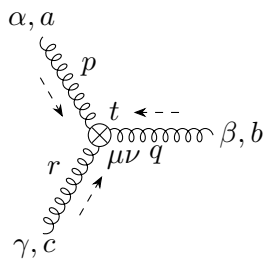

$$= \quad \begin{aligned} \mathrm{i} g_{\mathrm{B}}^3 f^{abc} \big[& (r_\mu \delta_{\rho\gamma} - r_\rho \delta_{\mu\gamma})(\delta_{\alpha\nu}\delta_{\beta\rho} - \delta_{\beta\nu}\delta_{\alpha\rho}) \\ & + (q_\mu \delta_{\beta\rho} - q_\rho \delta_{\beta\mu})(\delta_{\gamma\nu}\delta_{\rho\alpha} - \delta_{\nu\alpha}\delta_{\gamma\rho}) \\ & + (p_\mu \delta_{\rho\alpha} - p_\rho \delta_{\mu\alpha})(\delta_{\beta\nu}\delta_{\gamma\rho} - \delta_{\gamma\nu}\delta_{\beta\rho}) \\ & + (\mu \leftrightarrow \nu) \big] \end{aligned} \tag{B.24}$$

  - four-gluon vertex:

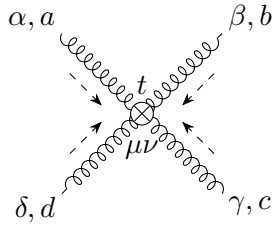

$$= \quad \begin{aligned} g_{\mathrm{B}}^4 \big[& f^{edc} f^{eba} (\delta_{\nu\beta}\delta_{\rho\alpha} - \delta_{\nu\alpha}\delta_{\rho\beta})(\delta_{\mu\delta}\delta_{\gamma\rho} - \delta_{\rho\delta}\delta_{\gamma\mu}) \\ & + f^{edb} f^{eca} (\delta_{\beta\rho}\delta_{\mu\delta} - \delta_{\rho\delta}\delta_{\mu\beta})(\delta_{\nu\gamma}\delta_{\alpha\rho} - \delta_{\gamma\rho}\delta_{\alpha\nu}) \\ & + f^{eda} f^{ecb} (\delta_{\alpha\rho}\delta_{\mu\delta} - \delta_{\alpha\mu}\delta_{\rho\delta})(\delta_{\beta\rho}\delta_{\nu\gamma} - \delta_{\beta\nu}\delta_{\gamma\rho}) \\ & + (\mu \leftrightarrow \nu) \big] \end{aligned} \tag{B.25}$$

- $\tilde{\mathcal{O}}_{2,\mu\nu}(t,x) \equiv \delta_{\mu\nu} G^a_{\rho\sigma}(t,x) G^a_{\rho\sigma}(t,x)$:
  - two-gluon vertex:

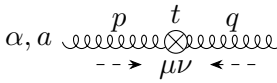

$$= \; 4 g_{\mathrm{B}}^2 \delta^{ab} \delta_{\mu\nu} \left[q_\alpha p_\beta - (q \cdot p) \delta_{\alpha\beta} \right] \tag{B.26}$$

  - three-gluon vertex:

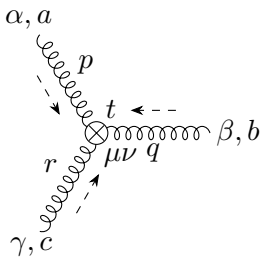

$$= \; \begin{aligned} & 4 \mathrm{i} g_{\mathrm{B}}^3 f^{abc} \delta_{\mu\nu} \left[\delta_{\alpha\beta} (q_\gamma - p_\gamma) + \delta_{\beta\gamma} (r_\alpha - q_\alpha) \right. \\ & \qquad \left. + \delta_{\alpha\gamma} (p_\beta - r_\beta) \right] \end{aligned} \tag{B.27}$$

  - four-gluon vertex:

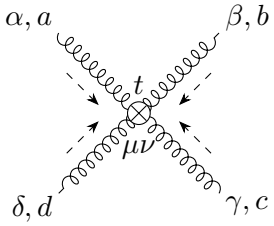

$$= \; \begin{aligned} & 4 g_{\mathrm{B}}^4 \delta_{\mu\nu} \left[f^{edc} f^{eba} (\delta_{\alpha\gamma} \delta_{\beta\delta} - \delta_{\alpha\delta} \delta_{\beta\gamma}) \right. \\ & \qquad + f^{edb} f^{eca} (\delta_{\alpha\beta} \delta_{\gamma\delta} - \delta_{\alpha\delta} \delta_{\beta\gamma}) \\ & \qquad \left. + f^{eda} f^{ecb} (\delta_{\alpha\beta} \delta_{\gamma\delta} - \delta_{\alpha\gamma} \delta_{\beta\delta}) \right] \end{aligned} \tag{B.28}$$

- $\tilde{\mathcal{O}}_{3_f,\mu\nu}(t,x) \equiv \bar{\chi}(t,x) \left(\gamma_\mu \overleftrightarrow{\mathcal{D}}^{\mathrm{F}}_\nu + \gamma_\nu \overleftrightarrow{\mathcal{D}}^{\mathrm{F}}_\mu \right) \chi(t,x)$:
  - quark-antiquark vertex:

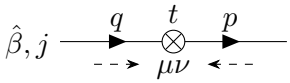

$$= \; \mathrm{i} \delta_{ij} \left[(p_\nu - q_\nu) \gamma_\mu + (p_\mu - q_\mu) \gamma_\nu \right]_{\hat{\alpha}\hat{\beta}} \tag{B.29}$$

  - quark-antiquark-gluon vertex:

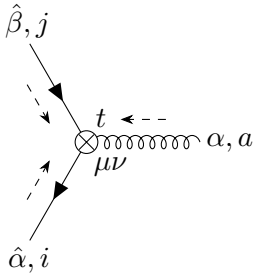

$$= \; -2 g_{\mathrm{B}} T^a_{ij} \left(\gamma_\mu \delta_{\alpha\nu} + \gamma_\nu \delta_{\alpha\mu} \right)_{\hat{\alpha}\hat{\beta}} \tag{B.30}$$

- $\tilde{\mathcal{O}}_{4_f,\mu\nu}(t,x) \equiv \delta_{\mu\nu}\bar{\chi}(t,x)\overleftrightarrow{\mathcal{D}}^{\mathrm{F}}\chi(t,x)$:
  - quark-antiquark vertex:

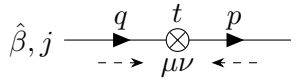

$$= \mathrm{i}\delta_{ij}\delta_{\mu\nu}\left(\not{p} - \not{q}\right)_{\hat{\alpha}\hat{\beta}} \tag{B.31}$$

  - quark-antiquark-gluon vertex:

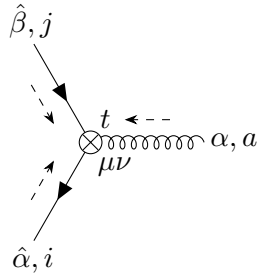

$$= -2g_{\mathrm{B}}T^a_{ij}\delta_{\mu\nu}\left(\gamma_\alpha\right)_{\hat{\alpha}\hat{\beta}} \tag{B.32}$$

B.4 ELECTROWEAK CURRENT-CURRENT OPERATORS

For the Feynman rules of the flowed current-current operators in the electroweak Hamiltonian defined in Eqs. (8.12) to (8.14) we use nested definitions to compress the expressions. Moreover, $\gamma_{\mu_1\cdots\mu_n} \equiv \gamma_{\mu_1}\cdots\gamma_{\mu_n}$ and $P_\pm = \frac{1}{2}(1 \pm \gamma_5)$. Note that the quarks have different flavors.

- $\tilde{\mathcal{O}}_1 \equiv -\left(\bar{\chi}_{1,\mathrm{L}}\gamma_\mu T^a \chi_{2,\mathrm{L}}\right)\left(\bar{\chi}_{3,\mathrm{L}}\gamma_\mu T^a \chi_{4,\mathrm{L}}\right)$:

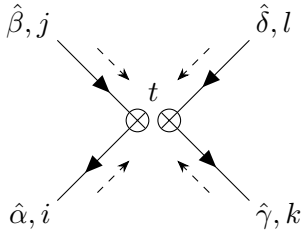

$$= -T^a_{ij}T^a_{kl}\{P_+\gamma_\mu P_-\}_{\hat{\alpha}\hat{\beta}}\{P_+\gamma_\mu P_-\}_{\hat{\gamma}\hat{\delta}} \tag{B.33}$$

$$\equiv \mathcal{O}_{1,ijkl,\hat{\alpha}\hat{\beta}\hat{\gamma}\hat{\delta}}$$

- $\tilde{\mathcal{O}}_2 \equiv \left(\bar{\chi}_{1,\mathrm{L}}\gamma_\mu \chi_{2,\mathrm{L}}\right)\left(\bar{\chi}_{3,\mathrm{L}}\gamma_\mu \chi_{4,\mathrm{L}}\right)$:

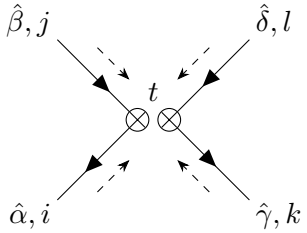

$$= \delta_{ij}\delta_{kl}\{P_+\gamma_\mu P_-\}_{\hat{\alpha}\hat{\beta}}\{P_+\gamma_\mu P_-\}_{\hat{\gamma}\hat{\delta}} \tag{B.34}$$

$$\equiv \mathcal{O}_{2,ijkl,\hat{\alpha}\hat{\beta}\hat{\gamma}\hat{\delta}}$$

- $\tilde{E}_1^{(1)} \equiv -\left(\bar{\chi}_{1,\mathrm{L}}\gamma_{\mu_1\mu_2\mu_3}T^a\chi_{2,\mathrm{L}}\right)\left(\bar{\chi}_{3,\mathrm{L}}\gamma_{\mu_1\mu_2\mu_3}T^a\chi_{4,\mathrm{L}}\right) - 16\tilde{\mathcal{O}}_1$:

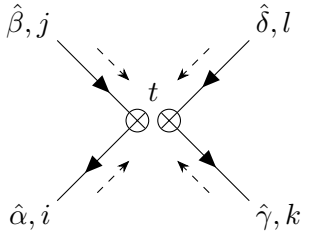

$$\begin{aligned} &= -T^a_{ij}T^a_{kl}\{P_+\gamma_{\mu_1\mu_2\mu_3}P_-\}_{\hat{\alpha}\hat{\beta}}\{P_+\gamma_{\mu_1\mu_2\mu_3}P_-\}_{\hat{\gamma}\hat{\delta}} \\ &\quad -16\,\mathcal{O}_{1,ijkl,\hat{\alpha}\hat{\beta}\hat{\gamma}\hat{\delta}} \\ &\equiv E^{(1)}_{1,ijkl,\hat{\alpha}\hat{\beta}\hat{\gamma}\hat{\delta}} \end{aligned} \tag{B.35}$$

- $\tilde{E}_2^{(1)} \equiv \left(\bar{\chi}_{1,\mathrm{L}}\gamma_{\mu_1\mu_2\mu_3}\chi_{2,\mathrm{L}}\right)\left(\bar{\chi}_{3,\mathrm{L}}\gamma_{\mu_1\mu_2\mu_3}\chi_{4,\mathrm{L}}\right) - 16\tilde{\mathcal{O}}_2$:

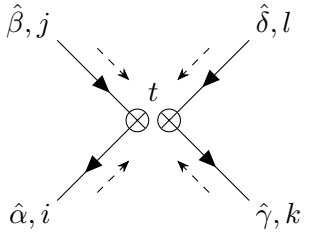

$$\begin{aligned} &= \delta_{ij}\delta_{kl}\{P_+\gamma_{\mu_1\mu_2\mu_3}P_-\}_{\hat{\alpha}\hat{\beta}}\{P_+\gamma_{\mu_1\mu_2\mu_3}P_-\}_{\hat{\gamma}\hat{\delta}} \\ &\quad -16\,\mathcal{O}_{2,ijkl,\hat{\alpha}\hat{\beta}\hat{\gamma}\hat{\delta}} \\ &\equiv E^{(1)}_{2,ijkl,\hat{\alpha}\hat{\beta}\hat{\gamma}\hat{\delta}} \end{aligned} \tag{B.36}$$

- $\tilde{E}_1^{(2)} \equiv -\left(\bar{\chi}_{1,\mathrm{L}}\gamma_{\mu_1\mu_2\mu_3\mu_4\mu_5}T^a\chi_{2,\mathrm{L}}\right)\left(\bar{\chi}_{3,\mathrm{L}}\gamma_{\mu_1\mu_2\mu_3\mu_4\mu_5}T^a\chi_{4,\mathrm{L}}\right) - 20\tilde{E}_1^{(1)} - 256\tilde{\mathcal{O}}_1$:

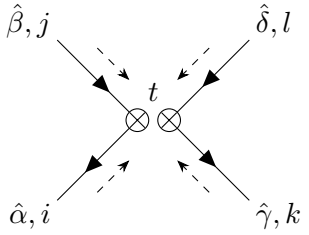

$$\begin{aligned} &= -T^a_{ij}T^a_{kl}\{P_+\gamma_{\mu_1\mu_2\mu_3\mu_4\mu_5}P_-\}_{\hat{\alpha}\hat{\beta}}\{P_+\gamma_{\mu_1\mu_2\mu_3\mu_4\mu_5}P_-\}_{\hat{\gamma}\hat{\delta}} \\ &\quad -20\,E^{(1)}_{1,ijkl,\hat{\alpha}\hat{\beta}\hat{\gamma}\hat{\delta}} - 256\,\mathcal{O}_{1,ijkl,\hat{\alpha}\hat{\beta}\hat{\gamma}\hat{\delta}} \end{aligned} \tag{B.37}$$

- $\tilde{E}_2^{(2)} \equiv \left(\bar{\chi}_{1,\mathrm{L}}\gamma_{\mu_1\mu_2\mu_3\mu_4\mu_5}\chi_{2,\mathrm{L}}\right)\left(\bar{\chi}_{3,\mathrm{L}}\gamma_{\mu_1\mu_2\mu_3\mu_4\mu_5}\chi_{4,\mathrm{L}}\right) - 20\tilde{E}_2^{(1)} - 256\tilde{\mathcal{O}}_2$:

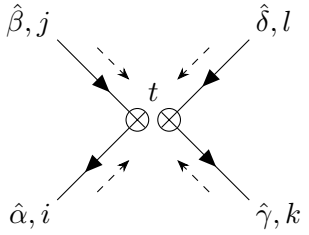

$$\begin{aligned} &= \delta_{ij}\delta_{kl}\{P_+\gamma_{\mu_1\mu_2\mu_3\mu_4\mu_5}P_-\}_{\hat{\alpha}\hat{\beta}}\{P_+\gamma_{\mu_1\mu_2\mu_3\mu_4\mu_5}P_-\}_{\hat{\gamma}\hat{\delta}} \\ &\quad -20\,E^{(1)}_{2,ijkl,\hat{\alpha}\hat{\beta}\hat{\gamma}\hat{\delta}} - 256\,\mathcal{O}_{2,ijkl,\hat{\alpha}\hat{\beta}\hat{\gamma}\hat{\delta}} \end{aligned} \tag{B.38}$$

B.5 AUXILIARY FEYNMAN RULES

The following Feynman rules are auxiliary Feynman rules for our implementation as described in Appendix C. They replace the vertices with four gluons or gluon-flow lines in our implementation and allow us to factorize the color structure of all Feynman diagrams.

- four-gluon vertex:
  - Σ propagator:

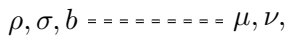

$$= \delta^{ab}\delta_{\mu\rho}\delta_{\nu\sigma} \tag{B.39}$$

  - Σ-gluon-gluon vertex:

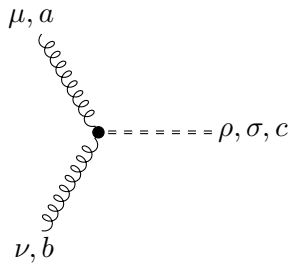

$$= \frac{\mathrm{i}g_{\mathrm{B}}}{\sqrt{2}} f^{abc}\left(\delta_{\mu\rho}\delta_{\nu\sigma} - \delta_{\nu\rho}\delta_{\mu\sigma}\right) \tag{B.40}$$

- three-plus-one gluon flow vertex:
  - Σ flow line:

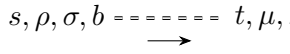

$$= \delta^{ab}\delta_{\mu\rho}\delta_{\nu\sigma}\delta(t-s) \tag{B.41}$$

  - outgoing Σ-gluon-gluon flow vertex:

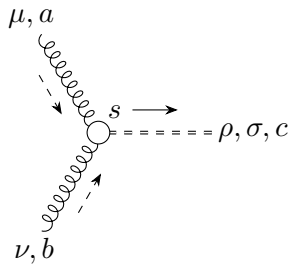

$$= \frac{\mathrm{i}g_{\mathrm{B}}}{\sqrt{2}} f^{abc}\left(\delta_{\mu\rho}\delta_{\nu\sigma} - \delta_{\nu\rho}\delta_{\mu\sigma}\right) \int_0^\infty \mathrm{d}s \tag{B.42}$$

  - incoming Σ-gluon-gluon flow vertex:

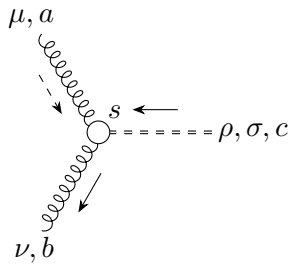

$$= \frac{\mathrm{i}g_{\mathrm{B}}}{\sqrt{2}} f^{abc}\left(\delta_{\mu\rho}\delta_{\nu\sigma} - \delta_{\nu\rho}\delta_{\mu\sigma}\right) \int_0^\infty \mathrm{d}s \tag{B.43}$$

- four-gluon vertex of $E(t,x) \equiv \frac{1}{4} G^a_{\mu\nu}(t,x) G^a_{\mu\nu}(t,x)$:
  - Σ_E flow line:

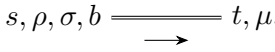

$$= \quad \delta^{ab} \delta_{\mu\rho} \delta_{\nu\sigma} \delta(t-s) \tag{B.44}$$

  - outgoing Σ_E-gluon-gluon vertex:

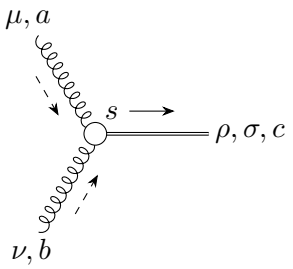

$$= \quad \frac{g_B^2}{\sqrt{2}} f^{abc} \left(\delta_{\mu\rho} \delta_{\nu\sigma} - \delta_{\nu\rho} \delta_{\mu\sigma} \right) \int_0^\infty \mathrm{d}s \tag{B.45}$$

  - incoming Σ_E-gluon-gluon vertex:

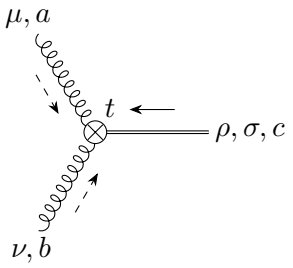

$$= \quad \frac{g_B^2}{\sqrt{2}} f^{abc} \left(\delta_{\mu\rho} \delta_{\nu\sigma} - \delta_{\nu\rho} \delta_{\mu\sigma} \right) \tag{B.46}$$

- four-gluon vertex of $\tilde{\mathcal{O}}_{1,\mu\nu}(t,x) \equiv G^a_{\mu\rho}(t,x) G^a_{\nu\rho}(t,x)$:
  - $\Sigma_{\tilde{\mathcal{O}}_{1,\mu\nu}}$ flow line:

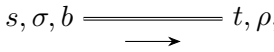

$$= \quad \delta^{ab} \delta_{\rho\sigma} \delta(t-s) \tag{B.47}$$

  - outgoing $\Sigma_{\tilde{\mathcal{O}}_{1,\mu\nu}}$-gluon-gluon vertex:

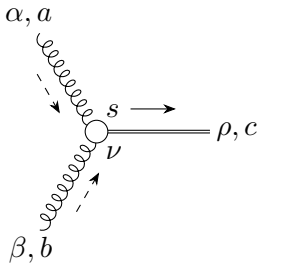

$$= \quad g_B^2 f^{abc} \left(\delta_{\nu\alpha} \delta_{\beta\rho} - \delta_{\nu\beta} \delta_{\alpha\rho} \right) \int_0^\infty \mathrm{d}s \tag{B.48}$$

– incoming $\Sigma_{\tilde{\mathcal{O}}_{1,\mu\nu}}$-gluon-gluon vertex:

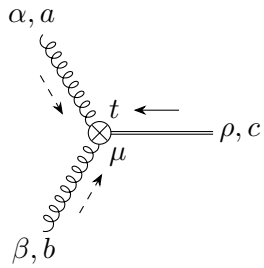

$$= \quad g_{\mathrm{B}}^2 f^{abc} \left(\delta_{\mu\alpha}\delta_{\beta\rho} - \delta_{\mu\beta}\delta_{\alpha\rho}\right) \tag{B.49}$$

- four-gluon vertex of $\tilde{\mathcal{O}}_{2,\mu\nu}(t,x) = \delta_{\mu\nu} G^a_{\rho\sigma}(t,x) G^a_{\rho\sigma}(t,x)$:
  – $\Sigma_{\tilde{\mathcal{O}}_{2,\mu\nu}}$ flow line:

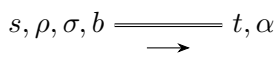

$$= \quad \delta^{ab}\delta_{\rho\alpha}\delta_{\sigma\beta}\delta(t-s) \tag{B.50}$$

  – outgoing $\Sigma_{\tilde{\mathcal{O}}_{2,\mu\nu}}$-gluon-gluon vertex:

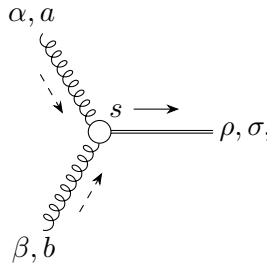

$$= \quad g_{\mathrm{B}}^2 f^{abc} \left(\delta_{\alpha\rho}\delta_{\beta\sigma} - \delta_{\alpha\sigma}\delta_{\beta\rho}\right) \int_0^\infty \mathrm{d}s \tag{B.51}$$

  – incoming $\Sigma_{\tilde{\mathcal{O}}_{2,\mu\nu}}$-gluon-gluon vertex:

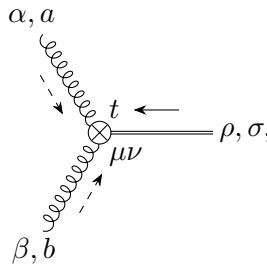

$$= \quad g_{\mathrm{B}}^2 f^{abc} \delta_{\mu\nu} \left(\delta_{\alpha\rho}\delta_{\beta\sigma} - \delta_{\alpha\sigma}\delta_{\beta\rho}\right) \tag{B.52}$$

C

AUTOMATED IMPLEMENTATION

We generate the Feynman diagrams including symmetry factors and signs (from closed fermion loops) with the help of the program `qgraf` [227, 228]. In the notation of this program, the propagators for the gluon, the ghost, and a single quark flavor can be defined as

```
[g,g,+], [c,C,-], [fq,fQ,-].
```

The sign in the third entry of each square bracket denotes whether the particle is a boson or a fermion. The flow lines for the gluon and the quark are implemented by introducing separate fields `b`, `fr`, and `fs` for L, λ, and $\bar{\lambda}$, respectively. They are implemented as

```
[b,B,+], [fr,fR,-], [fs,fS,-],
```

where the latter two represent the $\langle \chi \bar{\lambda} \rangle$ and $\langle \lambda \bar{\chi} \rangle$ bilinears (see Eqs. (2.53) and (2.54)). With these fields, we can then define the regular as well as the flow vertices. For example, for the trilinear flow vertex of the pure gauge theory defined in Eq. (2.55), we define

```
[B,b,b], [B,b,g], [B,g,g],
```

which corresponds to the three combinations of Fig. 2.1.

Already in regular QCD it is convenient to separate the color structure from the rest of the calculation. This becomes non-trivial in cases which involve the four-gluon vertex. It is thus convenient to introduce an auxiliary "particle" $\Sigma^a_{\mu\nu}$ whose "propagator" is given by (see [229] and the references therein)

$$\rho, \sigma, b \text{ ========= } \mu, \nu, a \qquad = \qquad \delta^{ab} \delta_{\mu\rho} \delta_{\nu\sigma}. \tag{C.1}$$

The four-gluon vertex can then be replaced by a trilinear $gg\Sigma$ vertex whose Feynman rule reads

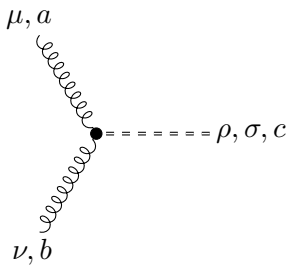

$$= \qquad \frac{\mathrm{i} g_{\mathrm{B}}}{\sqrt{2}} f^{abc} \left(\delta_{\mu\rho} \delta_{\nu\sigma} - \delta_{\nu\rho} \delta_{\mu\sigma} \right). \tag{C.2}$$

This allows to factorize the color factor off all Feynman diagrams, albeit at the cost of increasing their number.[1] We proceed correspondingly for the quartic gluon flow vertices

1 By constructing a general algorithm, it was shown in Ref. [62] that four-gluon (flow) vertices can always be factorized as long as the momentum dependence is polynomial.

by introducing an additional Σ particle which is directed in flow time. It forms trilinear vertices with gluons and gluon flow lines, as shown explicitly in Appendix B.5. Again, they contain exactly one outgoing (Σ or gluon) flow line. The quartic gluon vertices from operators like $E(t)$ with the vertex in Eq. (2.70) are treated in the same way. All of them can be found in Appendix B.5 as well.

By default, `qgraf` also generates diagrams with closed flow-line loops. We use a `Perl` script to parse the `qgraf` output in order to eliminate such diagrams before the actual calculation. They vanish trivially algebraically though, as discussed earlier. In the same way we multiply diagrams by a factor n_h or n_l for each closed heavy or light fermion loop, respectively. We then process the diagrams with the help of `q2e/exp` [230, 231] in order to insert the Feynman rules and convert the diagrams to `FORM` code.

Within `FORM` [225, 226], we contract the Lorentz indices, take the fermion traces, and simplify the resulting expressions to the standard form of scalar integrals in Eq. (2.77). The color factor is evaluated separately with the help of the `color` package [200]. The projectors for the calculations in Chapters 6 to 8 are implemented in `FORM` as well. More details of the implementation thus far can be found in Ref. [42] and some more details of the implementation of the projectors for the operators of the EMT in Ref. [151].

Afterwards, we collect all scalar integrals and try to map them onto each other by exploiting symmetries in the loop momenta and flow-time variables. For the remaining integrals, we then construct a system of equations employing the relations discussed in Section 3.1 with the help of a `Mathematica` [71] code developed in Ref. [45]. This system is then solved with `Kira` $\oplus$ `FireFly` [46–48, 70] employing the feature to reduce user-defined systems, as discussed at length in Chapter 3. The master integrals are computed with the strategies discussed in Chapter 4. Ultimately, we assemble the final results with `Mathematica`.

D

ACRONYMS

CKM *Cabibbo-Kobayashi-Maskawa*
CMM *Chetyrkin-Misiak-Münz*
CRT *Chinese remainder theorem*
CP *charge conjugation parity*
EMT *energy-momentum tensor*
EOM *equations of motion*
IBP *integration-by-parts*
LO *leading order*
NLO *next-to-leading order*
NNLO *next-to-next-to-leading order*
OPE *operator product expansion*
1PI *one-particle irreducible*
QCD *Quantum Chromodynamics*
QED *Quantum Electrodynamics*
RG *renormalization group*
RR *rational reconstruction*
UV *ultra-violet*
VEV *vacuum expectation value*
VPF *vacuum polarization function*

E

ACKNOWLEDGEMENTS

First and foremost, I would like to thank Prof. Dr. Robert V. Harlander for guiding me through my doctoral studies. Not only did he teach me valuable lessons and provided advice, he also encouraged me to pursue projects beyond his supervision. Moreover, his great humor made me laugh many times. In addition, he apparently provided a sufficiently positive letter of recommendation to secure me a postdoc position.

I thank Prof. Dr. Michał Czakon for agreeing to be the second referee of my thesis.

I would like to thank Dr. Jonas Klappert for pushing `FireFly` and `Kira` with his enthusiasm and skill. Without him, these projects would have never reached their current status. I also praise his skill in pretending to listen to my thoughts, which surprisingly often helped to solve problems. I thank Benjamin Summ for answering all my (stupid and naive) questions with his profound knowledge of Quantum Field Theories. Moreover, I thank both of them for many interesting and helpful discussions, the lively atmosphere in our office, and for proofreading my thesis.

Furthermore, I would like to thank my other collaborators Johannes Artz, Sven Yannick Klein, Yannick Kluth, Dr. Philipp Maierhöfer, Dr. Tobias Neumann, Dr. Mario Prausa, and Dr. Johann Usovitsch for their contributions to our joint projects and valuable discussions. I especially thank Dr. Philipp Maierhöfer and Dr. Tobias Neumann for providing me with additional letters of recommendation. Further thanks go to Dr. Philipp Maierhöfer and Dr. Mario Prausa for the "productive" week in Freiburg and to Dr. Johann Usovitsch for the productive days in Mainz. Moreover, I owe Dr. Alexander Voigt gratitude for always having time to discuss technical problems and helping me solving these with his great technical knowledge and skill. I would also like to thank Lucius Bushnaq for interesting discussions, not only on the gradient flow.

I thank Anke Bachtenkirch and Ketsia Omokoko for guiding me through the administrative jungle and Dr. Jonas Becker, Michael Margos, and especially Dr. Uwe Kahlert for their IT support.

I also thank all current and former members of the institute during my doctoral studies, especially the regular guests of the coffee break Alexander M., Christian, Daniel M., Fabian, Fredo, Harun, Josh, Lena, Lukas K., Magnus, Nicole, Robert, and Thorben for many interesting discussions. For some distracting activities in the evening, I would like to thank Arnd, Benjamin, Elias, Fredo, Lukas S., Marco B., Marco N., Rene, Sebastian P., and Torsten.

For the regular (before Corona) board game and movie evenings I thank Backi, Chris, Johannes, Lasse, Marcel, Martin, Sophie, Thilo, and Tim. Furthermore, I thank Jan Paul, Martin, and Tim for other distractions. In my old home, I thank Alex, Bene, Jonas, Marce, Marlit, Moritz A., and Moritz B. for our activities, including the yearly hike and the more frequent board game evenings.

Finally, I would like to thank my family, in particular my parents, for their continued support.

All Feynman rules throughout this thesis as well as the Feynman diagrams in Chapters 3 and 5 were produced with Ti*k*Z-Feynman [232]. The Feynman diagrams in Chapters 2, 7, and 8 were drawn with `FeynGame` [233].

I thank the *Deutsche Forschungsgemeinschaft* (DFG, German Research Foundation) for funding my position through grant 386986591 and for allowing me to collaborate within the Collaborative Research Centre TRR 257 funded through grant 396021762. Some of the calculations in Chapter 5 were performed with computing resources granted by RWTH Aachen University under project "rwth0244". Some of the calculations in Chapter 3 were performed with computing resources granted by RWTH Aachen University under project "rwth0541".

BIBLIOGRAPHY

[1] M. F. Atiyah and R. Bott, *The Yang-Mills equations over Riemann surfaces*, *Philos. Trans. Royal Soc. A* **308** (1982) 523–615, DOI: 10.1098/rsta.1983.0017.

[2] R. Narayanan and H. Neuberger, *Infinite N phase transitions in continuum Wilson loop operators*, *JHEP* **03** (2006) 064, DOI: 10.1088/1126-6708/2006/03/064, arXiv: hep-th/0601210.

[3] M. Lüscher, *Trivializing Maps, the Wilson Flow and the HMC Algorithm*, *Commun. Math. Phys.* **293** (2010) 899–919, DOI: 10.1007/s00220-009-0953-7, arXiv: 0907.5491 [hep-lat].

[4] M. Lüscher, *Properties and uses of the Wilson flow in lattice QCD*, *JHEP* **08** (2010) 071, DOI: 10.1007/JHEP08(2010)071, arXiv: 1006.4518 [hep-lat], Erratum: *JHEP* **03** (2014) 092, DOI: 10.1007/JHEP03(2014)092.

[5] Sz. Borsányi et al., *High-precision scale setting in lattice QCD*, *JHEP* **09** (2012) 010, DOI: 10.1007/JHEP09(2012)010, arXiv: 1203.4469 [hep-lat].

[6] R. Sommer, *Scale setting in lattice QCD*, *PoS* **LATTICE2013** (2014) 015, DOI: 10.22323/1.187.0015, arXiv: 1401.3270 [hep-lat].

[7] M. Lüscher, *Chiral symmetry and the Yang-Mills gradient flow*, *JHEP* **04** (2013) 123, DOI: 10.1007/JHEP04(2013)123, arXiv: 1302.5246 [hep-lat].

[8] M. Lüscher and P. Weisz, *Perturbative analysis of the gradient flow in non-abelian gauge theories*, *JHEP* **02** (2011) 051, DOI: 10.1007/JHEP02(2011)051, arXiv: 1101.0963 [hep-th].

[9] C. Monahan and K. Orginos, *Locally smeared operator product expansions in scalar field theory*, *Phys. Rev. D* **91** (2015) 074513, DOI: 10.1103/PhysRevD.91.074513, arXiv: 1501.05348 [hep-lat].

[10] H. Suzuki, *Energy–momentum tensor from the Yang–Mills gradient flow*, *PTEP* **2013** (2013) 083B03, DOI: 10.1093/ptep/ptt059, arXiv: 1304.0533 [hep-lat], Erratum: *PTEP* **2015** (2015) 079201, DOI: 10.1093/ptep/ptv094.

[11] H. Makino and H. Suzuki, *Lattice energy–momentum tensor from the Yang–Mills gradient flow—inclusion of fermion fields*, *PTEP* **2014** (2014) 063B02, DOI: 10.1093/ptep/ptu070, arXiv: 1403.4772 [hep-lat], Erratum: *PTEP* **2015** (2015) 079202, DOI: 10.1093/ptep/ptv095.

[12] M. Asakawa, T. Hatsuda, E. Itou, M. Kitazawa, and H. Suzuki, *Thermodynamics of $SU(3)$ gauge theory from gradient flow on the lattice*, *Phys. Rev. D* **90** (2014) 011501, DOI: 10.1103/PhysRevD.90.011501, arXiv: 1312.7492 [hep-lat], Erratum: *Phys. Rev. D* **92** (2015) 059902, DOI: 10.1103/PhysRevD.92.059902.

[13] Y. Taniguchi, S. Ejiri, R. Iwami, K. Kanaya, M. Kitazawa, H. Suzuki, T. Umeda, and N. Wakabayashi, *Exploring $N_f = 2+1$ QCD thermodynamics from the gradient flow*, *Phys. Rev. D* **96** (2017) 014509, DOI: 10.1103/PhysRevD.96.014509, arXiv: 1609.01417 [hep-lat], Erratum: *Phys. Rev. D* **99** (2019) 059904, DOI: 10.1103/PhysRevD.99.059904.

[14] M. Kitazawa, T. Iritani, M. Asakawa, T. Hatsuda, and H. Suzuki, *Equation of state for SU(3) gauge theory via the energy-momentum tensor under gradient glow*, *Phys. Rev. D* **94** (2016) 114512, DOI: 10.1103/PhysRevD.94.114512, arXiv: 1610.07810 [hep-lat].

[15] M. Kitazawa, T. Iritani, M. Asakawa, and T. Hatsuda, *Correlations of the energy-momentum tensor via gradient flow in SU(3) Yang-Mills theory at finite temperature*, *Phys. Rev. D* **96** (2017) 111502, DOI: 10.1103/PhysRevD.96.111502, arXiv: 1708.01415 [hep-lat].

[16] R. Yanagihara, T. Iritani, M. Kitazawa, M. Asakawa, and T. Hatsuda, *Distribution of stress tensor around static quark–anti-quark from Yang-Mills gradient flow*, *Phys. Lett. B* **789** (2019) 210–214, DOI: 10.1016/j.physletb.2018.09.067, arXiv: 1803.05656 [hep-lat].

[17] Z. Fodor, K. Holland, J. Kuti, D. Nogradi, and C. H. Wong, *The Yang-Mills gradient flow in finite volume*, *JHEP* **11** (2012) 007, DOI: 10.1007/JHEP11(2012)007, arXiv: 1208.1051 [hep-lat].

[18] P. Fritzsch and A. Ramos, *The gradient flow coupling in the Schrödinger Functional*, *JHEP* **10** (2013) 008, DOI: 10.1007/JHEP10(2013)008, arXiv: 1301.4388 [hep-lat].

[19] A. Ramos, *The gradient flow running coupling with twisted boundary conditions*, *JHEP* **11** (2014) 101, DOI: 10.1007/JHEP11(2014)101, arXiv: 1409.1445 [hep-lat].

[20] A. Ramos, *The Yang-Mills gradient flow and renormalization*, *PoS* **LATTICE2014** (2015) 017, DOI: 10.22323/1.214.0017, arXiv: 1506.00118 [hep-lat].

[21] R. V. Harlander and T. Neumann, *The perturbative QCD gradient flow to three loops*, *JHEP* **06** (2016) 161, DOI: 10.1007/JHEP06(2016)161, arXiv: 1606.03756 [hep-ph].

[22] M. Dalla Brida and M. Lüscher, *SMD-based numerical stochastic perturbation theory*, *Eur. Phys. J. C* **77** (2017) 308, DOI: 10.1140/epjc/s10052-017-4839-0, arXiv: 1703.04396 [hep-lat].

[23] M. Dalla Brida and A. Ramos, *The gradient flow coupling at high-energy and the scale of SU(3) Yang–Mills theory*, *Eur. Phys. J. C* **79** (2019) 720, DOI: 10.1140/epjc/s10052-019-7228-z, arXiv: 1905.05147 [hep-lat].

[24] C. Monahan and K. Orginos, *Quasi parton distributions and the gradient flow*, *JHEP* **03** (2017) 116, DOI: 10.1007/JHEP03(2017)116, arXiv: 1612.01584 [hep-lat].

[25] C. Monahan, *Smeared quasidistributions in perturbation theory*, *Phys. Rev. D* **97** (2018) 054507, DOI: 10.1103/PhysRevD.97.054507, arXiv: 1710.04607 [hep-lat].

[26] S. Aoki, K. Kikuchi, and T. Onogi, *Geometries from field theories*, *PTEP* **2015** (2015) 101B01, DOI: 10.1093/ptep/ptv131, arXiv: 1505.00131 [hep-th].

[27] S. Aoki, J. Balog, T. Onogi, and P. Weisz, *Flow equation for the large N scalar model and induced geometries*, *PTEP* **2016** (2016) 083B04, DOI: 10.1093/ptep/ptw106, arXiv: 1605.02413 [hep-th].

[28] S. Aoki and S. Yokoyama, *AdS geometry from CFT on a general conformally flat manifold*, *Nucl. Phys. B* **933** (2018) 262–274, DOI: 10.1016/j.nuclphysb.2018.06.004, arXiv: 1709.07281 [hep-th].

[29] S. Aoki and S. Yokoyama, *Flow equation, conformal symmetry, and anti-de Sitter geometry*, *PTEP* **2018** (2018) 031B01, DOI: 10.1093/ptep/pty013, arXiv: 1707.03982 [hep-th].

[30] S. Aoki, J. Balog, and S. Yokoyama, *Holographic computation of quantum corrections to the bulk cosmological constant*, *PTEP* **2019** (2019) 043B06, DOI: 10.1093/ptep/ptz026, arXiv: 1804.04636 [hep-th].

[31] S. Aoki, S. Yokoyama, and K. Yoshida, *Holographic geometry for nonrelativistic systems emerging from generalized flow equations*, *Phys. Rev. D* **99** (2019) 126002, DOI: 10.1103/PhysRevD.99.126002, arXiv: 1902.02578 [hep-th].

[32] F. V. Tkachov, *A theorem on analytical calculability of 4-loop renormalization group functions*, *Phys. Lett. B* **100** (1981) 65–68, DOI: 10.1016/0370-2693(81)90288-4.

[33] K. G. Chetyrkin and F. V. Tkachov, *Integration by parts: The algorithm to calculate β-functions in 4 loops*, *Nucl. Phys. B* **192** (1981) 159–204, DOI: 10.1016/0550-3213(81)90199-1.

[34] M. Kauers, *Fast Solvers for Dense Linear Systems*, *Nucl. Phys. B Proc. Suppl.* **183** (2008) 245–250, DOI: 10.1016/j.nuclphysbps.2008.09.111.

[35] P. Kant, *Finding linear dependencies in integration-by-parts equations: A Monte Carlo approach*, *Comput. Phys. Commun.* **185** (2014) 1473–1476, DOI: 10.1016/j.cpc.2014.01.017, arXiv: 1309.7287 [hep-ph].

[36] A. von Manteuffel and R. M. Schabinger, *A novel approach to integration by parts reduction*, *Phys. Lett. B* **744** (2015) 101–104, DOI: 10.1016/j.physletb.2015.03.029, arXiv: 1406.4513 [hep-ph].

[37] T. Peraro, *Scattering amplitudes over finite fields and multivariate functional reconstruction*, *JHEP* **12** (2016) 030, DOI: 10.1007/JHEP12(2016)030, arXiv: 1608.01902 [hep-ph].

[38] F. Jegerlehner, *The Anomalous Magnetic Moment of the Muon*, *Springer Tracts Mod. Phys.* **274** (2017), DOI: 10.1007/978-3-319-63577-4.

[39] T. Aoyama et al., *The anomalous magnetic moment of the muon in the Standard Model*, *Phys. Rep.* **887** (2020) 1–166, DOI: 10.1016/j.physrep.2020.07.006, arXiv: 2006.04822 [hep-ph].

[40] Sz. Borsanyi et al., *Leading hadronic contribution to the muon magnetic moment from lattice QCD*, *Nature* **593** (2021) 51–55, DOI: 10.1038/s41586-021-03418-1, arXiv: 2002.12347 [hep-lat].

[41] J. Artz, R. V. Harlander, F. Lange, T. Neumann, and M. Prausa, *Results and techniques for higher order calculations within the gradient-flow formalism*, *JHEP* **06** (2019) 121, DOI: 10.1007/JHEP06(2019)121, arXiv: 1905.00882 [hep-lat], Erratum: *JHEP* **10** (2019) 032, DOI: 10.1007/JHEP10(2019)032.

[42] J. Artz, *Automatic approach to the perturbative gradient flow*, MA thesis, RWTH Aachen University, 2017.

[43] R. V. Harlander, Y. Kluth, and F. Lange, *The two-loop energy–momentum tensor within the gradient-flow formalism*, *Eur. Phys. J. C* **78** (2018) 944, DOI: 10.1140/epjc/s10052-018-6415-7, arXiv: 1808.09837 [hep-lat], Erratum: *Eur. Phys. J. C* **79** (2019) 858, DOI: 10.1140/epjc/s10052-019-7327-x.

[44] S. Laporta, *High-precision calculation of multiloop Feynman integrals by difference equations*, *Int. J. Mod. Phys. A* **15** (2000) 5087–5159, DOI: 10.1016/S0217-751X(00)00215-7, arXiv: hep-ph/0102033.

[45] F. Lange, *The Perturbative Gradient Flow at Higher Orders*, MA thesis, RWTH Aachen University, 2017.

[46] J. Klappert and F. Lange, *Reconstructing rational functions with* `FireFly`, *Comput. Phys. Commun.* **247** (2020) 106951, DOI: 10.1016/j.cpc.2019.106951, arXiv: 1904.00009 [cs.SC].

[47] J. Klappert, S. Y. Klein, and F. Lange, *Interpolation of dense and sparse rational functions and other improvements in FireFly*, *Comput. Phys. Commun.* **264** (2021) 107968, DOI: 10.1016/j.cpc.2021.107968, arXiv: 2004.01463 [cs.MS].

[48] J. Klappert, F. Lange, P. Maierhöfer, and J. Usovitsch, *Integral reduction with Kira 2.0 and finite field methods*, *Comput. Phys. Commun.* **266** (2021) 108024, DOI: 10.1016/j.cpc.2021.108024, arXiv: 2008.06494 [hep-ph].

[49] T. Gehrmann and E. Remiddi, *Differential equations for two-loop four-point functions*, *Nucl. Phys. B* **580** (2000) 485–518, DOI: 10.1016/S0550-3213(00)00223-6, arXiv: hep-ph/9912329.

[50] R. N. Lee, *Group structure of the integration-by-part identities and its application to the reduction of multiloop integrals*, *JHEP* **07** (2008) 031, DOI: 10.1088/1126-6708/2008/07/031, arXiv: 0804.3008 [hep-ph].

[51] A. V. Smirnov and A. V. Petukhov, *The Number of Master Integrals is Finite*, *Lett. Math. Phys.* **97** (2011) 37–44, DOI: 10.1007/s11005-010-0450-0, arXiv: 1004.4199 [hep-th].

[52] S. G. Gorishny, S. A. Larin, L. R. Surguladze, and F. V. Tkachov, *Mincer: Program for multiloop calculations in quantum field theory for the Schoonschip system*, *Comput. Phys. Commun.* **55** (1989) 381–408, DOI: 10.1016/0010-4655(89)90134-3.

[53] S. A. Larin, F. V. Tkachov, and J. A. M. Vermaseren, *The FORM version of MINCER*, 1991, NIKHEF-H-91-18.

[54] D. J. Broadhurst, *Three-loop on-shell charge renormalization without integration: $\Lambda^{\overline{MS}}_{QED}$ to four loops*, *Z. Phys. C* **54** (1992) 599–606, DOI: 10.1007/BF01559486.

[55] M. Steinhauser, *MATAD: a program package for the computation of MAssive TADpoles*, *Comput. Phys. Commun.* **134** (2001) 335–364, DOI: 10.1016/S0010-4655(00)00204-6, arXiv: hep-ph/0009029.

[56] K. Melnikov and T. van Ritbergen, *Three-Loop Slope of the Dirac Form Factor and the 1S Lamb Shift in Hydrogen*, *Phys. Rev. Lett.* **84** (2000) 1673–1676, DOI: 10.1103/PhysRevLett.84.1673, arXiv: hep-ph/9911277.

[57] K. Melnikov and T. van Ritbergen, *The three-loop relation between the $\overline{MS}$ and the pole quark masses*, *Phys. Lett. B* **482** (2000) 99–108, DOI: 10.1016/S0370-2693(00)00507-4, arXiv: hep-ph/9912391.

[58] K. Melnikov and T. van Ritbergen, *The three-loop on-shell renormalization of QCD and QED*, *Nucl. Phys. B* **591** (2000) 515–546, DOI: 10.1016/S0550-3213(00)00526-5, arXiv: hep-ph/0005131.

[59] B. Ruijl, T. Ueda, and J. A. M. Vermaseren, FORCER, *a* FORM *program for the parametric reduction of four-loop massless propagator diagrams*, *Comput. Phys. Commun.* **253** (2020) 107198, DOI: 10.1016/j.cpc.2020.107198, arXiv: 1704.06650 [hep-ph].

[60] R. N. Lee, *Presenting* `LiteRed`*: a tool for the Loop InTEgrals REDuction*, 2012, arXiv: 1212.2685 [hep-ph].

[61] R. N. Lee, `LiteRed` *1.4: a powerful tool for reduction of multiloop integrals*, *J. Phys. Conf. Ser.* **523** (2014) 012059, DOI: 10.1088/1742-6596/523/1/012059, arXiv: 1310.1145 [hep-ph].

[62] L. Bushnaq, *Calculational methods in the Gradient Flow Formalism*, MA thesis, RWTH Aachen University, 2019.

[63] C. Anastasiou and A. Lazopoulos, *Automatic integral reduction for higher order perturbative calculations*, *JHEP* **07** (2004) 046, DOI: 10.1088/1126-6708/2004/07/046, arXiv: hep-ph/0404258.

[64] A. V. Smirnov, *Algorithm FIRE — Feynman Integral REduction*, *JHEP* **10** (2008) 107, DOI: 10.1088/1126-6708/2008/10/107, arXiv: 0807.3243 [hep-ph].

[65] A. V. Smirnov and V. A. Smirnov, *FIRE4, LiteRed and accompanying tools to solve integration by parts relations*, *Comput. Phys. Commun.* **184** (2013) 2820–2827, DOI: 10.1016/j.cpc.2013.06.016, arXiv: 1302.5885 [hep-ph].

[66] A. V. Smirnov, *FIRE5: A C++ implementation of Feynman Integral REduction*, *Comput. Phys. Commun.* **189** (2015) 182–191, DOI: 10.1016/j.cpc.2014.11.024, arXiv: 1408.2372 [hep-ph].

[67] A. V. Smirnov and F. S. Chuhkarev, *FIRE6: Feynman Integral REduction with modular arithmetic*, *Comput. Phys. Commun.* **247** (2020) 106877, DOI: 10.1016/j.cpc.2019.106877, arXiv: 1901.07808 [hep-ph].

[68] C. Studerus, *Reduze – Feynman integral reduction in C++*, *Comput. Phys. Commun.* **181** (2010) 1293–1300, DOI: 10.1016/j.cpc.2010.03.012, arXiv: 0912.2546 [physics.comp-ph].

[69] A. von Manteuffel and C. Studerus, *Reduze 2 – Distributed Feynman Integral Reduction*, 2012, arXiv: 1201.4330 [hep-ph].

[70] P. Maierhöfer, J. Usovitsch, and P. Uwer, *Kira—A Feynman integral reduction program*, *Comput. Phys. Commun.* **230** (2018) 99–112, DOI: 10.1016/j.cpc.2018.04.012, arXiv: 1705.05610 [hep-ph].

[71] Wolfram Research, Inc., *Mathematica, Version 11.3*, Champaign, IL, 2018, URL: https://www.wolfram.com/mathematica.

[72] R. H. Lewis, *Computer Algebra System Fermat*, URL: https://home.bway.net/lewis.

[73] J. von zur Gathen and J. Gerhard, *Modern Computer Algebra*, third ed., Cambridge University Press, 2013, DOI: 10.1017/CBO9781139856065.

[74] W. S. Brown, *On Euclid's Algorithm and the Computation of Polynomial Greatest Common Divisors*, *J. ACM* **18** (1971) 478–504, DOI: 10.1145/321662.321664.

[75] M. J. Encarnación, *Computing GCDs of Polynomials over Algebraic Number Fields*, *J. Symb. Comp.* **20** (1995) 299–313, DOI: 10.1006/jsco.1995.1052.

[76] J. de Kleine, M. Monagan, and A. Wittkopf, *Algorithms for the Non-monic Case of the Sparse Modular GCD Algorithm*, *Proc. Int. Symp. Symbolic Algebraic Comp.* **2005** (2005) 124–131, DOI: 10.1145/1073884.1073903.

[77] R. Zippel, *Probabilistic algorithms for sparse polynomials*, *Symbolic Algebraic Comp. EUROSAM* **1979** (1979) 216–226, DOI: 10.1007/3-540-09519-5_73.

[78] M. Ben-Or and P. Tiwari, *A Deterministic Algorithm for Sparse Multivariate Polynomial Interpolation*, *Proc. ACM Symp. Theory Comp.* **20** (1988) 301–309, DOI: 10.1145/62212.62241.

[79] E. Kaltofen and Lakshman Y., *Improved Sparse Multivariate Polynomial Interpolation Algorithms*, *Symbolic Algebraic Comp. ISSAC* **1988** (1989) 467–474, DOI: 10.1007/3-540-51084-2_44.

[80] R. Zippel, *Interpolating Polynomials from their Values*, *J. Symb. Comp.* **9** (1990) 375–403, DOI: 10.1016/S0747-7171(08)80018-1.

[81] E. Kaltofen, W.-s. Lee, and A. A. Lobo, *Early Termination in Ben-Or/Tiwari Sparse Interpolation and a Hybrid of Zippel's Algorithm*, *Proc. Int. Symp. Symbolic Algebraic Comp.* **2000** (2000) 192–201, DOI: 10.1145/345542.345629.

[82] E. Kaltofen and W.-s. Lee, *Early termination in sparse interpolation algorithms*, *J. Symb. Comp.* **36** (2003) 365–400, DOI: 10.1016/S0747-7171(03)00088-9.

[83] A. Cuyt and W.-s. Lee, *Sparse interpolation of multivariate rational functions*, *Theor. Comp. Sci.* **412** (2011) 1445–1456, DOI: 10.1016/j.tcs.2010.11.050.

[84] P. S. Wang, *A p-adic Algorithm for Univariate Partial Fractions*, *Proc. ACM Symp. Symbolic Algebraic Comp.* **1981** (1981) 212–217, DOI: 10.1145/800206.806398.

[85] M. Monagan, *Maximal Quotient Rational Reconstruction: An Almost Optimal Algorithm for Rational Reconstruction*, *Proc. Int. Symp. Symbolic Algebraic Comp.* **2004** (2004) 243–249, DOI: 10.1145/1005285.1005321.

[86] R. A. DeMillo and R. J. Lipton, *A probabilistic remark on algebraic program testing*, *Inf. Process. Lett.* **7** (1978) 193–195, DOI: 10.1016/0020-0190(78)90067-4.

[87] J. T. Schwartz, *Fast Probabilistic Algorithms for Verification of Polynomial Identities*, *J. ACM* **27** (1980) 701–717, DOI: 10.1145/322217.322225.

[88] S. Abreu, J. Dormans, F. Febres Cordero, H. Ita, M. Kraus, B. Page, E. Pascual, M. S. Ruf, and V. Sotnikov, CARAVEL*: A C++ Framework for the Computation of Multi-Loop Amplitudes with Numerical Unitarity*, 2020, arXiv: 2009.11957 [hep-ph].

[89] T. Peraro, FINITEFLOW*: multivariate functional reconstruction using finite fields and dataflow graphs*, *JHEP* **07** (2019) 031, DOI: 10.1007/JHEP07(2019)031, arXiv: 1905.08019 [hep-ph].

[90] S. Y. Klein, *Reduktion von Feynmanintegralen mit vielen Skalen*, BA thesis, RWTH Aachen University, 2019.

[91] M. Abramowitz and I. A. Stegun, eds., *Handbook of Mathematical Functions With Formulas, Graphs, and Mathematical Tables*, first ed., Dover Publications, 1964, ISBN: 0-486-61272-4.

[92] E. Kaltofen and B. M. Trager, *Computing with Polynomials Given By Black Boxes for Their Evaluations: Greatest Common Divisors, Factorization, Separation of Numerators and Denominators*, *J. Symb. Comp.* **9** (1990) 301–320, DOI: 10.1016/S0747-7171(08)80015-6.

[93] D. Y. Grigoriev, M. Karpinski, and M. F. Singer, *Interpolation of Sparse Rational Functions Without Knowing Bounds on Exponents*, *Proc. Symp. Foundations Comp. Sci.* **31** (1990) 840–846, DOI: 10.1109/FSCS.1990.89616.

[94] D. Y. Grigoriev and M. Karpinski, *Algorithms for Sparse Rational Interpolation*, *Proc. Int. Symp. Symbolic Algebraic Comp.* **1991** (1991) 7–13, DOI: 10.1145/120694.120696.

[95] D. Grigoriev, M. Karpinski, and M. F. Singer, *Computational Complexity of Sparse Rational Interpolation*, *SIAM J. Comp.* **23** (1994) 1–11, DOI: 10.1137/S0097539791194069.

[96] E. Kaltofen and Z. Yang, *On Exact and Approximate Interpolation of Sparse Rational Functions*, *Proc. Int. Symp. Symbolic Algebraic Comp.* **2007** (2007) 203–210, DOI: 10.1145/1277548.1277577.

[97] Q.-L. Huang and X.-S. Gao, *Sparse Rational Function Interpolation with Finitely Many Values for the Coefficients*, *Math. Aspects Comp. Information Sci.* **2017** (2017) 227–242, DOI: 10.1007/978-3-319-72453-9_16, arXiv: 1706.00914 [cs.SC].

[98] A. Díaz and E. Kaltofen, FOXBOX*: A System for Manipulating Symbolic Objects in Black Box Representation*, *Proc. Int. Symp. Symbolic Algebraic Comp.* **1998** (1998) 30–37, DOI: 10.1145/281508.281538.

[99] Ø. Ore, *Über höhere Kongruenzen*, *Norsk Mat. Forenings Skrifter Ser.* **I** (1922).

[100] P. S. Wang, M. J. T. Guy, and J. H. Davenport, *P-adic Reconstruction of Rational Numbers*, *ACM SIGSAM Bulletin* **16** (1982) 2–3, DOI: 10.1145/1089292.1089293.

[101] A. V. Smirnov and V. A. Smirnov, *How to choose master integrals*, *Nucl. Phys. B* **960** (2020) 115213, DOI: 10.1016/j.nuclphysb.2020.115213, arXiv: 2002.08042 [hep-ph].

[102] J. Usovitsch, *Factorization of denominators in integration-by-parts reductions*, 2020, arXiv: 2002.08173 [hep-ph].

[103] MPI Forum, *Message Passing Interface*, URL: https://www.mpi-forum.org.

[104] X. Guan, X. Liu, and Y.-Q. Ma, *Complete reduction of integrals in two-loop five-light-parton scattering amplitudes*, *Chin. Phys. C* **44** (2020) 093106, DOI: 10.1088/1674-1137/44/9/093106, arXiv: 1912.09294 [hep-ph].

[105] T. Binoth and G. Heinrich, *An automatized algorithm to compute infrared divergent multi-loop integrals*, *Nucl. Phys. B* **585** (2000) 741–759, DOI: 10.1016/S0550-3213(00)00429-6, arXiv: hep-ph/0004013.

[106] T. Binoth and G. Heinrich, *Numerical evaluation of multiloop integrals by sector decomposition*, *Nucl. Phys. B* **680** (2004) 375–388, DOI: 10.1016/j.nuclphysb.2003.12.023, arXiv: hep-ph/0305234.

[107] T. Neumann, *Perturbative calculations for Standard Model precision physics: Higgs production and Yang-Mills gradient flow*, PhD thesis, Bergische Universität Wuppertal, 2015, URL: http://nbn-resolving.org/urn:nbn:de:hbz:468-20151005-111240-6.

[108] A. V. Kotikov, *Differential equations method. New technique for massive Feynman diagram calculation*, *Phys. Lett. B* **254** (1991) 158–164, DOI: 10.1016/0370-2693(91)90413-K.

[109] A. V. Kotikov, *Differential equations method: the calculation of vertex-type Feynman diagrams*, *Phys. Lett. B* **259** (1991) 314–322, DOI: 10.1016/0370-2693(91)90834-D.

[110] A. V. Kotikov, *Differential equation method. The Calculation of N-point Feynman diagrams*, *Phys. Lett. B* **267** (1991) 123–127, DOI: 10.1016/0370-2693(91)90536-Y, Erratum: *Phys. Lett. B* **295** (1992) 409, DOI: 10.1016/0370-2693(92)91582-T.

[111] E. Remiddi, *Differential equations for Feynman graph amplitudes*, *Nuovo Cim. A* **110** (1997) 1435–1452, arXiv: hep-th/9711188.

[112] O. V. Tarasov, *Connection between Feynman integrals having different values of the space-time dimension*, *Phys. Rev. D* **54** (1996) 6479–6490, DOI: 10.1103/PhysRevD.54.6479, arXiv: hep-th/9606018.

[113] R. N. Lee, *Space–time dimensionality D as complex variable: Calculating loop integrals using dimensional recurrence relation and analytical properties with respect to D*, *Nucl. Phys. B* **830** (2010) 474–492, DOI: 10.1016/j.nuclphysb.2009.12.025, arXiv: 0911.0252 [hep-ph].

[114] V. A. Smirnov, *Analytical result for dimensionally regularized massless on-shell double box*, *Phys. Lett. B* **460** (1999) 397–404, DOI: 10.1016/S0370-2693(99)00777-7, arXiv: hep-ph/9905323.

[115] J. B. Tausk, *Non-planar massless two-loop Feynman diagrams with four on-shell legs*, *Phys. Lett. B* **469** (1999) 225–234, DOI: 10.1016/S0370-2693(99)01277-0, arXiv: hep-ph/9909506.

[116] M. Prausa, *Mellin–Barnes meets Method of Brackets: a novel approach to Mellin–Barnes representations of Feynman integrals*, *Eur. Phys. J. C* **77** (2017) 594, DOI: 10.1140/epjc/s10052-017-5150-9, arXiv: 1706.09852 [hep-ph].

[117] M. Czakon, *Automatized analytic continuation of Mellin–Barnes integrals*, *Comput. Phys. Commun.* **175** (2006) 559–571, DOI: 10.1016/j.cpc.2006.07.002, arXiv: hep-ph/0511200.

[118] A. V. Smirnov and V. A. Smirnov, *On the resolution of singularities of multiple Mellin–Barnes integrals*, *Eur. Phys. J. C* **62** (2009) 445–449, DOI: 10.1140/epjc/s10052-009-1039-6, arXiv: 0901.0386 [hep-ph].

[119] T. Huber and D. Maître, *HypExp, a Mathematica package for expanding hypergeometric functions around integer-valued parameters*, *Comput. Phys. Commun.* **175** (2006) 122–144, DOI: 10.1016/j.cpc.2006.01.007, arXiv: hep-ph/0507094.

[120] T. Huber and D. Maître, *HypExp 2, Expanding hypergeometric functions about half-integer parameters*, *Comput. Phys. Commun.* **178** (2008) 755–776, DOI: 10.1016/j.cpc.2007.12.008, arXiv: 0708.2443 [hep-ph].

[121] E. Panzer, *On hyperlogarithms and Feynman integrals with divergences and many scales*, *JHEP* **03** (2014) 071, DOI: 10.1007/JHEP03(2014)071, arXiv: 1401.4361 [hep-th].

[122] Maplesoft, a division of Waterloo Maple Inc., *Maple 2020*, Waterloo, Ontario.

[123] E. Panzer, *Algorithms for the symbolic integration of hyperlogarithms with applications to Feynman integrals*, *Comput. Phys. Commun.* **188** (2015) 148–166, DOI: 10.1016/j.cpc.2014.10.019, arXiv: 1403.3385 [hep-th].

[124] E. Panzer, *Feynman integrals and hyperlogarithms*, PhD thesis, Humboldt-Universität zu Berlin, 2015, DOI: 10.18452/17157, arXiv: 1506.07243 [math-ph].

[125] A. B. Goncharov, *Multiple polylogarithms, cyclotomy and modular complexes*, *Math. Res. Lett.* **5** (1998) 497–516, DOI: 10.4310/MRL.1998.v5.n4.a7, arXiv: 1105.2076 [math.AG].

[126] J. M. Borwein, D. M. Bradley, D. J. Broadhurst, and P. Lisonek, *Special values of multiple polylogarithms*, *Trans. Am. Math. Soc.* **353** (2001) 907–941, DOI: 10.1090/S0002-9947-00-02616-7, arXiv: math/9910045.

[127] A. V. Smirnov and M. N. Tentyukov, *Feynman Integral Evaluation by a Sector decomposiTion Approach (FIESTA)*, *Comput. Phys. Commun.* **180** (2009) 735–746, DOI: 10.1016/j.cpc.2008.11.006, arXiv: 0807.4129 [hep-ph].

[128] A. V. Smirnov, V. A. Smirnov, and M. Tentyukov, *FIESTA 2: Parallelizeable multiloop numerical calculations*, *Comput. Phys. Commun.* **182** (2011) 790–803, DOI: 10.1016/j.cpc.2010.11.025, arXiv: 0912.0158 [hep-ph].

[129] A. V. Smirnov, *FIESTA 3: Cluster-parallelizable multiloop numerical calculations in physical regions*, *Comput. Phys. Commun.* **185** (2014) 2090–2100, DOI: 10.1016/j.cpc.2014.03.015, arXiv: 1312.3186 [hep-ph].

[130] A. C. Genz and A. A. Malik, *An Imbedded Family of Fully Symmetric Numerical Integration Rules*, *SIAM J. Numer. Anal.* **20** (1983) 580–588, DOI: 10.1137/0720038.

[131] L. Fousse, G. Hanrot, V. Lefèvre, P. Pélissier, and P. Zimmermann, *MPFR: A Multiple-Precision Binary Floating-Point Library With Correct Rounding*, *ACM Trans. Math. Softw.* **33** (2007) 13, DOI: 10.1145/1236463.1236468.

[132] R. V. Harlander, F. Lange, and T. Neumann, *Hadronic vacuum polarization using gradient flow*, *JHEP* **08** (2020) 109, DOI: 10.1007/JHEP08(2020)109, arXiv: 2007.01057 [hep-lat].

[133] T. Iritani, M. Kitazawa, H. Suzuki, and H. Takaura, *Thermodynamics in quenched QCD: energy–momentum tensor with two-loop order coefficients in the gradient-flow formalism*, *PTEP* **2019** (2019) 023B02, DOI: 10.1093/ptep/ptz001, arXiv: 1812.06444 [hep-lat].

[134] K. G. Chetyrkin, J. H. Kühn, and M. Steinhauser, *RunDec: a Mathematica package for running and decoupling of the strong coupling and quark masses*, *Comput. Phys. Commun.* **133** (2000) 43–65, DOI: 10.1016/S0010-4655(00)00155-7, arXiv: hep-ph/0004189.

[135] F. Herren and M. Steinhauser, *Version 3 of RunDec and CRunDec*, *Comput. Phys. Commun.* **224** (2018) 333–345, DOI: 10.1016/j.cpc.2017.11.014, arXiv: 1703.03751 [hep-ph].

[136] H. Makino, O. Morikawa, and H. Suzuki, *Gradient flow and the Wilsonian renormalization group flow*, *PTEP* **2018** (2018) 053B02, DOI: 10.1093/ptep/pty050, arXiv: 1802.07897 [hep-th].

[137] M. Beneke and V. A. Smirnov, *Asymptotic expansion of Feynman integrals near threshold*, *Nucl. Phys. B* **522** (1998) 321–344, DOI: 10.1016/S0550-3213(98)00138-2, arXiv: hep-ph/9711391.

[138] V. A. Smirnov, *Applied Asymptotic Expansions in Momenta and Masses*, *Springer Tracts Mod. Phys.* **177** (2002), DOI: 10.1007/3-540-44574-9.

[139] V. A. Smirnov, *Analytic Tools for Feynman Integrals*, *Springer Tracts Mod. Phys.* **250** (2012), DOI: 10.1007/978-3-642-34886-0.

[140] E. Lambrou, *Determining α_s by using the gradient flow in the quenched theory*, *PoS* **LATTICE2016** (2016) 196, DOI: 10.22323/1.256.0196.

[141] S. Caracciolo, G. Curci, P. Menotti, and A. Pelissetto, *The energy-momentum tensor on the lattice: The scalar case*, *Nucl. Phys. B* **309** (1988) 612–624, DOI: 10.1016/0550-3213(88)90332-X.

[142] S. Caracciolo, G. Curci, P. Menotti, and A. Pelissetto, *The Energy-Momentum Tensor for Lattice Gauge Theories*, *Annals Phys.* **197** (1990) 119–153, DOI: 10.1016/0003-4916(90)90203-Z.

[143] S. Caracciolo, P. Menotti, and A. Pelissetto, *Analytic determination at one loop of the energy–momentum tensor for lattice QCD*, *Phys. Lett. B* **260** (1991) 401–406, DOI: 10.1016/0370-2693(91)91632-6.

[144] S. Caracciolo, P. Menotti, and A. Pelissetto, *One-loop analytic computation of the energy–momentum tensor for lattice gauge theories*, *Nucl. Phys. B* **375** (1992) 195–239, DOI: 10.1016/0550-3213(92)90339-D.

[145] S. Capitani and G. Rossi, *Deep inelastic scattering in improved lattice QCD (I). The first moment of structure functions*, *Nucl. Phys. B* **433** (1995) 351–389, DOI: 10.1016/0550-3213(94)00428-H, arXiv: hep-lat/9401014.

[146] G. Burgio, S. Caracciolo, and A. Pelissetto, *Algebraic algorithm for the computation of one-loop Feynman diagrams in lattice QCD with Wilson fermions*, *Nucl. Phys. B* **478** (1996) 687–719, DOI: 10.1016/0550-3213(96)00428-2, arXiv: hep-lat/9607010.

[147] L. Giusti and M. Pepe, *Energy-momentum tensor on the lattice: Nonperturbative renormalization in Yang-Mills theory*, *Phys. Rev. D* **91** (2015) 114504, DOI: 10.1103/PhysRevD.91.114504, arXiv: 1503.07042 [hep-lat].

[148] M. Dalla Brida, L. Giusti, and M. Pepe, *Non-perturbative definition of the QCD energy-momentum tensor on the lattice*, *JHEP* **04** (2020) 043, DOI: 10.1007/JHEP04(2020)043, arXiv: 2002.06897 [hep-lat].

[149] S. G. Gorishny, S. A. Larin, and F. V. Tkachov, *The algorithm for OPE coefficient functions in the MS scheme*, *Phys. Lett. B* **124** (1983) 217–220, DOI: 10.1016/0370-2693(83)91439-9.

[150] S. G. Gorishny and S. A. Larin, *Coefficient functions of asymptotic operator expansions in minimal subtraction scheme*, *Nucl. Phys. B* **283** (1987) 452–476, DOI: 10.1016/0550-3213(87)90283-5.

[151] Y. Kluth, *Gradient Flow and the Energy-Momentum Tensor*, MA thesis, RWTH Aachen University, 2018.

[152] N. K. Nielsen, *The energy-momentum tensor in a non-Abelian quark gluon theory*, *Nucl. Phys. B* **120** (1977) 212–220, DOI: 10.1016/0550-3213(77)90040-2.

[153] H. Suzuki and H. Takaura, *Renormalon-free definition of the gluon condensate within the large-β_0 approximation*, *PTEP* **2019** (2019) 103B04, DOI: 10.1093/ptep/ptz100, arXiv: 1807.10064 [hep-ph].

[154] M. Kitazawa, S. Mogliacci, I. Kolbé, and W. A. Horowitz, *Anisotropic pressure induced by finite-size effects in SU(3) Yang-Mills theory*, *Phys. Rev. D* **99** (2019) 094507, DOI: 10.1103/PhysRevD.99.094507, arXiv: 1904.00241 [hep-lat].

[155] Y. Taniguchi, S. Ejiri, K. Kanaya, M. Kitazawa, H. Suzuki, and T. Umeda, *$N_f = 2+1$ QCD thermodynamics with gradient flow using two-loop matching coefficients*, *Phys. Rev. D* **102** (2020) 014510, DOI: 10.1103/PhysRevD.102.014510, arXiv: 2005.00251 [hep-lat].

[156] R. Yanagihara, M. Kitazawa, M. Asakawa, and T. Hatsuda, *Distribution of energy-momentum tensor around a static quark in the deconfined phase of SU(3) Yang-Mills theory*, *Phys. Rev. D* **102** (2020) 114522, DOI: 10.1103/PhysRevD.102.114522, arXiv: 2010.13465 [hep-lat].

[157] K. G. Chetyrkin, J. H. Kühn, and A. Kwiatkowski, *QCD corrections to the e^+e^- cross-section and the Z boson decay rate*, *Phys. Rept.* **277** (1996) 189–281, DOI: 10.1016/S0370-1573(96)00012-9, arXiv: hep-ph/9503396.

[158] K. G. Chetyrkin, J. H. Kühn, A. Maier, P. Maierhöfer, P. Marquard, M. Steinhauser, and C. Sturm, *Precise charm- and bottom-quark masses: Theoretical and experimental uncertainties*, *Theor. Math. Phys.* **170** (2012) 217–228, DOI: 10.1007/s11232-012-0024-7, arXiv: 1010.6157 [hep-ph].

[159] A. Crivellin, M. Hoferichter, C. A. Manzari, and M. Montull, *Hadronic Vacuum Polarization: $(g-2)_\mu$ versus Global Electroweak Fits*, *Phys. Rev. Lett.* **125** (2020) 091801, DOI: 10.1103/PhysRevLett.125.091801, arXiv: 2003.04886 [hep-ph].

[160] A. Keshavarzi, W. J. Marciano, M. Passera, and A. Sirlin, *Muon $g-2$ and $\Delta\alpha$ connection*, *Phys. Rev. D* **102** (2020) 033002, DOI: 10.1103/PhysRevD.102.033002, arXiv: 2006.12666 [hep-ph].

[161] T. Blum, N. Christ, M. Hayakawa, T. Izubuchi, L. Jin, C. Jung, and C. Lehner, *Hadronic Light-by-Light Scattering Contribution to the Muon Anomalous Magnetic Moment from Lattice QCD*, *Phys. Rev. Lett.* **124** (2020) 132002, DOI: 10.1103/PhysRevLett.124.132002, arXiv: 1911.08123 [hep-lat].

[162] E.-H. Chao, A. Gérardin, J. R. Green, R. J. Hudspith, and H. B. Meyer, *Hadronic light-by-light contribution to $(g-2)_\mu$ from lattice QCD with SU(3) flavor symmetry*, *Eur. Phys. J. C* **80** (2020) 869, DOI: 10.1140/epjc/s10052-020-08444-3, arXiv: 2006.16224 [hep-lat].

[163] C. A. Dominguez, *Analytical determination of the QCD quark masses*, *Int. J. Mod. Phys. A* **29** (2014) 1430069, DOI: 10.1142/S0217751X14300695, arXiv: 1411.3462 [hep-ph].

[164] V. P. Spiridonov, *Anomalous Dimension of $G^2_{\mu\nu}$ and β-function*, 1984, IYaI-P-0378.

[165] V. P. Spiridonov and K. G. Chetyrkin, *Nonleading mass corrections and renormalization of the operators $m\bar{\psi}\psi$ and $G^2_{\mu\nu}$*, *Sov. J. Nucl. Phys.* **47** (1988) 522–527.

[166] K. G. Chetyrkin and J. H. Kühn, *Quartic mass corrections to R_{had}*, *Nucl. Phys. B* **432** (1994) 337–350, DOI: 10.1016/0550-3213(94)90605-X, arXiv: hep-ph/9406299.

[167] P. A. Baikov and K. G. Chetyrkin, *QCD vacuum energy in 5 loops*, *PoS* **RADCOR2017** (2018) 025, DOI: 10.22323/1.290.0025.

[168] G. Källén and A. Sabry, *Fourth order vacuum polarization*, *Kong. Dan. Vid. Sel. Mat. Fys. Med.* **29** (1955) 1–20, DOI: 10.1007/978-3-319-00627-7_93.

[169] D. J. Broadhurst, *Chiral symmetry breaking and perturbative QCD*, *Phys. Lett. B* **101** (1981) 423–426, DOI: 10.1016/0370-2693(81)90167-2.

[170] B. A. Kniehl, *Two-loop corrections to the vacuum polarizations in perturbative QCD*, *Nucl. Phys. B* **347** (1990) 86–104, DOI: 10.1016/0550-3213(90)90552-O.

[171] A. Djouadi and P. Gambino, *Electroweak gauge bosons self-energies: Complete QCD corrections*, *Phys. Rev. D* **49** (1994) 3499–3511, DOI: 10.1103/PhysRevD.49.3499, arXiv: hep-ph/9309298, Erratum: *Phys. Rev. D* **53** (1996) 4111, DOI: 10.1103/PhysRevD.53.4111.

[172] D. J. Broadhurst, J. Fleischer, and O. V. Tarasov, *Two-loop two-point functions with masses: asymptotic expansions and Taylor series, in any dimension*, *Z. Phys. C* **60** (1993) 287–302, DOI: 10.1007/BF01474625, arXiv: hep-ph/9304303.

[173] J. Fleischer and O. V. Tarasov, *Calculation of Feynman diagrams from their small momentum expansion*, *Z. Phys. C* **64** (1994) 413–425, DOI: 10.1007/BF01560102, arXiv: hep-ph/9403230.

[174] D. J. Broadhurst, P. A. Baikov, V. A. Ilyin, J. Fleischer, O. V. Tarasov, and V. A. Smirnov, *Two-loop gluon-condensate contributions to heavy-quark current correlators: exact results and approximations*, *Phys. Lett. B* **329** (1994) 103–110, DOI: 10.1016/0370-2693(94)90524-X, arXiv: hep-ph/9403274.

[175] P. A. Baikov and D. J. Broadhurst, *Three-loop QED Vacuum Polarization and the four-loop Muon Anomalous Magnetic Moment*, 1995, arXiv: hep-ph/9504398.

[176] K. G. Chetyrkin, J. H. Kühn, and M. Steinhauser, *Heavy quark vacuum polarization to three loops*, *Phys. Lett. B* **371** (1996) 93–98, DOI: 10.1016/0370-2693(95)01593-0, arXiv: hep-ph/9511430.

[177] K. G. Chetyrkin, J. H. Kühn, and M. Steinhauser, *Heavy quark current correlators to $\mathcal{O}(\alpha_s^2)$*, *Nucl. Phys. B* **505** (1997) 40–64, DOI: 10.1016/S0550-3213(97)00481-1, arXiv: hep-ph/9705254.

[178] K. G. Chetyrkin, R. Harlander, and M. Steinhauser, *Singlet polarization functions at $O(\alpha_s^2)$*, *Phys. Rev. D* **58** (1998) 014012, DOI: 10.1103/PhysRevD.58.014012, arXiv: hep-ph/9801432.

[179] A. H. Hoang, V. Mateu, and S. Mohammad Zebarjad, *Heavy quark vacuum polarization function at $\mathcal{O}(\alpha_s^2)$ and $\mathcal{O}(\alpha_s^3)$*, *Nucl. Phys. B* **813** (2009) 349–369, DOI: 10.1016/j.nuclphysb.2008.12.005, arXiv: 0807.4173 [hep-ph].

[180] Y. Kiyo, A. Maier, P. Maierhöfer, and P. Marquard, *Reconstruction of heavy quark current correlators at $\mathcal{O}(\alpha_s^3)$*, *Nucl. Phys. B* **823** (2009) 269–287, DOI: 10.1016/j.nuclphysb.2009.08.010, arXiv: 0907.2120 [hep-ph].

[181] D. Greynat and S. Peris, *Resummation of threshold, low- and high-energy expansions for heavy-quark correlators*, *Phys. Rev. D* **82** (2010) 034030, DOI: 10.1103/PhysRevD.82.034030, arXiv: 1006.0643 [hep-ph], Erratum: *Phys. Rev. D* **82** (2010) 119907, DOI: 10.1103/PhysRevD.82.119907.

[182] D. Greynat, P. Masjuan, and S. Peris, *Analytic reconstruction of heavy-quark two-point functions at $\mathcal{O}(\alpha_s^3)$*, *Phys. Rev. D* **85** (2012) 054008, DOI: 10.1103/PhysRevD.85.054008, arXiv: 1104.3425 [hep-ph].

[183] A. Maier and P. Marquard, *Validity of Padé approximations in vacuum polarization at three- and four-loop order*, *Phys. Rev. D* **97** (2018) 056016, DOI: 10.1103/PhysRevD.97.056016, arXiv: 1710.03724 [hep-ph].

[184] W. Celmaster and R. J. Gonsalves, *Quantum-Chromodynamics Perturbation Expansions in a Coupling Constant Renormalized by Momentum-Space Subtraction*, *Phys. Rev. Lett.* **42** (1979) 1435–1438, DOI: 10.1103/PhysRevLett.42.1435.

[185] K. G. Chetyrkin, A. L. Kataev, and F. V. Tkachov, *Higher-order corrections to $\sigma_{tot}(e^+e^- \to hadrons)$ in quantum chromodynamics*, *Phys. Lett. B* **85** (1979) 277–279, DOI: 10.1016/0370-2693(79)90596-3.

[186] M. Dine and J. Sapirstein, *Higher-Order Quantum Chromodynamic Corrections in e+ e- Annihilation*, *Phys. Rev. Lett.* **43** (1979) 668–671, DOI: 10.1103/PhysRevLett.43.668.

[187] S. G. Gorishny, A. L. Kataev, and S. A. Larin, *Three-Loop Corrections of Order $O(m^2)$ to the Correlator of Electromagnetic Quark Currents*, *Nuovo Cim. A* **92** (1986) 119–131, DOI: 10.1007/BF02727185.

[188] K. G. Chetyrkin, R. Harlander, J. H. Kühn, and M. Steinhauser, *Mass corrections to the vector current correlator*, *Nucl. Phys. B* **503** (1997) 339–353, DOI: 10.1016/S0550-3213(97)00383-0, arXiv: hep-ph/9704222.

[189] R. Harlander and M. Steinhauser, *Higgs boson decay to top quarks at $O(\alpha_s^2)$*, *Phys. Rev. D* **56** (1997) 3980–3990, DOI: 10.1103/PhysRevD.56.3980, arXiv: hep-ph/9704436.

[190] R. Harlander and M. Steinhauser, *$\mathcal{O}(\alpha_s^2)$ corrections to top quark production at e^+e^- colliders*, *Eur. Phys. J. C* **2** (1998) 151–158, DOI: 10.1007/s100520050129, arXiv: hep-ph/9710413.

[191] P. A. Baikov, K. G. Chetyrkin, and J. H. Kühn, *Vacuum polarization in pQCD: First complete $O(\alpha_s^4)$ result*, *Nucl. Phys. B Proc. Suppl.* **135** (2004) 243–246, DOI: 10.1016/j.nuclphysbps.2004.09.013.

[192] P. A. Baikov, K. G. Chetyrkin, and J. H. Kühn, *$R(s)$ and hadronic τ-Decays in Order α_s^4: technical aspects*, *Nucl. Phys. B Proc. Suppl.* **189** (2009) 49–53, DOI: 10.1016/j.nuclphysbps.2009.03.010, arXiv: 0906.2987 [hep-ph].

[193] P. A. Baikov, K. G. Chetyrkin, and J. H. Kühn, *Scalar Correlator at $\mathcal{O}(\alpha_s^4)$, Higgs Boson Decay into Bottom Quarks, and Bounds on the Light-Quark Masses*, *Phys. Rev. Lett.* **96** (2006) 012003, DOI: 10.1103/PhysRevLett.96.012003, arXiv: hep-ph/0511063.

[194] K. G. Chetyrkin and A. Khodjamirian, *Strange quark mass from pseudoscalar sum rule with $O(\alpha_s^4)$ accuracy*, *Eur. Phys. J. C* **46** (2006) 721–728, DOI: 10.1140/epjc/s2006-02508-8, arXiv: hep-ph/0512295.

[195] P. A. Baikov, K. G. Chetyrkin, J. H. Kühn, and J. Rittinger, *Complete $O(\alpha_s^4)$ QCD Corrections to Hadronic Z Decays*, *Phys. Rev. Lett.* **108** (2012) 222003, DOI: 10.1103/PhysRevLett.108.222003, arXiv: 1201.5804 [hep-ph].

[196] P. A. Baikov, K. G. Chetyrkin, J. H. Kühn, and J. Rittinger, *Adler function, sum rules and Crewther relation of order $\mathcal{O}(\alpha_s^4)$: The singlet case*, *Phys. Lett. B* **714** (2012) 62–65, DOI: 10.1016/j.physletb.2012.06.052, arXiv: 1206.1288 [hep-ph].

[197] K. G. Chetyrkin, S. G. Gorishny, and V. P. Spiridonov, *Wilson expansion for correlators of vector currents at the two-loop level: Dimension-four operators*, *Phys. Lett. B* **160** (1985) 149–153, DOI: 10.1016/0370-2693(85)91482-0.

[198] K. G. Chetyrkin, R. V. Harlander, and J. H. Kühn, *Quartic mass corrections to R_{had} at $\mathcal{O}(\alpha_s^3)$*, *Nucl. Phys. B* **586** (2000) 56–72, DOI: 10.1016/S0550-3213(00)00393-X, arXiv: hep-ph/0005139, Erratum: *Nucl. Phys. B* **634** (2002) 413–414, DOI: 10.1016/S0550-3213(02)00353-X.

[199] R. Harlander, *Quarkmasseneffekte in der Quantenchromodynamik und asymptotische Entwicklung von Feynman-Integralen*, PhD thesis, Universität Karlsruhe, 1998.

[200] T. van Ritbergen, A. N. Schellekens, and J. A. M. Vermaseren, *Group theory factors for Feynman diagrams*, *Int. J. Mod. Phys. A* **14** (1999) 41–96, DOI: 10.1142/S0217751X99000038, arXiv: hep-ph/9802376.

[201] M. Lüscher, *Future applications of the Yang–Mills gradient flow in lattice QCD*, *PoS* **LATTICE2013** (2014) 016, DOI: 10.22323/1.187.0016, arXiv: 1308.5598 [hep-lat].

[202] A. Kagimura, A. Tomiya, and R. Yamamura, *Effective lattice action for the configurations smeared by the Wilson flow*, 2015, arXiv: 1508.04986 [hep-lat].

[203] R. Yamamura, *The Yang–Mills gradient flow and lattice effective action*, *PTEP* **2016** (2016) 073B10, DOI: 10.1093/ptep/ptw097, arXiv: 1510.08208 [hep-lat].

[204] Y. Abe and M. Fukuma, *Gradient flow and the renormalization group*, *PTEP* **2018** (2018) 083B02, DOI: 10.1093/ptep/pty081, arXiv: 1805.12094 [hep-th].

[205] A. Carosso, A. Hasenfratz, and E. T. Neil, *Nonperturbative Renormalization of Operators in Near-Conformal Systems Using Gradient Flows*, *Phys. Rev. Lett.* **121** (2018) 201601, DOI: 10.1103/PhysRevLett.121.201601, arXiv: 1806.01385 [hep-lat].

[206] A. Carosso, A. Hasenfratz, and E. T. Neil, *Renormalization Group Properties of Scalar Field Theories using Gradient Flow*, *PoS* **LATTICE2018** (2019) 248, DOI: 10.22323/1.334.0248, arXiv: 1811.03182 [hep-lat].

[207] H. Sonoda and H. Suzuki, *Derivation of a gradient flow from the exact renormalization group*, *PTEP* **2019** (2019) 033B05, DOI: 10.1093/ptep/ptz020, arXiv: 1901.05169 [hep-th].

[208] A. Carosso, *Stochastic renormalization group and gradient flow*, *JHEP* **01** (2020) 172, DOI: 10.1007/JHEP01(2020)172, arXiv: 1904.13057 [hep-th].

[209] G. Buchalla, A. J. Buras, and M. E. Lautenbacher, *Weak decays beyond leading logarithms*, *Rev. Mod. Phys.* **68** (1996) 1125–1244, DOI: 10.1103/RevModPhys.68.1125, arXiv: hep-ph/9512380.

[210] S. Aoki et al., *FLAG Review 2019: Flavour Lattice Averaging Group (FLAG)*, *Eur. Phys. J. C* **80** (2020) 113, DOI: 10.1140/epjc/s10052-019-7354-7, arXiv: 1902.08191 [hep-lat].

[211] K. Chetyrkin, M. Misiak, and M. Münz, $||\Delta F|| = 1$ *nonleptonic effective Hamiltonian in a simpler scheme*, *Nucl. Phys. B* **520** (1998) 279–297, DOI: 10.1016/S0550-3213(98)00131-X, arXiv: hep-ph/9711280.

[212] H. E. Haber, *Useful relations among the generators in the defining and adjoint representations of SU(N)*, *SciPost Phys. Lect. Notes* **21** (2021), DOI: 10.21468/SciPostPhysLectNotes.21, arXiv: 1912.13302 [math-ph].

[213] F. J. Gilman and M. B. Wise, *Effective Hamiltonian for* $\Delta S = 1$ *weak nonleptonic decays in the six-quark model*, *Phys. Rev. D* **20** (1979) 2392–2407, DOI: 10.1103/PhysRevD.20.2392.

[214] A. J. Buras, M. Jamin, M. E. Lautenbacher, and P. H. Weisz, *Effective hamiltonians for* $\Delta S = 1$ *and* $\Delta B = 1$ *non-leptonic decays beyond the leading logarithmic approximation*, *Nucl. Phys. B* **370** (1992) 69–104, DOI: 10.1016/0550-3213(92)90345-C, Addendum: *Nucl. Phys. B* **375** (1992) 501–502, DOI: 10.1016/0550-3213(92)90042-A.

[215] F. Jegerlehner, *Facts of life with* γ_5, *Eur. Phys. J. C* **18** (2001) 673–679, DOI: 10.1007/s100520100573, arXiv: hep-th/0005255.

[216] G. 't Hooft and M. Veltman, *Regularization and Renormalization of Gauge Fields*, *Nucl. Phys. B* **44** (1972) 189–213, DOI: 10.1016/0550-3213(72)90279-9.

[217] N. Zerf, *Fermion traces without evanescence*, *Phys. Rev. D* **101** (2020) 036002, DOI: 10.1103/PhysRevD.101.036002, arXiv: 1911.06345 [hep-ph].

[218] A. J. Buras and P. H. Weisz, *QCD nonleading corrections to weak decays in dimensional regularization and 't Hooft-Veltman schemes*, *Nucl. Phys. B* **333** (1990) 66–99, DOI: 10.1016/0550-3213(90)90223-Z.

[219] M. J. Dugan and B. Grinstein, *On the vanishing of evanescent operators*, *Phys. Lett. B* **256** (1991) 239–244, DOI: 10.1016/0370-2693(91)90680-O.

[220] S. Herrlich and U. Nierste, *Evanescent operators, scheme dependences and double insertions*, *Nucl. Phys. B* **455** (1995) 39–58, DOI: 10.1016/0550-3213(95)00474-7, arXiv: hep-ph/9412375.

[221] P. Gambino, M. Gorbahn, and U. Haisch, *Anomalous dimension matrix for radiative and rare semileptonic B decays up to three loops*, *Nucl. Phys. B* **673** (2003) 238–262, DOI: 10.1016/j.nuclphysb.2003.09.024, arXiv: hep-ph/0306079.

[222] M. Gorbahn and U. Haisch, *Effective Hamiltonian for non-leptonic* $|\Delta F| = 1$ *decays at NNLO in QCD*, *Nucl. Phys. B* **713** (2005) 291–332, DOI: 10.1016/j.nuclphysb.2005.01.047, arXiv: hep-ph/0411071.

[223] A. Suzuki, Y. Taniguchi, H. Suzuki, and K. Kanaya, *Four quark operators for kaon bag parameter with gradient flow*, *Phys. Rev. D* **102** (2020) 034508, DOI: 10.1103/PhysRevD.102.034508, arXiv: 2006.06999 [hep-lat].

[224] M. D. Rizik, C. J. Monahan, and A. Shindler, *Short flow-time coefficients of CP-violating operators*, *Phys. Rev. D* **102** (2020) 034509, DOI: 10.1103/PhysRevD.102.034509, arXiv: 2005.04199 [hep-lat].

[225] J. A. M. Vermaseren, *New features of FORM*, 2000, arXiv: math-ph/0010025.

[226] J. Kuipers, T. Ueda, J. A. M. Vermaseren, and J. Vollinga, *FORM version 4.0*, *Comput. Phys. Commun.* **184** (2013) 1453–1467, DOI: 10.1016/j.cpc.2012.12.028, arXiv: 1203.6543 [cs.SC].

[227] P. Nogueira, *Automatic Feynman Graph Generation*, *J. Comput. Phys.* **105** (1993) 279–289, DOI: 10.1006/jcph.1993.1074.

[228] P. Nogueira, *Abusing QGRAF*, *Nucl. Instrum. Methods Phys. Res.* **559** (2006) 220–223, DOI: 10.1016/j.nima.2005.11.151.

[229] R. Harlander and M. Steinhauser, *Automatic Computation of Feynman Diagrams*, *Prog. Part. Nucl. Phys.* **43** (1999) 167–228, DOI: 10.1016/S0146-6410(99)00095-2, arXiv: hep-ph/9812357.

[230] R. Harlander, T. Seidensticker, and M. Steinhauser, *Corrections of $\mathcal{O}(\alpha\alpha_s)$ to the decay of the Z boson into bottom quarks*, *Phys. Lett. B* **426** (1998) 125–132, DOI: 10.1016/S0370-2693(98)00220-2, arXiv: hep-ph/9712228.

[231] T. Seidensticker, *Automatic application of successive asymptotic expansions of Feynman diagrams*, 1999, arXiv: hep-ph/9905298.

[232] J. P. Ellis, *TikZ-Feynman: Feynman diagrams with TikZ*, *Comput. Phys. Commun.* **210** (2017) 103–123, DOI: 10.1016/j.cpc.2016.08.019, arXiv: 1601.05437 [hep-ph].

[233] R. V. Harlander, S. Y. Klein, and M. Lipp, *FeynGame*, *Comput. Phys. Commun.* **256** (2020) 107465, DOI: 10.1016/j.cpc.2020.107465, arXiv: 2003.00896 [physics.ed-ph].